REGULATION OF LIPID HOMEOSTASIS DURING LOW OXYGEN ADAPTATION IN *SCHIZOSACCHAROMYCES POMBE*

by
Risa Burr

A dissertation submitted to Johns Hopkins University in conformity with the requirements of the degree of Doctor of Philosophy

Baltimore, Maryland
August, 2017

Abstract

Adaptation to environmental change is a hallmark of life, and fundamental factors including oxygen, lipids, nutrients, pH, and temperature are in a constant state of flux in many cellular environments. All organisms, from single-celled yeast to multicellular humans, must sense and adapt to these changing environmental conditions in order to survive and reproduce. This sensing and response is often regulated on the level of transcription factors, so that a broad set of genes can be altered in concert through changes in a single or small number of sensors. Due to the essential nature of these adaptations, the relevant transcription factor pathways are often conserved across species and can be highly complex in order to precisely tune the response. Therefore, study of these transcription factor pathways in the non-pathogenic fungus *Schizosaccharomyces pombe* may establish universal paradigms that are broadly applicable to other fungal species or to eukaryotes in general.

In this thesis, I defined a novel role for the AAA+ ATPase Cdc48 and its cofactor Ufd1 in the Golgi localization of the Dsc E3 ligase complex. This role ultimately impinges on cleavage of the SREBP transcription factor responsible for regulation of sterol biosynthesis in response to low oxygen in fission yeast. Through that work I also generated the first list of Cdc48 binding proteins in *S. pombe*, which can be used in the future to identify new Cdc48 cofactors and pathways that may be important to other cellular processes. I also uncovered a new regulator of the low oxygen response - Mga2. I demonstrated that Mga2 transcriptionally regulates phospholipid biosynthesis in response to low oxygen, acting alongside SREBPs to regulate lipid homeostasis. Further, I showed evidence of potential coordination of SREBP and Mga2 activation, suggesting broader co-regulation of these two pathways to keep overall lipid homeostasis in balance. In the future, I hope these insights will lead to establishment of Mga2 as important for low oxygen adaptation in pathogenic fungi.

PhD Dissertation Referees for Risa Burr

Peter Espenshade, PhD, Professor of Cell Biology, Johns Hopkins University School of Medicine (faculty sponsor)

Steven Claypool, PhD, Associate Professor of Physiology, Johns Hopkins University School of Medicine (reader)

Note to readers: Throughout this text, *S. pombe* gene names are in italics and the first letter of protein names are capitalized, in keeping with convention. This work was supported by NIH grants HL077588 (PJE) and T32 GM007445 (BCMB training grant).

Acknowledgements

I would like to start by thanking my advisor and mentor, Peter Espenshade, for his extraordinarily dedicated and thoughtful guidance throughout my graduate education. I appreciate Peter's generosity with his time, his critical and rigorous approach to science, and his tireless support in all scientific and professional activities. Every graduate student has an advisor to provide research direction, but I was lucky enough to find a mentor and, more importantly, a role model, to help me grow as a scientist, professional, and person. I also owe a lot of thanks to current and past members of the Espenshade lab. They selflessly provided reagents, protocols, and troubleshooting, not to mention friendship. I literally would not have finished without you.

I also thank my thesis committee members, Susan Michaelis, Cynthia Wolberger, and Steven Claypool for your advice and encouragement. I learned an enormous amount from BCMB and Cell Biology faculty members in classes and seminars. I owe a special thanks to the members of the BCMB and Cell Biology administrative offices, whose work behind the scenes has made the graduate school machine run much more smoothly. I also thank the members of the BCMB policy committee, the MA/PhD committee, the PDCO, and Eric Lee. What I learned from them about communication and professionalism has made me a much stronger scientist.

Finally, I would not have made it through graduate school without my friends and family. To my friends in Baltimore, I have appreciated their scientific input, their constancy, their laughter, and their support. I hope I have given them even a portion of what they gave me, and that these friendships will last far into the future, no matter where we end up. I thank my sister for always being by my side, and for her example of empathy. My parents inspire me to be my best scientist and person. As professors, they set the example for all that higher education has to offer. They could have also set expectations for my career, but they never did. I have only felt support and love from them for whoever I am and whatever path I chose, and I cannot thank them enough for that rare freedom. Last, I thank my grandfather, Dr. Calvin Mutchler, the original PhD, to whom this thesis is dedicated.

Table of Contents

List of Figures

List of Tables

Chapter 1

Introduction

This chapter is an edited version of the manuscript, “Oxygen-responsive transcriptional regulation of lipid homeostasis in fungi: Implications for anti-fungal drug development” by R. Burr and P. J. Espenshade, under revision at Seminars in Cell and Developmental Biology. It also incorporates material from the manuscript, “Dsc E3 ligase localization to the Golgi requires the ATPase Cdc48 and cofactor Ufd1 for activation of Sterol Regulatory Element-binding Protein in fission yeast” by R. Burr, D. Ribbens, S. Raychaudhuri, E. V. Stewart, J. Ho, and P. J. Espenshade, under revision at the Journal of Biological Chemistry, the manuscript, “Mga2 transcription factor regulates an oxygen-responsive lipid homeostasis pathway in fission yeast” by R. Burr, E. V. Stewart, W. Shao, S. Zhao, H. K. Hannibal-Bach, C. S. Ejsing, and P. J. Espenshade, published in the Journal of Biological Chemistry, Volume 291, Issue 23, 12171-12183. , and the manuscript, “Coordinate regulation of yeast Sterol Regulatory Element-Binding Protein (SREBP) and Mga2 transcription factors” by R. Burr, E. V. Stewart, and P. J. Espenshade, published in the Journal of Biological Chemistry, Volume 292, Issue 13, 5311-5324.

1.1 Environmental sensing in human disease

Environmental variability is a major challenge for life. Indeed, it can be argued that it is the constant flux of the environment that drives evolution. Within the human body, variations in temperature, pH, oxygen, carbon dioxide, nutrients, toxins, and hormones are common depending on location. For example, atmospheric air contains 21% oxygen, but human tissues have oxygen concentrations of 2.5-14% and oxygen can fall below 1% at sites of wounding or at the center of a poorly vascularized tumor (1). Sensing and adaptation to these environmental changes is crucial for maintenance of homeostasis and optimal growth and reproduction. As a result, sensing defects have been implicated in numerous human diseases. Many of these diseases are related to hormone insensitivity - mutations in the androgen receptor cause androgen insensitivity syndrome, resulting in genetic males that present with a female appearance (2). Growth hormone insensitivities, such as Laron dwarfism, are caused by defects in growth hormone receptor (3). Insulin resistance is caused by defects in the insulin receptor and is associated with type-2 diabetes, atherosclerosis, and hepatic steatosis in obese individuals (4).

Aside from hormone sensing, aberrant nutrient and metabolite sensing is also associated with human diseases. Defects in the extracellular calcium receptor cause diseases of abnormal calcium homeostasis leading to parathyroid gland dysfunction (5). Aberrant HIF-1 activity, which normally responds to oxygen levels, is associated with cancer progression and mortality (6). And dysregulated lipid sensing via SREBP is implicated in metabolic syndrome, hypertriglyceridemia, hepatic steatosis, and Huntington's disease (7-9). Study of the ways in which organisms sense and respond to their environment can lead to increased understanding of how homeostasis is maintained during constant environmental change and generate targets for treatments of disease in which environmental sensing is defective.

1.2 Cellular lipid homeostasis and physiological roles

Our lab seeks to elucidate the mechanisms of lipid and oxygen sensing and the resulting transcriptional response in eukaryotes. In the cell, lipid homeostasis is important for maintenance of membrane structure, barrier function, fluidity, and curvature, formation of lipid rafts, signaling, energy storage, and as substrates for posttranslational protein modification (10-13). The lipid category encompasses multiple classes, including sterols, sterol esters, and other isoprenoids (such as dolichol), free fatty acids, glycerophospholipids (such as phosphatidylcholine, lysophosphatidic acid, and cardiolipin), ether lipids, glycerolipids (such as diacylglycerol), sphingolipids, and polyketides. Lipid homeostasis is maintained through the balance of synthesis and breakdown. In eukaryotes, lipid synthesis centers around acetyl-CoA, which is primarily generated in the mitochondrion from pyruvate (at the end of glycolysis) and fatty acid oxidation.

To participate in lipid synthesis, mitochondrial acetyl-CoA must be converted to citrate through the TCA cycle, transported out of the mitochondrion and then converted back to acetyl-CoA in the cytoplasm by ATP citrate lyase (10). For this reason, all substrates of the TCA cycle that can generate citrate (many of which derive from amino acids such as glutamine) can also feed into the acetyl-CoA pool available for lipid synthesis. Acetyl-CoA becomes committed to isoprenoid and sterol synthesis upon condensation with another acetyl-CoA molecule to acetoacetyl-CoA, followed by conversion to HMG-CoA and then to mevalonate at the ER (10,12,14). Sterol synthesis is a highly oxygen-consumptive process, with synthesis of a single molecule of cholesterol requiring 11 molecules of oxygen. Synthesis of polyketides occurs by a unique mechanism involving decarboxylative condensation of acetate, proprionate, and butyrate into ring structures by polyketide synthase in a mechanism similar to fatty acid synthesis (15).

In contrast, synthesis of all other lipids begins with acetyl-CoA conversion to malonyl-CoA and then coupling of that malonyl-CoA to additional units of acetyl-CoA by fatty acid synthase to produce a long chain saturated acyl-CoA (10). At this point, the acyl-CoA may be mono- or poly-desaturated, or further elongated at the ER (16). Approximately 70-80% of all

fungal fatty acids are monounsaturated, and every bond desaturated on the acyl-CoA expends a molecule of oxygen (17). The acyl-CoA is then combined with glycerol 3-phosphate to form lysophosphatidic acid and a second acyl-CoA to form phosphatidic acid (PA) (11). The bond between the glycerol and the acyl-CoA is usually an ester bond, although ether bonds are produced at the peroxisome to generate ether lipids (18). At this point, the PA can be dephosphorylated to form diacylglycerol, which is then converted to phosphatidylcholine, phosphatidylethanolamine, phosphatidylserine, or triacylglycerol (11). Alternatively the PA can react with cytidine triphosphate to create CDP-diacylglycerol, which is then converted to phosphatidylglycerol, phosphatidylinositol (and its derivatives such as phosphatidylinositol phosphate), or cardiolipin (11) (16). Finally, an acyl-CoA can instead be combined with serine to start down the sphingolipid biosynthesis pathway or may be transferred to a sterol to generate a sterol ester (19,20).

Lipid catabolism is crucial to retrieve energy from lipids stored in lipid droplets or taken up from the extracellular environment, and to reformulate dietary essential fatty acids, damaged lipids, or excess lipids to rebalance the levels of different lipid classes in the cell. Most lipids are hydrolyzed to acyl-CoA and glycerol in the cytosol (21). However, lipid droplets are also shunted to the lysosome via lipophagy, where the triacylglycerols and sterol esters are hydrolyzed by lysosomal acid lipase (22). After hydrolysis, fatty acids are then catabolized in the mitochondrion (or peroxisomes if very long chain fatty acids) through the process of fatty acid oxidation (21,22). The acyl-CoA is first converted to acylcarnitine by carnitine palmitoyltransferase for transport across the membrane, at which point they are reconverted to acyl-CoA (21). In the mitochondrion (or peroxisome), the acyl-CoA is shortened two carbons at a time, producing acetyl-CoA, NADH, and $FADH_2$. The acetyl-CoA can enter the TCA cycle while the NADH and $FADH_2$ serve as electron carriers for the electron transport chain (21). Comparatively, sterol degradation is much less well understood, although in mammalian cells oxidation to bile acids is thought to be a major catabolic pathway and sterol and bile acid excretion is used to maintain sterol homeostasis (23).

Aside from lipid synthesis, acetyl-CoA is crucial for the TCA cycle and mitochondrial respiration and protein acetylation. Due to the many roles for acetyl-CoA in the cell, lipid synthesis is carefully coordinated with overall cellular metabolism.

1.3 Mammalian lipid and oxygen sensing pathways

We study both oxygen and lipid sensing because lipid biosynthesis is an oxygen-intensive process and therefore it is important to coordinate the regulation of lipid homeostasis with oxygen availability. Previous work from our lab and others has characterized the transcription factors that regulate lipid and oxygen sensing in mammals. Mammalian cells respond to changing lipid availability through a conserved family of ER membrane-bound SREBP transcription factors. SREBPs are bound and regulated by SCAP, a multi-pass transmembrane protein that senses sterols (24,25). Under conditions of low sterols, SCAP transports SREBPs from the ER to the Golgi. SREBPs in the Golgi are first cleaved by the Site-1 protease, releasing a membrane-bound N-terminal fragment that is further processed and released by the Site-2 protease, producing the active N-terminal transcription factor fragment (SREBP-N) (26). This process leaves the C-terminal fragment still bound to SCAP. At some point the C-terminus is removed and SCAP recycles back to the ER (27). After cleavage, the SREBP-N transcription factor domain enters the nucleus and upregulates transcription of target genes. In mammals, there are three isoforms of SREBP. SREBP-1 (a and c) regulate TAG and glycerophospholipid synthesis through activation of target genes including fatty acid synthase, stearoyl CoA desaturase, and long-chain fatty acid CoA ligase (24). SREBP-2 regulates cholesterol biosynthesis through genes such as HMG-CoA synthase, HMG-CoA reductase, and CYP51, as well as cholesterol uptake through control of LDL receptor expression (24,28). Interestingly, despite extensive experimentation, SREBP activation has not been found to be responsive to oxygen availability.

Instead, the mammalian oxygen response is largely regulated by the hypoxia-inducible factor (HIF) bHLH-PAS transcription factors, HIF1 and 2 (29). HIF is a heterodimer of an

unstable alpha subunit and a stable beta subunit (29). Under normoxic conditions, HIFα is hydroxylated on an asparaginyl residue by the Fe(II)- and 2-oxoglutarate-dependent dioxygenase FIH1, and on two different prolyl residues by the PHD family of prolyl hydroxylases (30,31). The asparaginyl hydroxylation interferes with HIF binding to transcriptional coactivators, while the prolyl hydroxylation targets HIFα to the pVHL ubiquitin ligase for ubiquitylation and proteasomal degradation. The FIH hydroxylase is functional at lower oxygen concentrations than the PHD, therefore together these inhibitors produce a graded response to oxygen availability. In response to low oxygen, HIF upregulates glycolysis, autophagy, and angiogenesis, and downregulates ATP consumption and oxidative phosphorylation (29). HIF also downregulates fatty acid oxidation and lipid synthesis genes (likely via downregulation of the SREBP pathway) and upregulates lipid uptake and storage in response to low oxygen, perhaps forming a link between the oxygen response and lipid homeostasis (32,33).

1.4 Pathogenic fungal infections

I study oxygen and lipid sensing in the fungus *Schizosaccharomyces pombe* as a model for sensing in fungal pathogens. Pathogenic fungi annually cause an estimated 1.6 million deaths worldwide (34). Mortality for invasive fungal infections can be high, with invasive *Candida* infections resulting in a mortality rate of 10-49% depending on the species (35-37). While most fungal infections are not life-threatening in immunocompetent hosts, an immunocompromised state is a major risk factor for invasive fungal infection (35). With improvements in HIV treatments, cancer immunotherapy, and organ transplant, as well as shifting demographics, the number of people living in an immunocompromised state is growing, leading to an increase in the number of fungal infections (35,38). Both *Candida* and *Aspergillus* infections have increased in incidence over the past two decades, and once-rare threats, such as *Mucor*, have gained in importance (37,39-41).

Moreover, antifungal resistance is increasing faster than new therapies are developed (42). The three main classes of antifungal drugs are azoles, polyenes, and echinocandins (35,42). Azoles, the largest class, target ergosterol biosynthesis by inhibiting the action of lanosterol demethylase (43). Polyenes, including amphotericin B, bind ergosterol to create pores in the fungal cell membrane (42). Introduced in 2001, echinocandins target cell wall integrity and were the last new class of antifungal therapies to become available (44,45). Due to increased, sometimes inappropriate, antifungal use in hospital and agricultural settings, antifungal resistance is increasing and becoming a serious public health threat. Fluconazole resistance in all *Candida* species is currently 7% (46). However, many pathogenic species show higher resistance and resulting increases in mortality. For example, 30% of *C. glabrata* cases are resistant to the first line antifungal fluconazole, and there has been a doubling of *C. glabrata* resistance to the second line antifungal echinocandin over the past 10 years (46-48). In 2009, a rare strain of *Candida auris* resistant to all three major antifungal classes was identified in Japan, and was since found in nine countries on four continents with high rates of mortality (49). Therefore, identification of new antifungal therapies, and particularly new fungal-specific targets outside the three major classes, will be crucial in future efforts to reduce mortality due to fungal infection.

The estimated 3.5-5 million species comprising the fungal kingdom populate a wide variety of environments including soil, tropical forests, city indoor air, dust, deserts, human tissue, and animal feces (50-52). Many of these environments differ greatly in oxygen availability and fungi that travel between environments of varying oxygen saturation must adapt in order to survive. This is particularly relevant for pathogenic fungi, which live in both the terrestrial environment and the low oxygen host environment (1,51,53). We predict that oxygen adaptation is a crucial aspect of host infection that leaves pathogens vulnerable to drugs targeting sensing and response pathways.

1.5 Conserved low oxygen transcriptional response in fungal species

Fungi do not have HIF homologs, and instead have developed different mechanisms for regulating the response to low oxygen. Numerous studies have identified hypoxic responsive transcriptional programs in different fungal species (54-60). As a foundation for my thesis, I analyzed the significantly up and down-regulated genes from those studies for gene ontology (GO) term enrichment and assembled broad categories of regulation from those GO terms. It is important to note that experimental protocols varied greatly among these reports, with oxygen concentrations ranging from 0-1% (or not defined when flasks were flushed with nitrogen) and low oxygen incubation times from 1.5-12 h. Despite these experimental differences and millions of years of divergence, we observed a shared program of transcriptional regulation among species. A large proportion of genes regulated in response to low oxygen fall into four significantly enriched categories: upregulation of lipid anabolism including sterols and glycerophospholipids, upregulation of carbohydrate catabolism, downregulation of gene expression including transcription and translation, and downregulation of aerobic respiration **(Fig. *1.1*)**. Lipid biosynthesis is a highly oxygen consumptive process and is crucial for maintenance of membrane integrity, cell growth, and proliferation. In order to adapt to low oxygen environments and maintain lipid homeostasis, fungi upregulate lipid biosynthetic enzymes to more efficiently utilize available oxygen. Lipid synthesis is also dependent on acetyl-CoA produced by pyruvate dehydrogenase during carbohydrate catabolism. Therefore, upregulating carbohydrate catabolism and acetyl-CoA production and downregulating aerobic respiration may serve to increase acetyl-CoA pools and free up molecular oxygen for lipid biosynthesis under hypoxic conditions. In contrast, non-specific downregulation of gene expression serves to reduce energy expenditure for protein synthesis, suggesting that general transcription is sacrificed during low oxygen stress. Thus, lipid biosynthesis seems to be the uniformly conserved anabolic pathway upregulated under low oxygen, while regulation of other pathways occurs with the purpose of generating energy and

components for lipid biosynthesis. Based on this finding, I focused my studies on the regulation of lipid homeostasis during low oxygen adaptation in fission yeast.

1.6 Ergosterol regulation in response to oxygen

GO biological process terms significantly upregulated in multiple fungal species under low oxygen include lipid metabolic process (GO:0006629), sterol biosynthetic process (GO:0016126), and ergosterol metabolic process (GO:0008204), implicating sterol anabolism in low oxygen adaptation **(Fig. *1.1*)**. The major fungal sterol, ergosterol, is essential for membrane organization and function. Synthesis of one molecule of ergosterol requires 12 molecules of oxygen (61). Accordingly, the ergosterol synthesis pathway is regulated by transcription factors that sense and respond to cellular oxygen availability in order to maintain lipid homeostasis.

Early work in our lab showed that fission yeast has SREBP transcription factor homologs, most notably *sre1* (54,62). Sre1 regulates ergosterol homeostasis in a way that is analogous to SREBP-2 in mammals (54,62). Interestingly, Sre1 also regulates a low oxygen response, representing the sole low oxygen-responsive program described in *S. pombe* (54,62). In fact, *sre1* is required for fission yeast survival under low oxygen conditions and regulates 22% of all oxygen responsive genes (54).

Sre1 is a basic-helix-loop-helix (bHLH) leucine zipper transcription factor that is initially synthesized as an inactive precursor form integral to the endoplasmic reticulum (ER) membrane (62). In the ER, Sre1 is bound by the multi-pass transmembrane protein and mammalian SCAP homolog, Scp1, which senses sterols through an N-terminal domain containing eight transmembrane segments (62) **(Fig. *1.2*)**. Whereas Insig proteins inhibit SREBP-SCAP binding under cholesterol-replete conditions in mammals, Sre1-Scp1 binding in fission yeast is not regulated by Insig (62). Instead, *S. pombe* Insig directly binds and inhibits the key ergosterol biosynthesis enzyme HMG-CoA reductase (63). Sre1 that is not bound by Scp1 in the ER is degraded by ER-associated degradation (ERAD); therefore it is probable that all Sre1 in the ER is

bound by Scp1 (64). There is a basal level of Sre1-Scp1 traffic to the Golgi under normoxia, but when oxygen (and subsequently ER ergosterol) is low, the rate of trafficking is greatly increased (65). These steps of Sre1 processing closely mirror the mammalian system for SREBP processing. In addition to Sre1, fission yeast has a second SREBP, Sre2, which is cleaved through the same mechanism as Sre1 but does not bind Scp1 and therefore is not regulated by ergosterol or oxygen levels (62,66). The constitutive activity of this homolog is useful for studying SREBP processing independent of Scp1 and the oxygen environment. The biological role of Sre2 is largely unknown, although it has been shown to repress flocculation (67).

Once *S. pombe* Sre1 reaches the Golgi, the remaining steps of activation are markedly different from the mammalian system. Large-scale genetic screens using the *S. pombe* deletion collection and methyl methanesulfonate (MMS) chemical mutagenesis identified seven genes (*dsc1-dsc5, cdc48, rbd2*) that are required for both Sre1 and Sre2 activation in the Golgi (68-71). Dsc1-Dsc5 are subunits of a Golgi-resident E3 ligase complex (the Dsc E3 ligase complex), which is homologous to the *Saccharomyces cerevisiae* Tul1 E3 ligase that has a recently ascribed function in vacuolar quality control (68,72). It is yet to be shown whether the Dsc E3 ligase ubiquitylates Sre1 itself or another pathway component during this process (73). Proper localization of the Dsc E3 ligase in the Golgi requires that it is a functional ligase, because Dsc E3 ligase subunits are retained in the ER when Dsc1 is catalytically dead or when complex members are missing (73). Therefore, ER-to-Golgi transport of multiple Sre1 pathway components, including Sre1-Scp1 and the Dsc E3 ligase, is required for Sre1 activation. Evidence in *S. cerevisiae* suggests that the Dsc E3 ligase plays a role in protein quality control outside of SREBP activation (72,74). In support of this role, over 30 fungal species have homologs of at least four of the five Dsc E3 ligase subunits, many species of which do not have Sre1 homologs **(Table *1.1*)**.

Rbd2 is a Golgi-resident rhomboid protease that is required for cleavage of SREBPs at the Golgi. Our current model is that the Dsc E3 ligase complex ubiquitylates SREBP to target it

to Rbd2 for cleavage. However, Rbd2 may not be the only protease involved as it is predicted to cleave the SREBP in the second transmembrane segment or luminal loop, whereas the active N-terminal transcription factor terminates before the first transmembrane segment (71). Indeed, in *Aspergillus nidulans*, where this system is conserved, a signal peptide peptidase provides the second cleavage of the SREBP homolog *SrbA*, indicating a requirement for two proteases in that species (75). However, the homologous peptidase is not required for SREBP cleavage in *S. pombe* (71). Alternatively, the cytosolic SREBP N-terminus could be mechanically extracted from the membrane before it can act as a transcription factor. In the mammalian system, Fleig *et al.* showed that Cdc48 acts downstream of substrate cleavage by the rhomboid protease RHBDL4 during ERAD (76).

cdc48 is the fission yeast homolog of mammalian *VCP* (also known as *p97*), a highly conserved gene that codes for an essential AAA+ ATPase making up 1% of total cellular protein (77). Cdc48 is a separase, using the energy from ATP hydrolysis for mechanical remodeling of ubiquitylated substrates (78). This function is required for many cellular processes including ERAD, autophagy, endosomal trafficking, chromosome-associated degradation, ribosomal quality control, membrane fusion, and cell cycle control (77-79). Cdc48 exists as a homohexamer, each monomer consisting of a N-terminal domain (N-domain), a D1 domain, a D2 domain, and a C-terminal domain (C-domain). Each D1 and D2 domain has an ATP binding and hydrolysis site, for a total of 12 ATP binding sites in the hexamer. ATP binding to D1 is required for ATP hydrolysis by the D2 domain, while ATP hydrolysis by D2 accounts for the majority of ATP hydrolysis by Cdc48 (80). Substrate binding inhibits ATP hydrolysis in the D1 domain but stimulates ATP hydrolysis in the D2 domain, resulting in an overall increase in Cdc48 ATP hydrolysis upon substrate binding (81). Recent *in vitro* work suggests that substrate unfolding occurs via ATP driven transport of ubiquitylated substrate through the central pore of the Cdc48 hexamer, after which the substrate is partially deubiquitylated and released (81). A series of Cdc48 cofactors target this ubiquitous protein to specific substrates and regulate its ATPase

activity (78,82). Autosomal dominant disease mutations clustered at the interface between the human VCP N and D1 domains change the balance of cofactors binding to VCP (83,84). These mutations lead to degenerative neuronal disorders including familial ALS, parkinsonism, and Inclusion Body Myopathy associated with Paget disease of bone and Frontotemporal Dementia (IBMPFD) (84-91).

Previous studies regarding the role of Cdc48 in SREBP cleavage highlight its versatility. Dsc5, the fission yeast homolog of FAF1, contains a canonical Cdc48-binding UBX domain that allows Cdc48 to bind the Dsc E3 ligase, but this domain is not required for SREBP cleavage (69). This suggests that the interaction between Cdc48 and the Dsc E3 ligase is not required for SREBP activation, but could be involved in the potential quality control role of the Dsc E3 ligase. Additionally, recent studies showed that Cdc48 binds Rbd2 through the SHP domain at the C-terminus of Rbd2, and that loss of this interaction inhibits SREBP cleavage (71). Rbd2 is not stably associated with the Dsc E3 ligase, therefore Cdc48 may serve to shuttle ubiquitylated SREBP from the Dsc E3 ligase to Rbd2. Indeed, experiments suggest that Cdc48 serves as a substrate adaptor between Rbd2 and SREBP because the block in SREBP cleavage due to a failure to form the Rbd2-Cdc48 complex can be overcome by overexpression of Rbd2 (71).

Following cleavage in the Golgi, cytosolic Sre1N is further regulated by the prolyl-hydroxylase Ofd1 and its inhibitor Nro1 (92-94). The Nro1 structure resembles that of known importins, and *nro1* is required for Ofd1 nuclear localization (93). Under normoxic conditions, Ofd1 binds Sre1N and inhibits DNA binding, leading to Sre1N degradation (95,96). However under low oxygen conditions, Nro1 binds and inhibits Ofd1, freeing Sre1N to exert transcription factor activity (97). Interestingly, Ofd1 and its human homolog OGFOD1 bind and hydroxylate the ribosomal protein Rps23, ultimately impacting translation termination (98). Whether the roles of *S. pombe* Ofd1 in Sre1N turnover and Rps23 hydroxylation are integrated is an unresolved question. Upon entering the nucleus, Sre1N binds SRE promoter elements and upregulates expression of hypoxic responsive and ergosterol biosynthesis pathway genes, including C-5 sterol

desaturase, C-4 methylsterol oxidase, cytochrome P450s, and coproporphyrinogen III oxidase, to scavenge the available oxygen and increase flux through the ergosterol biosynthesis pathway (54,62). Sre1N also binds to SRE elements in its own promoter, creating a positive feedback loop that amplifies small changes in ergosterol or oxygen availability into larger changes in pathway regulation (64). Ultimately, the Sre1 pathway in fission yeast is regulated by oxygen at two points – once indirectly through ergosterol and once through the oxygen-sensing Ofd1. In combination with the positive feedback present in the system, this results in a rapid and highly regulated transcriptional response to changing oxygen concentrations.

1.7 Phospholipid regulation in response to low oxygen

In addition to sterol synthesis, fungi regulate triacylglycerol (TAG) and glycerophospholipid (GPL) synthesis as well as fatty acid desaturation in response to changing oxygen availability. Enriched GO terms in this category include fatty acid biosynthetic process (GO:0006633), acyl-CoA biosynthetic process (GO:0071616), sphingolipid biosynthetic process (GO:0030148), long-chain fatty acid metabolic process (GO:0001676), membrane lipid metabolic process (GO:0006643), and triglyceride mobilization (GO:0006642). As with sterols, fatty acid desaturation requires oxygen and therefore desaturases are upregulated as oxygen decreases in order to maintain lipid homeostasis (54,99,100). Because desaturated fatty acids are incorporated into GPL and TAG, synthesis of these macromolecules is also oxygen-dependent.

In *S. cerevisiae*, Mga2 transcription factor homologs regulate these pathways in response to oxygen (101,102). Mga2 transcription factors have an IPT DNA-binding domain and an ankyrin repeat protein-protein interaction domain (103,104). Mga2 and its homolog Spt23 have overlapping functions in the low-oxygen response (103,105). Deletion of both *MGA2* and *SPT23* results in disrupted nuclear membrane morphology and is ultimately lethal even under normoxic conditions. Addition of exogenous unsaturated fatty acid rescues these defects (103). Mga2 is functionally more important in the oxygen response than Spt23 and will be the focus here

(101,105,106). The most-studied target of Mga2-Spt23 is *OLE1*, the only Δ9 fatty acid desaturase in *S. cerevisiae* (106). Mga2 upregulates transcription of *OLE1* and other target genes through binding to Low Oxygen Response Elements (LORE) in their promoters in response to low oxygen, unsaturated fatty acids (UFA), or temperature (101,106,107). Mga2 also regulates stability of the *OLE1* mRNA, although it is not known whether this activity is conserved for other target genes (101).

Like Sre1, Mga2 is initially membrane-bound and is activated by cleavage and release of the N-terminal transcription factor domain (103,104,108). Mga2 and Spt23 are activated by regulated ubiquitin/proteasome-dependent processing (RUP) **(Fig. *1.3*)** (108). Prior to processing, inactive Mga2 dimerizes through the IPT domain in the N-terminus (109). During RUP, Mga2 precursor is ubiquitylated by the NEDD4 E3 ligase Rsp5, which targets Mga2 to Cdc48 and the proteasome to release the N-terminal transcription factor domain through endoproteolytic cleavage, similar to NF-κB processing (108). It is still unknown what amino acid is ubiquitylated or how the proteasome selects a cleavage site (108). It was believed that Mga2 cleavage is regulated by membrane fatty acid saturation, with UFA blocking cleavage in a product inhibition mechanism similar to that observed for ergosterol and Sre1 (108). Recently however, it was shown that the transmembrane helix of Mga2 oligomerizes in the ER membrane where it senses the overall membrane lipid environment. Increased membrane order through saturated phospholipid or sterol incorporation stabilized a transmembrane helix rotational conformation that promoted Mga2 cleavage and activation (110). Therefore, it may be the fluidity of the membrane, rather than fatty acid saturation per se, that is sensed by the Mga2 pathway to regulate TAG and GPL biosynthesis. These results confirm that the *S. cerevisiae* Mga2 transcription factor is product inhibited in a very similar manner to the *S. pombe* transcription factor Sre1. Both systems detect the presence of product in the ER membrane and are only activated for cleavage when product is decreased. What if any transcription factor(s) regulates this fatty acid pathway under low oxygen in fission yeast is unknown.

1.8 Thesis aims

My work in the Espenshade lab sought to address three aspects of the transcriptional response to low oxygen adaptation in fission yeast:

(1) In response to the discovery of a requirement for *cdc48* in SREBP activation, I wanted to elucidate the role played by this multifunctional protein in the fungal SREBP pathway.

(2) Given that Sre1 regulates only 22% of all oxygen-responsive genes in fission yeast, I wanted to identify the transcriptional regulator(s) of those lipid metabolism genes not regulated by Sre1 under low oxygen conditions, namely, those involved in phospholipid metabolism.

(3) Finally, based on the fact that sterol and phospholipid biosynthesis pathways are coordinated in mammals via a shared activation mechanism of SREBP-1 and SREBP-2, I hypothesized that these two pathways may also be coordinated in fission yeast and sought to identify the mechanism of coordination.

1.9 Figures

FIGURE 1.1. **Pathways transcriptionally regulated in response to oxygen.** Genes significantly up and down regulated under low oxygen conditions in *S. pombe* (1.5 h, 0% O2) (54), *S. cerevisiae* (12 h, 0% O2) (55), *C. albicans* (3.5 h, 1% O2) (56), *C. parapsilosis* (3 h, 1% O2) (57), *A. fumigatus* (2 h, 0.2% O2) (60), *A. nidulans* (6 h, low O2) (58), and *Y. lipolytica* (~6 h, 1% O2) (59) were analyzed for GO term enrichment using AmiGO for *S. cerevisiae*, and FungiFun2 for the remaining species (111). Biological process annotations were identified using directly and indirectly annotated associations. Resulting enriched GO terms were grouped using REVIGO with an allowed similarity of 0.5 (112) and additional hand categorization. Broad categories were then analyzed for enrichment in each fungal species, represented as colored (enriched) or blank (not enriched) wedges.

FIGURE 1.2. **Sre1 cleavage activation pathway.** In the presence of oxygen or sterols, Sre1 is retained in the ER by the sterol sensor Scp1. Additionally, Sre1N produced from basal cycling is bound by Ofd1 and degraded. In the absence of oxygen or sterols, Sre1-Scp1 traffics to the Golgi where the Dsc E3 ligase complex, the rhomboid protease Rbd2, and Cdc48 are required for Sre1 cleavage and Sre1N release. Also under low oxygen, Ofd1 is inhibited by Nro1, releasing Sre1N to enter the nucleus and upregulate its own transcription as well as additional hypoxic responsive genes.

FIGURE 1.3. **Mga2 cleavage activation pathway.** Under conditions of high unsaturated fatty acids (UFA) when membranes are relatively disordered and loosely packed, Mga2 homodimers in the ER are in a rotational conformation that is not permissive to Rsp5 E3 ligase interaction and cleavage. When UFA decrease and the membrane becomes more ordered, the Mga2 transmembrane domains rotate into a cleavage-competent orientation. Rps5 then ubiquitylates Mga2 and the proteasome performs regulated ubiquitin-dependent partial proteolysis. Cdc48 releases the cleaved Mga2N from the homodimer complex and Mga2N enters the nucleus to bind Low Oxygen Response Elements (LORE) and upregulate target genes.

Species	*mga2*	*rsp5*	*cph2*	*sre1*	*scp1*	*dsc1*	*dsc2*	*dsc3*	*dsc4*	*dsc5*	*rbd2*	*ofd1*	*nro1*	*stp1*	*upc2*	*efg1*	*tye7*	*gal4*
S. cerevisiae	X		X			X	X	X		X	X	X	X		X	X	X	X
S. pombe	X	X		X	X	X	X	X	X	X	X	X	X					
H. sapiens		X		X	X							X		X				
Human																		
A. clavatus	X	X		X		X	X	X	X	X	X	X			X	X		X
A. flavus	X	X		X		X		X	X	X	X	X			X	X		X
A. fumigatus	X	X		X		X	X	X	X	X	X	X				X		X
A. niger	X	X		X		X	X	X	X	X	X	X				X		X
A. terreus	X	X		X		X		X	X	X		X				X		X
B. cinerea	X	X		X	X	X	X	X		X		X				X		
C. albicans	X	X	X			X	X	X	X	X	X	X	X		X	X	X	
C. dubliniensis	X	X	X			X	X	X	X	X	X	X	X		X	X	X	
C. glabrata	X	X	X			X	X	X		X	X	X	X		X	X	X	
C. parapsilosis	X	X	X			X	X	X	X	X	X	X	X		X	X	X	
C. tropicalis	X	X	X			X	X	X	X	X	X	X	X		X	X	X	
C. immitis	X	X		X		X	X	X	X	X	X	X				X		
C. posadasii	X	X		X		X	X	X	X	X	X	X				X		
C. gattii	X	X		X		X	X	X		X		X		X				X
C. neoformans	X	X		X		X	X	X		X		X		X				X
H. capsulatum	X	X		X		X	X	X	X	X	X	X				X		X
M. globosa	X	X				X		X		X		X		X			X	
P. brasiliensis	X	X		X		X	X	X	X	X		X				X		
P. lutzii	X	X		X		X	X	X	X	X		X				X		
P. marneffei	X	X		X		X	X		X	X	X	X				X		X
P. jirovecii	X	X				X	X	X	X	X		X						
R. oryzae	X	X				X	X			X		X	X	X		X	X	
Plant pathogens																		
A. aculeatus	X	X		X		X	X	X	X	X		X			X	X		X
F. verticillioides	X	X	X	X	X	X	X	X	X	X	X	X			X	X		X
M. oryzae	X	X		X	X	X	X	X	X	X	X	X				X		
M. larici-	X	X					X			X		X		X		X		
M. circinelloides	X	X				X	X	X		X	X	X		X				X
P. graminis		X				X	X	X		X		X		X				
S. sclerotiorum	X	X		X	X	X	X			X	X	X				X		
S. reilianum	X	X				X	X			X		X					X	X
U. maydis	X	X				X	X			X		X					X	X
Non-pathogenic																		
A. nidulans	X	X		X		X	X	X	X	X	X	X				X		X
A. oryzae	X	X		X		X		X	X	X	X	X			X	X		
K. lactis	X	X									X				X	X		
N. crassa	X	X		X	X	X	X	X	X	X	X	X			X	X		
T. reesei	X	X		X	X	X	X		X	X	X	X				X		X
Y. lipolytica	X	X		X		X	X			X	X	X	X		X	X		

Table 1.1. Gene conservation across select fungal species
Orthologs to genes of interest were identified by protein sequence using OrthoMCL. The *S. pombe* or *S. cerevisiae* genes were used to initiate the search with standard parameters. The below list is not comprehensive of all fungal species. An X represents detection of an ortholog, which may not be validated. Phyla: Ascomycete, **Basidiomycete,** Zygomycete

Figure 1.1

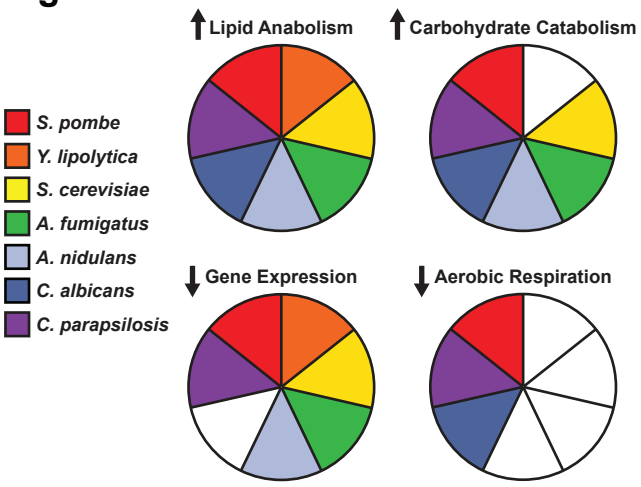
S. pombe
Y. lipolytica
S. cerevisiae
A. fumigatus
A. nidulans
C. albicans
C. parapsilosis
Lipid Anabolism
Carbohydrate Catabolism
Gene Expression
Aerobic Respiration

Figure 1.2

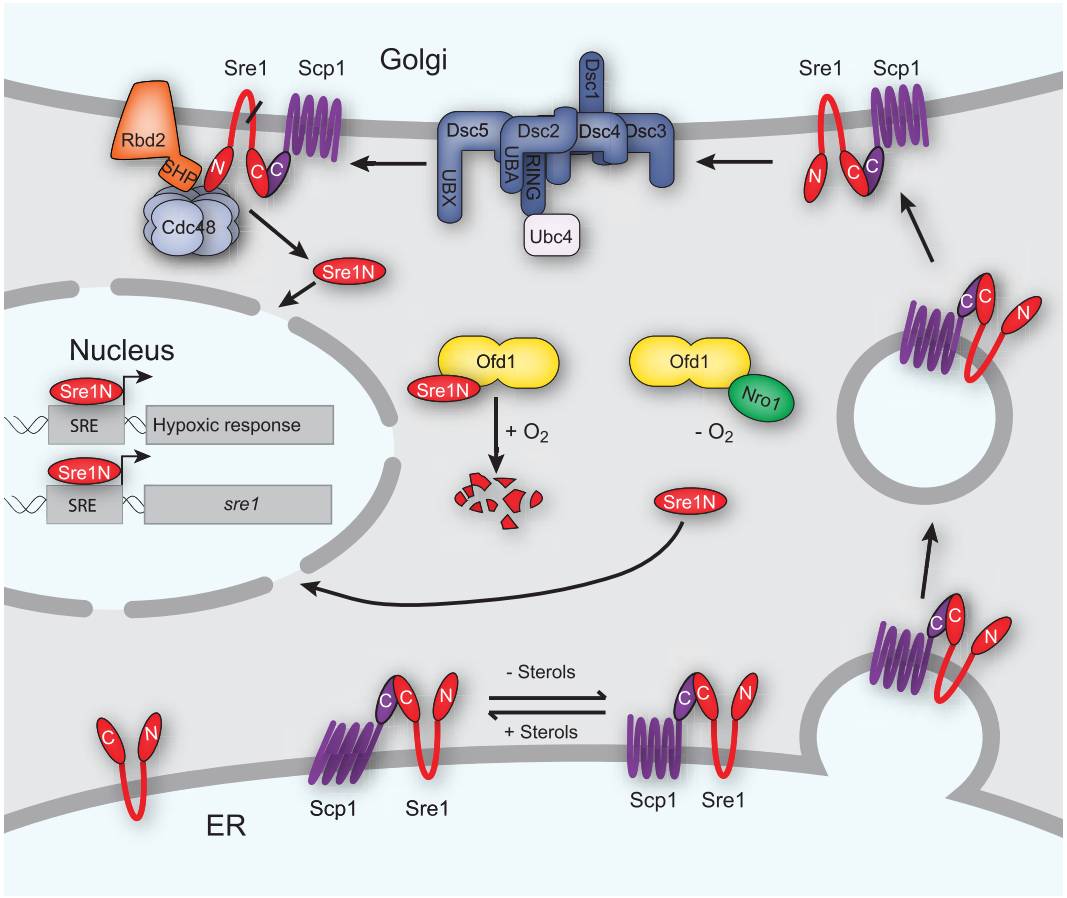
Golgi
Sre1
Scp1
Rbd2
SHP
N
C
C
Cdc48
Sre1N
Dsc1
Dsc5
Dsc2
Dsc4
Dsc3
UBX
UBA
RING
Ubc4
Sre1
Scp1
N
C
C
Nucleus
Sre1N
SRE
Hypoxic response
Sre1N
SRE
sre1
Ofd1
Sre1N
+ O2
Ofd1
Nro1
- O2
Sre1N
C
C
N
C
C
N
C
C
N
- Sterols
+ Sterols
C
N
ER
Scp1
Sre1
Scp1
Sre1

Figure 1.3

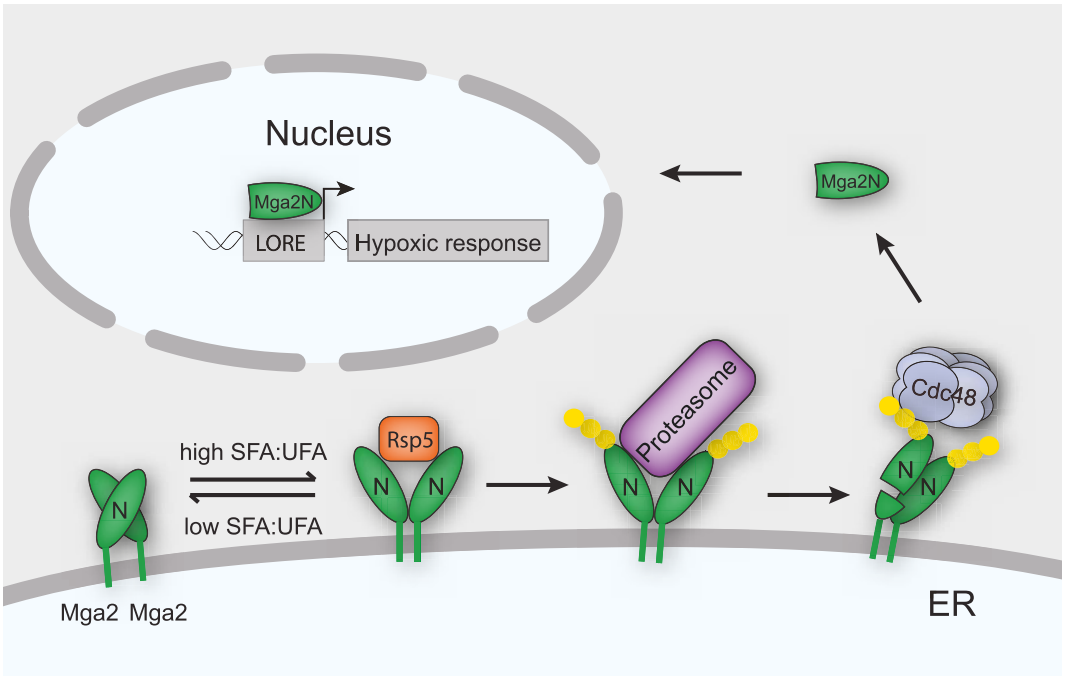
Nucleus
Mga2N
LORE
Hypoxic response
Mga2N
high SFA:UFA
low SFA:UFA
Rsp5
Proteasome
Cdc48
N
Mga2 Mga2
ER

Chapter 2

Dsc E3 ligase Golgi localization requires the ATPase Cdc48 and cofactor Ufd1 for Sterol Regulatory Element-binding Protein activation in fission yeast

This chapter is an edited version of the manuscript, "Dsc E3 ligase localization to the Golgi requires the ATPase Cdc48 and cofactor Ufd1 for activation of Sterol Regulatory Element-binding Protein in fission yeast" by R. Burr, D. Ribbens, S. Raychaudhuri, E. V. Stewart, J. Ho, and P. J. Espenshade, under revision at the Journal of Biological Chemistry

2.1 Summary

Schizosaccharomyces pombe sterol regulatory element-binding proteins (SREBP) regulate lipid homeostasis and the hypoxic response under conditions of low sterols or oxygen. SREBPs are cleaved in the Golgi through the combined action of the Dsc E3 ligase complex, the rhomboid protease Rbd2, and the essential AAA+ (ATPases Associated with diverse cellular Activities) ATPase Cdc48. The soluble SREBP N-terminal transcription factor domain is then released in the cytosol to enter the nucleus and regulate gene expression. Previously, we reported that Cdc48 binding to Rbd2 is required for the cleavage of SREBPs by Rbd2. The exact function of Cdc48 at Rbd2 is unknown, and Cdc48 may have additional roles in the pathway before or after cleavage of substrate by Rbd2. To determine whether Cdc48 performs additional roles during SREBP activation, we extended our analysis of *cdc48* point mutants in *S. pombe* (69). Here, we report identification of two new alleles of *cdc48* that impact SREBP cleavage. Five *cdc48* mutants show defects in both Sre1 and Sre2 cleavage, but had minimal impact on Cdc48 protein level or cellular growth rate. We also perform affinity chromatography and mass spectrometry to identify Cdc48 binding proteins in *S. pombe*, generating a list of many previously unknown potential binding partners. Of these binding partners, we demonstrate that the substrate-recruiting Cdc48 cofactor Ufd1 is required for SREBP cleavage. Importantly, we find that the Cdc48-Ufd1 complex is functionally distinct from the previously described Cdc48-Rbd2 complex. Cdc48-Ufd1 is instead required at a step prior to Rbd2 function, during Golgi localization of the Dsc E3 ligase complex. Together, these data demonstrate that two distinct Cdc48 complexes – Cdc48-Ufd1 and Cdc48-Rbd2 – are required for SREBP activation and low oxygen adaptation in *S. pombe*.

2.2 Results

Identification of cdc48 alleles – cdc48 is required for SREBP cleavage in fission yeast (69,71), but whether this multipurpose enzyme has additional functions in the SREBP pathway is

unknown. Further analysis of our four *cdc48* mutants revealed that two of the four showed relatively weak SREBP cleavage defects that are not suitable for dissecting the role of Cdc48 during SREBP cleavage (69). To expand our set of *cdc48* alleles and to identify other genes involved in SREBP activation, we revisited our MMS mutagenesis screen and performed additional linkage analysis on uncharacterized mutants (69). As previously reported, this screen was performed by generating a reporter strain in which Sre1 binding sites were in the promoter of the *ura4* gene, such that when Sre1 is functional, orotidine 5'-phosphate decarboxylase (Ura4) is produced (69). This reporter strain was mutagenized with either 0.024% or 0.012% MMS and the resulting isolates were plated on 5-fluoroorotic acid (5-FOA), which is converted to the toxic 5-fluorouracil by Ura4, thereby selecting for isolates with deficient Sre1 activity. The majority of surviving mutants (86%) from the original screen phenocopied *sre1* deletion and were sensitive to cobalt chloride ($CoCl_2$), a hypoxia mimetic (**Fig. *2.1A***).

Cobalt-sensitive mutants were transformed with plasmids expressing $sre1^+$ and $scp1^+$ to identify these frequent mutants. For mutants not rescued by these plasmids, we performed linkage analysis by mating uncharacterized mutants with known SREBP pathway mutants and tested if the resulting spores grew on $CoCl_2$. Matings from which no spores grew on $CoCl_2$ indicated linkage of the uncharacterized mutant to the known gene, most likely because the uncharacterized mutation was also within the known gene. In many cases, we identified the precise mutation in these strains by PCR amplification and sequencing of the gene of interest. After this analysis, 196 of the 305 cobalt chloride-sensitive mutants (64%) were assigned to linkage groups, while 109 strains remain to be tested (**Fig. *2.1A***). The specific mutations in the sequenced genes are available in **Supplementary Table 2.1**. The only new gene identified in this search was the essential translation initiation RNA helicase *sum3*, which was identified via whole genome sequencing of two linked mutagenized strains. Further analysis indicated that the *sum3* mutants were not rescued by Sre1N expression and had intermediate Sre1 cleavage defects (**Fig. *A.1***). We

concluded that the role of *sum3* in this pathway was likely a non-specific stress-response and did not study it further.

As expected, for non-essential genes we observed a linear relationship between the number of strains isolated and the length of the coding sequence (**Fig. *2.1B***). Notably, *cdc48* and *sum3* are essential and lie below the line, with fewer strains identified than would be expected for the given coding region length. In other words, the gene sequence that can be viably mutated is smaller for essential genes than non-essential genes. Analysis of the number of strains per gene found through the MMS screen indicated that the screen could identify non-essential genes larger than 750 base pairs (**Fig. *2.1B***). An additional 1100 *S. pombe* non-essential genes fall below this threshold, indicating that additional non-essential and essential genes required for Sre1 activity may remain unidentified.

This new analysis identified two *cdc48* point mutations (A366D and R764C) in addition to the four previously described (**Fig. *2.1C***) (69). To further examine these mutants, we compared the *S. pombe cdc48* point mutants to the human *VCP* sequence, to which the fission yeast protein shares 70% identity. All six mutated fission yeast *cdc48* residues are identical in human (**Fig. *2.1C***). These six mutations are dispersed throughout this essential protein and are not clustered in three-dimensional space (**Fig. *2.1D*** and data not shown). Importantly, none of these *cdc48* mutants are temperature sensitive (data not shown). Additionally, none are found in the N-domain, which is the major site of cofactor binding (78). One of these mutants, *cdc48-8*, is in the known ATP hydrolysis region of the D1 domain (**Fig. *2.1D***).

SREBP activation requires cdc48 - Cdc48 is a versatile protein that may function in multiple steps of SREBP activation. Our previous studies of *cdc48* mutants used the original isolates from the MMS mutagenesis screen (69). To evaluate and directly compare the *cdc48* alleles, we recreated all six *cdc48* mutations in a wild-type, non-mutagenized strain background. These strains were generated by homologous recombination and all strains, including the isogenic wild-type, were marked with the nourseothricin resistance gene (see Experimental Procedures).

Because these strains are in a non-mutagenized, marked background, we gave them the new allele numbers *cdc48-5* through *cdc48-10* to differentiate them from those previously studied (**Fig. *2.1C***).

To characterize these new mutant strains, we first assayed growth on $CoCl_2$. We observed no growth defect for *cdc48-7* and complete $CoCl_2$ growth defects for the other five mutants (**Fig. *2.2A***). To compare Sre1N production in all *cdc48* mutant strains, we assayed Sre1 cleavage by western blot. We cultured wild-type and the indicated *cdc48* mutant strains for 0 or 4 h minus oxygen. We then probed whole cell lysates with anti-Sre1N, which detects both the full-length ER-membrane bound precursor form (P) as well as the cleaved N-terminal transcription factor form (N). Wild-type cells accumulated Sre1N after 4 hours of growth under low oxygen (**Fig. *2.2B***, lanes 1-2). The *cdc48* mutant strains showed a range of Sre1N production defects, from complete blocks (*cdc48-8,-9,-10*) to partial defects (*cdc48-5,-6*) (**Fig. *2.2B***, lanes 3-14). Additionally, we examined cleavage of a N-terminally FLAG-tagged Sre2 model substrate, Sre2-MS, which recapitulates Sre2 constitutive activation (66). The *cdc48* mutant strains showed Sre2-MS cleavage defects consistent with their Sre1 cleavage defects, as had been previously shown for *cdc48-4* (**Fig. *2.2C***) (66). Notably, we observed no $CoCl_2$ growth, Sre1, or Sre2-MS cleavage defects in *cdc48-7*, which is inconsistent with our previously published results (**Fig. *2.2B***, lanes 7-8, ***2.2C***, lanes 7-8) (69). This may be due to the highly mutagenized background of the original mutant, and validates our decision to remake these strains in a non-mutagenized strain. Therefore we conclude that *cdc48-7* is a mutant allele with no effect on SREBP cleavage and serves as a wild-type control. Together, these data indicate that *cdc48* is required for SREBP cleavage in *S. pombe* at a step that is common to both Sre1 and Sre2 activation.

cdc48 mutations do not exhibit major defects in Cdc48 expression or cell growth – To better understand how these *cdc48* mutations affect SREBP cleavage, we characterized their effects on Cdc48 protein accumulation and cell growth. To assay Cdc48 expression, we probed whole cell lysates from each strain with anti-Cdc48 polyclonal antibody (**Fig. *2.3A***). Despite

some statistically significant changes, all mutants had levels of Cdc48 protein similar to wild-type, and expression levels did not show a correlation with strength of SREBP cleavage defect (**Fig. *2.3B***). This is consistent with the fact that *cdc48* is an essential gene and large changes in expression may not be tolerated. These data suggest that differential expression is not the cause of the observed SREBP cleavage defects.

To further examine the overall cellular effects of these *cdc48* point mutations, we assayed growth rate. We grew wild-type and *cdc48* mutants in liquid culture in the presence of oxygen for 12 h and calculated doubling time. Of the six *cdc48* mutants, only *cdc48-9* had a dramatically slower doubling time than wild-type cells under normoxic conditions (**Fig. *2.3C***). Because the *cdc48-8, cdc48-9,* and *cdc48-10* mutants have equally strong blocks in SREBP cleavage but different growth rates, it is unlikely that the change in growth rate is responsible for the block in SREBP cleavage. These results suggest that the effects of our *cdc48* mutations on essential Cdc48 activities are minimal.

Identification of Cdc48 binding proteins in S. pombe – It is well established in the literature that a complex network of cofactors direct Cdc48 to specific targets. However, we did not identify any Cdc48 cofactors that are required for SREBP cleavage in this MMS mutagenesis or a previous screen of non-essential genes (**Fig. *2.1A***) (70). Identification and assessment of Cdc48 cofactors could clarify the roles for Cdc48 in SREBP cleavage. To identify Cdc48 cofactors in fission yeast, we purified Cdc48 using a C-terminal 5xFLAG tag and quantitatively identified all bound proteins using TMT mass spectrometry (113). Tagging Cdc48 with 5xFLAG did not alter Cdc48 function as judged by the ability to accumulate Sre1N to wild-type levels under low oxygen (**Fig. *2.4A***, lane 2 vs 4). Purification of Cdc48-5xFLAG with anti-FLAG conjugated magnetic beads recovered the majority of Cdc48 protein, and no Cdc48 was isolated in the untagged strain (**Fig. *2.4B***, lanes 5-6). Quantitative mass spectrometry analysis of the bound fractions from wild-type and Cdc48-5xFLAG lysates identified 2283 proteins, of which 52 were enriched in the Cdc48-5xFLAG sample at least 2 standard deviations from the mean (fold

change ≥3.2) (**Fig. *2.4C***, red dots and **Table 2.1**). The full list of identified proteins and peptides is available in **Supplementary Table 2.2**. Of note, Dsc1, Dsc2, Dsc3, and Dsc5 were highly enriched in the Cdc48-bound population (**Table 2.1**). This result is consistent with our published observation that Cdc48 binds the Dsc E3 ligase through the Dsc5-UBX domain independent of any role in SREBP cleavage (69). Interestingly, Rbd2 was not identified as a Cdc48 binding protein. This could either be due to an inability to detect Rbd2 peptides by mass spectrometry or the reported transient nature of the Cdc48-Rbd2 interaction (71).

To determine which Cdc48 binding proteins were required for SREBP processing we tested deletions of the non-essential genes in *S. pombe* for growth on $CoCl_2$ (114). In addition, we created deletions of those genes not present in the Bioneer deletion collections and also tested temperature-sensitive mutants of the essential cofactor *ufd1* (kind gift of Boddy Lab) (115). We were unable to test a number of essential genes due to lack of availability of temperature-sensitive mutations and a failure to knock them down. Results of the $CoCl_2$ growth assays can be found in **Table 2.1**. Interestingly of all the genes tested, only the *ufd1* point mutants and *ubx3Δ* were sensitive to $CoCl_2$ and not previously known components of the SREBP pathway. Both of these genes code for known Cdc48 cofactors (**Table 2.1**, grey rows). Upon further examination, the $CoCl_2$ growth defect in *ubx3Δ* cells was minor, and we observed minor effects on Sre1 cleavage (**Fig. *A.2***). Therefore, we focused our analysis on Ufd1.

Ufd1 is a Cdc48 cofactor required for SREBP cleavage – Ufd1 is an established Cdc48 cofactor with homologs from yeast to humans (116,117). Together with the cofactor Npl4, it is thought to direct Cdc48 to ERAD functions (118,119). To test the requirement for *ufd1* in SREBP activation, we tested three temperature-sensitive mutations in this essential gene using strains generated by the Boddy Lab (115). These wild-type and *ufd1* mutant strains express *ufd1-13xMyc* from the endogenous locus. *ufd1-7* and *ufd1-8* have mutations in the conserved UFD1 domain, while *ufd1-5* and *ufd1-7* have mutations outside of that domain, near the C-terminus (**Fig. *2.5A***)

(115). We assayed growth of these wild-type and *ufd1* mutant strains on $CoCl_2$ and observed complete growth defects in the mutant strains consistent with **Table 2.1** (**Fig. *2.5A***). We also observed decreased growth at semi-permissive temperature on rich medium (30°C) (**Fig. *2.5A***) and in a liquid culture growth assay (**Fig. *2.5B***). These results are consistent with the previously published report that these strains are temperature-sensitive (115).

We next examined Ufd1-13xMyc and Cdc48 expression in the wild-type and *ufd1* mutants at 30°C. All point mutants had lower Ufd1-13xMyc protein than wild-type cells, although Cdc48 levels were normal (**Fig. *2.5C***). We then assayed Sre1 and Sre2-MS cleavage in each strain. *ufd1* mutants were deficient for Sre1 cleavage induction by low oxygen and had defects in Sre2-MS cleavage (**Fig. *2.5D-E***). Notably, *ufd1-5* and *ufd1-7* had complete blocks in Sre2-MS cleavage, while *ufd1-8* had a partial block indicating an incomplete defect. Importantly, all *ufd1* mutants had normal Sre1 precursor levels, indicating no defect in Sre1 expression in these strains (**Fig. *2.5D***). These data suggest that *ufd1-5* and *ufd1-7* are the strongest mutants but that all three have significant effects on SREBP cleavage. Therefore, we concluded that *ufd1* is a new component of the SREBP activation pathway.

SREBP activation requires Cdc48-Ufd1 during Dsc E3 ligase Golgi localization – SREBP activation requires ER-to-Golgi transport of SREBP, the Dsc E3 ligase, and Rbd2, as well as Dsc E3 ligase activity and cleavage by Rbd2. Defects in any of these steps would result in the cleavage defect observed in *cdc48* and *ufd1* mutants. We previously demonstrated that Cdc48 is required for Rbd2 cleavage of SREBPs in the Golgi. Rbd2 binds Cdc48 through its C-terminal SHP domain, and disruption of Rbd2-Cdc48 binding blocks cleavage (71). To determine whether Ufd1 is involved in the function of Cdc48 at Rbd2, we tested whether Ufd1 physically associates with Cdc48 when bound to Rbd2. We performed an *in vitro* pull-down experiment from wild-type and *ufd1-13xmyc* lysates using GST-tagged Dsc5 UBX domain, GST-tagged Rbd2 SHP domain, or GST alone. As expected, both GST-UBX and GST-SHP efficiently purified Cdc48 from lysates (**Fig. *2.6A***, lanes 9-14) (71). However, only GST-UBX also purified Ufd1-13xMyc

(**Fig. *2.6A***, lane 12 vs 14). The ability of Dsc5 UBX domain to purify Ufd1 suggests that a Cdc48-Ufd1 complex may interact with the Dsc E3 ligase in an uncharacterized function independent of SREBP cleavage (69). The fact that Ufd1-13xMyc is not bound to Cdc48 when Cdc48 is bound to the Rbd2-SHP domain suggests that Ufd1 is not part of the Cdc48-Rbd2 complex required for SREBP cleavage. These data indicate that two distinct Cdc48 complexes – Cdc48-Ufd1 and Cdc48-Rbd2 – are required for SREBP activation in fission yeast.

To determine whether Cdc48-Ufd1 is required prior to SREBP cleavage by Rbd2, we performed a genetic epistasis test that takes advantage of a useful *rbd2Δ* phenotype. In *rbd2Δ* cells, uncleaved SREBP precursor proteins do not accumulate as in wild-type cells, but are instead degraded (71). This degradation requires both the Dsc E3 ligase and the proteasome, and we proposed that it results from degradation of the ubiquitylated SREBP precursor when Rbd2 cleavage does not occur. In contrast, all *dsc* deletions, *cdc48*, and *ufd1* mutants have wild-type SREBP precursor levels (**Fig. *2.2B-C, 2.5B-C***) (68,69). Because these phenotypes are opposing, we can create double mutants between *rbd2Δ* and other pathway components and perform epistasis tests to determine their order of action in this SREBP activation pathway.

As previously shown, in wild-type cells endogenous Sre2 is constitutively cleaved and only the N-terminal form was detected (**Fig. *2.6B-C***, lane 1). In contrast, *rbd2* deletion resulted in a failure to cleave Sre2 without a corresponding increase in Sre2 precursor, resulting in minimal Sre2 signal (**Fig. *2.6B-C***, lane 2) (71). As expected, *rbd2Δ dsc1Δ* cells accumulated Sre2 precursor (**Fig. *2.6B***, lane 3, **Fig. *2.6C***, lane 4), because the Dsc E3 ligase acts before Rbd2 during SREBP activation and is required for precursor degradation by the proteasome (71). This is consistent with our model that the SREBP is ubiquitylated by the Dsc E3 ligase before transfer to Rbd2 for cleavage.

In *cdc48* mutant cells, Sre2 cleavage defects ranged from none (*cdc48-7)*, partial (*cdc48-5,-6*), to strong (*cdc48-8,-9,-10*) (**Fig. *2.6B***), consistent with observed Sre1 and Sre2-MS defects (**Fig. *2.2***). When the *cdc48* mutants were combined with *rbd2Δ*, the Sre2 precursor was retained

in the strongest mutants (*cdc48-8,-9,-10*) and partially retained in the weaker mutants (*cdc48-5,-6*) (**Fig. *2.6B***, lanes 3-14). This is consistent with the magnitude of the SREBP cleavage defect in each *cdc48* allele (**Fig. *2.2B-C, 2.6B***). These results demonstrate that *cdc48* functions prior to *rbd2*. Likewise, *ufd1 rbd2Δ* double mutants also accumulated Sre2 precursor, confirming that Ufd1 and Cdc48 act before Sre2 cleavage by Cdc48-Rbd2 (**Fig. *2.6C***, lane 2 vs lanes 6 and 8). The *ufd1-5 rbd2Δ* combination could not be tested because we were unable to generate this strain by mating or homologous recombination. Together, these data suggest that distinct Cdc48 complexes play multiple roles during SREBP cleavage, one of which is prior to Rbd2 cleavage at the Golgi.

Cdc48-Ufd1 is required for SREBP activation prior to cleavage by Rbd2, but it is unclear what role it performs at that stage. To test which step of SREBP cleavage is defective in *cdc48* and *ufd1* mutants, we assayed Dsc E3 ligase localization in these cells by taking advantage of the fact that the Dsc1 subunit is glycosylated in the Golgi. Glycosylation causes a change in apparent molecular weight on an SDS-PAGE gel with a high molecular weight band representing Golgi localization and a low molecular weight band representing ER localization (73). The Dsc E3 ligase is retained in the ER when *dsc1-dsc4* are deleted, when the Dsc E3 ligase is catalytically inactivated, or when the cognate E2, *ubc4*, is inactivated (73).

To examine Dsc E3 ligase localization, we subjected microsomal protein preparations from *cdc48* and *ufd1* mutant cells to SDS-PAGE and probed for Dsc1. As previously reported, wild-type cells showed primarily a higher molecular weight (Golgi) Dsc1 band representing 55% maturely glycosylated, while *dsc2Δ* cells showed only a lower molecular weight (ER) Dsc1 band representing 23% maturely glycosylated (**Fig. *2.6D***, lane 1 vs 8, ***2.6E***) (73). Consistent with the wild-type Sre1 cleavage observed in *dsc5-ΔUBX* cells, deletion of the UBX domain also had no effect on Dsc1 glycosylation (**Fig. *2.6D***, lane 9). Importantly, *rbd2* deletion also showed a wild-type Dsc1 glycosylation pattern, indicating that Rbd2 is not required for Dsc1 Golgi localization (**Fig. *2.6D***, lane 10). When we examined Dsc1 glycosylation in the strongest *cdc48* and *ufd1*

mutant strains (*cdc48-8,-9,-10,ufd1-5,-7*), we observed accumulation of the lower molecular weight form and between 25-35% maturely glycosylated, phenocopying *dsc2Δ* (**Fig. *2.6D,*** lanes 5-7, 12-13, ***2.6E***). *cdc48-7* had wild-type Dsc1 glycosylation while *cdc48-5,-6* and *ufd1-8* had partial Dsc1 glycosylation defects with 38-48% maturely glycosylated form, consistent with their SREBP cleavage effects (**Fig. *2.6D,*** lanes 2-4, 14, ***2.6E***). Because neither the *dsc5-ΔUBX* nor the *rbd2Δ* cells showed Dsc1 glycosylation defects, the impacts of the *cdc48* mutants on Dsc1 glycosylation are likely not due to Cdc48 binding to either of these proteins. These data suggest that the Cdc48-Ufd1 complex is required for Dsc E3 ligase Golgi localization in a role separate from the binding of Cdc48 to Dsc5 or Rbd2.

2.3 Discussion

Our previous efforts to discover components of the *S. pombe* SREBP activation pathway identified the AAA+ ATPase Cdc48, but failed to identify any Cdc48 cofactors. Here, we analyzed six *cdc48* point mutations and performed mass spectrometry identification of Cdc48 binding proteins to further elucidate the role of Cdc48 and any cofactors in SREBP activation. These data add to a growing body of evidence supporting multiple interactions between Cdc48 and SREBP pathway components. First, in this report we used *cdc48* and *ufd1* point mutants to show that the Cdc48 cofactor Ufd1 is required for SREBP cleavage and that Cdc48-Ufd1 act at an early step in the activation pathway, namely Golgi localization of the Dsc E3 ligase complex (**Fig. *2.6***). *cdc48* and *ufd1* mutants show defects in Dsc1 glycosylation, suggesting that the Dsc E3 ligase is trapped in the ER where it is unable to participate in SREBP activation (**Fig. *2.6D***). Importantly, in all cases, the strength of the Dsc1 glycosylation defect is consistent with the strength of the SREBP cleavage defect, indicating that the Dsc E3 ligase localization defect causes the SREBP cleavage defect. In our characterization of the *ufd1* mutants, we also observed growth and Ufd1 expression defects (**Fig. *2.5A-C***). This is likely due to the temperature-sensitive nature of these strains, but may have contributed to the SREBP cleavage defects (115). However,

we believe the consistency between the *cdc48* and *ufd1* mutant results support our conclusion that Cdc48-Ufd1 plays this essential role during Dsc E3 ligase localization.

Interestingly, *ufd1* was not identified in our MMS screen (**Fig. *2.1B***). This may be due to the fact that *ufd1* is an essential gene with a coding sequence of only 1029 bp, likely too small to come through our screen (**Fig. *2.1B***). Similarly, the Ufd1 binding partner Npl4 is also essential and could have been missed in our screen. While the literature suggests that Ufd1 usually is in complex with the binding partner Npl4 when bound to Cdc48, we were unable to generate temperature-sensitive mutants or tagged versions of *npl4*, and therefore cannot comment on its role in SREBP activation.

The second role for Cdc48 in the SREBP activation pathway is during SREBP cleavage by the rhomboid protease Rbd2. We previously showed that Cdc48 interacts with Rbd2 through the Rbd2 SHP domain, and that this interaction is required for SREBP cleavage (71). The function performed by Cdc48 at Rbd2 is unknown but could be as a substrate adaptor, as an activator of Rbd2 enzymatic activity, and/or to release the cleaved SREBP N-terminus into the cytosol. Here we show that both *cdc48* and *ufd1* mutants are epistatic to *rbd2Δ* and retain the Sre2 precursor in the absence of *rbd2* (**Fig. *2.6B-C***). This phenocopies *dsc1Δ rbd2Δ* and supports the requirement for Cdc48-Ufd1 in Dsc E3 ligase function. Further, we showed that the Rbd2-SHP domain binds to Cdc48 but not Ufd1 *in vitro* (**Fig. *2.6A***). While it is possible that Ufd1 interacts with Rbd2 at a location separate from the SHP domain, this suggests that Ufd1 cannot interact with Rbd2 through Cdc48. Together, these data indicate that Cdc48-Ufd1 is distinct from Cdc48-Rbd2, and that two Cdc48 complexes are required for the SREBP activation pathway.

Finally, we previously published the interaction between Cdc48 and the Dsc E3 ligase through the Dsc5 UBX domain (69). This interaction is not required for SREBP activation. However, it could play a role in a non-SREBP function of the Dsc E3 ligase in the Golgi, such as Golgi quality control. Indeed, there are homologs of the Dsc proteins in *S. cerevisiae*, despite a lack of SREBP homologs in that organism (120). There, the homologous Tul1 E3 ligase regulates

turnover of certain vacuolar membrane proteins in budding yeast during vacuolar quality control (72). These three related roles for Cdc48 highlight the versatility of this powerful molecular machine and the necessity of cofactors to target it to specific substrates.

Interestingly, although *cdc48* is an essential gene, none of these mutations is lethal, suggesting that they have relatively minor functional defects. However, we observe strong defects in SREBP cleavage in many of the mutants (**Fig. *2.2***). This may indicate synthetic effects between the roles for Cdc48 during Dsc E3 ligase Golgi localization and Rbd2 cleavage. The impacts of deficient Cdc48 activity on each step of the pathway may be relatively minor, but together they strongly affect SREBP cleavage. Therefore, the requirement for Cdc48 at multiple steps may make SREBP activation uniquely sensitive to alterations in Cdc48 function.

In addition to describing a novel role for Cdc48-Ufd1 during SREBP cleavage, this study generated two valuable resources for future studies of this pathway and low oxygen adaptation in fission yeast. Through the MMS screen, we report point mutations in *sum3*, *sre1*, *scp1*, Dsc E3 ligase subunits, *cdc48*, and *rbd2* that exhibit low oxygen adaptation defects (**Fig. *2.1A*, Supplemental Table 2.1**). These mutants will provide insight into the molecular function of these proteins in this and other pathways. Additionally, the mass spectrometry data contains a number of leads for future studies. 18 of the 51 proteins enriched at least two standard deviations from the mean in the Cdc48-bound fraction of our Cdc48-5xFLAG pull-down were known Cdc48 cofactors in *S. pombe* and/or other species (**Table 2.1**). In addition to Ufd1 and many known Cdc48 cofactors, four Dsc E3 ligase complex members were identified as Cdc48-binding proteins, consistent with our previously published results that Cdc48 interacts with the Dsc E3 ligase by binding to the Dsc5 UBX domain (69). These data validate our data set and suggest that the 33 unexpected binding proteins are very interesting candidates for future study. Included in this list are three predicted E3 ligases and an ubiquitin-metalloprotease fusion protein (**Table 2.1**). Interestingly, mammalian VCP was shown to interact with a large number of E3 ligases through UBX domain-containing proteins, including the Dsc5 homolog FAF1 (121). These proteins are

therefore likely Cdc48-binding proteins. The remaining candidates may be unidentified components of Cdc48-interacting complexes or possibly substrates. Further analysis of the interaction between Cdc48 and these binding partners may identify new pathways requiring Cdc48 function.

Together, these results highlight the ubiquitous value of Cdc48/VCP separase activity in organisms from yeast to humans. As careful structural and biochemical studies of Cdc48/VCP rapidly advance our understanding of Cdc48 mechanical function, future work will need to turn toward understanding the regulation of numerous cofactor interactions with Cdc48, as it is these interactions that ultimately define the fate of Cdc48 and the essential pathways in which it functions.

2.4 Experimental procedures

Materials – General chemicals and materials were obtained from Sigma or Fisher. Other sources include: yeast extract, peptone, and agar from BD Biosciences; Brefeldin A, Igepal CA-630 (NP-40), cobalt (II) chloride, amino acid supplements, 1X protease inhibitors (PI) (10 μg/ml leupeptin, 5 μg/ml pepstatin A, 0.5 μM PMSF), acid washed glass beads (425-600 μm), and FLAG M2 monoclonal IgGs (F1804 and F3165) from Sigma; alkaline phosphatase (Cat #713023) and complete EDTA-free PI from Roche Applied Sciences; oligonucleotides from Integrated DNA Technologies; IRDye donkey anti-rabbit and donkey anti-mouse from Li-Cor; Myc monoclonal 9E10 IgG, and GST monoclonal IgG from Santa Cruz Biotechnology, Inc; prestained protein standards from Bio-Rad; Dynabeads Coupling Kit from Life Technologies (14311D); Glutathione HiCap Matrix beads from Qiagen; MagneGST beads and Trypsin/Lys-C mix (Cat #V5073) from Promega; 5-fluoroorotic acid (Cat #F595000) from Thermo Fisher.

Strains and media - Yeast strains are described in **Table 2.2**. Strain PEY1516 was generated as described previously using seven tandem copies of the Tf2–1 sterol-regulatory element to drive *ura4*$^{+}$ reporter gene activation (92). *S. pombe* were cultured to exponential phase

at 30°C in rich YES medium (0.5% (w/v) yeast extract plus 3% (w/v) glucose supplemented with 225 μg/ml each of uracil, adenine, leucine, histidine, and lysine) or Edinburgh minimal medium plus supplements (EMM) (20 g/L glucose, 225 mg/L each of uracil, adenine, leucine, histidine, and lysine) unless otherwise indicated. YES+$CoCl_2$ medium was prepared by dissolving cobalt (II) chloride in H_2O and adding to a final concentration of 1.6 mM in YES medium.

Antibodies - Rabbit polyclonal antibody anti-Sre1 IgG (aa 1-260) was generated using a standard protocol as described previously (62). Briefly, antigen was expressed in *E. coli* and affinity purified by an N-terminal polyhistidine tag. Sre1-specific antibodies were isolated from rabbit serum by affinity to the polyhistidine-tagged Sre1 antigen. Specificity of this antibody was assayed by loss of immunoreactivity in an *sre1*Δ strain. We generated rabbit polyclonal antibody anti-Sre2 IgG (aa 1-426) using a standard protocol as described above for anti-Sre1 (62).

We generated monoclonal antibody 5B4 IgG1κ to Sre1 (aa 1–260) as described previously using recombinant protein that was purified from *E. coli* by nickel-affinity chromatography (Qiagen) and injected into BALB/c mice (70). Antibody specificity was tested by immunoblotting against *S. pombe* extracts from cells overexpressing *sre1*.

Generation of polyclonal antibodies to Dsc E3 ligase complex members (Dsc1 and Dsc5) was described previously (68,69). Hexa-histidine tagged recombinant protein antigens, Dsc1 (aa 20-319) and Dsc5 (aa 251-427) were purified from *E. coli* using Ni-NTA (Qiagen). Antisera were generated by Covance using a standard protocol. Dsc1 antibody was affinity purified by passing over a column containing Dsc1 N terminus (aa 1–300) coupled to agarose beads (AminoLink Plus immobilization kit, Thermo Scientific) according to the manufacturer's protocol as previously described (73). Antiserum to Cdc48 was the kind gift of R. Hartmann-Petersen (University of Copenhagen) (122).

Yeast mutagenesis and selection – S. pombe were mutagenized using methyl methanesulfonate (MMS) as previously described (69). Briefly, PEY1516 cells were grown to a

cell density of 1×10^7 cells/ml, washed in sterile water, and resuspended at a concentration of 1×10^8 cells/ml in EMM containing 0.024% or 0.012% (w/v) MMS. Cultures were then grown for 3 h at room temperature. Cells were washed with sterile water and resuspended in sterile water at a density of 5×10^6 cells/ml. Cells were plated onto selection medium [SM: EMM, 2% (w/v) agar, 20 g/L glucose, 225 mg/L each of adenine, leucine, and histidine, 50.25 mg/L uracil, 0.1% (w/v) 5-FOA, 0.2 mm $CoCl_2$] at a density of 5×10^5 cells/plate. Plates were wrapped in foil and incubated at 30°C. Colonies were picked and streaked onto SM. Single colonies were then patched onto SM and then streaked onto YES + $CoCl_2$. $CoCl_2$-sensitive isolates were then streaked from the SM patch a second time onto SM to isolate single colonies.

Mutant identification – Mutant genes were identified as previously described (69). To test whether strains contained mutations in *sre1* and *scp1*, $CoCl_2$-sensitive isolates were co-transformed with plasmids expressing *sre1*$^+$ and *scp1*$^+$ from the cauliflower mosaic virus promoter or the empty vector control plasmids pSLF101 and pSLF102 (123), respectively, and then screened again for $CoCl_2$ sensitivity. Strains whose growth on $CoCl_2$ was not rescued by plasmids expressing *sre1* and *scp1* were evaluated by western blotting for Sre1 cleavage. Strains that exhibited deficient Sre1 cleavage were mated to *dsc1–5Δ*, *cdc48-8*, *rbd2Δ*, *sre1Δ*, and *scp1Δ* cells. A suspension of spores from the mating was plated on YES or YES + $CoCl_2$. The inability to recover $CoCl_2$-resistant spores indicated tight linkage between the mutations. To identify the nucleotide mutations in each gene, genomic DNA was prepared, the full coding sequence of the relevant locus was PCR-amplified, and the coding region was sequenced.

Recreation of cdc48 point mutations – *cdc48* point mutations were created in a non-mutagenized wild-type KGY425 background by generating a plasmid containing *cdc48* (bp 4-2504) followed by the *NatMX6* marker. This wild-type plasmid was mutated using site-directed mutagenesis to create plasmids with the *cdc48* mutations of interest. Plasmids were digested to release the *cdc48-NatMX6* sequence and cdc48 fragment was transformed into KGY425 wild-type yeast for homologous recombination. Successful transformants were selected by

nourseothricin resistance (Nat) and tested for sensitivity to $CoCl_2$. An isogenic wild-type *cdc48* strain with the nourseothricin resistance cassette was also generated. All mutant strains were then confirmed by sequencing of genomic DNA as described above. Because these strains were generated in a non-mutagenized background and contained nourseothricin resistance, they were assigned allele numbers *cdc48-5 – cdc48-10* to distinguish them from the mutagenized versions published in Stewart et al 2012 (69).

SREBP cleavage assay – For Sre1 cleavage, cells were grown in YES medium to exponential phase inside an $InVivo_2$ 400 hypoxic workstation (Biotrace, Inc) at 30°C. For Sre2 and Sre2-MS cleavage, cells were grown in YES medium (Sre2) or EMM medium minus leucine (Sre2-MS) in normoxic conditions at 30°C.

Whole cell lysis - Cells were harvested for protein extraction and immunoblotting by the whole cell lysis method as previously described, unless otherwise indicated (124). Briefly, cell pellets were resuspended in 1.85 M NaOH/7.4% (v/v) BME and incubated on ice for 10 min. Tricholoroacetic acid (TCA) was added to a final concentration of 30% (w/v) and the samples were incubated on ice again. Lysate was centrifuged at 20,000 x *g* for 10 min at 4°C and pellet was washed with cold acetone. Samples were centrifuged at 20,000 x *g* for 5 min at 4°C and dried completely under vacuum. Pellets were resuspended in SDS lysis buffer (1% SDS, 150 mM NaCl, 50 mM Tris-HCl pH 8.0, 1x protease inhibitors) and sonicated 10 s. Protein was quantified using the BCA protein assay (Pierce). For alkaline phosphatase treatment, 20-50 µg lysate was diluted at least 1:2 in 50 mM Tris-HCl pH 8.0, then alkaline phosphatase was added to 20% (v/v). Samples were incubated at 37°C for 1 h then 1x loading dye was added (30 mM Tris-HCl, 3% SDS, 5% glycerol, 0.004% bromophenol blue, 2.5% 2-mercaptoethanol). Entire phosphatase-treated sample was loaded onto SDS-polyacrylamide gels and consistent loading was confirmed following electroblotting by staining the membrane with Ponceau S. Blots were imaged using the Odyssey CLx infrared imaging system (LI-COR Biosciences). Protein signal was quantified using

the LI-COR Biosciences Image Studio software to box the bands of interest, normalized to blot background, and then normalized to the indicated loading control.

Cdc48-5xFLAG affinity chromatography - Exponentially growing cells (1 x 10^{10}) were pelleted then washed with H_2O. Cell pellets were resuspended in 15 ml cold B88 buffer [20 mM HEPES pH 7.2, 150 mM KOAc, 5 mM $Mg(OAc)_2$, 250 mM sorbitol] + 1X protease inhibitors, 1x Complete EDTA-free PI. Cells were lysed by high pressure emulsifier (EmulsiFlex-C-3, Avestin), lysate was centrifuged for 10 min at 100,000 x *g* to pellet insoluble material, and supernatant was saved. Monoclonal FLAG antibody F3165 (Sigma) was conjugated to Dynabeads using the Dynabeads Coupling Kit (Life Technologies 14311D) to a final concentration of 10 µg antibody/1 mg beads. FLAG-conjugated Dynabeads (1.5 mg) were washed with IP buffer (B88 + 1x PI, 1x Complete EDTA-free PI, 0.5% Triton X-100). Lysate (25 mg) was diluted in IP buffer to 550 µl total volume, and Triton X-100 concentration was returned to 0.5%. Lysate (50 µl) was saved as input and 500 µl was incubated with the FLAG-Dynabeads for 30 min at 4°C. Beads were collected by magnet and unbound fraction was reserved. Beads were washed 3x in 200 µl IP buffer and transferred to a new tube on the last wash to minimize background. The bound fraction was eluted into SDS lysis buffer + 1x PI at 95°C for 5 min and transferred to a new tube. Aliquots of all fractions were run on SDS-PAGE and silver stained to analyze pull-down before sending total bound fraction for mass spectrometry analysis.

TMT labeling and proteomics analysis – Protein samples from three biological replicates of wild-type and Cdc48-5xFLAG samples subjected to anti-FLAG purification were pH adjusted to 8.0 using 500 mM Triethylammonium bicarbonate (TEAB) added dropwise. Cysteine residues were reduced using 0.5 µg/µl DTT for 1 h at 60°C then alkylated with 1 µg/µl iodoacetomide for 30 min in the dark. Samples were precipitated with 8x volume of 10% TCA-acetone at -20°C for 5 h, centrifuged at max speed for 10 min to remove supernatant, then washed with 8x acetone at -20°C for 20 min. Samples were centrifuged at max speed to remove supernatant and protein pellets were air-dried. For protein digestion, samples were incubated with 2 µg trypsin/LysC mix

in 50 µl 400 mM TEAB at 37°C for 4 h. After proteolysis, samples were labeled with amine reactive 6-plex tandem mass tag reagents (TMT, Thermo Scientific) dissolved in 41 µl anhydrous acetonitrile at room temperature for 1 h. Labels are as follows: 1_ctr: 126; 1_exp: 129; 2_ctr: 130; 2_exp: 127; 3_ctr: 131; 3_exp: 128. After labeling, 8 µl of 5% (v/v) hydroxylamine was added to quench the reaction. After labeling, all samples were mixed and dried, resulting in a total protein quantity of 140 µg.

The combined mixture of TMT 6-plex labeled tryptic peptides was reconstituted in 2 ml basic Reverse Phase (bRP) solvent A (10 mM TEAB pH 8.5), then pH checked and fractionated over 8 min on a XBridge C18 Column, 5 µm, 2.1 x 100 mm analytical column (Waters) with a XBridge C18 Guard Column, 5 µm, 2.1 x 10 mm (Waters), using an Agilent HPLC system containing 1100 series binary pump, 1200 series UV detector and a 1200 series micro-fraction collector. Fractionation of peptides were carried out by a linear gradient (starting at 16 min) between solvent A and solvent B (10 mM TEAB in 90% Acetonitrile), flow rate 250 µl/min. 12 flow through fractions between 1-20 min were not used for MS/MS. 84 x 225 µl bRP fractions collected between 20-95 min (0-100% solvent B), were recombined into 28 fractions for MS/MS analysis.

Each bRP fraction was completely dried then reconstituted in 2% (v/v) acetonitrile/0.1% (v/v) formic acid and 50% was loaded on a 75 µm x 2.5 cm ODS-A C18 HPLC column trap (YMC) at 600 nl/min 0.1% formic acid (solvent A). Peptides were fractionated by reverse-phase HPLC on a 75 um x 100 mm ProntoSil C18H reverse-phase column (5 µm, 120Å, Bischoff Chromatography) at 300 nl/min using a 2-10% solvent B (90% acetonitrile in 0.1% formic acid) gradient over the first 2 min, then up to 25% B by 55 min, 45% B by 67 min, and 100% B by 75 min. Eluting peptides were sprayed through 1 µm emitter tip (New Objective) at 2.0 kV directly into an LTQ Orbitrap Velos mass spectrometer in FTFT (Thermo Fisher Scientific) interfaced with nano-Acquity LC system (Waters). Survey scans (full MS) were acquired from 350 to 1800 m/z. Precursor ions were individually isolated with 15 ppm tolerance between 2.5-5.5 Da and

fragmented (MS/MS) using an HCD activation collision energy of 35 and dynamic exclusion of 30 s. Fragment ions were isolated with 0.03 Da tolerance. Precursor and the fragment ions were analyzed at resolution 30,000 and 15,000, respectively.

Protein quantification - MS/MS spectra (.RAW) were analyzed via Proteome Discoverer software (v1.4 Thermofisher Scientific) using 3Nodes (extracted, processed by MS2Processor, and PD1.4), with Mascot (v 2.2, Matrix Science) using the RefSeq2012 Complete Database with concatenated decoy database specifying *S. pombe* species (5020 entries). Fixed modifications of TMT 6-plex of N-termini and carboamidomethyl on Cys, and variable modifications of TMT 6-plex on Lys and oxidation of Met, were allowed. One missed cleavage was allowed. 80498 PSMs were matched to 16290 peptides. The peptide identifications and reporter ions with the highest Mascot score for the same peptide matched spectrum from the different extraction methods were processed within the Proteome Discoverer to identify peptides with a confidence threshold 1% False Discovery Rate. Peptides were grouped by mass and sequence into 2355 protein groups, considering only PSMs with delta Cn better than 0.15. Spectra were assessed using principle component analysis, quantile-quantile plots, and box and whisker plots using Partek statistical software (Genomic Solutions). Based on that analysis, spectral intensities were subjected to logarithmic transformation to more closely approximate a normal distribution. The relative protein abundance was obtained by taking the median value of all reporter ion intensities assigned to that protein. Protein abundance values were quantile normalized prior to averaging of the three biological replicates and fold change calculation between the FLAG-tagged experiment and the untagged control. p-values were calculated by 2-way ANOVA because principle component analysis showed evidence of significant batch effects among our three biological replicates.

GST in vitro pull-down – Exponentially growing KGY425 (WT) and NBY3824 (*ufd1-13xmyc)* cells (3.0×10^8) were collected and washed with H_2O. Cell pellets were resuspended in 500 µl cold B88 buffer + 1X protease inhibitors and lysed using glass beads for 20 min at 4°C.

Beads were washed with 400 µl B88 buffer and lysate was centrifuged at 47,000 rpm for 10 min at 4°C. Supernatant was saved as cleared lysate.

Recombinant GST-HA-V5, GST-Dsc5-UBX, and GST-Rbd2-SHP were purified from *E. coli* (4.0×10^{10}) after 4 h induction with IPTG. Bacterial pellets were resuspended in 5 ml PBS pH 7.2 and sonicated for 3 min total, with 15 sec on and 59 sec off. Triton X-100 was added to a final concentration of 1% (v/v) and lysate was rotated for 30 min at 4°C. Lysate was centrifuged at 15,000 x *g* for 20 min at 4°C. Supernatant was saved as unpurified protein. For purification, 500 µl Glutathione Hi-Cap Matrix beads (Qiagen) were washed 3x with 2.5 ml PBS-EW wash buffer (50 mM NaH_2PO_4, 150 mM NaCl, pH 7.2, 1 mM EDTA, 1 mM DTT) and centrifuged 4000 x *g* for 1.5 min after each wash. Cell lysate was added to beads and nutated for 1 h at 4°C. Beads were centrifuged 4000 x *g* for 1.5 min and washed 2x with 1.3 ml PBS-EW. Beads were washed 1x with 1.25 ml wash buffer (50 mM Tris pH 8.0, 0.4 M NaCl, 0.1% Triton X-100, 1 mM DTT). Elution buffer (250 µl) (50 mM Tris pH 8.0, 0.4 M NaCl, 0.1% Triton X-100, 1 mM DTT, 50 mM reduced glutathione) was added to beads and incubated for 10 min at 4°C. Beads were centrifuged 4000 x *g* for 1.5 min, eluate was removed, and beads were incubated 2x in elution buffer for 5 min each, saving eluates separately. SDS lysis buffer and loading dye was added to aliquots of eluates and intermediate steps. These samples were run on an SDS-PAGE gel and Coomassie stained to evaluate purity and concentration.

For pull-down, 25 µl of MagneGST beads (Promega) were washed 3x with 1 ml PBS pH 7.2 then blocked for 1 h with PBS + 5% BSA at 4°C. Beads were washed 1x with PBS then 50 µg purified GST-tagged protein was added, and volume was brought up to 500 µl with PBS before binding for 1 h at 4°C. Beads were collected by magnet and washed 3x with 1 ml PBS. Beads were washed 1x with 1 ml binding buffer (B88, 0.2% NP-40, 1X protease inhibitors). Cytosol (250 µg) and binding buffer was added to beads to a final volume of 200 µl and incubated 30 min at 4°C. Beads were collected by magnet and unbound fraction was saved before washing beads

3x with 1 ml binding buffer. Beads were resuspended in 100 µl SDS lysis buffer and 1x loading dye and boiled at 95°C for 5 min to elute bound proteins.

Dsc1 glycosylation assay - Exponentially growing cells (2.5 x 10^8) were collected and resuspended in 300 µl B88 buffer + 1X protease inhibitors, 1x Complete EDTA-free PI. Cells were lysed using glass beads for 12 min at 4°C then centrifuged for 5 min at 500 x *g* to clear cell debris. The supernatant was centrifuged at 20,000 x *g* for 20 min, and the pelleted membranes were resuspended in 100 µl B88 buffer with 1% NP-40 (v/v) then sonicated for 5 s. Membranes were solubilized at 4°C for 1 h, samples were centrifuged at 20,000 x *g* for 20 min, and the supernatant was collected as detergent-solubilized membrane. Loading dye was added and samples were incubated at 37°C for 30 min before running an SDS-PAGE gel. At no time were samples boiled, as Dsc1 aggregates at high temperature. % mature was calculated by quantifying the higher molecular weight band and the lower molecular weight band on the LiCor, and dividing the high signal by the total signal.

Acknowledgments/Author contributions: The authors thank Dr. M. N. Boddy (Scripps Research Institute) for the *ufd1* strains, Dr. R. Hartmann-Petersen (University of Copenhagen) for the Cdc48 antibody, Dr. J. Burg for generation of the *cdc48* homologous recombination plasmid, the Johns Hopkins Mass Spectrometry Core for Mass Spectrometry, the Johns Hopkins Microarray facility for data analysis, and S. Zhao and other members of the Espenshade lab for help and advice. RB designed and conducted the experiments, analyzed the results, and wrote the manuscript. EVS performed the MMS mutagenesis screen which was described in **Fig. *2.1A*** and which generated the *cdc48* mutants. DR and JH performed linkage analysis and sequencing to analyze results of the MMS mutagenesis screen. Sre1 cleavage assays for *cdc48-1* through *cdc48-4* were originally published in Stewart *et al.,* 2012. DR made the initial observation that *cdc48* point mutants are epistatic to *rbd2*Δ. SR made the initial observation that *cdc48* point mutants have defective Dsc1 glycosylation. PJE conceived of the project, designed experiments, and

wrote the manuscript. All authors reviewed the results and approved the final version of this manuscript.

2.5 Figures

FIGURE 2.1. **Identification of *cdc48* alleles** *A,* flow chart of results from two MMS mutagenesis screens [0.024% and 0.012% (w/v)]. Red numbers denote the number of isolates in each category. Numbers in parentheses are the number of isolates with mutations confirmed by sequencing (see **Supplementary Table 2.1** for specific mutations). Aside from the first box, all numbers are pooled from the two MMS dosages. *B,* comparison of gene coding sequence size with number of isolated mutants in MMS mutagenesis screen. Best-fit line calculated against non-essential genes (filled markers), R^2=0.87. *C,* table of remade *cdc48* alleles showing amino acid changes in *S. pombe,* corresponding homologous amino acid in human, and corresponding allele from our previous report (69). *D,* line diagram of *S. pombe cdc48,* where the *orange box* indicates the N-domain to which the majority of cofactors bind. The *blue box* indicates the minor ATPase D1 domain required for hexamer formation. The *green box* indicates the major ATPase D2 domain required for force generation. *Yellow boxes* in both domains indicate sequences essential for ATP binding and hydrolysis. The *grey box* indicates the C-domain to which a minority of cofactors bind. *Red asterisks* indicate the locations of our *cdc48* point mutations.

FIGURE 2.2. **SREBP cleavage requires *cdc48*** *A,* wild-type cells or the indicated mutants (5000 cells) were grown on rich medium plus or minus cobalt chloride ($CoCl_2$) for 2 or 10 days, respectively. *B,* western blots, probed with monoclonal anti-Sre1 IgG (5B4) and polyclonal anti-Dsc5 IgG (for loading), of lysates treated with alkaline phosphatase for 1 h from wild-type cells and the indicated *cdc48* mutants grown for 0 or 4 h in the absence of oxygen. P and N denote precursor and cleaved N-terminal transcription factor forms, respectively. Asterisk denotes nonspecific band. The blot is representative of three biological replicates. *C,* western blots,

probed with monoclonal anti-FLAG M2 and polyclonal anti-Dsc5 IgG (for loading), of lysates treated with alkaline phosphatase for 1 h from wild-type cells and the indicated *cdc48* mutants containing a plasmid expressing *sre2-MS* (+) or the empty vector (-) grown in the presence of oxygen. P and N denote precursor and cleaved N-terminal transcription factor forms, respectively. The blot is representative of three biological replicates.

FIGURE 2.3. ***cdc48* mutants have minimal effect on Cdc48 expression or growth rate** *A,* western blots, probed with polyclonal anti-Cdc48 IgG and polyclonal anti-Dsc5 IgG (for loading), of lysates from wild-type cells and the indicated *cdc48* mutants. *B,* quantification of *A* from three biological replicates, each indicated by a different marker shape, normalized for loading to Dsc5 and then normalized to wild-type cells for comparison among blots. Error bars are 1 S.D. (*, $p < 0.05$; **, $p < 0.01$ vs WT by two-tailed Student's t-test). *C,* indicated strains were grown in liquid culture for 12 h. Cell density was measured by absorbance at 600 nm every 3 h. Doubling times were calculated using 3- and 9-h optical density readings using the formula: doubling time = (culture time x log(2))/log(final OD) - log(initial OD). Doubling times are displayed as mean±S.D. from four biological replicates as indicated by marker shape. (*, $p < 0.05$; **, $p < 0.01$ vs WT by two-tailed Student's t-test).

FIGURE 2.4. **Identification of Cdc48 binding proteins in *S. pombe*** *A,* western blots, probed with monoclonal anti-Sre1 IgG (5B4) and polyclonal anti-Dsc5 IgG (for loading), of lysates treated with alkaline phosphatase for 1 h from wild-type cells, *cdc48-5xFLAG* (cdc48-F) cells, or *sre1Δ* cells grown for 0 or 4 h in the absence of oxygen. P and N denote precursor and cleaved N-terminal transcription factor forms, respectively. Asterisks denote nonspecific bands. The blot is representative of two biological replicates. *B,* Cdc48 was immunoprecipitated (IP) from wild-type or *cdc48-5xFLAG* cells using monoclonal anti-FLAG M2 IgG as described in Experimental Procedures. Input, unbound, and 10-fold enriched bound fractions were analyzed by western

blotting using polyclonal anti-Cdc48 IgG. The blot is representative of four biological replicates. *C,* volcano plot of all proteins identified during TMT mass spectrometry of Cdc48-5xFLAG bound proteins. Points in red are proteins with enrichment > 2 S.D. from the mean in the Cdc48-5xFLAG versus wild-type samples. p-values were calculated using two-way ANOVA with quantile normalization for 3 biological replicates.

FIGURE 2.5. **Ufd1 is a Cdc48 cofactor required for SREBP cleavage** *A,* wild-type cells or the indicated mutants (5000 cells) were grown on rich medium plus or minus $CoCl_2$ for 10 days. *B,* indicated strains were grown in liquid culture for 12 h. Cell density was measured by absorbance at 600 nm every 3 h. Doubling times were calculated using 3- and 9-h optical density readings using the formula: doubling time = (culture time x log(2))/log(final OD) - log(initial OD). Doubling times are displayed as mean±S.D. for three biological replicates as indicated by marker shape. (**, $p < 0.01$ vs WT by two-tailed Student's t-test). *C,* western blots, probed with monoclonal anti-Myc IgG, polyclonal anti-Cdc48 IgG, and polyclonal anti-Dsc5 IgG (for loading), of lysates from wild-type cells and the indicated *ufd1* mutants. The blot is representative of three biological replicates. *D,* western blots, probed with monoclonal anti-Sre1 IgG (5B4) and polyclonal anti-Dsc5 IgG (for loading), of lysates treated with alkaline phosphatase for 1 h from wild-type cells, *sre1Δ*, or the indicated *ufd1* mutants grown for 0 or 4 h in the absence of oxygen. P and N denote precursor and cleaved N-terminal transcription factor forms, respectively. Asterisk denotes nonspecific band. The blot is representative of three biological replicates. *E,* western blots, probed with monoclonal anti-FLAG M2 and polyclonal anti-Dsc5 IgG (for loading), of lysates treated with alkaline phosphatase for 1 h from wild-type cells and the indicated *ufd1* mutants containing a plasmid expressing *sre2-MS* (+) or the empty vector (-) grown in the presence of oxygen. P and N denote precursor and cleaved N-terminal transcription factor forms, respectively. The blot is representative of three biological replicates.

FIGURE 2.6. **SREBP cleavage requires Cdc48-Ufd1 during Dsc E3 ligase Golgi localization** *A,* recombinant GST-HA-V5 control (GST), GST-Dsc5 UBX ($Dsc5_{323–425}$, UBX), and GST-Rbd2 C-terminus ($Rbd2_{200–251}$, SHP) were bound to GST magnetic beads and incubated with *S. pombe* cytosol from wild-type (-) or *ufd1-13xmyc* (+) cells. Input, unbound, and 10-fold enriched bound fractions were probed with monoclonal anti-Myc IgG, polyclonal anti-Cdc48 IgG, and monoclonal anti-GST IgG. The blot is representative of five replicates. *B-C,* western blots, probed with polyclonal anti-Sre2 IgG and polyclonal anti-Dsc5 IgG (for loading), of lysates treated with alkaline phosphatase for 1 h from wild-type, *dsc1Δ* (*1Δ*), or the indicated *cdc48 (B)* or *ufd1 (C)* mutant cells. *rbd2* (+) or *rbd2Δ* (-) genotype is indicated. P and N denote precursor and cleaved N-terminal transcription factor forms, respectively. The blot is representative of three *(B)* or five *(C)* biological replicates. *D,* western blot, probed with polyclonal anti-Dsc1 IgG, of Nonidet P-40-solubilized membrane protein from wild-type, *dsc2Δ*, *dsc5ΔUBX* (*ΔUBX*)*, rbd2Δ,* or the indicated *cdc48* or *ufd1* mutant cells. M and I indicate mature and intermediate glycosylated forms, respectively. The blot is representative of three biological replicates. *E*, quantification of Dsc1 from *(D)* of three biological replicates each denoted by different marker symbols. The quantity of the mature form was divided by total Dsc1 signal for percent mature, allowing comparison between lanes and blots. Error bars are 1 S.D. (*, $q < 0.05$ FDR by one-way ANOVA with post-hoc comparison to matched wild-type and Benjamini, Krieger, Yekutieli multiple comparison correction).

Table 2.1. Cdc48 binding proteins in *S. pombe*. Cdc48 binding proteins, identified by TMT mass spectrometry, of 3 biological replicates, enriched at least 2 S.D. from the mean. Rows highlighted in grey are known Cdc48 binding proteins.
[a] Descriptions were obtained from PomBase (www.pombase.org) with some additional hand editing.

Common Name	Systematic ID	Gene Description[a]	Log_2 (FC)	p-value	$CoCl_2$ sensitive
SPBC1711.10c	*npl4*	Hrd1p ubiquitin ligase complex Npl4 (predicted)	6.03	0.05	
SPCC1442.07c	*wss2*	ubiquitin/metalloprotease fusion protein Udp7	5.45	0.03	NO
SPBC21C3.11	*ubx4*	UBX domain protein Ubx4 (predicted)	5.11	0.02	NO
SPCC1020.01c	*pma2*	P-type proton ATPase, P3-type Pma2	4.94	0.03	NO
SPBC16A3.09c	*ufd1*	Hrd1 ubiquitin ligase complex subunit Ufd1 (predicted)	4.71	0.02	YES
SPAC6G10.08	*idp1*	isocitrate dehydrogenase Idp1 (predicted)	4.66	0.09	NO
SPAC343.09	*ubx3*	UBX domain protein Ubx3, Cdc48 cofactor	4.53	0.05	YES
SPBC947.10	*dsc1*	Golgi Dsc E3 ligase complex subunit Dsc1	4.51	0.06	YES
SPAP32A8.03c	*bop1*	ubiquitin-protein ligase E3 (predicted)	4.39	0.01	NO
SPAC2C4.15c	*ubx2*	Hrd1 ubiquitin ligase complex UBX domain Ubx2	4.31	0.02	NO
SPAC1565.08	*cdc48*	AAA family ATPase, ubiquitin-mediated degradation	4.21	0.03	YES
SPAC17C9.11c	*SPAC17C9.11c*	zf-C2H2 type zinc finger protein/UBA domain protein	4.06	0.05	NO
SPAC20H4.02	*dsc3*	Golgi Dsc E3 ligase complex subunit Dsc3	3.65	0.12	YES
SPCC1827.04	*vms1*	Cdc48p-Npl4p-Vms1p AAA ATPase complex subunit	3.59	0.09	NO
SPAC26H5.09c	*SPAC26H5.09c*	oxidoreductase involved in NADPH regeneration	3.58	0.02	NO
SPCC4G3.12c	*SPCC4G3.12c*	ubiquitin-protein ligase E3 (predicted)	3.30	0.01	NO
SPAC6B12.13	*SPAC6B12.13*	protein phosphatase inhibitor (predicted)	3.23	0.04	
SPAC26A3.16	*dph1*	UBA domain protein Dph1	3.22	0.01	NO
SPCC285.11	*dsc5*	UBX domain protein required for Sre1 cleavage	3.21	0.10	YES
SPCC1281.07c	*gst4*	glutathione S-transferase (predicted)	3.21	0.04	NO
SPBC1105.07c	*pci2*	TREX complex subunit Pci2 (predicted)	3.12	0.08	
SPBC21B10.05c	*pop3*	WD repeat protein Pop3	2.96	0.09	NO
SPAC29A4.06c	*SPAC29A4.06c*	splicing protein, human NSRP1 ortholog	2.94	0.03	
SPAC4A8.12c	*sds22*	protein phosphatase regulatory subunit Sds22	2.71	0.11	
SPAC57A7.08	*pzh1*	serine/threonine protein phosphatase Pzh1	2.63	0.08	NO
SPAC1486.02c	*dsc2*	Golgi Dsc E3 ligase complex subunit Dsc2	2.63	0.05	YES
SPBC354.07c	*SPBC354.07c*	oxysterol binding protein (predicted)	2.45	0.07	NO
SPBP4H10.07	*SPBP4H10.07*	ubiquitin-protein ligase E3 (predicted)	2.37	0.04	NO
SPAC2F3.15	*lsk1*	P-TEFb-associated cyclin-dependent protein kinase	2.16	0.28	NO
SPBC216.03	*SPBC216.03*	conserved fungal protein	2.13	0.23	NO
SPAC1A6.04c	*plb1*	phospholipase B homolog Plb1	2.12	0.26	NO
SPAC24C9.14	*otu1*	ubiquitin-specific cysteine protease, OTU family, Otu1	2.09	0.19	NO
SPAC18B11.03c	*SPAC18B11.03c*	N-acetyltransferase (predicted)	2.09	0.34	NO
SPAC4F8.07c	*hxk2*	hexokinase 2	2.05	0.06	NO
SPBC29A10.08	*gas2*	1,3-beta-glucanosyltransferase Gas2 (predicted)	2.03	0.21	NO
SPCC4B3.01	*tum1*	thiosulfate sulfurtransferase, tRNA wobble thiolation	1.97	0.39	NO
SPBC15D4.11c	*SPBC15D4.11c*	mitochondrial Mam33 family protein (predicted)	1.94	0.15	
SPAC343.12	*rds1*	conserved fungal protein	1.93	0.10	NO
SPAC22E12.06c	*gmh3*	alpha-1,2-galactosyltransferase Gmh3	1.92	0.02	NO
SPBC354.13	*rga6*	Rho-type GTPase activating protein Rga6 (predicted)	1.88	0.11	NO
SPCC306.08c	*mdh1*	malate dehydrogenase Mdh1 (predicted)	1.86	0.31	NO
SPBC365.06	*pmt3*	SUMO	1.85	0.09	NO
SPAC2C4.17c	*msy2*	MS ion channel protein 2 (predicted)	1.85	0.04	NO
SPAC637.07	*moe1*	translation initiation factor eIF3d Moe1	1.83	0.15	NO
SPAC1B3.03c	*wis2*	cyclophilin family peptidyl-prolyl cis-trans isomerase	1.83	0.08	NO
SPAC25G10.05c	*his1*	ATP phosphoribosyltransferase	1.83	0.04	NO
SPAC13G7.02c	*ssa1*	heat shock protein Ssa1 (predicted)	1.81	0.09	NO
SPBC106.03	*SPBC106.03*	DUF1776 family protein	1.78	0.26	NO
SPBC18H10.04c	*sce3*	translation initiation factor (predicted)	1.77	0.03	NO
SPBC887.05c	*cwf29*	RNA-binding protein Cwf29	1.74	0.22	
SPAC19B12.11c	*SPAC19B12.11c*	zinc finger protein, human ZNF593 ortholog	1.70	0.09	NO
SPBC17D11.02c	*hrd1*	Hrd1 ubiquitin ligase complex E3 subunit, Hrd1	1.67	0.06	NO

Table 2.2. *S. pombe* strain list

Strains	Genotype	Source	Figure
PEY1516	*h- leu1-32 ade6-M210 ura4-D18::7xSRE ura4+ kanR, his3-D1::7xSRE lacZ*	(Stewart et al., 2012)	1
KGY425	*h- leu1-32 ura4-D18 ade6-M210 his3-D1*	ATCC	2,4,6
PEY522	*h- leu1-32 ura4-D18 ade6-M210 his3-D1 ∆sre1-D1::kanMX6*	(Hughes et al., 2005)	2,4,5
PEY1653	*h- leu1-32 ura4-D18 ade6-M210 his3-D1 cdc48+::natMX6*	This study	2,3,6
PEY1654	*h- leu1-32 ura4-D18 ade6-M210 his3-D1 cdc48-N558I::natMX6*	This study	2,3,6
PEY1655	*h- leu1-32 ura4-D18 ade6-M210 his3-D1 cdc48-A586V::natMX6*	This study	2,3,6
PEY1656	*h- leu1-32 ura4-D18 ade6-M210 his3-D1 cdc48-E731D::natMX6*	This study	2,3,6
PEY1657	*h- leu1-32 ura4-D18 ade6-M210 his3-D1 cdc48-E325K::natMX6*	This study	2,3,6
PEY1659	*h- leu1-32 ura4-D18 ade6-M210 his3-D1 cdc48-A366D::natMX6*	This study	2,3,6
PEY1660	*h- leu1-32 ura4-D18 ade6-M210 his3-D1 cdc48-R764C::natMX6*	This study	2,3,6
PEY1820	*h- leu1-32 ura4-D18 ade6-M210 his3-D1 cdc48-5xFLAG::kanMX6*	This study	4
ED666	*h+ leu1-32 ura4-D18 ade6-M210*	Bioneer Inc.	Table 1
deletion strains	*h+ leu1-32 ura4-D18 ade6-M210 ∆[GOI]-D1::kanMX4 (GOI: SPCC1442.07c, ubx4, idp1, bop1, ubx2, SPAC17C9.11c, vms1, SPAC26H5.09c, dph1, SPCC1281.07c, pop3, pzh1, SPBC354.07c, lsk1, plb1, otu1, SPAC18B11.03c, tum1, fds1, gmh1, rga6, SPCC306.08c, pmt3, msy2, moe1, wis2, his1, ssa1, SPBC106.03, sce3, SPAC19B12.11c, hrd1)*	Bioneer Inc.	Table 1
PEY1831	*h- leu1-32 ura4-D18 ade6-M210 his3-D1 ∆ubx3-D1::natMX6*	This study	Table 1
PEY1832	*h- leu1-32 ura4-D18 ade6-M210 his3-D1 ∆SPCC4G3.12c-D1::natMX6*	This study	Table 1
PEY1833	*h- leu1-32 ura4-D18 ade6-M210 his3-D1 ∆SPBP4H10.07-D1::natMX6*	This study	Table 1
PEY1834	*h- leu1-32 ura4-D18 ade6-M210 his3-D1 ∆SPBC216.03-D1::natMX6*	This study	Table 1
PEY1835	*h- leu1-32 ura4-D18 ade6-M210 his3-D1 ∆pma2-D1::natMX6*	This study	Table 1
PEY1836	*h- leu1-32 ura4-D18 ade6-M210 his3-D1 ∆gas2-D1::natMX6*	This study	Table 1
PEY1837	*h- leu1-32 ura4-D18 ade6-M210 his3-D1 ∆hxk2-D1::natMX6*	This study	Table 1
NBY3824	*h+ leu1-32 ura4-D18 ade6-M210 his3-D1 ufd1-13xmyc::kanMX6*	(Nie et al., 2012)	5-6
NBY3921	*h+ leu1-32 ura4-D18 ade6-M210 his3-D1 ufd1 (L281S)-13xmyc::kanMX6*	(Nie et al., 2012)	5,6
NBY4402	*h+ leu1-32 ura4-D18 ade6-M210 his3-D1 ufd1 (L68P, G226D)-13xmyc::kanMX6*	(Nie et al., 2012)	5-6
NBY4403	*h+ leu1-32 ura4-D18 ade6-M210 his3-D1 ufd1 (L78P)-13xmyc::kanMX6*	(Nie et al., 2012)	5-6
PEY1821	*h- leu1-32 ura4-D18 ade6-M210 his3-D1 Δrbd2-D1::kanMX6, cdc48+::natMX6*	This study	6
PEY1822	*h+ leu1-32 ura4-D18 ade6-M210 his3-D1 Δrbd2-D1::kanMX6, cdc48-N558I::natMX6*	This study	6
PEY1823	*h+ leu1-32 ura4-D18 ade6-M210 his3-D1 Δrbd2-D1::kanMX6, cdc48-E325K::natMX6*	This study	6
PEY1824	*h90 leu1-32 ura4-D18 ade6-M210 his3-D1 Δrbd2-D1::kanMX6, cdc48-A366D::natMX6*	This study	6
PEY1825	*h- leu1-32 ura4-D18 ade6-M210 his3-D1 Δrbd2-D1::kanMX6, cdc48-R764C::natMX6*	This study	6
PEY1826	*h90 leu1-32 ura4-D18 ade6-M210 his3-D1 Δrbd2-D1::kanMX6, cdc48-A586V::natMX6*	This study	6
PEY1827	*h90 leu1-32 ura4-D18 ade6-M210 his3-D1 Δrbd2-D1::kanMX6, cdc48-E731D::natMX6*	This study	6
PEY1828	*h+ leu1-32 ura4-D18 ade6-M210 his3-D1 ufd1-13xmyc::kanMX6, Δrbd2-D1::natMX6*	This study	6
PEY1829	*h+ leu1-32 ura4-D18 ade6-M210 his3-D1 ufd1 (L68P, G226D)-13xmyc::kanMX6, Δrbd2-D1::natMX6*	This study	6
PEY1830	*h+ leu1-32 ura4-D18 ade6-M210 his3-D1 ufd1 (L78P)-13xmyc::kanMX6, Δrbd2-D1::natMX6*	This study	6
PEY1569	*h+ leu1-32 ura4-D18 ade6-M210 his3-D1 ∆dsc1-D1::kanMX6*	(Burr et al., 2017)	6
PEY1685	*h+ leu1-32 ura4-D18 ade6-M210 his3-D1 Δdsc1-D1::kanMX6 Δrbd2-D1::natMX6*	(Hwang et al., 2016)	6
PEY1792	*h+ leu1-32 ura4-D18 ade6-M210 his3-D1 ∆dsc2-D1::kanMX6*	(Burr et al., 2017)	6
PEY1681	*h+ leu1-32 ura4-D18 ade6-M210 his3-D1 Δrbd2-D1::natMX6*	(Hwang et al., 2016)	6
PEY1556	*h- leu1-32 ura4-D18 ade6-M210 his3-D1 dsc5ΔUBX-D1::kanMX6*	(Stewart et al., 2012)	6

Figure 2.1

A

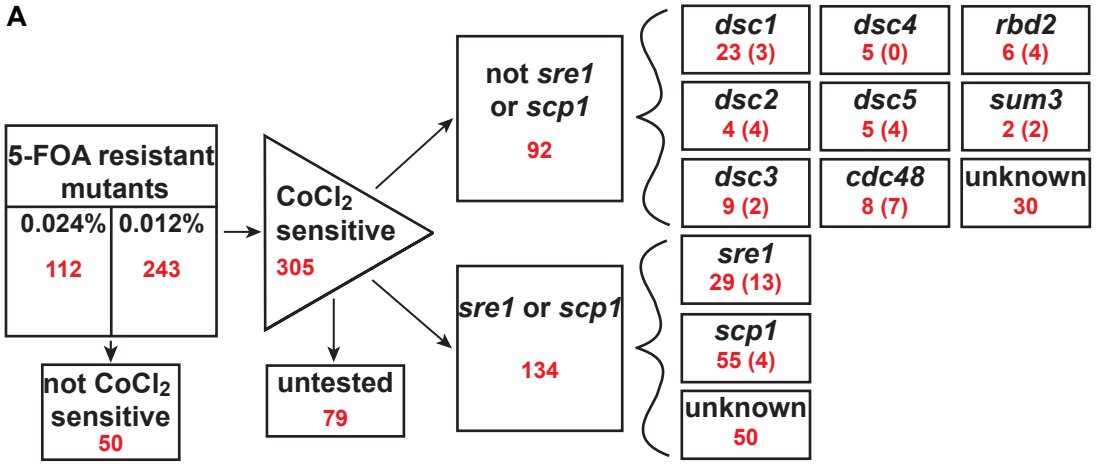

B

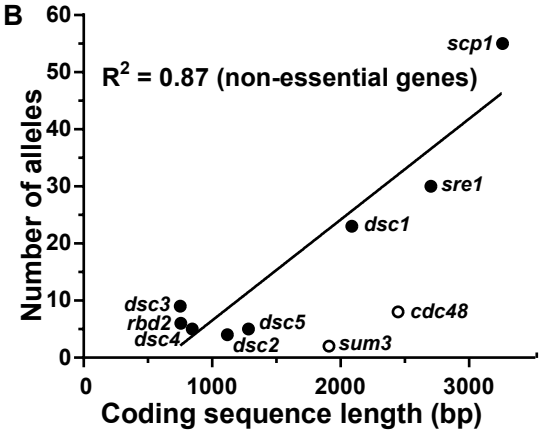

C

Allele	*S. pombe*	Human	Stewart et al. 2012
cdc48-5	N558I	N538	*cdc48-1*
cdc48-6	A586V	A567	*cdc48-3*
cdc48-7	E731D	E712	*cdc48-2*
cdc48-8	E325K	E305	*cdc48-4*
cdc48-9	A366D	A346	
cdc48-10	R764C	R744	

D

Figure 2.2

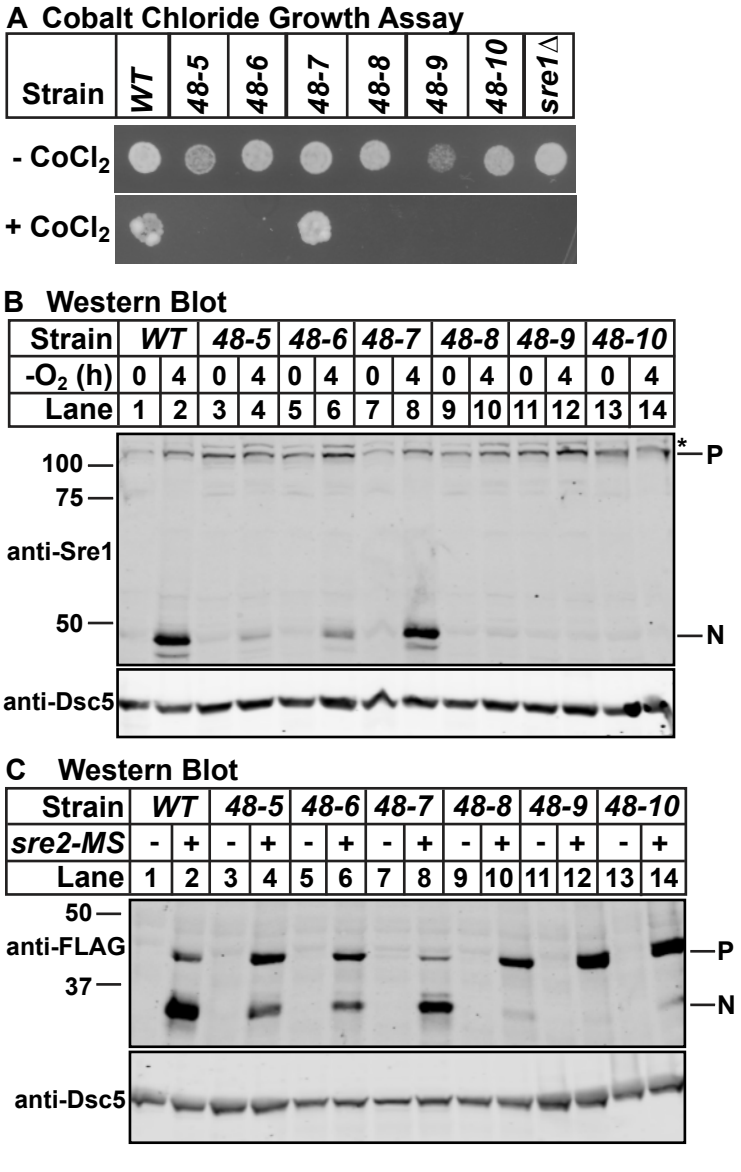
A Cobalt Chloride Growth Assay
Strain
WT
48-5
48-6
48-7
48-8
48-9
48-10
sre1Δ
- CoCl2
+ CoCl2
B Western Blot
Strain
WT
48-5
48-6
48-7
48-8
48-9
48-10
-O2 (h)
0 4 0 4 0 4 0 4 0 4 0 4 0 4
Lane
1 2 3 4 5 6 7 8 9 10 11 12 13 14
100
75
anti-Sre1
50
anti-Dsc5
*
P
N
C Western Blot
Strain
WT
48-5
48-6
48-7
48-8
48-9
48-10
sre2-MS
- + - + - + - + - + - + - +
Lane
1 2 3 4 5 6 7 8 9 10 11 12 13 14
50
anti-FLAG
37
anti-Dsc5
P
N

Figure 2.3

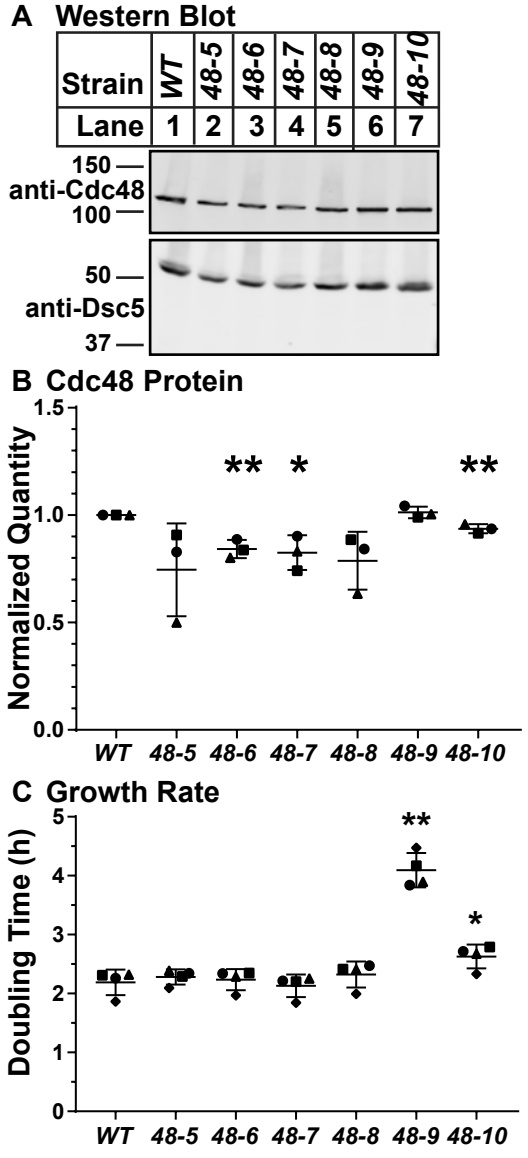
A Western Blot
Strain
WT
48-5
48-6
48-7
48-8
48-9
48-10
Lane
1
2
3
4
5
6
7
150
anti-Cdc48
100
50
anti-Dsc5
37
B Cdc48 Protein
Normalized Quantity
1.5
1.0
0.5
0.0
**
*
**
WT
48-5
48-6
48-7
48-8
48-9
48-10
C Growth Rate
Doubling Time (h)
5
4
3
2
1
0
**
*
WT
48-5
48-6
48-7
48-8
48-9
48-10

Figure 2.4

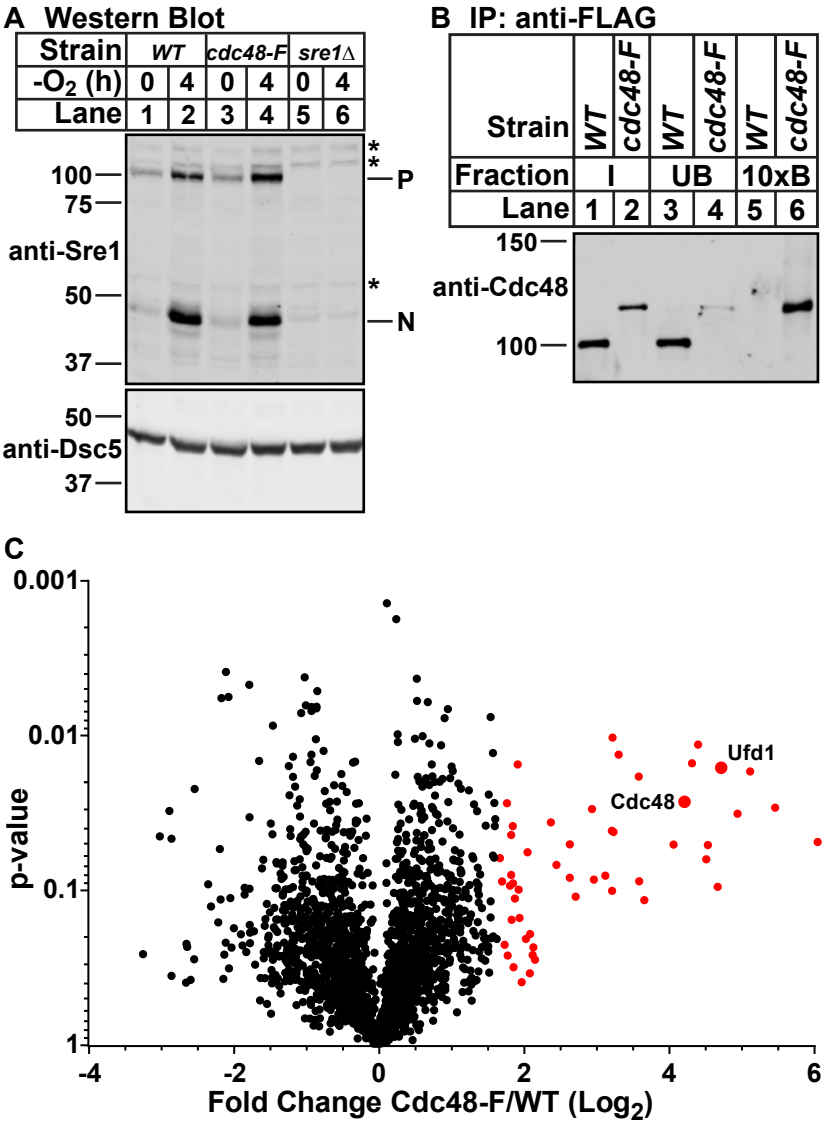
A Western Blot
Strain
WT
cdc48-F
sre1Δ
-O2 (h)
0
4
0
4
0
4
Lane
1
2
3
4
5
6
100
75
anti-Sre1
50
37
*
*
P
*
N
50
anti-Dsc5
37
B IP: anti-FLAG
Strain
WT
cdc48-F
WT
cdc48-F
WT
cdc48-F
Fraction
I
UB
10xB
Lane
1
2
3
4
5
6
150
anti-Cdc48
100
C
0.001
0.01
0.1
1
p-value
Ufd1
Cdc48
-4
-2
0
2
4
6
Fold Change Cdc48-F/WT (Log2)

Figure 2.5

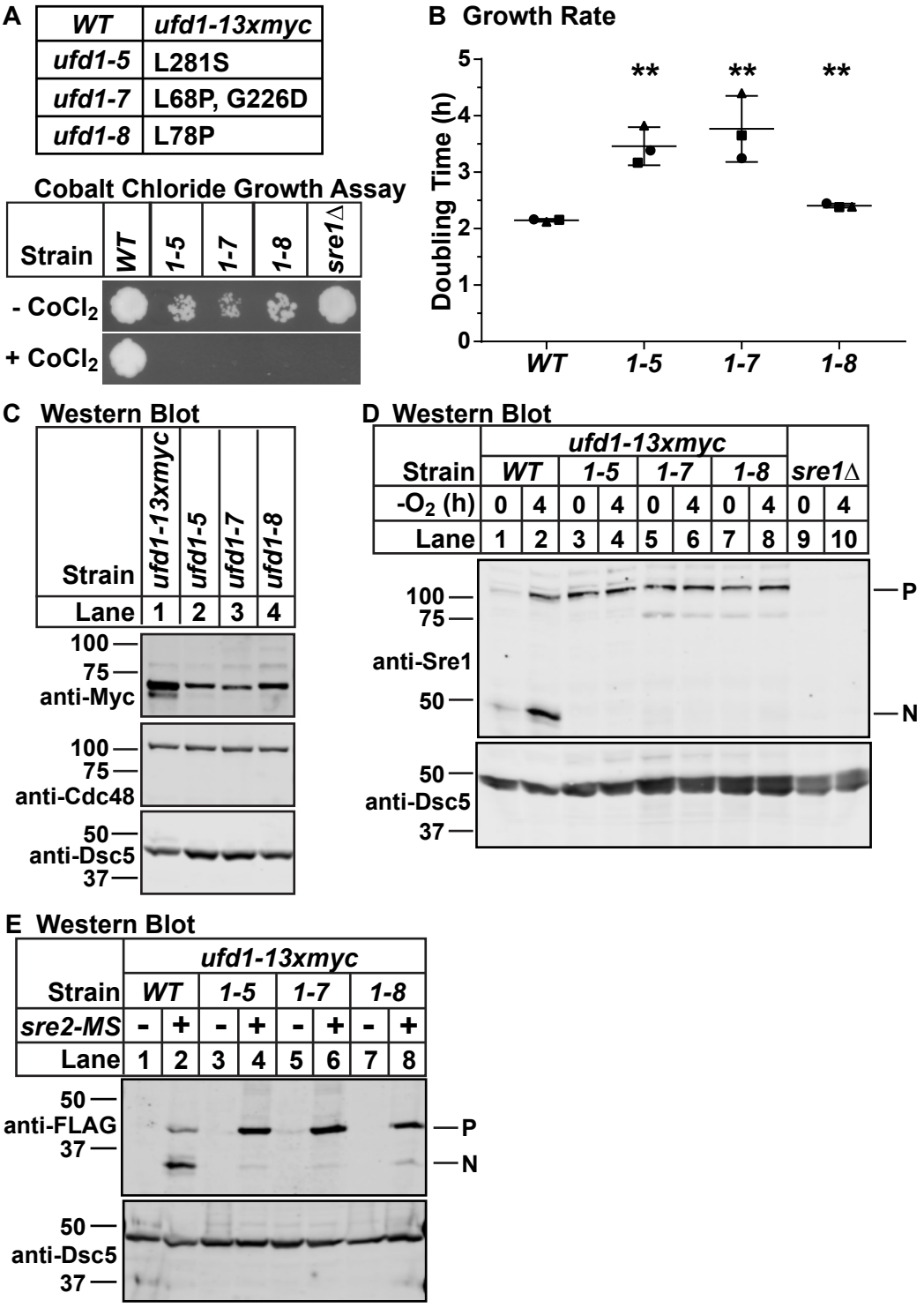
A
WT
ufd1-13xmyc
ufd1-5
L281S
ufd1-7
L68P, G226D
ufd1-8
L78P
Cobalt Chloride Growth Assay
Strain
WT
1-5
1-7
1-8
sre1Δ
- CoCl2
+ CoCl2
B Growth Rate
Doubling Time (h)
0
1
2
3
4
5
**
**
**
WT
1-5
1-7
1-8
C Western Blot
Strain
ufd1-13xmyc
ufd1-5
ufd1-7
ufd1-8
Lane
1
2
3
4
100
75
anti-Myc
100
75
anti-Cdc48
50
anti-Dsc5
37
D Western Blot
Strain
ufd1-13xmyc
WT
1-5
1-7
1-8
sre1Δ
-O2 (h)
0
4
0
4
0
4
0
4
0
4
Lane
1
2
3
4
5
6
7
8
9
10
100
75
anti-Sre1
50
P
N
50
anti-Dsc5
37
E Western Blot
Strain
ufd1-13xmyc
WT
1-5
1-7
1-8
sre2-MS
-
+
-
+
-
+
-
+
Lane
1
2
3
4
5
6
7
8
50
anti-FLAG
37
P
N
50
anti-Dsc5
37

Figure 2.6

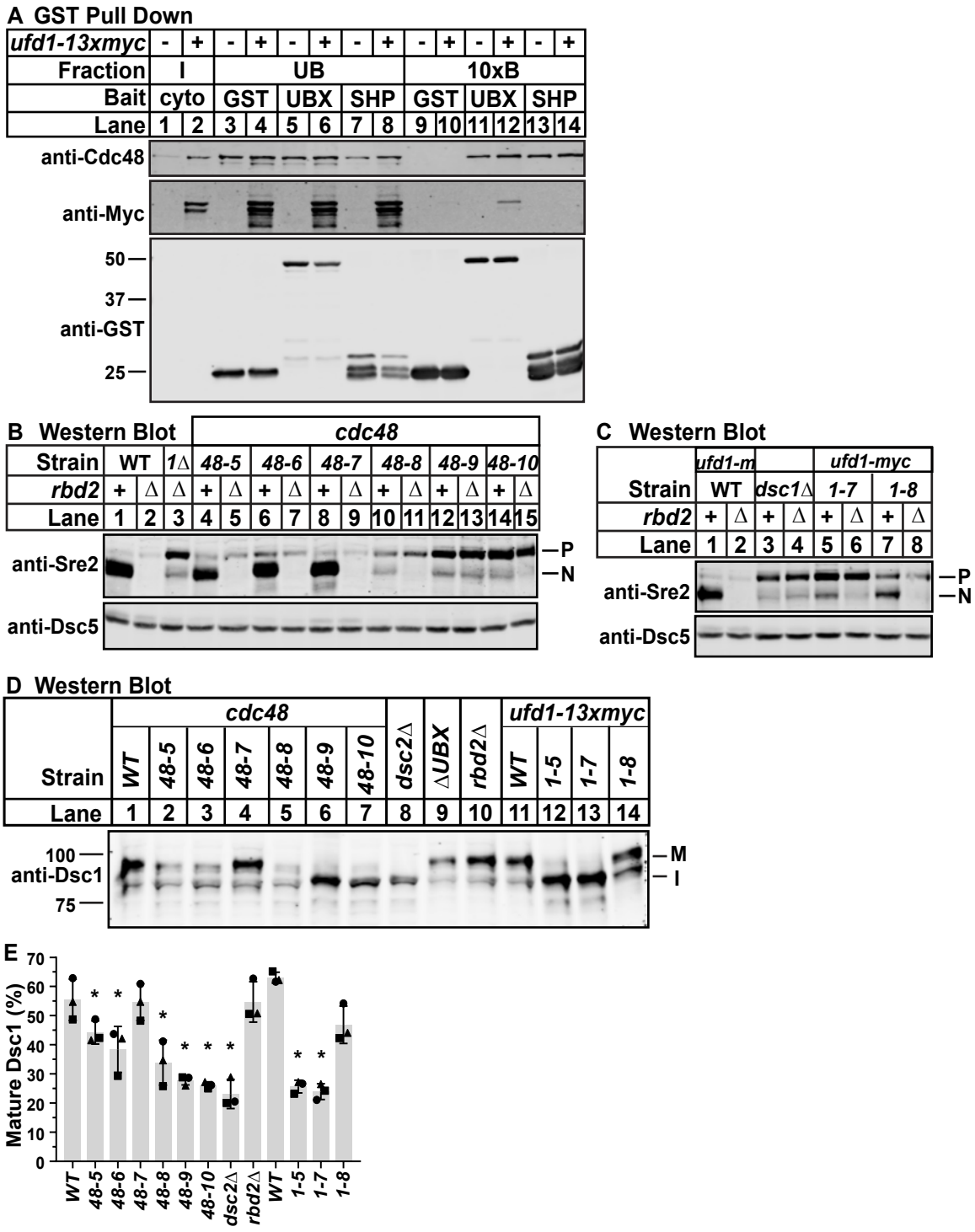
A GST Pull Down
ufd1-13xmyc
Fraction
Bait
Lane
anti-Cdc48
anti-Myc
50
37
anti-GST
25
B Western Blot
cdc48
Strain
rbd2
Lane
anti-Sre2
anti-Dsc5
P
N
C Western Blot
ufd1-myc
dsc1Δ
1-7
1-8
D Western Blot
dsc2Δ
ΔUBX
rbd2Δ
100
anti-Dsc1
75
M
I
E
Mature Dsc1 (%)

Chapter 3

Mga2 transcription factor regulates an oxygen-responsive lipid homeostasis pathway in fission yeast

This chapter is an edited version of the manuscript, "Mga2 transcription factor regulates an oxygen-responsive lipid homeostasis pathway in fission yeast" by R. Burr, E. V. Stewart, W. Shao, S. Zhao, H. K. Hannibal-Bach, C. S. Ejsing, and P. J. Espenshade, published in the Journal of Biological Chemistry, Volume 291, Issue 23, 12171-12183.

3.1 Summary

Eukaryotic lipid synthesis is oxygen-dependent with cholesterol synthesis requiring 11 oxygen molecules and fatty acid desaturation requiring 1 oxygen molecule per double bond. Accordingly, organisms evaluate oxygen availability to control lipid homeostasis. The sterol regulatory element-binding protein (SREBP) transcription factors regulate lipid homeostasis. In mammals, SREBP-2 controls cholesterol biosynthesis, while SREBP-1 controls triacylglycerol and glycerophospholipid biosynthesis. In the fission yeast *Schizosaccharomyces pombe*, the SREBP-2 homolog Sre1 regulates sterol homeostasis in response to changing sterol and oxygen levels. However, notably missing is an SREBP-1 analog that regulates triacylglycerol and glycerophospholipid homeostasis in response to low oxygen. Consistent with this, studies have shown that the Sre1 transcription factor regulates only a fraction of all genes upregulated under low oxygen. Our previous study identified 404 genes that are upregulated under low oxygen but are not Sre1 targets (54). Therefore, additional low oxygen-responsive pathways remain to be discovered. Given that fission yeast adaptation to low oxygen is a model for low oxygen responses in pathogenic fungi, identification of these pathways could highlight novel targets for inhibitors of fungal pathogenesis (125-128).

To identify new regulators of low oxygen adaptation, we screened the *S. pombe* nonessential haploid deletion collection and identified 27 gene deletions sensitive to both low oxygen and cobalt chloride, a hypoxia mimetic. One of these genes, *mga2*, is a putative transcriptional activator. *mga2* has homologs in *S. cerevisiae* that are ER membrane-bound transcriptional activators required for expression of the Δ9 fatty acid desaturase *OLE1* (103,106). In the absence of *mga2*, fission yeast exhibited growth defects under both normoxia and low oxygen conditions. We demonstrate that fission yeast Mga2 regulates a low oxygen-responsive gene expression program distinct from Sre1. Genes regulated by Mga2 include the fatty acid synthases *fas1* and *fas2*, the fatty acid desaturase *ole1*, and the long chain fatty acid CoA ligase *lcf1*, all of which are homologs of SREBP-1 targets in mammals. We also find that *mga2Δ* cells

showed disrupted triacylglycerol and glycerophospholipid homeostasis, most notably with an increase in fatty acid saturation. Indeed, addition of exogenous oleic acid to *mga2Δ* cells rescued the observed growth defects. Together, these results establish Mga2 as a transcriptional regulator of triacylglycerol and glycerophospholipid homeostasis in *S. pombe*, analogous to mammalian SREBP-1.

3.2 Results

Identification of genes required for growth under low oxygen and on cobalt chloride – Adaptation to low oxygen in fission yeast requires the coordinated regulation of many genes (54). The Sre1 transcription factor only regulates expression of 22% of low oxygen-responsive genes, suggesting that additional oxygen-regulated transcription factors exist (54). Successful low oxygen adaptation can be assayed by growth of fission yeast under low oxygen or on the low oxygen mimetic, $CoCl_2$. Indeed, *sre1Δ* cells fail to grow under both of these conditions (68). To identify genes required for hypoxic adaptation we screened 2,601 mutants from the *Schizosaccharomyces pombe* non-essential, haploid deletion collection for growth in these two conditions. We found that 105 gene deletions were sensitive to low oxygen and/or $CoCl_2$, exhibiting reduced growth in these conditions (**Fig. *3.1A***). This included 38 deletion mutants sensitive to only low oxygen (1.5% of all tested gene deletions, **Supplementary Table 3.2**), 40 mutants sensitive to $CoCl_2$ (1.5%, **Supplementary Table 3.3**), and 27 mutants sensitive to both conditions (1.0%, **Table 3.2**). Growth data for the complete screen can be found in **Supplementary Table 3.1**. GO term enrichment analysis of deletions sensitive to both low oxygen and $CoCl_2$ (**Table 3.2**) showed enrichment for genes involved in "retrograde transport, endosome to Golgi" and the retromer complex ($p < 4E\text{-}3$).

Our previous work identified four of the 27 genes required for growth under low oxygen and on $CoCl_2$ as *dsc1-dsc4*, members of the Dsc E3 ligase complex required for Sre1 cleavage in the Golgi (68). Genes required for Sre1 cleavage fail to accumulate the N-terminal transcription

factor (Sre1N) in the absence of oxygen (68). To identify genes functioning in the Sre1 pathway, we assayed low oxygen induction of Sre1N in a number of deletion strains, including the remaining 23 mutants required for growth under low oxygen and on $CoCl_2$ (**Fig. *3.1B* and Table 3.2**). Immunoblotting against the Sre1 N-terminus permits detection of both the full-length precursor form of Sre1 and the transcriptionally active cleaved N-terminus. Wild-type cells showed robust cleavage and Sre1N production after 6 h at low oxygen (**Fig. *3.1B***, lanes 7-8), and four of the deletions sensitive to both low oxygen and $CoCl_2$ (*mga2, cpp1, ppr6, trx2*) showed reduced Sre1N accumulation (**Fig. *3.1B* and Table 3.2**). These deletions represent new candidates for genes required for Sre1 activation in *S. pombe*. The remaining 19 deletions showed normal Sre1N accumulation (**Table 3.2**) and thus are genes that could be involved in low oxygen-responsive pathways distinct from Sre1 target gene transcription.

To test whether a failure to produce Sre1N caused the observed growth defects in the absence of these four genes (*mga2, cpp1, ppr6, trx2*), we expressed *sre1N* from a plasmid and assayed growth on $CoCl_2$. Notably, none of these deletion strains was rescued by *sre1N* expression (**Fig. *3.1C-D***), suggesting that either the Sre1N production defect occurs after cleavage (e.g. Sre1N is highly unstable) or that the deletion mutant is $CoCl_2$-sensitive for reasons unrelated to Sre1N function.

Of the four genes, we focused our studies on *mga2* because Mga2 is a putative transcriptional activator in fission yeast based on homology to two related transcriptional activators in *S. cerevisiae*, *MGA2 and SPT23* (103). Therefore Mga2 was a candidate for a new regulator of a low oxygen response. To confirm that the defect in growth of *mga2*Δ cells on cobalt chloride was not due to the observed Sre1 cleavage defect, we expressed the *sre1N* transcription factor from the endogenous *sre1* locus and assayed transcription factor activity and growth on $CoCl_2$. As with the plasmid-based *sre1N* previously examined, expression of *sre1N* from the endogenous locus did not rescue $CoCl_2$ growth of *mga2*Δ cells (**Fig. *3.1E***). Importantly,

full activation of Sre1 production under low oxygen requires positive feedback regulation in which Sre1 stimulates *sre1* transcription (92). In the absence of *mga2,* Sre1N upregulated its own expression under low oxygen through positive feedback to wild-type levels (**Fig. *3.1F***). These data suggest (1) that *mga2Δ* cells are defective for proteolytic activation of Sre1 precursor, rather than at a step downstream of cleavage, and (2) that the Sre1 cleavage defect cannot fully account for the observed growth defects of *mga2Δ* cells on $CoCl_2$. Based on our interest in the hypoxic transcriptional response and the known function of *S. cerevisiae mga2* homologs as transcriptional activators, we further analyzed the requirement for *mga2* in fission yeast low oxygen adaptation.

Cell growth requires mga2 in the presence and absence of oxygen – To characterize the requirement for *mga2* in response to changes in environmental oxygen, we measured growth in liquid culture of wild-type and *mga2*Δ cells in either the presence or absence of oxygen. *mga2*Δ cells showed significantly reduced growth compared to wild-type cells in both conditions, and further reduced growth in the absence of oxygen compared to the presence of oxygen (**Fig. *3.2A***). Consistent with the observation that functional Sre1N transcription factor does not rescue $CoCl_2$ growth in the absence of *mga2* (**Fig. *3.1E-F***), Sre1N did not rescue either the plus oxygen or minus oxygen liquid growth defects (**Fig. *3.2B***). Given that *sre1*Δ cells exhibit wild-type growth in the presence of oxygen (54), these growth assays demonstrate that *mga2* functions in adaptation to low oxygen and $CoCl_2$ through Sre1-independent pathway(s).

Mga2 functions as a transcriptional regulator of lipid metabolism – Uncharacterized in *S. pombe*, *mga2* is the sole fission yeast homolog of *S. cerevisiae MGA2* and *SPT23. S. cerevisiae MGA2*, but not *SPT23*, is required for low oxygen induction of transcription of the Δ9 fatty acid desaturase *OLE1* and modulates the stability of *OLE1* mRNA in response to fatty acid availability (101,106). *S. cerevisiae* Mga2 also upregulates transcription of other genes involved in fatty acid and sterol homeostasis under oxidative stress, including *ERG1, FAS1, ELO1, FAA4* and *ATF1*

(129). Although a combined deletion of both *MGA2* and *SPT23* in *S. cerevisiae* is lethal, deletion of *mga2* in *S. pombe* was slow growing but viable under normoxia (**Fig. *3.1D, 3.2A***). The low oxygen sensitivity of the *mga2*Δ mutant led us to investigate Mga2-dependent transcription in *S. pombe* under low oxygen.

To determine the transcriptional targets of *S. pombe* Mga2, we performed genome-wide expression profiling under low oxygen. We compared gene expression in *sre1Δ* cells to *sre1Δ mga2Δ* cells after 1.5 h growth in the absence of oxygen. We deleted *sre1* in both strains so that observed changes in gene expression would be due to loss of *mga2*, and not indirect effects of the Sre1 cleavage block that occurs in *mga2Δ* cells (**Fig. *3.1B***). Of the 5,057 genes examined, 291 (5.8%) were significantly decreased in *mga2*Δ cells by SAM. The full list of Mga2-dependent genes can be found in **Supplementary Tables 3.4-3.5**. GO term enrichment analysis of the decreased genes identified fatty acid metabolism and lipid metabolism as affected pathways (p-value <0.0001). **Table 3.3** lists genes that decreased expression at least two standard deviations from the mean in *mga2*Δ cells. These included long-chain fatty acid CoA ligases (*lcf1* and *lcf2*), TAG lipases (*ptl1* and *ptl2*), and the Δ9 fatty acid desaturase (*ole1*). Additionally, Mga2 controls expression of the biotin transporter *vht1* and biotin synthase *bio2*, as well as *hem1*. Biotin is required for acetyl-CoA carboxylase function while heme is a prosthetic group for Ole1 in *S. cerevisiae* (130). While transcriptome profiling for *S. cerevisiae MGA2*-dependent genes under low oxygen conditions has not been performed, homologs of known *S. cerevisiae* Mga2-dependent genes were decreased in our *mga2*Δ cells (**Table 3.3 and Supplementary Table 3.5**). Our microarray results suggest that fission yeast Mga2 regulates many lipid metabolism genes.

To confirm the microarray results, we assayed low oxygen expression of candidate Mga2 target genes in wild-type and *mga2Δ* cells by quantitative real-time PCR. Expression of *ole1*, *lcf1*, *vht1*, *ptl1*, *fas1*, and *fas2* increased in the absence of oxygen, and this induction required *mga2*

(**Fig. *3.3A***). Expression of *ole1, lcf1*, and *fas2* was also reduced even in the presence of oxygen, indicating that *mga2* is required for gene expression both in the presence and absence of oxygen.

To assess the oxygen regulation of all Mga2 targets, we compared our microarray results with known data sets. A previous study in our lab identified *S. pombe* genes upregulated after 1.5 h low oxygen treatment (54). 37% of Mga2 target genes were upregulated under low oxygen in that study (**Supplementary Table 3.5, Fig. *3.3B***). This accounts for 21% of all low oxygen upregulated genes (54). If we consider those genes most dependent on Mga2 (those showing expression reduced more than 2 standard deviations from the mean in the absence of *mga2*), 68% of these genes were upregulated under low oxygen in our previous study (**Table 3.3**, underlined IDs). Only 21% of Sre1 target genes were also regulated by Mga2 under low oxygen, confirming that Mga2 promotes a low oxygen-responsive pathway that is distinct from the Sre1 pathway (**Table 3.3, Supplementary Table 3.5, Fig. *3.3B***) (54). We conclude that *S. pombe* Mga2 regulates lipid metabolism gene expression in the presence of oxygen, and that there is an additional requirement when oxygen is limiting.

Maintenance of lipid homeostasis requires mga2 - We hypothesized that failure to upregulate genes involved in lipid biosynthesis in *mga2Δ* cells may lead to alterations in lipid homeostasis. To measure levels of cellular lipids, we performed quantitative mass spectrometry-based lipidomics on wild-type and *mga2Δ* cells grown in the presence of oxygen (131). We examined cells in the presence of oxygen because oxygen is required for fatty acid desaturation and ergosterol synthesis (132-134), so the absence of oxygen would alter lipid synthesis regardless of strain background. Additionally, Mga2 target genes showed reduced expression in *mga2Δ* cells in the presence of oxygen (**Fig. *3.3A***). Full data and data analysis of this lipidomics experiment can be found in **Supplementary Table 3.6**.

Our lipidomics experiment showed that in *mga2Δ* cells, diacylglycerol (DAG) and TAG levels decreased, while glycerophospholipid levels varied, with PA and PE increasing, PI

decreasing, and PS and CL levels unchanged (**Fig. *3.4A***). Interestingly, these alterations in glycerophospholipids were largely not reflected in the lysophospholipids that are inputs and products of glycerophospholipids. LPC and LPE levels decreased, despite the fact that PC was unchanged and PE levels were higher in *mga2Δ* cells (**Fig. *3.4A***). Although levels of both ceramide and MIPC were unchanged, levels of the intermediate IPC increased in the absence of *mga2* (**Fig. *3.4A***). Levels of ergosterol increased in *mga2Δ* cells, while lanosterol decreased (**Supplementary Table 3.6**).

In the absence of *mga2*, glycerophospholipids decreased in chain length, especially in PC, PA and PE, although PI chain lengths increased slightly (**Fig. *3.4B***). No significant changes occurred in lysophospholipid chain length (**Supplementary Table 3.6**). Decreased acetyl-CoA carboxylase *cut6* and enoyl reductase *tcs13* expression (**Table 3.3**) may play a role in the observed decreases in fatty acid chain length. Taken together, these data demonstrate widespread lipidome disruption in the absence of *mga2*, and thus position this transcriptional activator as a crucial regulator of TAG and glycerophospholipid homeostasis.

Glycerophospholipid saturation increases in the absence of mga2 – MGA2 and *SPT23*, the *S. cerevisiae* homologs of *mga2,* regulate the Δ9 fatty acid desaturase *OLE1* required for fatty acid desaturation. Notably, Mga2 in fission yeast also regulated the Δ9 fatty acid desaturase *ole1* (**Fig. *3.3A***). To determine if decreased expression of *ole1* resulted in altered glycerophospholipid saturation in *mga2Δ* cells, we examined fatty acid saturation in our lipidomics experiment. All glycerophospholipids measured, as well as LPA, LPI, LPE, LPS, DAG, and TAG showed increased saturation in *mga2*Δ cells (**Fig. *3.5A***). Together, these data suggest that even in the presence of oxygen, *mga2Δ* cells exhibit strongly decreased levels of lipid molecules with unsaturated fatty acid moieties.

To test whether the observed plus and minus oxygen growth defects resulted from reduced fatty acid desaturation, we grew wild-type and *mga2Δ* cells in liquid medium

supplemented with monounsaturated oleic acid (18:1) conjugated to BSA (oleic acid), or with BSA alone. Oleic acid is the most abundant unsaturated fatty acid in fission yeast, representing about 75% of all fatty acids in the cell (135). Oleic acid or BSA was added to the media at the 0 h time point and cell density was measured for the following 12 h. Oleic acid addition had no effect on growth of wild-type cells, but rescued growth of *mga2Δ* cells in both the presence and absence of oxygen (**Fig. *3.5B***).

Although the oleic acid-treated *mga2Δ* cells did not reach a density equal to that of wild-type after 12 h, calculation of the cellular growth rates showed rescue. Oleic acid-treated *mga2Δ* cells exhibited a doubling time similar to that of BSA-treated *mga2Δ* cells during the first 6 hours of treatment, but grew like wild-type cells during the second 6 hours of treatment (**Table 3.4**). These data suggest that normal growth of *mga2Δ* cells requires a lag phase, perhaps to allow oleic acid uptake and incorporation into cellular lipids.

To test this hypothesis, we grew wild-type and *mga2Δ* cells under normoxia for 16 hours plus oleic acid, then diluted the cells into fresh oleic acid-containing medium and grew the cells in the presence or absence of oxygen for another 12 hours (**Fig. *3.5C*)**. As expected, preincubation of *mga2Δ* cells with oleic acid eliminated the lag phase and *mga2Δ* cells showed wild-type growth from the 0 hour time point (**Fig. *3.5C* and Table 3.5**). Therefore, we conclude that addition of exogenous oleic acid fully rescues growth defects of *mga2Δ* cells both in the presence and absence of oxygen.

3.3 Discussion

While Sre1 is regarded as the SREBP-2 analog that regulates sterol synthesis in *S. pombe*, no SREBP-1 analog regulating TAG and glycerophospholipid synthesis has been described. Given the results described in this study, we propose that *mga2* is the SREBP-1 analog in fission yeast. Mga2 regulates 21% of all oxygen responsive genes, primarily those involved in TAG and glycerophospholipid homeostasis, including the fatty acid synthases *fas1* and *fas2*, the fatty acid

desaturase *ole1*, and the long chain fatty acid CoA ligase *lcf1* (**Table 3.3, Fig. *3.3A***). This list of Mga2 gene targets is strikingly similar to the known gene targets of mammalian SREBP-1 (8/9 targets conserved, **Supplementary Table 3.5**) (24,136). Further, overall lipid homeostasis, and especially fatty acid saturation, is disrupted in the absence of *mga2,* even under normoxic conditions (**Fig. *3.4***). Therefore, we conclude that Mga2 serves as the analogous transcription factor to SREBP-1 in *S. pombe* by coordinately regulating TAG and glycerophospholipid metabolism.

Multiple lines of evidence support the conclusion that Mga2 regulates this oxygen-responsive transcriptional program independent of the Sre1 pathway. First, transcriptionally active Sre1N did not rescue low oxygen and $CoCl_2$ growth of *mga2Δ* cells (**Fig. *3.1E-F, 3.2B***). Second, *mga2Δ* cells exhibited a growth defect in the presence of oxygen, whereas *sre1Δ* cells have no normoxia growth defects (**Fig. *2A***) (62); Third, Mga2 regulates numerous genes not known to be oxygen-dependent, while Sre1 activity is only required under low oxygen (**Fig. *3.3A-B*, Supplementary Table 3.5**) (54); Finally, comparison of our list of Mga2 low oxygen gene expression targets with the known list of Sre1 expression targets showed only 22% overlap (most notably *csr101, lcf2, fsh2, hmg1*) (**Table 3.3, Fig. *3.3B***). This study positions Mga2 at the head of a new oxygen-responsive pathway in fission yeast.

While this study is the first characterizing the transcriptional regulation of glycerophospholipid and TAG metabolism in fission yeast, glycerophospholipid regulation is much better characterized in *S. cerevisiae*. There, PA signals the glycerophospholipid state of the cell, as all membrane phospholipids and TAG are synthesized from PA. Low levels of membrane PA cause the Opi1 repressor to leave the perinuclear ER membrane and enter the nucleus. There it represses phospholipid synthesis genes to maintain lipid homeostasis (137). Interestingly, there is no known Opi1 homolog in *S. pombe*, raising the question as to whether a different method is used to sense PA availability. Given the high degree of functional conservation between fission

yeast and mammals, studies of phospholipid homeostasis in fission yeast may provide insight into the regulation of this pathway in mammals.

These results support a model for *S. pombe* low oxygen lipid homeostasis in which decreased oxygen availability results in reduced ergosterol synthesis. This activates Sre1, increasing expression of enzymes required for ergosterol synthesis and restoring homeostasis (62). At the same time, low oxygen availability also results in reduced fatty acid desaturation. This activates Mga2, increasing expression of *ole1* and upregulating unsaturated fatty acid synthesis. Interestingly, while both SREBP-1 and SREBP-2 are activated by the same machinery in mammalian cells, Sre1 and Mga2 are not processed coordinately (26). Instead, Sre1 is activated through the function of a Golgi-resident Dsc E3 ligase and a rhomboid protease, while *S. cerevisiae* Mga2 and Spt23 are activated by the Rsp5 ubiquitin ligase and the proteasome (68,108,138). Independent activation of Sre1 and Mga2 is supported by the fact that cells lacking a Dsc E3 ligase component show wild-type normoxic growth unlike *mga2*Δ cells, indicating that the Dsc E3 ligase is not required for Mga2 activation (data not shown).

Despite differing mechanisms of regulation, both of these pathways are likely product inhibited. Work in mammalian cells has shown that SREBP trafficking by Scap is inhibited by exogenous cholesterol, although the parallel experiment cannot be performed in *S. pombe* as fission yeast do not uptake ergosterol (62,139,140). Similarly, work in *S. cerevisiae* showed a block in Mga2 activation when exogenous unsaturated fatty acid was added to the medium (108). Consistent with this result, activation of SREBP-1, but not SREBP-2, is inhibited by addition of exogenous arachidonate (20:4) in HEK293 cells (141). An important next step will be to examine whether unsaturated fatty acids regulate Mga2 through protein levels or activation. Alternatively, there could be other modes of regulation of these genes by oxygen. Our observation that Mga2 activates genes under normoxia and that expression is further increased under low oxygen conditions (**Fig. *3.3A***) suggests that there may be constitutive activation of Mga2 under all oxygen conditions, and that an additional oxygen-responsive transcription factor may cooperate

with Mga2 under low oxygen. Interestingly, a recent report suggested that the CSL transcription factor Cbf11 binds to the promoters of 7 Mga2 target genes in *S. pombe* (142). While *cbf11* is not itself an Mga2 target gene (**Supplementary Table 3.4**), deletion of *cbf11* results in a low oxygen growth defect in our screen (**Supplementary Tables 3.1 and 3.2**), and Cbf11 was found to bind Mga2 in an affinity capture screen for the fission yeast protein interactome network (143). The human homologs of Cbf11, RBPJ and RBPJL, share ~19% protein sequence identity (clustered in the functional domains), raising the possibility that these proteins perform similar functions. These RBP family transcription factors mediate Notch signaling and are required for pancreas development (144,145). It is intriguing to speculate that fission yeast Mga2 and Cbf11 may act together to regulate phospholipid and TAG metabolism in response to low oxygen. More work is required to determine if and how these two transcription factors work together to regulate lipid homeostasis. Because both ergosterol and unsaturated fatty acids require oxygen for synthesis, product inhibition of these two pathways would allow indirect sensing of oxygen availability. Additionally, as membrane production requires coordinated supply of both ergosterol and glycerophospholipids, crosstalk between these two pathways is likely. Future studies will examine coordination of these two oxygen-responsive pathways.

3.4 Experimental procedures

Materials – We obtained general chemicals and materials from Sigma or Fisher. Other sources include: yeast extract, peptone, and agar from BD Biosciences; *S. pombe* haploid deletion collection version 1 from Bioneer; cobalt (II) chloride and amino acid supplements from Roche Applied Sciences; M-MuLV Reverse Transcriptase from New England Biolabs; RNA STAT-60 from Tel-Test; GoTaq qPCR Master Mix from Promega; oligonucleotides from Integrated DNA Technologies; horseradish peroxidase-conjugated, affinity-purified donkey anti-rabbit IgG from Jackson ImmunoResearch; IRDye donkey anti-rabbit and from Li-Cor; prestained protein standards from Bio-Rad; fatty acid free bovine serum albumin from SeraCare Life Sciences.

Antibodies - Rabbit polyclonal antibody against amino acids 1-260 of Sre1 (anti-Sre1 IgG) was generated using a standard protocol as was previously described: we purified the antigen with an N-terminal polyhistidine tag and a tobacco etch virus (TEV) protease cleavage sequence from *E. coli* using Ni-NTA agarose (Qiagen). We then cleaved with TEV protease (Invitrogen) to remove the histidine tag. We isolated Sre1-specific antibodies from rabbit serum by affinity chromatography using NHS-Sepharose resin (Pierce) conjugated to the polyhistidine-tagged Sre1 antigen (62). Specificity of this antibody was assayed by loss of immunoreactivity in a *sre1*Δ strain.

We generated monoclonal antibody 5B4 IgG1κ to Sre1 (aa 1-260) using recombinant protein that was purified from *E. coli* by nickel-affinity chromatography (Qiagen). We immunized BALB/c mice with this antigen and screened for immunoreactivity by ELISA and Western blotting. We fused spleen cells from immunopositive mice with SP2/0 myeloma cells to make monoclonal antibodies. We identified positive clones by ELISA screening using the immunizing antigen. After dilution cloning, antibody specificity was tested by immunoblotting against *S. pombe* extracts from cells overexpressing Sre1. We determined isotype using Mouse Isotyping Kit (Boehringer Mannheim). We purified final antibodies from either tissue culture supernatant or ascites fluid using protein-G Sepharose (Pharmacia).

Yeast culture - Yeast strains are described in **Table 3.1**. *S. pombe* cells were grown to exponential phase at 30°C in rich YES medium [0.5% (w/v) yeast extract plus 3% (w/v) glucose supplemented with 225 μg/ml each of uracil, adenine, leucine, histidine, and lysine (20)]. YES+$CoCl_2$ medium was prepared by dissolving cobalt (II) chloride in H_2O and adding to a final concentration of 1.6 mM in YES medium. For fatty acid supplementation, fatty acids were added to 1 mM in YES medium from a 12.7 mM stock in 12% (w/v) fatty acid free BSA.

BSA conjugation of free fatty acids - Fatty acid free BSA (24% w/v) was made by adding 12 g of fatty acid free bovine serum albumin to 35 mL of 150 mM NaCl in six 2 g doses over 5 h.

pH was adjusted to 7.4 with 5N NaOH and the volume was brought up to 50 mL with 150 mM NaCl. This solution was diluted 1:1 with 150 mM NaCl to produce 12% fatty acid free BSA prior to use as an experimental control.

Fatty acid conjugation to BSA was performed by dissolving 319 μmoles of the conjugating fatty acid in 2 mL EtOH. 100 μl of 5N NaOH was added to precipitate sodium salt of the fatty acid. EtOH was evaporated under nitrogen gas. 10 mL of 150 mM NaCl were added to the dried fatty acid, and the solution was heated until the fatty acid dissolved. The solution was then stirred and slowly cooled to just before the fatty acid precipitated, at which point 12.5 mL of ice-cold fatty acid free BSA (24% w/v) was added. The solution was stirred for 10 min and the final volume was adjusted to 25 mL with 150 mM NaCl.

S. pombe deletion collection screen - The Bioneer Haploid Deletion Mutant Library v1.0 was screened as described previously (21). 2,601 deletion mutants were streaked for single colonies on YES or YES+$CoCl_2$ medium and placed at 30°C in the presence of oxygen. An additional YES plate was grown at 30°C in anaerobic conditions using the BBL GasPak system [Becton Dickson]. Mutants were compared to wild-type and *sre1Δ* strains and scored for growth after 7 days. Full screen results can be found in **Supplementary Table 3.1**.

Sre1 cleavage assay – Cells were grown in YES medium to exponential phase inside an $InVivo_2$ 400 hypoxic workstation [Biotrace, Inc] and collected for protein extraction and immunoblotting as described previously using polyclonal or monoclonal 5B4 anti-Sre1 antibody as indicated (8). SDS-PAGE gels were equally loaded for total protein, which was quantified using the BCA protein assay (Pierce). Consistent loading was confirmed following electroblotting by staining the membrane with Ponceau S. Blots were imaged using enhanced chemiluminescence and film or the Odyssey CLx infrared imaging system [Li-Cor], as noted in the figure legend.

Microarray - Data in **Supplementary Tables 3.4** and **3.5** represent the log2 fold changes in expression between *sre1Δ* and *sre1Δ mga2Δ* cells grown anaerobically for 1.5 h. Microarray analysis was performed as described previously (11). Total RNA was isolated using RNA STAT-60 and amplified and labeled using the RNA Amplification and Labeling Kit [Agilent Technologies] with oligo dT primers [System Bioscience] and cyanine CTPs [Perkin Elmer]. RNA was fragmented, denatured and hybridized to a custom Agilent array at 60°C for 17 h. Two dye-reversal hybridizations were performed with cells cultured on different days (biological replicates), yielding two data points per probe. Arrays were scanned by an Agilent G2505B Scanner and features were flagged using Agilent Feature Extraction Software. These data were imported into Partek Genomics Suite as the median of the arrays' three replicate probes' g/r processed signals. These log2 signal values were quantile normalized and the dye-swapped samples compared in a 1-way ANOVA. Because there were only 2 biological replicates, a pseudo p-value is presented alongside a Significance Analysis of Microarrays (SAM) q-value. SAM parameters were Δ=1.87646, false discovery rate (median) = 0.05447. Mga2-dependent genes showed lower expression in *sre1Δ mga2Δ* versus *sre1Δ* cells. The microarray gene expression data described in this paper have been deposited in NCBI's Gene Expression Omnibus (146) and are accessible through GEO Series accession number GSE60544 (http://www.ncbi.nlm.nih.gov/geo/query/acc.cgi?acc=GSE60544).

Quantitative PCR - Yeast cells (1 x 10^8) growing exponentially in the presence or absence of oxygen were pelleted, resuspended in RNA STAT 60, and vortexed. Samples were mixed with chloroform to 16% (v/v), then centrifuged at 10,000 x *g* for 15 min at 4ºC. The aqueous fraction was mixed with isopropanol to 33% (v/v), then centrifuged at 10,000 x *g* for 10 min. Precipitated RNA was washed with 75% (v/v) EtOH and air-dried. cDNA was synthesized following DNase and reverse transcription instructions for M-MuLV Reverse Transcriptase. RT-qPCR was performed using the indicated primers and GoTaq qPCR Master Mix. Each reaction

was performed with two technical replicates per the five biological replicates. Error bars are one standard deviation.

Lipid extraction - Lipid extraction was performed as described previously (131,147,148). Six biological replicate cultures of wild-type and *mga2Δ* cells growing exponentially in the presence of oxygen (6.8 x 10^7 – 1.3 x 10^8 cells) were pelleted and washed twice in 155 mM ammonium acetate then frozen under liquid nitrogen. Lipids were extracted at 4°C by breaking cell pellet with beads, then 20 internal lipid standards were spiked into the lysate. Samples were subjected to 2-step extraction with chloroform/methanol. The collected lipid extracts were then vacuum-evaporated and dissolved in chloroform/methanol.

Shotgun lipidomics – Mass spectrometry was performed as described previously (131,147,148). Extracts were analyzed on a LTQ Orbitrap XL mass spectrometer (Thermo Fisher Scientific) equipped with the robotic nanoflow ion source TriVersa NanoMate (Advion Biosciences).

Lipidomics data analysis - Lipidomics data analysis was performed as described previously using ALEX software (147,148). Species were annotated using sum composition: <lipid class><total # of C in the fatty acid moieties>:<total # of double bonds in the fatty acid moieties>. Sphingolipids were annotated as <lipid class><total # C in the long-chain base and fatty acid moiety>:<total # of double bonds in the long-chain base and fatty acid moiety>;<total # OH groups in the long-chain base and fatty acid moiety>. Visualization and calculation of mol% values were performed using the commercially available Tableau Software (www.tableausoftware.com). p-values were calculated using a Mann-Whitney U test. p-values were corrected for multiple hypotheses post-hoc using Benjamini and Hochberg False Discovery Rate. The following equations were utilized to calculate the presented mol% values, where n is molar abundance of lipid species i belonging to lipid class j:

$$\text{Mol\% of lipid species per all lipids} = \frac{n_{i,j}}{\sum\sum(n_{i,j})} \times 100$$

Mol% of lipid species per lipid class = $\frac{n_{i,j}}{\sum(n_{i,j})} \times 100$

*Mol% of monounsaturated fatty acids per lipid class =

$$\frac{\sum(n_{i,j} \times \#\text{ double bonds})}{\Sigma(n_{i,j} \times \#\text{ acyl chains per lipid molecule})} \times 100$$

* Calculated based on the fact that that *S. pombe* only synthesizes saturated (SFA) and mono-unsaturated fatty acids (MUFA) (27). In the case where fatty acid saturation was determined, lipid species were hydrolyzed *in silico* prior to normalization (148). For example for triacylglycerol (TAG) 42:2, two of the fatty acid moieties must be monounsaturated and one must be saturated; this is taken into account when tabulating the number of saturated and unsaturated fatty acids across all TAG species. Supplementary **Table 3.6** lists the full results of the lipidomics analysis.

Acknowledgments/Author contributions: We thank J. Hwang for critical reading of the manuscript, C. Talbot for microarray data analysis, and W. Lai and L.C. Hung from the Department of Pathology at UT-Southwestern Medical Center at Dallas for generating monoclonal antibody 5B4 to Sre1. RB conducted the experiments except as noted below, analyzed the results, and wrote the paper. EVS and SZ performed the deletion collection screen and western blots in **Fig. *3.1***. EVS performed the microarray experiment and provided preliminary results for the *mga2*Δ growth curve. WS assisted with qPCR experiments. HKHB and CSE performed the lipidomics experiments and analysis. PJE conceived of the project and wrote the paper. All authors reviewed the results and approved the final version of this manuscript.

3.5 Figures

FIGURE 3.1. **Screen for gene deletions sensitive to low oxygen and cobalt chloride.** *A,* Venn diagram of deletion collection screen results showing overlap between deletions defective for growth under low oxygen and those defective for growth on $CoCl_2$. *B*, Western blots imaged by

film probed with anti-Sre1 IgG of lysates from wild-type cells or the indicated deletion strains grown for 0 or 6 h in the absence of oxygen. P and N denote precursor and cleaved N-terminal transcription factor forms, respectively. Different blots are separated by solid black lines. This experiment was performed one time. *C-E*, Wild-type or the indicated deletion strains carrying empty vector or a plasmid expressing *sre1N (C-D)* or with *sre1N* integrated at the endogenous locus (*E*) were grown as indicated for 4 days. Cells were plated in 10-fold serial dilutions (16 - $1.6x10^6$ cells). Each experiment was performed with at least 2 biological replicates. *F*, Indicated strains were grown for 0 or 4 h in the absence of oxygen, and cell lysates were immunoblotted with monoclonal anti-Sre1 5B4 IgG1κ and imaged by Li-Cor. N denotes Sre1 N-terminal form. This experiment was performed with 3 biological replicates.

FIGURE 3.2. **Sre1N does not rescue *mga2Δ* growth defect.** Indicated strains were grown in liquid culture in the presence or absence of oxygen for 12 h. Cell density was measured by absorbance at 600 nm. Data points are average of three biological replicates. Error bars are one standard deviation (** $p<0.01$ by two-tailed student's t-test for 12 hour time point). *A,* Absorbance at time 0 among the samples ranged from 0.13-0.18. To focus on the difference in growth rate among conditions, we normalized the data for each sample to a value of 0.15 at time-point 0 before averaging. *B*, Absorbance at time 0 among the samples ranged from 0.09-0.16. To focus on the difference in growth rate among the 6 conditions, we normalized the data for each sample to a value of 0.13 at time-point 0 before averaging.

FIGURE 3.3. **Mga2 controls low oxygen gene expression.** *A*, Wild-type and *mga2Δ* cells were grown for 4 h in the presence or absence of oxygen. qPCR analysis was performed for the indicated genes. Error bars are standard deviation of five biological replicates. Two technical replicates were performed per sample. *p-value < 0.05, **p-value < 0.005 by two-tailed student's

t-test. The two graphs represent two independently performed sets of experiments. *B*, Pie chart comparing gene populations from different data sets: anaerobically upregulated genes from Todd *et al*., 2006 (54) reside in the circle; BLUE, Sre1 targets from Todd *et al*., 2006 (54); YELLOW, Mga2 targets from this study (**Supplementary Table 3.5**); GREEN, targets of both Sre1 and Mga2; WHITE, targets of neither Sre1 or Mga2. Mga2 targets that are not anaerobically upregulated are represented in a wedge outside of the circle.

FIGURE 3.4. **Mga2 regulates lipid homeostasis.** *WT* or *mga2*Δ cells were grown to exponential phase in liquid culture in the presence of oxygen. High resolution shotgun lipidomics was performed on six biological replicates (two technical replicates) to quantify the abundances of lipid species in the *S. pombe* lipidome. Full results are available in **Supplementary Table 3.6**. Error bars represent one standard deviation. p-values were calculated using a two-tailed Mann-Whitney U test and corrected for multiple comparisons using Benjamini and Hochberg's method to produce a false discovery rate, q. *q-value < 0.05.

FIGURE 3.5. **Unsaturated fatty acids rescue *mga2Δ* growth defect.** *A*, Saturation of fatty acyl chains in wild-type and *mga2Δ* cells. Saturation of each chain was determined rather than the saturation of a lipid species as a whole (see Experimental Procedures). SFA is saturated fatty acids and MUFA is monounsaturated fatty acids. Error bars are one standard deviation. p-values were calculated using a two-tailed Mann-Whitney U test and corrected for multiple comparisons using Benjamini and Hochberg's method to produce a false discovery rate, q. *q-value < 0.05, **q-value < 0.01. *B-C*, *WT* and *mga2*Δ cells were grown for 12 hours in the presence (red) or absence (blue) of oxygen, with the addition of BSA alone or oleic acid (18:1) conjugated to BSA. Cell density was measured by absorbance at 600nm. Data points are average of three biological replicates. Error bars are one standard deviation. *B,* BSA alone or oleic acid (18:1) was added at

time 0. Absorbance at time 0 among the samples ranged from 0.13-0.18. To focus on the difference in growth rate among the conditions, we normalized the data for each sample to a value of 0.15 at time-point 0 before averaging. The BSA only data are identical to those in **Fig. *2A***. *C*, Oleic acid (18:1) was added 16 hours prior to time 0, then cells were diluted into fresh oleic acid medium at time 0. Absorbance at time 0 among the samples ranged from 0.09-0.14. To focus on the difference in growth rate among the conditions, we normalized the data for each sample to a value of 0.12 at time-point 0 before averaging.

Table 3.1. *S. pombe* strain list

Strains	Genotype	Source	Figure
ED666	*h+ leu1-32 ura4-D18 ade6-M210*	Bioneer Inc.	1
Deletion strains	*h+ leu1-32 ura4-D18 ade6-M210 ∆[GOI]-D1::kanMX4*	Bioneer Inc.	1
KGY425	*h- leu1-32 ura4-D18 ade6-M210 his3-D1*	ATCC	1,2,3,4,5
PEY522	*h- leu1-32 ura4-D18 ade6-M210 his3-D1 ∆sre1-D1::kanMX6*	(Hughes et al., 2005)	1
PEY1762	*h- leu1-32 ura4-D18 ade6-M210 his3-D1 ∆mga2-D1::kanMX6*	This study	1,2,3,4,5
PEY875	*h- leu1-32 ura4-D18 ade6-M210 his3-D1 sre1N*	(Hughes and Espenshade, 2008)	1,2
PEY1763	*h+ leu1-32 ura4-D18 ade6-M210 his3-D1 ∆mga2-D1::kanMX6*	This study	1,2
PEY1764	*h+ leu1-32 ura4-D18 ade6-M210 his3-D1 ∆mga2-D1::kanMX6 sre1N*	This study	1,2

Table 3.2. Gene deletions sensitive to both hypoxia and cobalt chloride

Strains from the Bioneer haploid deletion collection version 1 found sensitive to both hypoxia and cobalt chloride were tested for rescue of the growth defect by exogenous expression of Sre1 N.

[a] Descriptions were obtained from PomBase (www.pombase.org) with some additional hand editing

[b] + indicates accumulation of the Sre1N transcription factor to wild type levels

[c] rescue of $CoCl_2$ growth defect by Sre1N. + indicates rescue, - no rescue, n.d. not determined

Functional category and systematic ID	Common name	Product[a]	Sre1N production[b]	Rescue with Sre1N[c]
DNA repair				
SPAC13C5.07	*mre11*	nuclease	+	n.d.
SPAC644.14c	*rad51*	RecA family recombinase Rad51/Rhp51	+	n.d.
SPCC338.08	*ctp1*	CtIP-related endonuclease	+	n.d.
Transcription				
SPAC17G8.05	*med20*	mediator complex subunit	+	n.d.
SPBC31F10.09c	*nut2*	mediator complex subunit Med10	+	n.d.
SPCC18.06c	*caf1*	CCR4-Not complex CAF1 family ribonuclease subunit	+	n.d.
SPAC26H5.05	*mga2*	IPT/TIG ankyrin repeat containing transcription regulator of FA biosynthesis	-	-
Protein modification				
SPBC947.10	*dsc1*	Golgi Dsc E3 ligase complex subunit	-	+
SPAC1486.02c	*dsc2*	Golgi Dsc E3 ligase complex subunit	-	+
SPAC20H4.02	*dsc3*	Golgi Dsc E3 ligase complex subunit	-	+
SPAC4D7.11	*dsc4*	Golgi Dsc E3 ligase complex subunit	-	+
SPBC4F6.06	*kin1*	microtubule affinity-regulating kinase	+	n.d.
SPCC1919.03c	*amk2*	AMP-activated protein kinase beta subunit	+	n.d.
Protein transport				
SPBC409.20c	*psh3*	ER chaperone (SHR3 homolog)	+	n.d.
Retrograde transport, endosome to Golgi				
SPAC4C5.02c	*ryh1*	GTPase	+	n.d.
SPAPJ696.01c	*vps17*	retromer complex subunit	+	n.d.
SPAC4G9.13c	*vps26*	retromer complex subunit	+	n.d.
SPCC777.13	*vps35*	retromer complex subunit	+	n.d.
Late endosome to vacuole transport				
SPAC1142.07c	*vps32*	ESCRT III complex subunit	+	n.d.
Other				
SPBC12D12.07c	*trx2*	mitochondrial thioredoxin	-	-
SPAC4G8.11c	*atp10*	mitochondrial F1-F0 ATPase assembly protein	+	n.d.
SPCC306.06c	*big1*	ER membrane protein, BIG1 family	+	n.d.
SPAC821.05	*tif38*	translation initiation factor eIF3h	+	-
SPAC17G6.04c	*cpp1*	protein farnesyltransferase beta subunit	-	-
SPBC27B12.10c	*tom7*	mitochondrial TOM complex subunit	+	n.d.
SPCC11E10.04	*ppr6*	mitochondrial PPR repeat protein	-	-
SPBC16A3.03c	*ppr7*	mitochondrial PPR repeat protein	+	n.d.

Table 3.3. *mga2*Δ transcriptional targets hypoxic microarray

[a] Descriptions and homologs were obtained from PomBase (www.pombase.org) with some additional hand editing.

[b] Data are presented as the average changes in expression of genes in *sre1*Δ ("WT") samples after 1.5 hours without O_2 compared to the expression of genes in *sre1*Δ*mga2*Δ ("*mga2*Δ") samples after 1.5 hours without O_2. For clarity, only data greater than 2 standard deviations from the average fold change are presented in this table. Full results are detailed in Supplementary Tables S4-S5.

[c] Statistically significant target assignment from low oxygen microarray in Todd et al, MCB 2006.

[d] Genes showing anaerobic induction in Todd et al, MCB 2006 are underlined.

Functional Category and Systematic ID[d]	Common Name	*S. cerevisiae* Homolog[a]	Product[a]	Log2 Fold Change[b] WT/*mga2*Δ	Sre1 target[c]
Lipid metabolism					
SPAC1B3.16c	*vht1*	*VHT1*	biotin transporter	2.69	-
SPBC18H10.02	*lcf1*	*FAA1,FAA3, FAA4*	long-chain-fatty-acid-CoA ligase	2.66	-
SPCC1450.16c	*ptl1*	*TGL3*	triacylglycerol lipase	2.57	-
SPAC1786.01c	*ptl2*	*TGL4,TGL5*	triacylglycerol lipase	2.32	-
SPAC30D11.11	-	*IZH3*	Haemolysin-III family protein (homolog to adipoQ receptor)	2.31	-
SPAC589.09	*csr101*	*CSR1*	sec14 cytosolic factor family, glycerophospholipid transfer protein	1.69	+
SPBP4H10.11c	*lcf2*	*FAA1,FAA3, FAA4*	long-chain-fatty-acid-CoA ligase	1.79	+
SPCC1281.06c	*ole1*	*OLE1*	acyl-CoA desaturase, ole1	1.74	-
SPCC1235.02	*bio2*	*BIO2*	biotin synthase	1.68	-
SPAC2F3.09	*hem1*	*HEM1*	5-aminolevulinate synthase	1.63	-
SPAC4A8.10	*rog1*	*ROG1*	acylglycerol lipase	1.62	-
SPAC22A12.06c	*fsh2*	*FSH2*	serine hydrolase-like protein	1.61	+
SPBC646.07c	*tsc13*	*TSC13*	enoyl reductase (predicted)	1.60	-
SPAC56E4.04c	*cut6*	*ACC1,HFA1*	acetyl-CoA/biotin carboxylase	1.58	-
Other					
SPBC1778.04	*spo6*	*DBF4*	Spo4-Spo6 kinase complex regulatory subunit	3.19	-
SPBC359.04c	*pfl7*	-	cell surface glycoprotein, DIPSY family	3.05	-
SPAC3G6.05	-	*YOR292C*	Mpv17/PMP22 family protein 1	2.27	-
SPBC359.02	*alr2*	-	alanine racemase	2.18	-
Unknown					
SPAC17A2.02c	-	*TDA4*	DUF887 family protein	2.01	-
SPAC5H10.07	-	-	sequence orphan	1.54	-
SPCP20C8.03	-	-	pseudogene	1.51	-
SPCC1281.08	*wtf11*	-	wtf element Wtf11	1.50	-

Table 3.4. Doubling time of *WT* and *mga2*Δ cells after oleate addition

Doubling times for growth curves shown in Figure 3.5B. Cells were grown in BSA-oleate or BSA alone for 12 hours +/- oxygen. Doubling times calculated using 0 and 6 hour or 6 and 12 hour optical density readings as indicated, using the formula:

$$\text{doubling time} = \frac{\text{culture time} \times \log(2)}{\log(\text{final OD}) - \log(\text{initial OD})}$$

Doubling times are displayed as mean± SD for 3 biological replicates.

		0-6h		6-12h	
Strain	**Oxygen**	**-Oleate**	**+Oleate**	**-Oleate**	**+Oleate**
WT	+	3.1±0.1	2.9±0.2	2.2±0.1	2.1±0.0
WT	-	3.2±0.2	3.1±0.3	2.9±0.0	2.5±0.1
mga2Δ	+	5.8±0.6	5.1±0.4	7.3±0.5	2.8±0.1
mga2Δ	-	7.6±0.2	5.8±0.6	39.2±29.3	3.2±0.0

Table 3.5. Doubling time of *WT* and *mga2*Δ cells after oleate preincubation

Doubling times for growth curves shown in Figure 3.5C. Cells were grown for 16 hours in BSA-oleate under normoxia, then in BSA-oleate for 12 hours +/- oxygen. Doubling times calculated using 0 and12 hour optical density readings as indicated, using the formula:

$$\text{doubling time} = \frac{\text{culture time} \times \log(2)}{\log(\text{final OD}) - \log(\text{initial OD})}$$

Doubling times are displayed as mean± SD for 3 biological replicates.

Strain	Oxygen	dt (h)
WT	+	2.6±0.1
WT	-	2.7±0.2
mga2Δ	+	3.1±0.1
mga2Δ	-	3.1±0.3

Figure 3.1

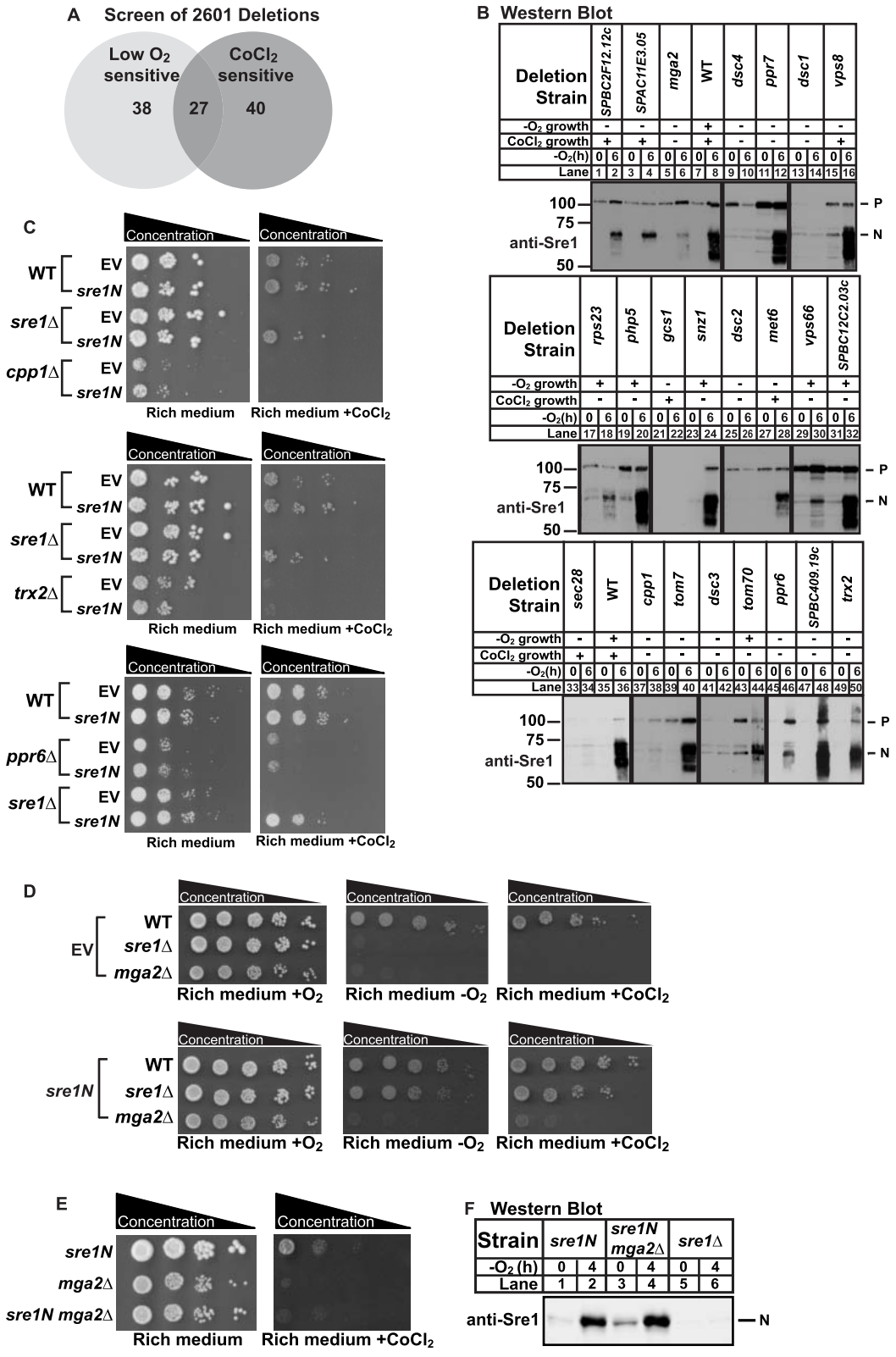
A Screen of 2601 Deletions
Low O2 sensitive
CoCl2 sensitive
38
27
40
B Western Blot
Deletion Strain
SPBC2F12.12c
SPAC11E3.05
mga2
WT
dsc4
ppr7
dsc1
vps8
-O2 growth
CoCl2 growth
-O2(h)
Lane
anti-Sre1
100
75
50
P
N
rps23
php5
gcs1
snz1
dsc2
met6
vps66
SPBC12C2.03c
sec28
cpp1
tom7
dsc3
tom70
ppr6
SPBC409.19c
trx2
C
Concentration
WT
sre1Δ
cpp1Δ
trx2Δ
ppr6Δ
EV
sre1N
Rich medium
Rich medium +CoCl2
D
mga2Δ
Rich medium +O2
Rich medium -O2
E
sre1N mga2Δ
F Western Blot
Strain
sre1N
sre1N mga2Δ
sre1Δ

Figure 3.2

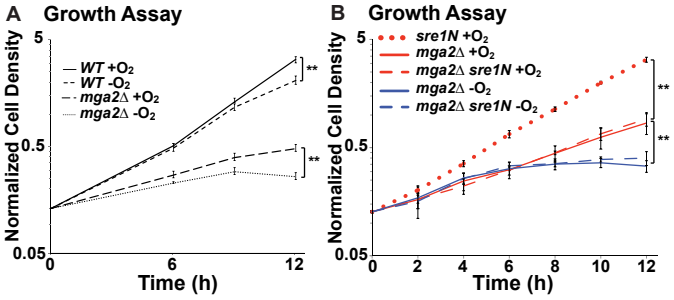
A Growth Assay
Normalized Cell Density
5
0.5
0.05
0
6
12
Time (h)
WT +O2
WT -O2
mga2Δ +O2
mga2Δ -O2
**
**
B Growth Assay
Normalized Cell Density
5
0.5
0.05
0
2
4
6
8
10
12
Time (h)
sre1N +O2
mga2Δ +O2
mga2Δ sre1N +O2
mga2Δ -O2
mga2Δ sre1N -O2
**
**

Figure 3.3

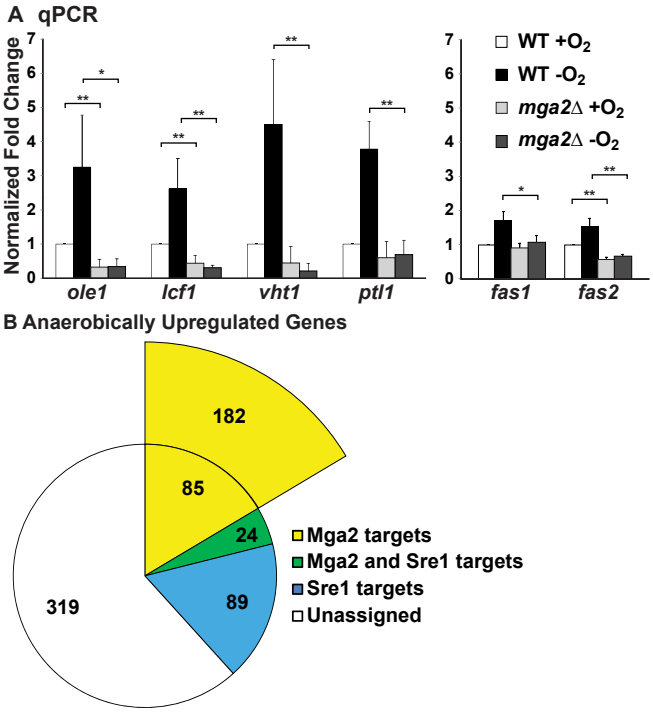
A qPCR
Normalized Fold Change
WT +O2
WT -O2
mga2Δ +O2
mga2Δ -O2
ole1
lcf1
vht1
ptl1
fas1
fas2
B Anaerobically Upregulated Genes
182
85
24
89
319
Mga2 targets
Mga2 and Sre1 targets
Sre1 targets
Unassigned

Figure 3.4

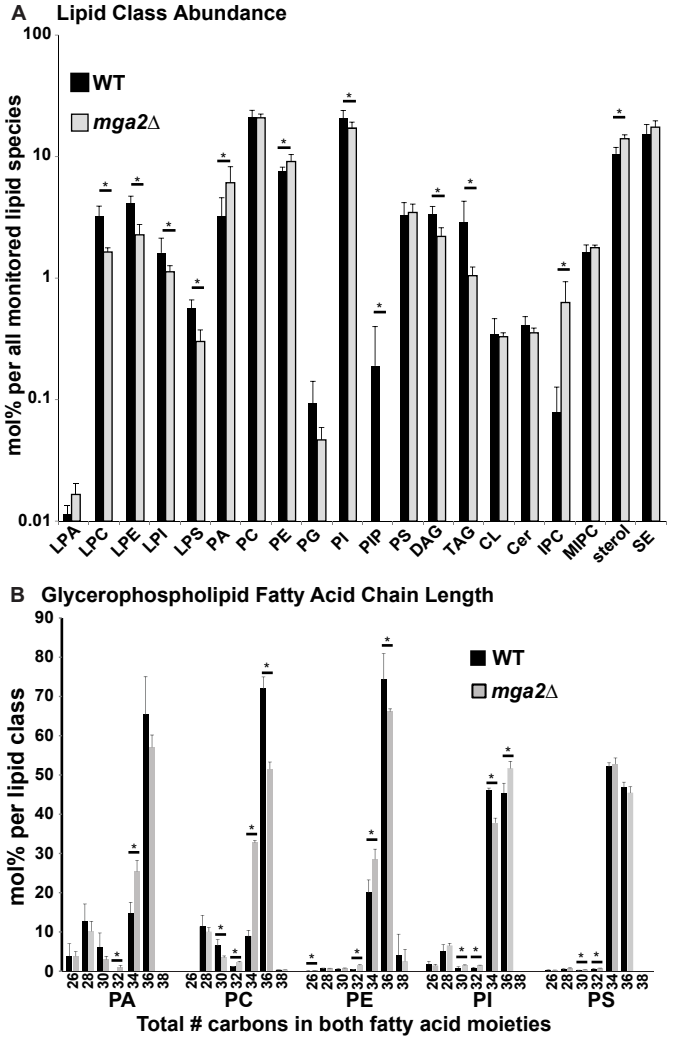
A Lipid Class Abundance
mol% per all monitored lipid species
100
10
1
0.1
0.01
WT
mga2Δ
LPA
LPC
LPE
LPI
LPS
PA
PC
PE
PG
PI
PIP
PS
DAG
TAG
CL
Cer
IPC
MIPC
sterol
SE
B Glycerophospholipid Fatty Acid Chain Length
mol% per lipid class
90
80
70
60
50
40
30
20
10
0
WT
mga2Δ
26 28 30 32 34 36 38
PA
PC
PE
PI
PS
Total # carbons in both fatty acid moieties

Figure 3.5

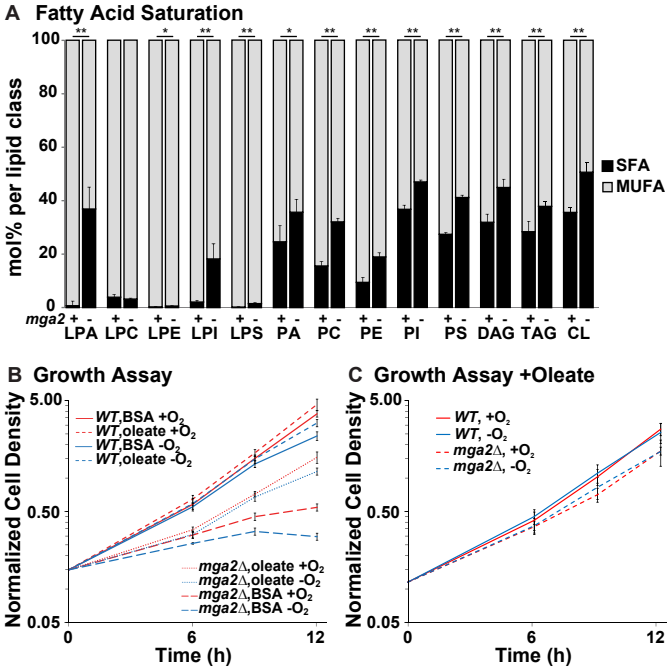
A Fatty Acid Saturation
mol% per lipid class
100
80
60
40
20
0
mga2 + - + - + - + - + - + - + - + - + - + - + - + - + -
LPA LPC LPE LPI LPS PA PC PE PI PS DAG TAG CL
SFA
MUFA
B Growth Assay
Normalized Cell Density
5.00
0.50
0.05
0
6
12
Time (h)
WT,BSA +O2
WT,oleate +O2
WT,BSA -O2
WT,oleate -O2
mga2Δ,oleate +O2
mga2Δ,oleate -O2
mga2Δ,BSA +O2
mga2Δ,BSA -O2
C Growth Assay +Oleate
Normalized Cell Density
5.00
0.50
0.05
0
6
12
Time (h)
WT, +O2
WT, -O2
mga2Δ, +O2
mga2Δ, -O2

Chapter 4

Coordinate regulation of yeast Sterol Regulatory Element-Binding Protein (SREBP) and Mga2 transcription factors

This chapter is an edited version of the manuscript, "Coordinate regulation of yeast Sterol Regulatory Element-Binding Protein (SREBP) and Mga2 transcription factors" by R. Burr, E. V. Stewart, and P. J. Espenshade, published in the Journal of Biological Chemistry, Volume 292, Issue 13, 5311-5324.

4.1 Summary

The Mga2 and Sre1 transcription factors regulate oxygen-responsive lipid homeostasis in the fission yeast *Schizosaccharomyces pombe* in a manner analogous to the mammalian Sterol Regulatory Element-Binding Protein transcription factors SREBP-1 and SREBP-2. Recently, we found that the transcription factor Mga2 regulates triacylglycerol (TAG) and glycerophospholipid (GPL) homeostasis in S. pombe (70). Deletion of *mga2* resulted in broad lipidome disruption, a decrease in fatty acid desaturation, and an Sre1 cleavage defect. Therefore, Mga2 and SREBP-1 regulate triacylglycerol and glycerophospholipid synthesis, while Sre1 and SREBP-2 regulate sterol synthesis. In mammals, a shared activation mechanism allows for coordinate regulation of SREBP-1 and SREBP-2. In contrast, distinct pathways activate fission yeast Mga2 and Sre1. Therefore, it is unclear whether and how these two related pathways are coordinated to maintain lipid balance in fission yeast. Previously, we showed that Sre1 cleavage is defective in the absence of *mga2*. Here, we report that this defect is due to deficient unsaturated fatty acid synthesis resulting in a general membrane transport defect of multiple Golgi proteins. This defect is recapitulated by treatment with the fatty acid synthase inhibitor, cerulenin, and is rescued by addition of exogenous unsaturated fatty acids. We conclude that the Sre1 cleavage defect is due to mislocalization of Sre1 pathway components when fatty acid homeostasis is disrupted. Thus, Sre1 is uniquely positioned to detect changes in membrane fatty acid homeostasis, due to the requirement for ER-to-Golgi transport of multiple Sre1 pathway components as well as positive feedback in the system, which magnifies small changes in Sre1 cleavage. Furthermore, we demonstrate that Mga2 cleavage in *S. pombe* is induced by treatment with cerulenin and inhibited by treatment with proteasome inhibitor. Chemical inhibition of sterol synthesis blocked Mga2-dependent target gene expression. Together, these data demonstrate that Sre1 and Mga2 are each regulated by the lipid product of the other transcription factor pathway, providing a source of coordination for these two branches of lipid synthesis.

4.2 Results

mga2Δ cells have reduced Sre1N accumulation in the presence and absence of oxygen – We previously screened the fission yeast deletion collection to identify regulators of Sre1 and found that *mga2* deletion blocked Sre1 cleavage induction by low oxygen (70). Here, we confirmed this requirement by creating our own *mga2* deletion strain (70). We cultured wild-type (WT), *mga2Δ*, *dsc2Δ*, and *sre1Δ* cells for 0 or 4 h minus oxygen. We then probed a western blot of whole cell lysates with antibody against Sre1N, which detects both the Sre1 inactive membrane-bound precursor form (P) and the cleaved N-terminal transcription factor form (N). As expected, WT cells accumulated cleaved Sre1N after 4 h minus oxygen, and the precursor increased due to Sre1N activation of sre1 transcription through positive feedback regulation (**Fig. *4.1A***, lanes 1-2) (62). In contrast, deletion of the Dsc E3 ligase subunit *dsc2* resulted in a failure to cleave Sre1 (**Fig. *4.1A***, lanes 5-6). As reported, deletion of *mga2* also resulted in a failure to accumulate Sre1N (**Fig. *4.1A***, lanes 3-4), leading to a 4-fold decrease in Sre1N accumulation compared to WT (**Fig. *4.1B***, lane 2 vs 4). To test if Sre1 activation requires *mga2* only under low oxygen, we assayed Sre1 cleavage in the presence of oxygen with addition of the statin drug compactin (CPN) that inhibits HMG-CoA reductase and blocks ergosterol synthesis (149). CPN induces Sre1 cleavage regardless of oxygen availability (62). CPN treatment induced Sre1 cleavage in WT cells, but not *mga2Δ* cells (**Fig. *4.1C-D***). Therefore, we conclude that the Sre1N accumulation defect in the absence of *mga2* is independent of oxygen supply. This is consistent with results from our previous study showing that loss of *mga2* disrupts TAG and GPL homeostasis under normoxic conditions (70).

Defect in Sre1 cleavage in the absence of mga2 is amplified by positive feedback - Interestingly, the Sre1N accumulation defect in *mga2Δ* cells was not as strong as in the control *dsc2Δ*□□□□□□□(**Fig. *4.1B,D***, lane 4 vs 6). Although low oxygen or CPN could not induce Sre1N accumulation in the absence of *mga2*, basal levels of Sre1N in *mga2Δ* cells were close to WT in the presence of oxygen (**Fig. *4.1A-D***, compare lanes 1 and 3). This indicated that in the

absence of *mga2* there was a failure to fully induce Sre1N accumulation rather than a strict block. To further dissect this, we examined Sre1N accumulation in a strain expressing *sre1* from a mutant promoter (sre1-MP) in which Sre1 is not able to activate its own transcription via positive feedback (64). Thus, accumulation of Sre1N in this strain reflects only the rate of Sre1 cleavage and Sre1N degradation. While *mga2Δ* cells showed a 4- to 8-fold decrease in Sre1N accumulation compared to WT cells (**Fig. *4.1A***, lane 2 vs 4, **Fig. *4.2A-B***, lane 2 vs 4), *mga2Δ sre1-MP* cells exhibited only a 1.5-fold decrease in accumulation compared to *sre1-MP* cells (**Fig. *4.2A-B***, lane 6 vs 8). These data indicate that positive feedback to the *sre1* promoter accounts for the majority of the observed difference in Sre1N accumulation, and that *mga2Δ* cells likely fail to accumulate Sre1N to a threshold level that induces maximal *sre1* transcription and positive feedback. Our previous work established that in the absence of *mga2* Sre1 is successfully transcribed, translated, and induces its own transcription when expressed without the membrane-anchoring domain (70). Together, these data show that the defect occurs in a step after Sre1 translation and prior to membrane release of the Sre1N transcription factor, referred to hereafter as the cleavage step.

Cleavage defect in mga2Δ cells occurs at a step downstream of Sre1-Scp1 complex formation and is not specific to Sre1 – We next wanted to further narrow down which step of Sre1 cleavage was defective in *mga2*Δ cells. A major point of regulation for the Sre1 pathway is the formation and ER-to-Golgi transport of the Sre1-Scp1 complex (65). Scp1 senses and responds to changes in sterol synthesis, transporting Sre1 to the Golgi for activation when sterols decrease (68). We showed previously that loss of Scp1 results in degradation of the Sre1 precursor via the Hrd1 E3 ligase (64). In *mga2*Δ cells, we observed wild-type levels of Sre1 precursor (**Fig. *4.1,4.2***) and Scp1 (**Fig. *4.3A***, lane 2). Therefore, low *scp1* expression does not account for the observed Sre1 cleavage defect in *mga2*Δ cells. To test if complex formation between Scp1 and Sre1 was disrupted in *mga2*Δ cells, we assayed Sre1-Scp1 binding. Immunopurification of Scp1-13xMyc recovered Sre1 precursor from *scp1-13xmyc* cells in both the presence and absence of mga2 (**Fig.**

4.3B, lanes 4-5). Together, these data indicate that the Sre1-Scp1 complex forms normally in *mga2*Δ cells.

Previous work in our lab established that Sre1-Scp1 transport to the Golgi for cleavage is regulated both by the rate of ER-to-Golgi transport as well as by the amount of Sre1-Scp1 complex available in the ER (65). That model predicts that increasing Sre1-Scp1 complex concentration will increase Sre1 cleavage as long as no step of the pathway is completely blocked. Consistent with this, overexpressing scp1 in WT cells increased Sre1 cleavage under low oxygen (**Fig. *4.3C***, lanes 1-4) (150). Overexpression of *scp1* in *mga2*Δ cells increased Sre1N to a similar proportion, although overall Sre1N accumulation was not rescued to WT levels (**Fig. *4.3C***, lanes 5-8). As expected, expression of *scp1* in *scp1*Δ cells supported wild-type levels of Sre1 cleavage (**Fig. *4.3C***, lanes 9-12). Thus, overexpression of *scp1* partially rescues the Sre1 cleavage defect in the absence of *mga2*, further demonstrating that there is not a complete block in Sre1 cleavage in *mga2*Δ cells and that Sre1-Scp1 complex formation is normal. However, overexpression of *scp1* in *mga2*Δ cells does not rescue cleavage as well as overexpression of *scp1* in *scp1*Δ cells, suggesting that the overexpressed Scp1 is affected by the same inhibition that blocks endogenous Sre1 cleavage in *mga2*Δ cells. This suggests that the defect in Sre1 activation in *mga2*Δ cells occurs at a step after Sre1-Scp1 complex formation.

Given our observed block in Sre1N accumulation under normoxic conditions and the normal expression and function of Scp1 in the absence of *mga2*, we tested cleavage of the Sre1 homolog Sre2 under normoxic conditions, where Sre2 is constitutively activated independently of Scp1 or sterol levels (62). We cultured *WT*, *mga2Δ*, *dsc2Δ*, and *sre2Δ* cells under normoxia and probed a western blot with antibody against the Sre2 N-terminus (Sre2N). As observed for Sre1, deletion of the Dsc E3 ligase subunit *dsc2* resulted in a failure to cleave Sre2 and accumulation of Sre2 precursor (**Fig. *4.3D***, lane 3). Deletion of *mga2* resulted in an intermediate Sre2 cleavage defect (**Fig. *4.3D*** lane 2) resulting in a 2-fold decrease in Sre2N (**Fig. *4.3E*** lane 1 vs 2).

Therefore we conclude that Sre2 cleavage is also defective in the absence of *mga2*, and that the defect in these cells is not specific to the Sre1-Scp1 complex activity.

Dsc E3 ligase is functional in mga2Δ cells – In addition to Sre1-Scp1 complex formation, Sre1 and Sre2 cleavage both require Dsc E3 ligase activity (68,69). To examine Dsc E3 ligase function in the absence of *mga2*, we first assayed Dsc E3 ligase complex assembly by immunopurifying Dsc2 in WT, *dsc2Δ*, or *mga2*Δ cells in the presence and absence of oxygen (**Fig. *4.4A***). We efficiently purified the Dsc E3 ligase complex from WT, but not *dsc2*Δ cells, and found no difference in complex formation between WT and *mga2Δ* cells in both oxygen conditions (**Fig. *4.4A***, lanes 9-14). This result indicates that Dsc E3 ligase complex assembly is not disrupted in *mga2*Δ cells.

To confirm that the Dsc E3 ligase is not only assembled but also functional, we forced co-localization of the Dsc E3 ligase and Sre1 in the presence and absence of oxygen using Brefeldin A (BFA). In BFA-treated cells, the ER and Golgi compartments mix, the Dsc E3 ligase and Sre1 co-localize, and the Sre1 precursor is degraded in a Dsc-dependent manner (68). To assess function of the Dsc E3 ligase, we assayed Sre1 precursor degradation in *mga2*Δ cells after BFA treatment. As expected, Sre1 precursor decreased upon BFA treatment in WT cells in both the presence and absence of oxygen (**Fig. *4.4B***, lanes 1-2, 7-8). Degradation of Sre1 precursor upon BFA treatment was blocked in *dsc1*Δ cells (**Fig. *4.4B***, lanes 5-6, 11-12), indicating that this Sre1 precursor degradation requires Dsc E3 ligase activity (68). Interestingly, the Sre1 precursor level increased upon addition of BFA in *dsc1*Δ cells (**Fig. *4.4B***, lanes 5-6 and 11-12), suggesting that BFA treatment prevented degradation of Sre1 by multiple mechanisms in *dsc1*Δ cells. Notably, Sre1 precursor was degraded normally in *mga2*Δ cells, demonstrating that the Dsc E3 ligase is functional in *mga2*Δ cells (**Fig. *4.4B***, lanes 3-4, 9-10). Therefore, the Sre1 cleavage defect in the absence of *mga2* is not due to a defect in Dsc E3 ligase activity, suggesting that the defect occurs before Sre1 cleavage at the Golgi, such as during ER-to-Golgi transport of pathway components.

We next tested whether the Dsc E3 ligase complex localizes properly to the Golgi (68). We can monitor Dsc E3 ligase localization by assaying maturation of Dsc1 N-linked glycosylation, which requires transport to the Golgi (73). As previously described, in WT cells transport of the Dsc E3 ligase to the Golgi led to the accumulation of Dsc1 primarily as a slower-migrating, mature glycosylated form by SDS-PAGE (**Fig. *4.4C-D***, lane 1). In contrast, failure to properly assemble the Dsc E3 ligase complex in *dsc2*Δ cells resulted in detection of only the faster-migrating, incompletely glycosylated form due to ER retention of Dsc1 (**Fig. *4.4C-D***, lane 3) (73). In *mga2*Δ cells, Dsc1 existed in both forms, representing accumulation of some incompletely glycosylated protein (**Fig. *4.4C-D***, lane 2). This suggested that the majority of Dsc1 was appropriately glycosylated. However, there was a small decrease in the percentage of Dsc1 that was fully glycosylated compared to WT, suggesting a defect in Dsc E3 ligase transport to the Golgi. These results demonstrate that the Dsc E3 ligase is assembled and functional in the absence of *mga2*, but that there may be a membrane trafficking defect in *mga2*Δ cells.

Membrane transport is disrupted in the absence of mga2 - We wondered if the small change in Golgi localization of the Dsc E3 ligase was due to a general defect in membrane transport caused by the altered lipid composition in *mga2*Δ cells. Lipid homeostasis, especially proper fatty acid saturation, is essential for proper membrane structure and fluidity (151). Defects in lipid homeostasis have wide ranging effects, including altering membrane-bound enzyme function and activating signal transduction pathways (70,152,153). To determine if general membrane transport is deficient in the absence of *mga2*, we visualized localization of the Golgi marker Anp1-GFP and the ER marker Ost1-mCherry. Previous work in our lab showed that Anp1 localized to the ER when ER exit is blocked using a *sar1ts* mutant that is defective in COPII vesicle formation (68,154). Anp1-GFP localized to punctate Golgi structures in 98% of WT cells (**Fig. *4.5A-B***). However, 34% of *mga2Δ* cells exhibited altered Anp1-GFP localization phenotypes, defined as no discernable GFP signal or complete or partial co-localization with Ost1-mCherry in the ER (perinuclear and around the cell periphery) (**Fig. *4.5A-B***). Anp1-GFP

also localized to the vacuole in *mga2Δ* cells (**Fig. *4.5A***). In addition, we observed a 2-fold increase in the ER signal for Ost1-mCherry in *mga2Δ* cells (**Fig. *4.5A,C***).

To determine whether changes in Anp1-GFP and Ost1-mCherry signal were due to changes in protein expression, we probed a western blot of whole cell lysate from these strains with antibodies against GFP, mCherry, and the loading control Dsc2 (**Fig. *4.5D***). In the absence of *mga2* we observed a slight decrease in full-length Anp1-GFP signal and an increase in free GFP (**Fig. *4.5D-E***). This suggests that the vacuolar GFP staining observed by microscopy is free GFP from partially degraded Anp1-GFP. We detected no change in Ost1-mCherry expression (**Fig. *4.5D,F***). This indicates that the observed increase in Ost1-mCherry signal in the ER is due to changes in localization rather than changes in expression. These data demonstrate that localization of the Golgi protein Anp1 and the ER protein Ost1 is altered in the absence of *mga2*. These two proteins are not components of the Sre1 pathway, suggesting that membrane transport is broadly defective in *mga2*Δ cells.

Exogenous oleate addition rescues Sre1 cleavage and general membrane transport in mga2Δ cells - To examine whether the observed Sre1 cleavage and general membrane transport defects in *mga2Δ* cells result from defects in fatty acid homeostasis, we tested whether saturated (SFA) or unsaturated fatty acids (UFA) could rescue Sre1 cleavage in *mga2Δ* cells under low oxygen and CPN treatment. We assayed Sre1 cleavage with the addition of BSA-conjugated stearate (18:0), oleate (18:1), or BSA control. WT cells showed robust cleavage under low oxygen that was unaffected by addition of 18:0, 18:1, or both (**Fig. *4.6A***, lanes 1-5). Addition of 18:1 alone, but not 18:0, rescued Sre1 cleavage under low oxygen in mga2Δ cells (**Fig. *4.6A***, lanes 7-9). Supplementing 18:1 with 18:0 had no additional effect on Sre1 cleavage (**Fig. *4.6A***, lane 10). Similarly, pre-incubation of *mga2*Δ cells with 18:1, but not 18:0, rescued CPN-induced Sre1 cleavage (**Fig. *4.6B***, lane 8). Therefore addition of exogenous oleate is sufficient to rescue the Sre1 cleavage defect in *mga2*Δ cells.

To test whether alterations in fatty acid composition also cause the observed defects in general membrane transport, we examined Anp1-GFP and Ost1-mCherry localization under parallel conditions. Incubation of *mga2*Δ cells with 18:1 or both 18:0 and 18:1 (referred to as 18:X), but not 18:0 alone, significantly restored Golgi localization of Anp1-GFP, reducing the percentage of mutant cells to 14% and 12%, respectively (**Fig. *4.6C-D***). Similarly, all of the fatty acid treatments significantly reduced Ost1-mCherry intensity in the ER, but not to wild-type levels (**Fig. *4.6C,E***). These data suggest that defects in fatty acid homeostasis in *mga2*Δ cells are responsible for the observed Sre1 cleavage and membrane transport defects.

Chemical inhibition of fatty acid homeostasis recapitulates mga2Δ phenotype – After observing rescue of membrane transport and Sre1 cleavage defects by 18:1 in *mga2Δ* cells (**Fig. *4.6A-B***), we wanted to independently test whether fatty acid homeostasis regulates Sre1 cleavage and membrane transport in WT cells. We were unable to genetically modulate expression of the fatty acid desaturase *ole1* by either knock down or overexpression (data not shown), and no Ole1 inhibitor is available. Instead, we treated WT cells with cerulenin (CER), an irreversible fatty acid synthase inhibitor that affects both SFA and UFA homeostasis (21-23). To determine the effects of CER on *S. pombe*, we grew WT cells with CER or DMSO control for 6 h and measured growth (**Fig. *4.7A***). CER inhibited cell division after 3 h of treatment. We then tested the effects of CER on Sre1 cleavage. After 2 h of treatment with CER followed by 4 h of low oxygen treatment without CER, Sre1 cleavage was fully blocked in WT cells (**Fig. *4.7B***). Addition of exogenous 16:1 or 18:1 during the 4 h low oxygen treatment rescued this defect, but exogenous 16:0 or 18:0 did not support full cleavage (**Fig. *4.7C*** compare lanes 11,14 to lanes 10,13). Addition of 18:0 and 18:1 together showed similar cleavage rescue to 18:1 alone (**Fig. *4.7C***, lanes 12,15). Therefore, CER treatment recapitulates the Sre1 cleavage defect and exogenous 18:1 rescues Sre1 cleavage as observed in mga2Δ cells.

We next examined Golgi localization of Anp1-GFP after 3 h of CER treatment. Anp1-GFP localized to punctate Golgi structures in 99% of control WT cells (**Fig. *4.7D-E***, -CER

treatment). However in CER-treated cells, 75% of cells showed altered Anp1-GFP localization (**Fig. *4.7D-E***, BSA treatment). Addition of exogenous 18:0 had no effect on Anp1-GFP localization, while addition of 18:1 or both 18:0 and 18:1 partially rescued Anp1 localization to the Golgi (**Fig. *4.7D-E***). Treatment of cells with cerulenin increased Ost1-mCherry signal 2-fold, and only addition of both 18:0 and 18:1 significantly reduced Ost1-mCherry signal in the ER (**Fig. *4.7D,F***). These data demonstrate that fatty acid homeostasis regulates both membrane transport and Sre1 cleavage in WT cells.

Inhibition of sterol synthesis blocks Mga2 transcription factor activity – Having established that products of the Mga2 transcription factor pathway regulate Sre1 activity, we wanted to test whether products of the Sre1 pathway, namely sterols, regulate Mga2 cleavage and activity. To develop an Mga2 cleavage assay in fission yeast, we N-terminally tagged *mga2* at the *his3* locus with *2xFLAG* to create a construct that allows detection of the full-length, precursor form and the cleaved, active N-terminal transcription factor form. To characterize the function of this fusion protein, we treated WT and *2xFLAG-mga2* cells with the proteasome inhibitor bortezomib (BZ) or cerulenin (CER) and examined Mga2 processing by western blot. Treatment of cells with BZ resulted in a strong accumulation of the precursor form and a slower migrating form of the Mga2 N-terminus that may represent an ubiquitylated species seen in *S. cerevisiae* (108). Conversely, treatment with CER induced Mga2 N-terminus accumulation and decreased the precursor form (**Fig. *4.8A***). These results were consistent with data in *S. cerevisiae* showing that the proteasome is required for Mga2 cleavage and that Mga2 activation is regulated by unsaturated fatty acids (108,155).

To test whether sterols have an effect on Mga2 cleavage and activity, we treated *2xFLAG-mga2* cells with the statin CPN or the lanosterol 14α-demethylase inhibitor itraconazole (ITR) alongside CER and BZ treatment controls, and we assayed Mga2 processing and target gene expression. CPN and ITR treatment caused accumulation of both the Mga2 precursor and N-terminal transcription factor, but the ratio of the two forms remained the same (**Fig. *4.8B***, lanes 3-

5). While the overall amount of Mga2 protein appears to change among these different treatments, there was no change in *mga2* expression (**Fig. *4.8B-C***), indicating that the increase in Mga2 protein results from a post-transcriptional mechanism. Importantly, treatment with of *2xFLAG-mga2* cells with CPN induced Sre1 cleavage to the same level as WT cells (**Fig. *4.8B***, lane 2 vs 4), confirming that this tagged protein is functional. Consistent with the observed changes in Mga2 N-terminus accumulation, CER treatment induced expression of the Mga2 target genes *ole1* and *vht1*, while treatment with BZ reduced expression to levels seen in *mga2Δ* cells (**Fig. *4.8D,E***) (70). Interestingly, despite the increase in Mga2 N-terminus accumulation in CPN and ITR treated cells, *ole1* expression was reduced to the basal level seen with BZ treatment (**Fig. *4.8D***). Likewise, inhibition of sterol synthesis reduced vht1 expression (**Fig. *4.8E***). These data demonstrate that the *2xFLAG-mga2* fusion protein is functional, and that Mga2 activation is regulated by fatty acids and requires the proteasome in *S. pombe*. Furthermore, Mga2 transcriptional activity requires sterol synthesis.

4.3 Discussion

Taken as a whole, the data in this study show that unsaturated fatty acids regulate Sre1 transcription factor activation in *S. pombe*. Disrupting fatty acid homeostasis, either through deletion of the *mga2* transcription factor, which regulates fatty acid desaturation and TAG and GPL synthesis, or through treatment with the fatty acid synthase inhibitor CER, blocked induction of Sre1 cleavage by sterols or low oxygen (**Fig. *4.1*, Fig. *4.7B***) (70). Importantly, the Sre1 cleavage defects in both *mga2Δ* and CER treated cells were rescued by addition of exogenous 18:1, indicating that UFA regulate Sre1 cleavage and that a defect in fatty acid homeostasis is responsible for the Sre1 cleavage defect (**Fig. *4.6A-B*, Fig. *4.7C***). Interestingly, the Sre1 cleavage defect that results from CER treatment of WT cells was more fully rescued by UFA than that observed in the absence of *mga2* (**Fig. *4.6A-B* vs Fig. *4.7C***). This is likely due to

the fact that CER specifically inhibits fatty acid synthesis, while *mga2* regulates a number of other lipid homeostasis pathways (70).

Multiple lines of evidence indicate that SREBP cleavage is disrupted due to a kinetic defect in the membrane transport component of the SREBP activation pathway when fatty acid homeostasis is disrupted. First, the observed Sre1 cleavage defect is largely a failure to induce cleavage under low oxygen conditions and is magnified by positive feedback within the system (**Fig. *4.1, 4.2***), suggesting that the disruption in the absence of *mga2* is incomplete and therefore more likely a kinetic defect than a complete block in cleavage. Second, overexpression of the Sre1 binding and trafficking partner *scp1* increased Sre1 cleavage in *mga2Δ* cells to a similar extent as WT cells, suggesting the Sre1 cleavage defect in these cells can be bypassed and occurs at a step after Sre1-Scp1 complex formation (**Fig. *4.3C***). Third, the Sre1 homolog Sre2 also exhibited a cleavage defect in the absence of *mga2*, indicating a shared deficiency between these two pathways, which do not share Scp1 (**Fig. *4.3D-E***). Fourth, the Dsc E3 ligase was functional in *mga2Δ* cells, supporting the existence of a defect prior to cleavage at the Golgi and narrowing the defective step to transport of pathway components (**Fig. *4.4***). Finally, *mga2* deletion or treatment of WT cells with the fatty acid synthesis inhibitor CER altered the localization of the Golgi-resident protein Anp1 and the ER-resident protein Ost1 (**Fig. *4.5*, Fig. *4.7D***) indicating a general membrane transport defect when fatty acid homeostasis is disrupted. Both the Sre1 cleavage defects and the Anp1/Ost1 localization defects were rescued by addition of unsaturated fatty acid (**Fig. *4.6*, Fig. *4.7***). It is probable that the other components of the SREBP activation pathway are affected by these same membrane transport defects. Interestingly, the rescue of the Sre1 cleavage defect with exogenous 18:1 was more robust than the rescue of Anp1 and Ost1 localization (**Fig. *4.6, 4.7***). These observations suggest that both the defects and rescue observed for membrane transport in these systems are small, but that they have a large effect on Sre1 N-terminal accumulation. This is consistent with our observation that positive feedback in the system amplifies the small defect in membrane transport, and that in the absence of this positive

feedback Sre1 cleavage only decreases 1.5-fold (**Fig. *4.2***). Alternatively, if multiple Sre1 pathway components are negatively affected by the membrane transport defect, then small improvements in transport of all of those pathway components could combine to produce a larger improvement in Sre1 cleavage. We favor a model that incorporates both of these possibilities. Together, these data suggest that the observed Sre1 cleavage defects are due to membrane transport defects.

While this study did not identify the precise step in membrane transport affected by fatty acid supply, membrane dynamics are highly sensitive to the lipid composition of the cell and alterations in lipid composition have wide-ranging effects, including on protein trafficking. Generally, increased saturated phospholipids, sterols, and sphingolipids result in more tightly packed, less fluid membranes, while phospholipid desaturation results in less densely packed, more fluid membranes (151). One possible source of the observed membrane transport defect that affects Sre1 and Sre2 cleavage is during COPII vesicle budding from the ER. Liposomes composed of diunsaturated glycerophospholipids form more COPII vesicles *in vitro* than liposomes composed of monounsaturated glycerophospholipids (156). This suggests that increasing saturated phospholipids reduces vesicle budding. Consistent with our study, treatment of *S. cerevisiae* with cerulenin blocked secretory protein transport from the transitional-ER to the Golgi (157). Membrane curvature and saturation are also important for vesicle targeting to the appropriate cellular compartment. Diunsaturated phospholipids with bulky headgroups favor membrane curvature, while sterols disfavor curvature (13). In mammalian cells, small artificial liposomes containing diunsaturated phospholipids bound to the Golgi more strongly than liposomes containing monounsaturated or saturated phospholipids, and binding also decreased with increasing liposome size (158). Because the Dsc E3 ligase showed some accumulation in the ER, *mga2Δ* cells are most likely defective in ER exit, although we cannot rule out additional effects on vesicle targeting and fusion to the Golgi.

In our previous report, we highlighted similarities between Mga2 and Sre1 regulation of lipid homeostasis in fission yeast and SREBP-1 and SREBP-2 regulation of lipid homeostasis in mammalian cells. Both Mga2 and SREBP-1 regulate TAG and GPL biosynthesis, most notably through the regulation of stearoyl-CoA desaturases (*ole1* in *S. pombe* and *SCD1* in mammals) (70,159). Likewise both Sre1 and SREBP-2 regulate sterol biosynthesis (62,160). Although regulation of mammalian SREBPs by sterols is well understood, how fatty acids regulate SREBPs is less clear (161-164). On the one hand, reports suggest that exogenous polyunsaturated fatty acids negatively regulate SREBP-1 cleavage (141,165-167). Another study showed that exogenous 18:1 does not impact SREBP cleavage under normal culture conditions, but rather potentiates inhibition of cleavage by exogenous sterols (168). On the other hand, others report a failure to induce SREBP-1 in the absence of SCD1, indicating that fatty acid desaturation is required for SREBP-1 activation (159). It will be important to continue this line of inquiry in the mammalian system to better understand the regulation of SREBPs by fatty acids and glycerophospholipids.

Membrane fluidity affects multiple cellular functions ranging from secretion to apoptosis (169). Programmed co-regulation and coordination of sterol synthesis and TAG/GPL synthesis is necessary for maintenance of membrane fluidity. Despite parallels between the mammalian and yeast pathways, a crucial difference exists in how these cells coordinate sterol and TAG/GPL synthesis. In mammalian cells, SREBP-1 and SREBP-2 are activated by the same proteases and have a shared requirement for ER-to-Golgi transport by the Scp1 homolog SCAP, providing an opportunity for strict balance of these related metabolic pathways (160). In contrast, although both Mga2 and Sre1 are synthesized as membrane-anchored proteins, their mechanisms of activation are distinct, raising the question of how their activities are coordinated.

Given the results presented here, we propose that regulation of Sre1 cleavage by unsaturated fatty acids (the products of Mga2 activity) and regulation of Mga2 cleavage by sterols (the products of Sre1 activity) is one mechanism for coordinating these two interdependent

pathways in fission yeast (**Fig. *4.9***). Coordination of the oxygen-responsive pathways at the transcription factor level would efficiently maintain cellular metabolic homeostasis, especially given the requirement for acetyl-CoA in lipid biosynthesis. Additionally, coordination of sterol levels with biosynthesis of their strongest membrane interactor, sphingolipids, is crucial to maintain membrane homeostasis (170). Interestingly, Covino *et al.* showed that sterols increased membrane order and stabilized *S. cerevisiae* Mga2 in an active conformation *in vitro* (110). In *S. pombe*, we observed an accumulation of Mga2 protein when sterol synthesis was inhibited with CPN or ITR (**Fig. *4.8B***). However, rather than induce expression of Mga2 target genes, CPN and ITR inhibited *ole1* and *vht1* expression to levels seen in *mga2*Δ cells (**Fig. *4.8D-E***) (70). Thus, Mga2 activity requires sterol synthesis. Understanding how sterols regulate Mga2 activity and protein levels will be the focus of future studies.

Collectively, these results outline a model in which both Mga2 and Sre1 are feedback inhibited by their respective products, but are also regulated by products of the other pathway (**Fig. *4.9***). In this way, both arms of lipid synthesis communicate and the pathways can act in balance. While our results suggest that crosstalk exists, further studies are needed to demonstrate the role for this regulatory network in physiological control of lipid homeostasis.

4.4 Experimental procedures

Materials – General chemicals and materials were obtained from Sigma or Fisher. Other sources include: yeast extract, peptone, and agar from BD Biosciences; digitonin from EMD Chemicals; Brefeldin A, Compactin, Itraconazole, Cerulenin, Igepal CA-630 (NP-40), amino acid supplements, and 1X protease inhibitors (PI) (10 μg/ml leupeptin, 5 μg/ml pepstatin A, 0.5 μM PMSF) from Sigma; bortezomib from LC Laboratories; alkaline phosphatase (Cat #713023) and complete EDTA-free PI from Roche Applied Sciences; M-MuLV Reverse Transcriptase from New England Biolabs; RNA STAT-60 from Tel-Test; GoTaq qPCR Master Mix from Promega; oligonucleotides from Integrated DNA Technologies; horseradish peroxidase-conjugated,

affinity-purified donkey anti-rabbit and anti-mouse IgG from Jackson ImmunoResearch; IRDye donkey anti-rabbit and donkey anti-mouse from Li-Cor; Myc monoclonal 9E10 IgG and β-actin monoclonal C4 IgG from Santa Cruz Biotechnology, Inc; anti-Myc polyclonal IgG (#06-549) from Upstate Biotechnology; anti-FLAG M2 monoclonal IgG from Sigma (F1804); anti-GFP monoclonal IgG from Roche (1814460); anti-mCherry polyclonal IgG from Invitrogen (PA5-34974); prestained protein standards from Bio-Rad; protein G magnetic beads from NEB; protein A Sepharose from GE; fatty acid free bovine serum albumin (BSA) from SeraCare Life Sciences.

Antibodies - Rabbit polyclonal antibody anti-Sre1 IgG (aa 1-260) was generated using a standard protocol as described previously (62). Briefly, antigen was expressed in E. coli and affinity purified by an N-terminal polyhistidine tag. Sre1-specific antibodies were isolated from rabbit serum by affinity to the polyhistidine-tagged Sre1 antigen. Specificity of this antibody was assayed by loss of immunoreactivity in an sre1Δ strain. We generated rabbit polyclonal antibody anti-Sre2 IgG (aa 1-426) using a standard protocol as described above for anti-Sre1 (62).

We generated monoclonal antibody 5B4 IgG1κ to Sre1 (aa 1–260) as described previously using recombinant protein that was purified from E. coli by nickel-affinity chromatography (Qiagen) and injected into BALB/c mice (70). Antibody specificity was tested by immunoblotting against S. pombe extracts from cells overexpressing sre1.

Generation of polyclonal antibodies to Dsc E3 ligase complex members 1-5 (Dsc1-Dsc5) was described previously (68,69). Hexa-histidine tagged recombinant protein antigens, Dsc1 (aa 20-319), Dsc2 (aa 250-372), Dsc3 (aa 1-190), Dsc4 (aa 150-281), and Dsc5 (aa 251-427) were purified from E. coli using Ni-NTA (Qiagen). Dsc1-5 antisera were generated by Covance using a standard protocol. Horseradish peroxidase (HRP) conjugation of Dsc2-Dsc5 antisera was prepared using the Thermo Scientific (Pierce) EZ-link Plus Activated Peroxidase kit, according to the manufacturer's protocol. HRP conjugation of Dsc1 antiserum was performed using the One-Hour Western Detection System (GenScript).

Monoclonal antibodies to 6xHis-Scp1 (aa 446–544) were made using recombinant protein that was purified from E. coli by nickel-affinity chromatography (Qiagen) as previously described (150). Antibody specificity of the final clones was tested by immunoblotting against S. pombe extracts from cells overexpressing scp1. 8G4C11 (IgG1k), 1G1D6 (IgG2ak), and 7B4A3 (IgG1k) were mixed for western blotting.

Antiserum to Cdc48 was the kind gift of R. Hartmann-Petersen (University of Copenhagen) (122).

Yeast culture – Yeast strains are described in **Table 4.1**. *S. pombe* were cultured to exponential phase at 30°C in rich YES medium [0.5% (w/v) yeast extract plus 3% (w/v) glucose supplemented with 225 µg/ml each of uracil, adenine, leucine, histidine, and lysine (171)] unless otherwise indicated. For fatty acid supplementation, fatty acids were added to 1 mM in YES medium from a 12.7 mM stock in 12% (w/v) fatty acid free BSA. Fatty acids were conjugated to fatty acid free BSA as described previously (70). Brefeldin A was added from a stock concentration of 5 mg/mL EtOH to a final concentration of 100 µg/mL in 2% EtOH. Compactin was added to a final concentration of 200 µM from a 10 mM stock in 6% EtOH, 20 mM NaCl. Cerulenin was added to a final concentration 112 nM in media from a 1000x stock in DMSO.

Sre1 cleavage assay - Cells were grown in YES medium to exponential phase inside an InVivo2 400 hypoxic workstation [Biotrace, Inc] and harvested for protein extraction and immunoblotting. Cell pellets were resuspended in 17 µl 1.85 M NaOH/7.4% (v/v) BME and vortexed. Samples were incubated on ice for 10 min. TCA was added to a final concentration of 30% (w/v) and the samples were vortexed and incubated on ice for 10 min. Lysate was centrifuged at 20,000 x g for 10 min at 4°C and pellet was washed with cold acetone. Samples were centrifuged at 20,000 x g for 5 min at 4°C and dried completely under vacuum. Pellets were resuspended in 150 µl SDS lysis buffer [1% SDS, 150 mM NaCl, 50 mM Tris-HCl pH 8.0, 1x protease inhibitors] and sonicated 10 s. Protein was quantified using the BCA protein assay (Pierce). For alkaline phosphatase treatment, lysate was diluted at least 1:2 in 50 mM Tris-HCl

pH 8.0, then alkaline phosphatase was added to 20% (v/v). Samples were incubated at 37°C for 1 h. SDS-polyacrylamide gels were loaded evenly for total protein, and consistent loading was confirmed following electroblotting by staining the membrane with Ponceau S. Blots were imaged using enhanced chemiluminescence and film or the Odyssey CLx infrared imaging system [Li-Cor] as noted in the figure legends.

Dsc2 immunoprecipitation - Exponentially growing cells (5 x 10^8) were subjected to co-immunoprecipitation as described previously (172). Briefly, cell pellets were resuspended in 200 µl digitonin lysis buffer [50 mM HEPES pH 6.8, 50 mM KOAc, 2 mM MgOAc, 1 mM CaCl2, 200 mM sorbitol, 1 mM NaF, 0.3 mM Na3VO4, 1% (w/v) digitonin, 2x PI, 1x Complete EDTA-free PI]. Cells were lysed by bead beating for 10 min at 4°C, then beads were washed with 800 µl digitonin lysis buffer to collect all lysate. Lysate was incubated with rotation for 40 min at 4°C then centrifuged for 10 min at 100,000 x g to pellet insoluble material. 1.3 mg of supernatant protein was incubated with 10 µl anti-Dsc2 antiserum for 15 min then incubated with 80 µl Protein A Sepharose beads overnight at 4°C. Beads were washed 3x with digitonin lysis buffer and the bound fraction was eluted into SDS lysis buffer + 1x PI and 1x loading dye [30 mM Tris-HCl, 3% SDS, 5% glycerol, 0.004% BPB, 2.5% 2-mercaptoethanol] at 95°C for 5 min.

Dsc1 glycosylation assay - Exponentially growing cells (2.5 x 108) were collected and resuspended in 300 µl B88 buffer [20 mM HEPES pH 7.2, 150 mM KOAc, 5 mM Mg(OAc)2, 250 mM sorbitol] + 1X protease inhibitors, 1x Complete EDTA-free PI. Cells were lysed using glass beads for 12 min then centrifuged for 5 min at 500 x g to clear cell debris. The supernatant was centrifuged at 20,000 x g for 20 min, and the pelleted membranes were resuspended in 100 µl B88 buffer with 1% NP-40 (v/v). The membranes were solubilized at 4ºC for 1 h, then samples were centrifuged at 20,000 x g for 20 min and the supernatant was collected as detergent-solubilized membrane. Loading dye was added and samples were incubated at 37ºC for 1 h before running an SDS-PAGE gel. At no time were samples boiled as Dsc1 aggregates at high temperature.

Microsome preparation for Scp1 immunoblot – Cell pellets from exponentially growing cells (5 x 107) were resuspended in 50 µl B88 buffer + 2x PI. Cells were lysed by bead beating 10 min with 200 µl glass beads at 4°C. Beads were washed with 500 µl B88 buffer + 1x PI and lysate was transferred to a new tube. Lysate was centrifuged for 5 min at 500 x g at 4°C. 80% of supernatant was transferred to a new tube and centrifuged for 10 min at 20,000 x g at 4°C. Supernatant was discarded and microsome pellet was resuspended in 50 µl SDS lysis buffer + 1x PI + 1x DTT. Microsomes were incubated at 37°C for 30 min before BCA assay. Samples were diluted 1:2 with Urea Buffer (50 mM Tris-HCl pH 6.8, 6 M urea, 2% SDS) and 1x loading dye before loading SDS-PAGE gel.

Scp1-13x Myc immunoprecipitation – Cell pellets from exponentially growing cells (5 x 10^8) were resuspended in 200 µl NP-40 lysis buffer [50 mM HEPES pH 7.4, 100 mM NaCl, 1.5 mM MgCl2, 1% NP-40 (v/v), 2x PI, 2x Complete EDTA-free PI]. Cells were lysed by bead beating for 10 min at 4°C, then beads were washed with 800 µl NP-40 lysis buffer to collect all lysate. Lysate was incubated with rotation for 40 min at 4°C then centrifuged for 5 min at 500 x g to clear intact cells and nuclei. 3 mg of supernatant protein was incubated with 4 µg anti-Myc 9E10 IgG (Santa Cruz) for 15 min then incubated with 80 µl protein G magnetic beads (NEB) for 2 h at 4°C. Beads were washed 3x with NP-40 lysis buffer, and the bound fraction was eluted into SDS lysis buffer + 1x PI and 1x loading dye at 95°C for 5 min.

Fluorescence microscopy – S. pombe cells expressing fluorescently-tagged proteins were imaged on 2% agarose pads using an AxioObserver.Z1 inverted microscope (Zeiss) with a Yokogawa CSU22 High-speed spinning Nipkow disk with microlenses (3i), 3 >40mW solid state lasers (473, 561, 658 nm), and a Cascade II, EM-CCD camera (Roper Scientific/Photometrics). Images were captured using a 100x oil objective and SlideBook software for data acquisition (3i). Images were analyzed using Image J software (NIH). All images were acquired and processed in an identical manner. For each frame a Z-stack was captured of 5 slices, 0.2 µm apart.

For analysis of microscopy data for Anp1-GFP localization, each slice was evaluated independently and quantification data from all slices was used to calculate the mean and standard deviation. For statistical analysis we divided the number of cells by 5 to account for the 5x sampling of each cell during analysis of all Z-slices. This method conservatively under-estimated the number of mutant cells in any frame, as a truly mutant cell may appear mutant in one Z-slice and WT in another. For quantification, cells were divided into 2 bins: WT (Golgi localization of Anp1, appearing as punctate signal with no ER staining around the nucleus or periphery), or mutant (3 different phenotypes: no specific signal, ER signal only, and both ER and Golgi signal). For each experiment, we performed pairwise chi-square analysis of all treatments (28 comparisons) and a post-hoc Bonferroni correction.

For analysis of microscopy data for Ost1-mCherry signal intensity, the middle Z-slice was selected from each frame and all images were normalized for overall signal. A straight line was drawn along the long axis of each cell through the nucleus and the Max and Min signal intensity values were recorded. To normalize for comparison between biological replicates and cell background, the Min value was subtracted from the Max value to get the normalized Ost1-mCherry intensity. Experimental data was represented by box-and-whisker plot with the midline the median and the whiskers extending to the largest and smallest values. Experiments were compared by one-way ANOVA followed by post-hoc multiple comparison of means between all of the treatments and Bonferroni correction.

Acknowledgments/Author contributions: The authors thank Dr. J. Mutchler (University of Massachusetts, Boston) for advice on statistical analysis and S. Zhao and other members of the Espenshade lab for help and advice. RB designed and conducted the experiments, analyzed the results, and wrote the manuscript. EVS conducted preliminary experiments for the Sre1 and Sre2 cleavage assays and cerulenin Sre1 cleavage block, and generated the *2xFLAG-mga2* strain. PJE

conceived of the project, designed experiments, and wrote the manuscript. All authors reviewed the results and approved the final version of this manuscript.

4.5 Figures

FIGURE 4.1. ***mga2*Δ cells have reduced Sre1N accumulation in the presence and absence of oxygen.** *A and C,* Western blots imaged by Li-Cor probed with monoclonal anti-Sre1 IgG (5B4) and polyclonal anti-Dsc5 IgG (for loading) of lysates treated with alkaline phosphatase for 1 h from *WT, mga2Δ, dsc2Δ*, or *sre1Δ* cells grown for 0 or 4 h in the absence of oxygen (*A*) or 6 h in the presence of the statin compactin (200 μM, CPN) or vehicle (0.12% EtOH, 400 μM NaCl) (*C*). P and N denote precursor and cleaved N-terminal transcription factor forms, respectively. Asterisks denote non-specific bands. *B and D,* Quantification from (*A*) and (*C*) of three (*A,B*) or four (*C,D*) biological replicates normalized for loading to Dsc5 then normalized to maximum signal (WT N-terminus band after treatment, lane 2) for comparison between blots. Error bars are 1 S.D. (**, $p<0.01$ for N-terminus by two-tailed student's t-test). Quantities of precursor and nuclear form are stacked to give an approximation of total signal per treatment. Average percent cleavage is calculated by dividing the quantity of N-terminus by the sum of both N-terminus and precursor.

FIGURE 4.2. **Defect in Sre1 cleavage in the absence of *mga2* is amplified by positive feedback.** *A,* Western blot imaged by Li-Cor probed with monoclonal anti-Sre1 IgG (5B4) and polyclonal anti-Dsc5 IgG (for loading) of lysates treated with alkaline phosphatase for 1 h from *WT, mga2Δ*, or *sre1Δ* cells with WT or mutant promoter (MP) sre1 as indicated. Cells were grown for 0 or 4 h in the absence of oxygen. P and N denote precursor and cleaved N-terminal transcription factor forms, respectively. *B,* Quantification from (*A*) of four biological replicates normalized for loading to Dsc5 then normalized to maximum signal (WT N-terminus band after treatment, lane 2) for comparison between blots. Error bars are 1 S.D. (**, $p<0.01$ for N-terminus

by two-tailed student's t-test). Quantities of precursor and nuclear form are stacked to give an approximation of total Sre1 signal per treatment.

FIGURE 4.3. **Cleavage defect in *mga2*Δ cells occurs at a step downstream of Sre1-Scp1 complex formation and is not specific to Sre1.** *A,* Western blot of cell lysates from the indicated strains grown in the presence of oxygen, probed with a mixture of anti-Scp1 IgG monoclonal antibodies 8G4C11, 1G1D6, and 7B4A3 (imaged by film) or anti-Dsc5 IgG (imaged by Li-Cor). Blot is representative of four biological replicates. *B, WT* or *mga2Δ* cells expressing *scp1-13xmyc* and *mga2Δ* cells expressing untagged scp1 were grown in the presence of oxygen, and Scp1-13xMyc was immunoprecipitated from NP-40-solubilized membranes using monoclonal anti-Myc 9E10 IgG as described in Experimental Procedures. Input and 5-fold enriched bound fractions were analyzed by western blot and imaged by Li-Cor using polyclonal anti-Sre1 IgG and polyclonal anti-Myc IgG. Blot is representative of three biological replicates. *C,* Indicated strains expressing vector (-) or scp1 (+) from a CaMV promoter were precultured in minimal medium lacking leucine, transferred to YES complete medium, and grown for 4 h in the presence or absence of oxygen. Western blot probed with anti-Sre1 IgG polyclonal antibody and imaged by Li-Cor is representative of five biological replicates. P and N denote Sre1 precursor and N-terminal forms. Asterisks indicate non-specific bands. *D,* Western blots imaged by Li-Cor probed with polyclonal anti-Sre2 and polyclonal anti-Cdc48 (for loading) of lysates treated with alkaline phosphatase for 1 h from *WT, mga2Δ, dsc2Δ*, or *sre2Δ* cells grown in the presence of oxygen. *E,* Quantification from (*D*) of six biological replicates normalized for loading to Cdc48 then normalized to WT N-terminus band for comparison between blots. Error bars are 1 S.D. (**, $p<0.01$ for N-terminus by two-tailed student's t-test). Quantities of precursor and nuclear form are stacked to give an approximation of total signal per treatment. Average percent cleavage is calculated by dividing the quantity of N-terminus by the sum of both N-terminus and precursor.

FIGURE 4.4. **Dsc E3 ligase is functional in *mga2*Δ cells.** *A,* Digitonin-solubilized membrane protein was prepared from *WT, mga2Δ*, or *dsc2Δ* cells grown in the presence or absence of oxygen for 6 h, and the Dsc E3 ligase complex was immunoprecipitated with anti-Dsc2 polyclonal IgG as described in Experimental Procedures. Equal quantities of input and unbound, and 10-fold bound fractions were analyzed by immunoblotting using HRP-conjugated antibodies against Dsc1, Dsc2, Dsc3, Dsc4, and Dsc5 (imaged by film). Blot is representative of three biological replicates. *B,* Western blot imaged by Li-Cor probed with polyclonal anti-Sre1 IgG and monoclonal anti-actin (for loading) of lysates from *WT, mga2Δ, dsc1Δ*, or *sre1Δ* yeast grown for 2 h in the presence or absence of oxygen, then treated with Brefeldin A (100 μg/mL, BFA) or EtOH vehicle for another 2 h in the presence or absence of oxygen. Quantification of Sre1 precursor (Sre1-P) normalized to WT vehicle in the absence of oxygen (lane 7) is shown below. Blot is representative of two biological replicates. *C,* Western blot imaged by Li-Cor probed with polyclonal anti-Dsc1 IgG of NP-40-solubilized membrane protein from *WT, mga2Δ*, or *dsc2Δ* cells grown in the presence of oxygen. M and I indicate mature and intermediate glycosylated forms, respectively. *D,* Quantification of Dsc1 from (*C*) of seven replicates. Quantity of M form was divided by total Dsc1 signal for % mature, allowing comparison between lanes and blots. Error bars are 1 S.D. (*, $p<0.05$, **, $p<0.01$ by two-tailed student's t-test).

FIGURE 4.5. ***mga2*** **deletion disrupts general membrane transport.** *A, anp1-GFP ost1-mCherry* (*WT*) and *mga2Δ anp1-GFP ost1-mCherry* (*mga2Δ*) cells were cultured in the presence of oxygen and 0.9% (w/v) BSA for 6 h and imaged by confocal microscopy. These images are representative of three biological replicates. Scale bar equals 5 μm. *B,* Quantification of cells with altered Anp1-GFP localization from (*A*) of three biological replicates denoted by different marker symbols. $n \geq 150$ cells per replicate. Error bars are mean +/- 1 S.D. (**, $p<0.01$ by chi-square analysis with Bonferroni correction). *C,* Box-and-whisker quantification of normalized Ost1-mCherry signal intensity from (*A*) of $n \geq 300$ cells from three biological replicates. Whiskers are

the max and min intensity values. (**, $p<0.01$ by one-way ANOVA and post-hoc multiple comparisons with Bonferroni correction). *D,* Western blots imaged by Li-Cor probed with monoclonal anti-GFP IgG, polyclonal anti-mCherry IgG, and polyclonal anti-Dsc2 IgG (for loading) of lysates from anp1-GFP *ost1-mCherry* (*WT*) and *mga2Δ anp1-GFP ost1-mCherry* (*mga2Δ*) cells cultured in the presence of oxygen and 0.9% (w/v) BSA for 6 h. *E,* GFP quantification from (*D*) of three biological replicates represented by different marker symbols. Quantity of free GFP was divided by total GFP signal for % GFP that is free, allowing comparison between lanes and blots. Error bars are 1 S.D. (*, $p<0.05$ by paired two-tailed student's t-test, with pairing of *WT* and *mga2Δ* data on same blot due to significant inter-blot variance in WT signal). *F,* mCherry quantification from (*D*) of four biological replicates represented by different marker symbols, normalized for loading to Anp1-GFP signal then normalized to WT signal for comparison between blots. (n.s. no significant difference by paired two-tailed student's t-test).

FIGURE 4.6. **Exogenous oleate addition rescues Sre1 cleavage and membrane trafficking in *mga2Δ* cells.** *A-B,* Western blot imaged by Li-Cor probed with monoclonal anti-Sre1 IgG (5B4) and polyclonal anti-Dsc5 IgG (for loading) of lysates treated with alkaline phosphatase for 1 h from *WT* or the indicated mutants grown for 4 h in the presence or absence of oxygen (*A*) or 6 h in the presence of 200 μM CPN or vehicle (0.12% EtOH, 400 μM NaCl) (*B*). All lanes contain 0.9% (w/v) BSA, and lanes with supplemental fatty acids conjugated to BSA are indicated. *A,* BSA-conjugated fatty acids were added at time 0 and were present for 4 h of growth. *B,* Cells were grown overnight with the indicated fatty acid, washed with H2O, and then grown for 6 h with CPN or vehicle. P and N denote precursor and cleaved N-terminal transcription factor forms, respectively. Asterisks (*) indicate non-specific bands. Blots are representative of three biological replicates. *C, anp1-GFP ost1-mCherry* (*WT*) and *mga2Δ anp1-GFP ost1-mCherry* (*mga2Δ*) cells were cultured with the indicated fatty acid supplement for 6 h and imaged by confocal

microscopy. 18:X indicates supplementation of both 18:0 and 18:1. Experimental data for *WT* BSA and *mga2Δ* BSA are the same as reported in **Fig. *5A-C***. Images are representative of three biological replicates. Scale bar equals 5 μm. *D,* Quantification of cells with altered Anp1-GFP localization from (*C*) of three biological replicates denoted by different marker symbols. n ≥ 150 cells per replicate. Error bars are mean +/- 1 S.D. (*, $p<0.05$, **, $p<0.01$ by chi-square analysis with Bonferroni correction). *E,* Box-and-whisker quantification of normalized Ost1-mCherry signal intensity from (*C*) of n ≥ 300 cells from three biological replicates. Whiskers are the max and min intensity values. (*, $p<0.05$, **, $p<0.01$ by one-way ANOVA and post-hoc multiple comparisons with Bonferroni correction).

FIGURE 4.7. **Disrupting fatty acid homeostasis blocks general membrane transport and Sre1 cleavage.** *A,* WT cells were grown in liquid culture in 112 nM CER or 0.1% (v/v) DMSO for 6 h. Cell density was measured by absorbance at 600 nm. Data points are average of four biological replicates. Error bars are 1 S.D. Absorbance at time 0 among the samples ranged from 0.10 to 0.29. To focus on the difference in growth rate between conditions, data were normalized for each sample to a value of 0.2 at time point 0 before averaging. *B-C,* Western blot imaged by Li-Cor probed with monoclonal anti-Sre1 IgG (5B4) and polyclonal anti-Dsc5 (for loading) of lysates treated with alkaline phosphatase for 1 h from WT cells. Cells were grown in 112 nM CER or 0.1% (v/v) DMSO for 2 h under normoxia. Cells were then washed, resuspended in fresh medium and grown without cerulenin for 4 h in the presence or absence of oxygen (*B,C*) with the indicated BSA-conjugated fatty acid supplemented (*C*). P and N denote precursor and cleaved N-terminal transcription factor forms, respectively. Asterisks (*) indicate non-specific bands. Blots are representative of two biological replicates. *D, anp1-GFP ost1-mCherry* cells were pre-cultured for 1 h in the indicated BSA-conjugated fatty acid. Then, 112 nM CER or 0.1% (v/v) DMSO (-CER) was added, and cells were cultured for an additional 3 h before imaging by confocal microscopy. 18:X indicates supplementation of both 18:0 and 18:1. Images are

representative of three biological replicates. Scale bar equals 5 μM. *E,* Quantification of cells with altered Anp1-GFP localization from (*D*) of three biological replicates denoted by different marker symbols. n ≥ 100 cells per replicate. Error bars are mean +/- 1 S.D. (**, $p<0.01$ by chi-square analysis with Bonferroni correction). *E,* Box-and-whisker quantification of normalized Ost1-mCherry signal intensity from (*D*) of n ≥ 300 cells from three biological replicates. Whiskers are the max and min intensity values. (**, $p<0.01$ by one-way ANOVA and post-hoc multiple comparisons with Bonferroni correction).

FIGURE 4.8. **Inhibition of sterol synthesis blocks Mga2 transcription factor activity.** *A,* Western blots imaged by Li-Cor probed with monoclonal anti-FLAG M2 IgG of lysates treated with alkaline phosphatase for 1 h from WT and 2xFLAG-mga2 cells grown for 2 h in 0.1% (v/v) DMSO (*D*), bortezomib (500 μM, BZ), or cerulenin (112 nM, CER). P and N denote precursor and cleaved N-terminal transcription factor forms, respectively. Asterisks denote non-specific bands. *B,* Western blots imaged by Li-Cor probed with monoclonal anti-FLAG M2 IgG, monoclonal anti-Sre1 IgG (5B4), and polyclonal anti-Dsc5 IgG (for loading) of lysates treated with alkaline phosphatase for 1 h from *WT* and *2xFLAG-mga2* cells grown in the following treatments: 8 h in vehicle (0.12% EtOH, 400 μM NaCl, V), compactin (200 μM, CPN), or itraconazole (2 μM, ITR) or 2 h in 0.1% (v/v) DMSO (D), bortezomib (500 μM, BZ), or cerulenin (112 nM, CER). P and N denote precursor and cleaved N-terminal transcription factor forms, respectively. Asterisks denote non-specific bands. *C-E,* qPCR of the indicated genes of lysates from *2xFLAG-mga2* cells treated as indicated. Error bars are mean +/- 1 S.D. of three biological replicates normalized to DMSO treatment. (*, $p<0.05$, **, $p<0.01$, by two-tailed student's t-test).

FIGURE 4.9. **Model of coordination of Mga2 and Sre1 pathways.** Sterol and TAG/GPL lipid biosynthetic pathways are positively regulated by the transcription factors Sre1 and Mga2,

respectively. Both Sre1 and Mga2 are product inhibited; Sre1 by sterols and Mga2 by UFA. Mga2 regulates Sre1 through the requirement for UFA, and Sre1 regulates Mga2 through the requirement of sterols for Mga2 activity.

Table 4.1. *S. pombe* strain list

Strains	Genotype	Source	Figure
KGY425	*h- leu1-32 ura4-D18 ade6-M210 his3-D1*	ATCC	1,2,3,4,5,6
PEY1762	*h- leu1-32 ura4-D18 ade6-M210 his3-D1 ∆mga2-D1::kanMX6*	(Burr et al., 2016)	1,2,3,4,5
PEY1792	*h+ leu1-32 ura4-D18 ade6-M210 his3-D1 ∆dsc2-D1::kanMX6*	This study	1,3,5
PEY522	*h- leu1-32 ura4-D18 ade6-M210 his3-D1 ∆sre1-D1::kanMX6*	(Hughes et al., 2005)	1,2,3,4,5
PEY888	*h- leu1-32 ura4-D18 ade6-M210 his3-D1 sre1-MP (mutant promoter)*	(Hughes et al., 2009)	2
PEY1793	*h+ leu1-32 ura4-D18 ade6-M210 his3-D1 sre1-MP ∆mga2-D1::kanMX6*	This study	2
PEY1794	*h- leu1-32 ade6-M216 ∆dsc2-D1::kanMX6, anp1-mCherry::ura4+, his3::dsc2-6xmGFP-his3*	This study	3
PEY1795	*h- leu1-32 ade6-M216 ∆mga2-D1::natMX6, ∆dsc2-D1::kanMX6, anp1-mCherry::ura4+, his3::dsc2-6xmGFP-his3*	This study	3,5
PEY1569	*h+ ∆dsc1-D1::kanMX6*	This study	3,5
PEY554	*h- leu1-32 ura4-D18 ade6-M210 his3-D1 ∆scp1-D1::kanMX6*	(Hughes et al., 2005)	4
PEY546	*h- ura4-D18 leu1-32 his3-D1 ade6-M210 scp1-13xmyc::kanMX6*	(Burg et al., 2008)	4
PEY1796	*h+ ura4-D18 leu1-32 his3-D1 ade6-M210 scp1-13xmyc::kanMX6 ∆mga2-D1::natMX6*	This study	4
PEY1797	*h+ leu1-32 his3-D1 ade6-M216 anp1-GFP::ura4+, ost1-mCherry::ura4+*	This study	6

Figure 4.1

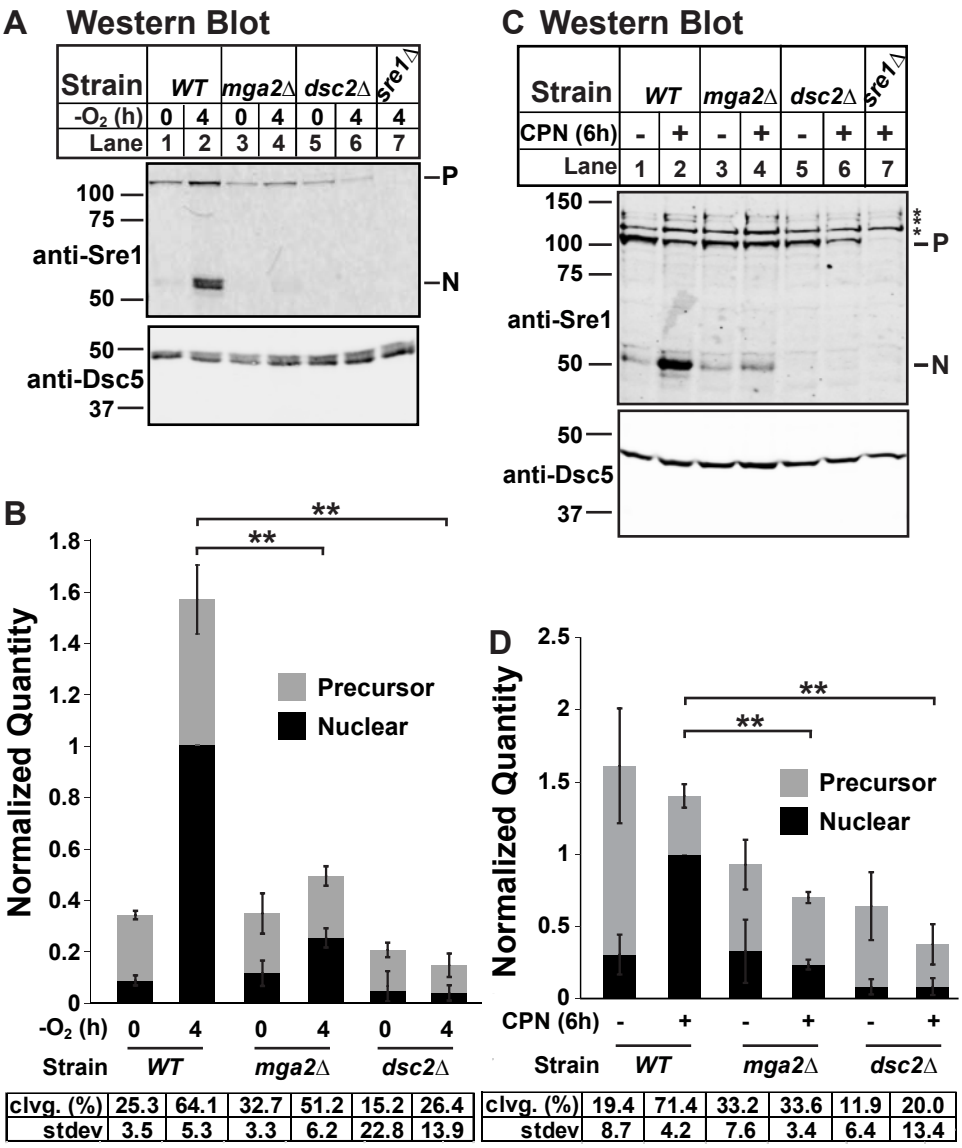

clvg. (%)	25.3	64.1	32.7	51.2	15.2	26.4
stdev	3.5	5.3	3.3	6.2	22.8	13.9

clvg. (%)	19.4	71.4	33.2	33.6	11.9	20.0
stdev	8.7	4.2	7.6	3.4	6.4	13.4

Figure 4.2

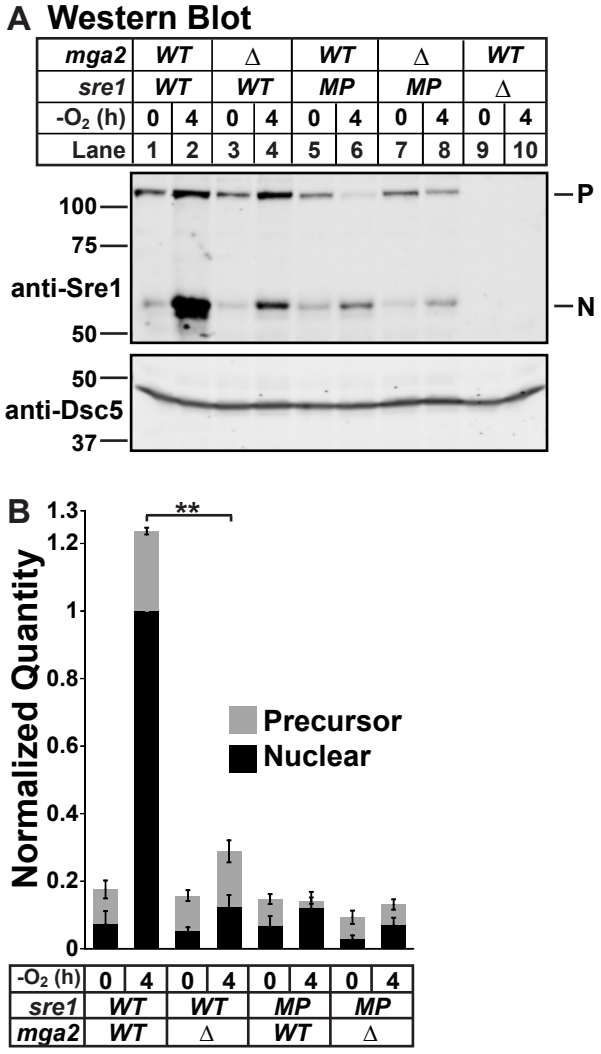
A Western Blot
mga2 WT Δ WT Δ WT
sre1 WT WT MP MP Δ
-O2 (h) 0 4 0 4 0 4 0 4 0 4
Lane 1 2 3 4 5 6 7 8 9 10
100
75
anti-Sre1
50
P
N
50
anti-Dsc5
37
B
Normalized Quantity
1.3
1.2
1
0.8
0.6
0.4
0.2
0
**
Precursor
Nuclear
-O2 (h) 0 4 0 4 0 4 0 4
sre1 WT WT MP MP
mga2 WT Δ WT Δ

Figure 4.3

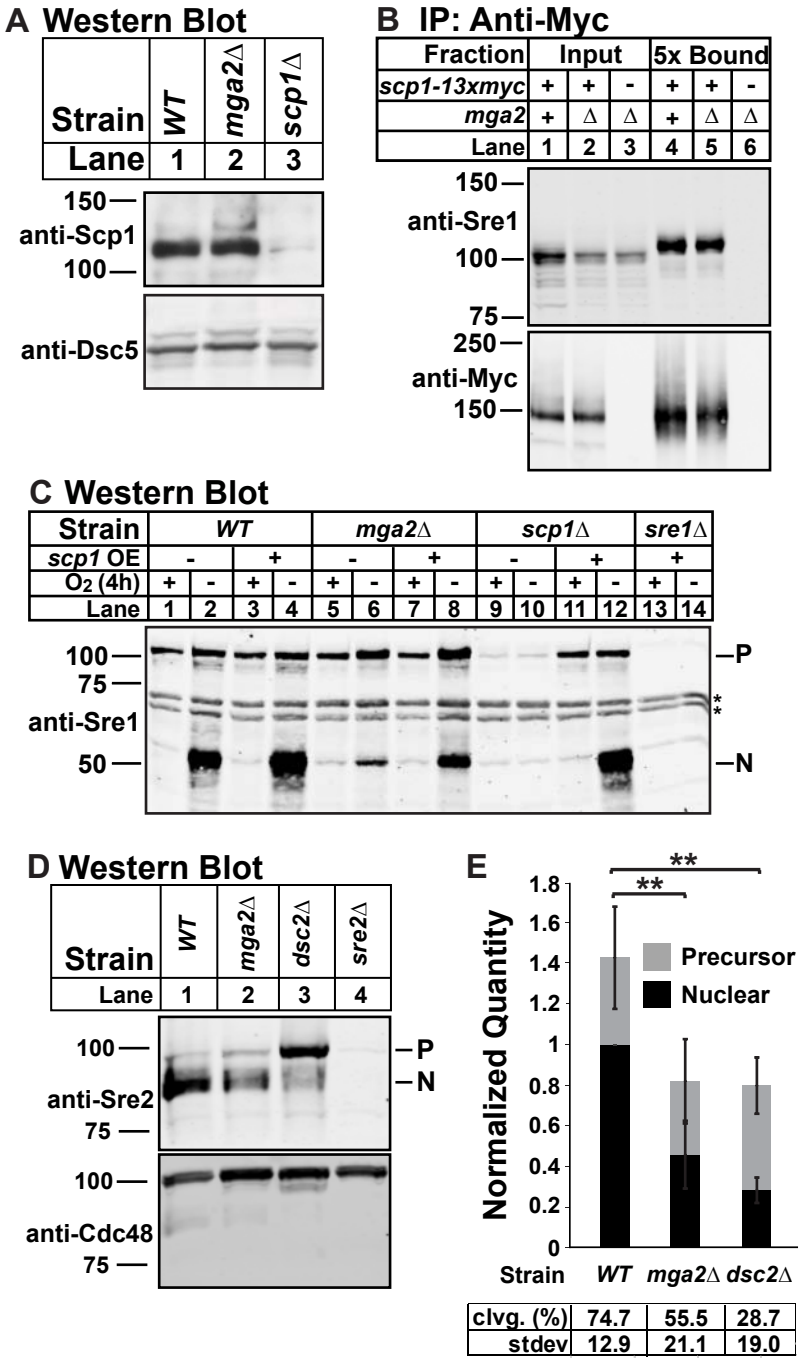
A Western Blot
Strain
WT
mga2Δ
scp1Δ
Lane
1
2
3
150
anti-Scp1
100
anti-Dsc5
B IP: Anti-Myc
Fraction
Input
5x Bound
scp1-13xmyc
mga2
Lane
1
2
3
4
5
6
150
anti-Sre1
100
75
250
anti-Myc
150
C Western Blot
Strain
WT
mga2Δ
scp1Δ
sre1Δ
scp1 OE
O2 (4h)
Lane
1
2
3
4
5
6
7
8
9
10
11
12
13
14
100
75
anti-Sre1
50
P
N
D Western Blot
Strain
WT
mga2Δ
dsc2Δ
sre2Δ
Lane
1
2
3
4
100
anti-Sre2
75
100
anti-Cdc48
75
P
N
E
Normalized Quantity
1.8
1.6
1.4
1.2
1
0.8
0.6
0.4
0.2
0
Precursor
Nuclear
Strain
WT
mga2Δ
dsc2Δ
clvg. (%)
74.7
55.5
28.7
stdev
12.9
21.1
19.0

Figure 4.4

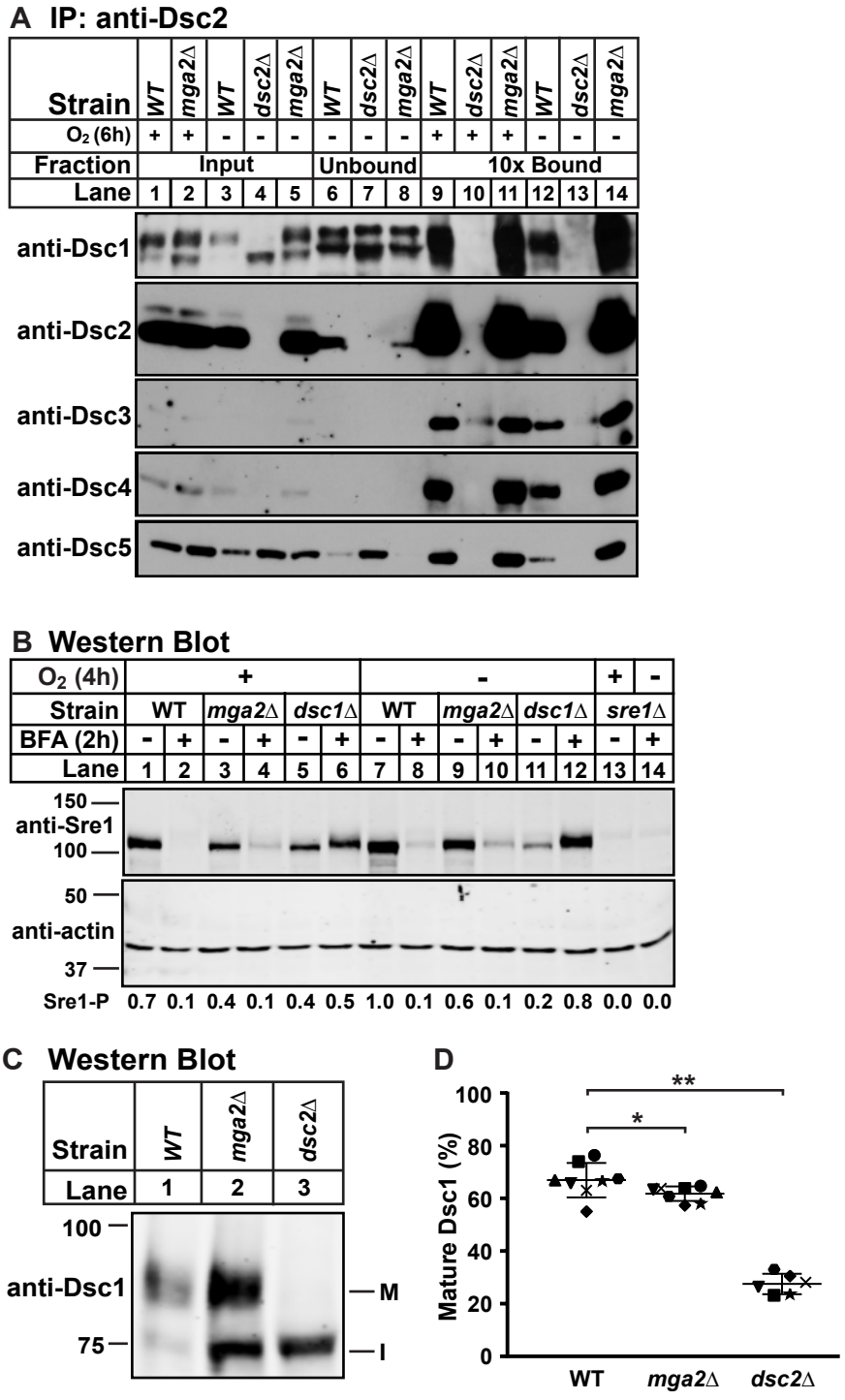
A IP: anti-Dsc2
Strain
WT
mga2Δ
WT
dsc2Δ
mga2Δ
WT
dsc2Δ
mga2Δ
WT
dsc2Δ
mga2Δ
WT
dsc2Δ
mga2Δ
O2 (6h)
+ + - - - - - - + + + - - -
Fraction
Input
Unbound
10x Bound
Lane
1 2 3 4 5 6 7 8 9 10 11 12 13 14
anti-Dsc1
anti-Dsc2
anti-Dsc3
anti-Dsc4
anti-Dsc5
B Western Blot
O2 (4h)
+
-
+ -
Strain
WT
mga2Δ
dsc1Δ
WT
mga2Δ
dsc1Δ
sre1Δ
BFA (2h)
- + - + - + - + - + - + - +
Lane
1 2 3 4 5 6 7 8 9 10 11 12 13 14
150
anti-Sre1
100
50
anti-actin
37
Sre1-P
0.7 0.1 0.4 0.1 0.4 0.5 1.0 0.1 0.6 0.1 0.2 0.8 0.0 0.0
C Western Blot
Strain
WT
mga2Δ
dsc2Δ
Lane
1 2 3
100
anti-Dsc1
75
M
I
D
Mature Dsc1 (%)
100
80
60
40
20
0
**
*
WT
mga2Δ
dsc2Δ

Figure 4.5

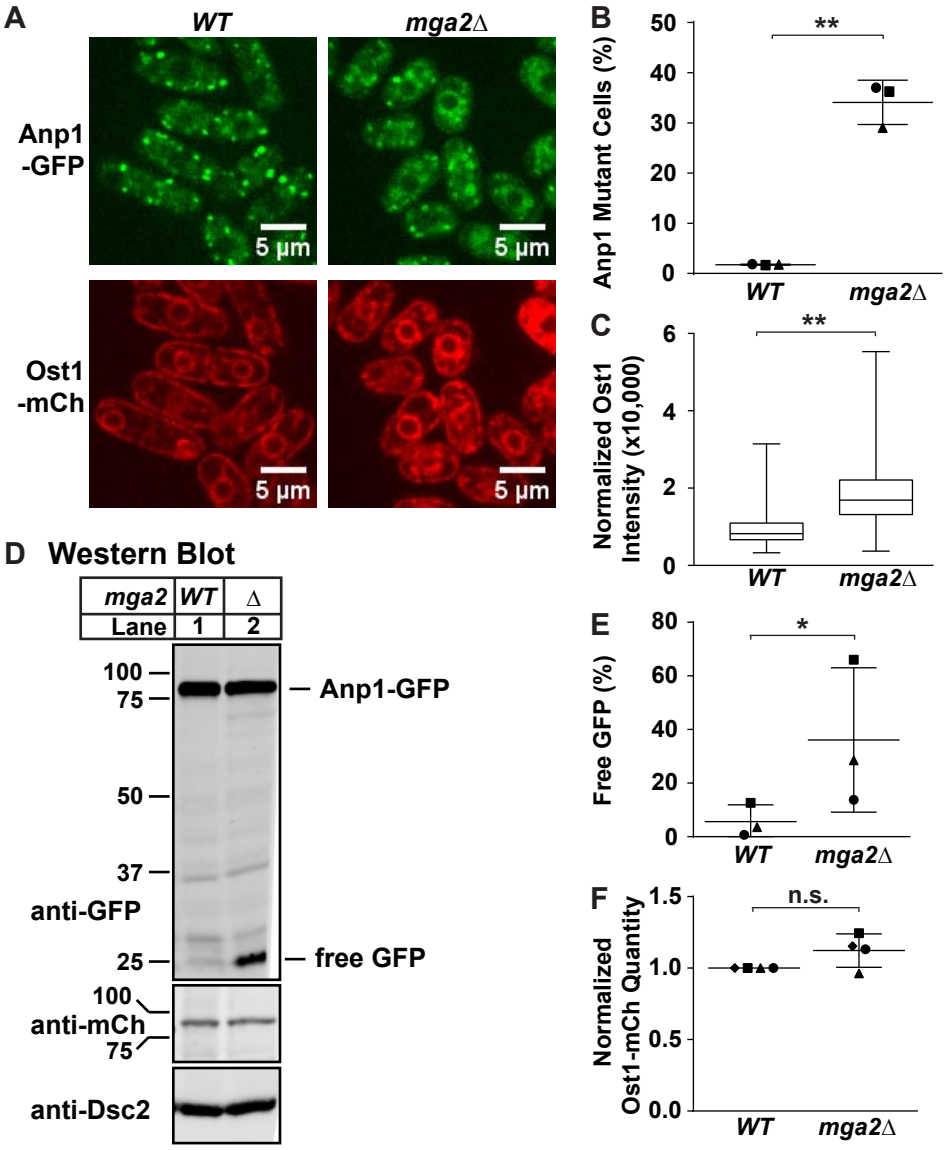
A
WT
mga2Δ
Anp1
-GFP
Ost1
-mCh
5 μm
B
Anp1 Mutant Cells (%)
**
WT
mga2Δ
C
Normalized Ost1
Intensity (x10,000)
**
D Western Blot
mga2
WT
Δ
Lane
1
2
100
75
50
37
25
anti-GFP
Anp1-GFP
free GFP
anti-mCh
anti-Dsc2
E
Free GFP (%)
*
F
Normalized
Ost1-mCh Quantity
n.s.

Figure 4.6

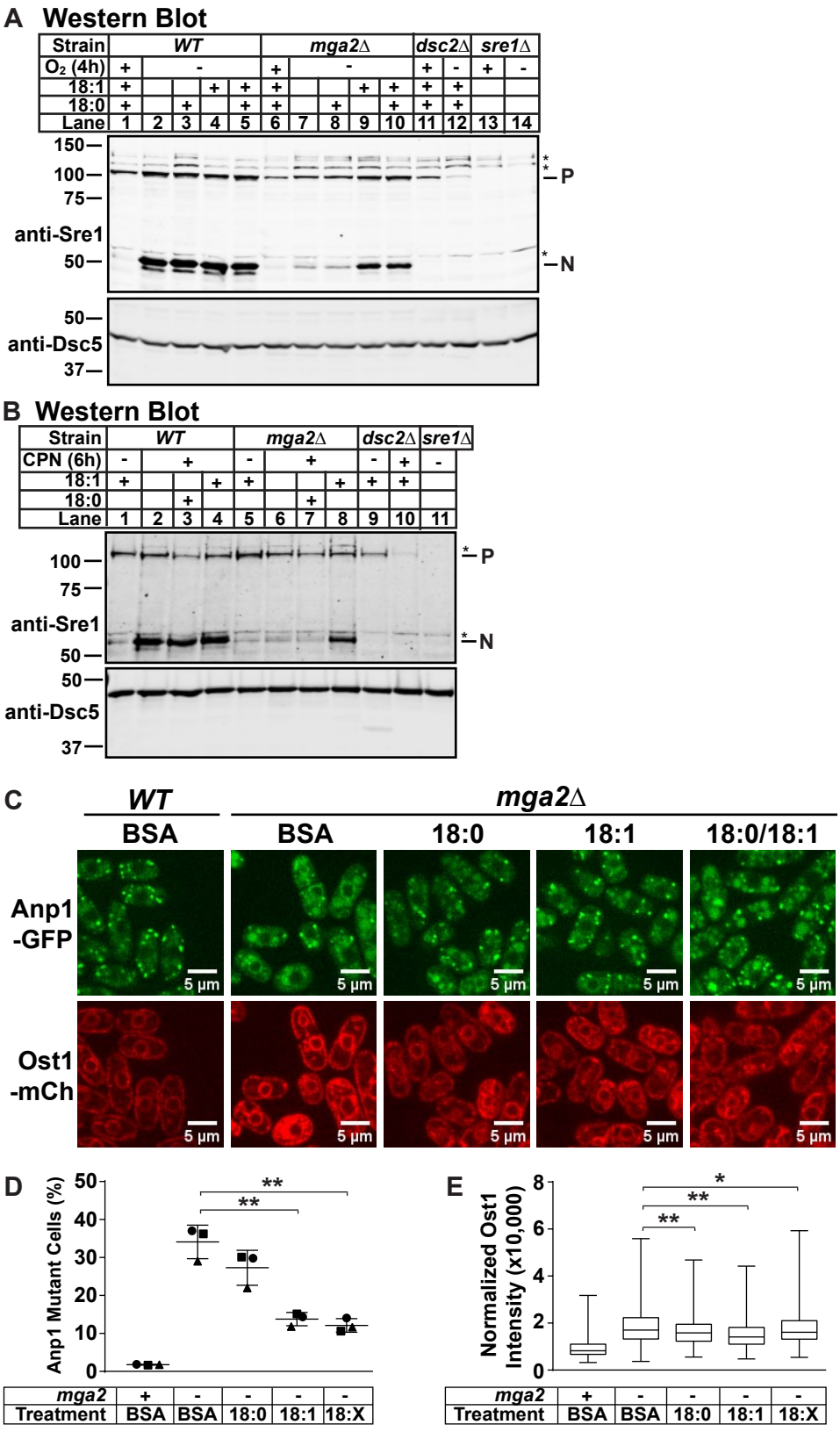
A Western Blot
Strain
WT
mga2Δ
dsc2Δ
sre1Δ
O2 (4h)
18:1
18:0
Lane
1 2 3 4 5 6 7 8 9 10 11 12 13 14
150
100
75
anti-Sre1
50
P
N
50
anti-Dsc5
37
B Western Blot
Strain
WT
mga2Δ
dsc2Δ
sre1Δ
CPN (6h)
18:1
18:0
Lane
1 2 3 4 5 6 7 8 9 10 11
100
75
anti-Sre1
50
50
anti-Dsc5
37
P
N
C
WT
mga2Δ
BSA
BSA
18:0
18:1
18:0/18:1
Anp1
-GFP
Ost1
-mCh
5 μm
D
Anp1 Mutant Cells (%)
50
40
30
20
10
0
**
**
mga2
Treatment
+
BSA
-
BSA
-
18:0
-
18:1
-
18:X
E
Normalized Ost1
Intensity (x10,000)
8
6
4
2
0
*
**
**
mga2
Treatment
+
BSA
-
BSA
-
18:0
-
18:1
-
18:X

Figure 4.7

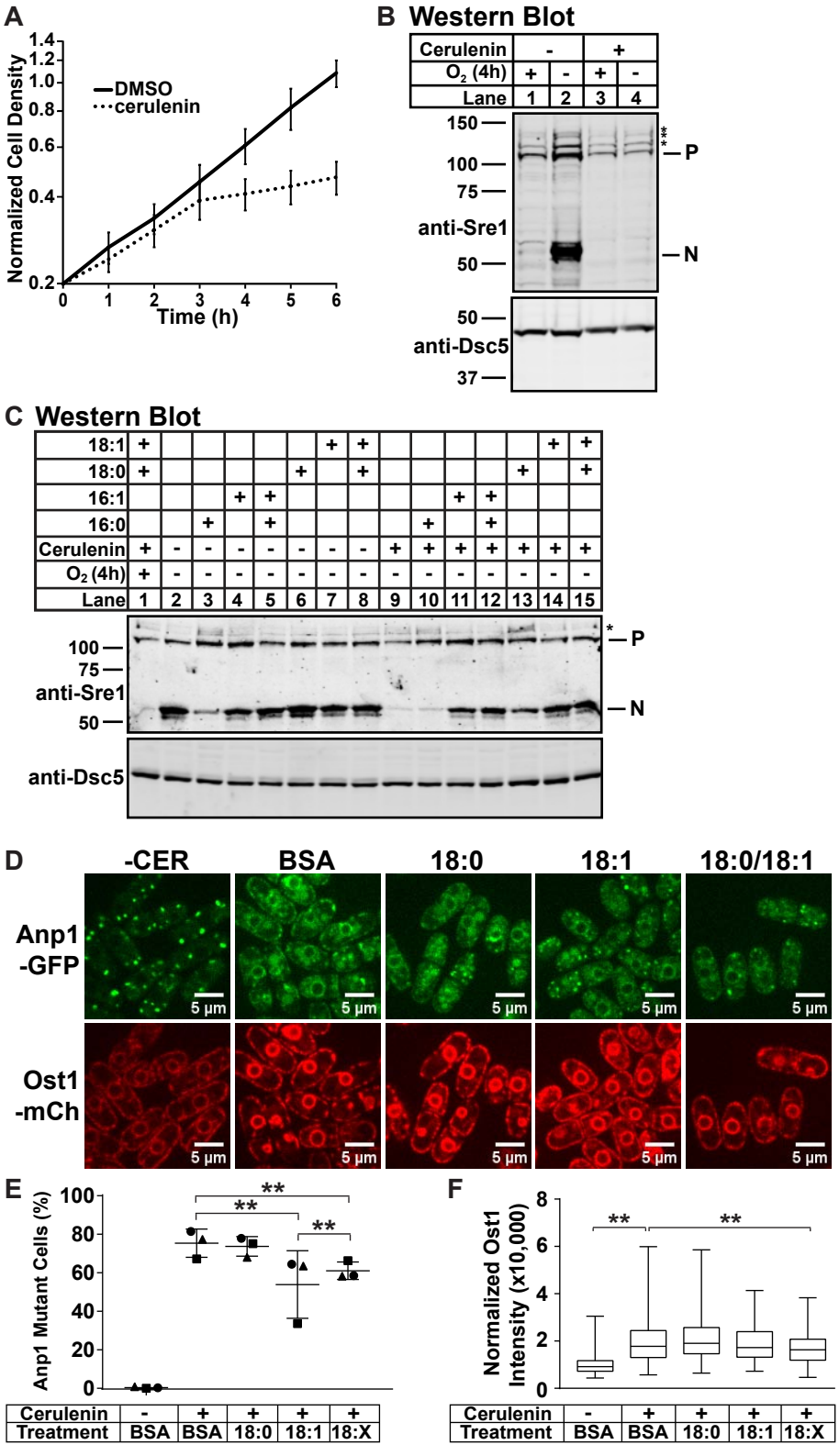
A
Normalized Cell Density
DMSO
cerulenin
Time (h)
B Western Blot
Cerulenin
O2 (4h)
Lane
anti-Sre1
anti-Dsc5
P
N
C Western Blot
18:1
18:0
16:1
16:0
Cerulenin
O2 (4h)
Lane
anti-Sre1
anti-Dsc5
D
-CER
BSA
18:0
18:1
18:0/18:1
Anp1 -GFP
Ost1 -mCh
5 µm
E
Anp1 Mutant Cells (%)
Cerulenin
Treatment
BSA
18:0
18:1
18:X
F
Normalized Ost1 Intensity (x10,000)

Figure 4.8

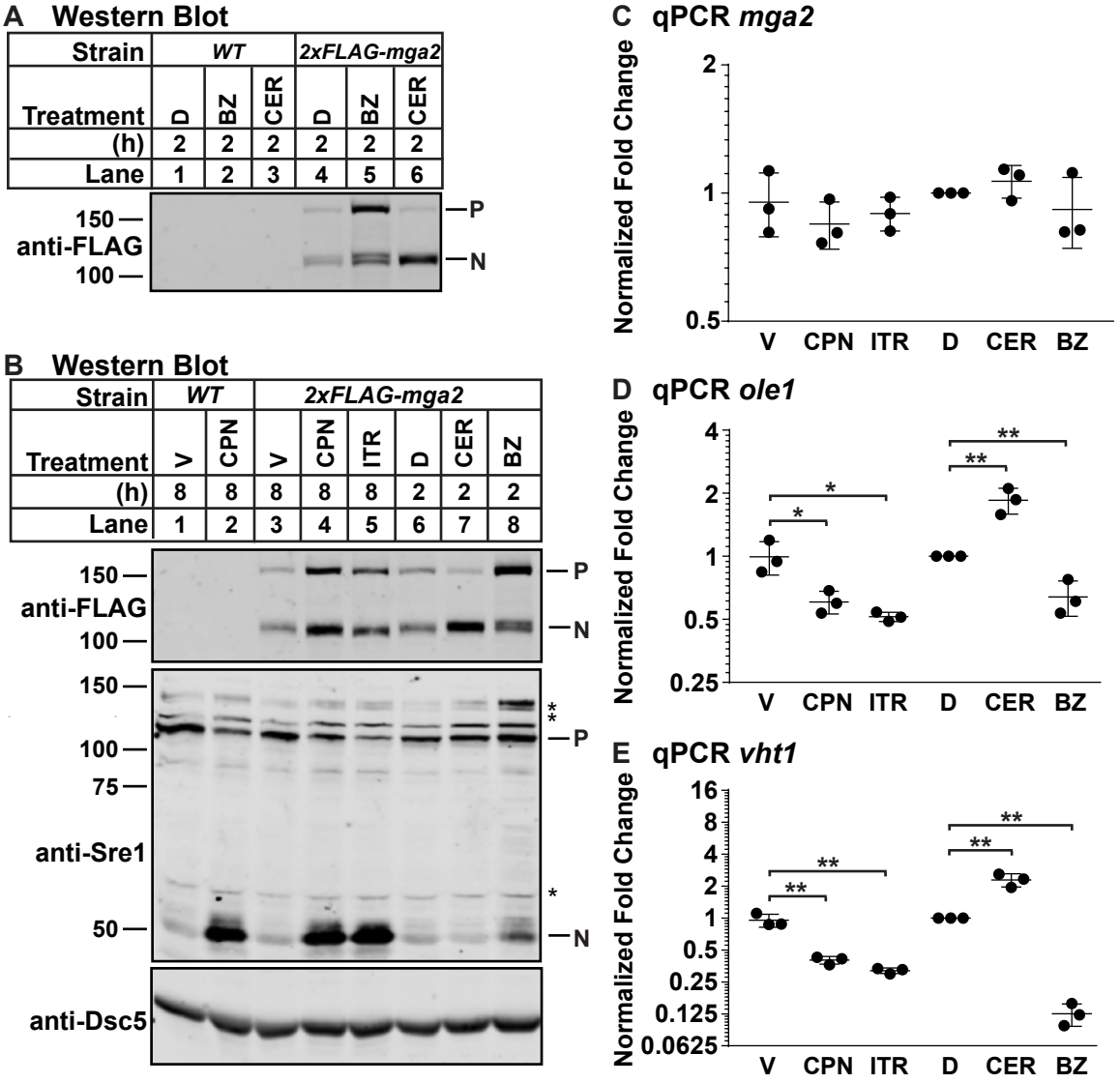
A Western Blot
Strain
WT
2xFLAG-mga2
Treatment
D
BZ
CER
D
BZ
CER
(h)
2
2
2
2
2
2
Lane
1
2
3
4
5
6
150
anti-FLAG
100
P
N
B Western Blot
Strain
WT
2xFLAG-mga2
Treatment
V
CPN
V
CPN
ITR
D
CER
BZ
(h)
8
8
8
8
8
2
2
2
Lane
1
2
3
4
5
6
7
8
150
anti-FLAG
100
P
N
150
100
75
anti-Sre1
50
**
*
P
N
anti-Dsc5
C qPCR mga2
Normalized Fold Change
2
1
0.5
V
CPN
ITR
D
CER
BZ
D qPCR ole1
Normalized Fold Change
4
2
1
0.5
0.25
*
*
**
**
V
CPN
ITR
D
CER
BZ
E qPCR vht1
Normalized Fold Change
16
8
4
2
1
0.5
0.25
0.125
0.0625
**
**
**
**
V
CPN
ITR
D
CER
BZ

Figure 4.9

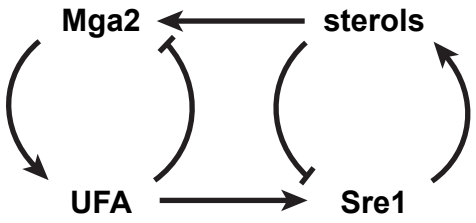

Chapter 5

Conclusions and future directions

This chapter is an edited version of the manuscript, “Oxygen-responsive transcriptional regulation of lipid homeostasis in fungi: Implications for anti-fungal drug development” by R. Burr and P. J. Espenshade, under revision at Seminars in Cell and Developmental Biology. It also incorporates material from the manuscript, “Dsc E3 ligase localization to the Golgi requires the ATPase Cdc48 and cofactor Ufd1 for activation of Sterol Regulatory Element-binding Protein in fission yeast” by R. Burr, D. Ribbens, S. Raychaudhuri, E. V. Stewart, J. Ho, and P. J. Espenshade, under revision at the Journal of Biological Chemistry, the manuscript, “Mga2 transcription factor regulates an oxygen-responsive lipid homeostasis pathway in fission yeast” by R. Burr, E. V. Stewart, W. Shao, S. Zhao, H. K. Hannibal-Bach, C. S. Ejsing, and P. J. Espenshade, published in the Journal of Biological Chemistry, Volume 291, Issue 23, 12171-12183. , and the manuscript, “Coordinate regulation of yeast Sterol Regulatory Element-Binding Protein (SREBP) and Mga2 transcription factors” by R. Burr, E. V. Stewart, and P. J. Espenshade, published in the Journal of Biological Chemistry, Volume 292, Issue 13, 5311-5324.

5.1 Summary

In my graduate work, I determined that Cdc48 plays multiple roles during SREBP cleavage in *S. pombe*. In addition to the previously described role at Rbd2, I discovered that Cdc48 and its cofactor Ufd1 are required at an earlier step of the pathway, namely during Dsc E3 ligase Golgi localization. Importantly, Ufd1 does not interact with Rbd2, suggesting that these two roles for Cdc48 are performed by distinct complexes. This work highlights the versatility of Cdc48, the need to focus on cofactors in order to characterize specific functions of Cdc48, and the important role that cellular localization of pathway components plays during SREBP activation.

In separate work, I defined Mga2 as the transcription factor that regulates fatty acid metabolism during low oxygen adaptation in fission yeast. This places Mga2 alongside Sre1 in regulating the low oxygen lipid response and supports my hypothesis that Mga2 and Sre1 mimic mammalian SREBP-1 and SREBP-2, respectively, in their joint regulation of lipid homeostasis. Further, I showed that Mga2 and Sre1 activities are coordinated via a unique mechanism of product cross talk. Therefore, evolution has devised a way to retain coordination of these two lipid homeostasis pathways in fission yeast despite lacking the shared activation mechanism of the mammalian SREBP system. This suggests that coordination of sterol and fatty acid biosynthesis is crucial for overall lipid homeostasis.

Many intriguing questions arise from these results. I expand upon three of these in this chapter:

1. What is the effect of the *cdc48* mutants on Cdc48 function, and what roles is Cdc48 playing during Dsc E3 ligase transport and at Rbd2?
2. What regulates the other genes that respond to low oxygen?
3. Are these pathways and their coordination conserved in other fungi?

5.2 What is Cdc48 doing during Dsc E3 ligase transport?

The specific function for Cdc48-Ufd1 during Dsc E3 ligase Golgi localization is unknown. Further understanding of how the *cdc48* point mutations characterized in this study affect Cdc48 activity could be helpful in elucidating that function. The mutations are spread throughout the D1 and D2 domains, are notably absent from the N-domain, and are not clustered in three-dimensional space. Two of the mutations (E325K and A366D) are in or near the ATP-binding region of the D1 domain. Although the enzymatic consequence of a lysine mutation at E325 is untested, the homologous residue has been extensively studied in both budding yeast and mammalian cells and has effects on the ATP hydrolysis rate of the D1 domain (81,173). Interestingly, a report in fission yeast independently isolated the E325K mutation as a cold-sensitive suppressor of the temperature sensitive *cdc48-353* (G338D) mutation (174). The authors concluded that E325K likely alters Cdc48 structure in a way that is compensatory to the effects of *cdc48-353.* Therefore, fission yeast *cdc48-8* (E325K), and possibly *cdc48-9* (A366D), may produce structural changes that impact Cdc48 ATPase activity.

Because our *cdc48* mutants are distributed throughout the sequence and do not cluster in three-dimensional space, the mutations are unlikely to directly impact a single binding interaction with a specific cofactor or substrate in order to cause the observed SREBP cleavage defects. Instead they may alter hexamer assembly, ATPase activity, or substrate release, thereby reducing enzymatic efficiency. Similarly, of the three *ufd1* mutants, only *ufd1-7* has a mutation in the predicted Cdc48-binding region (aa 219-235 based on homology to *S. cerevisiae*), and none are mutant in the predicted Npl4 binding region (aa 251-266) (115,119). It may be that these mutants more generally destabilize the protein, or that the binding regions in *S. pombe* are different from those in *S. cerevisiae*.

In contrast, the known *VCP* IBMPFD disease mutations are all clustered in the N and D1 domains at the N-D1 interface (ClinVar). These mutations increase ATPase activity and alter

cofactor binding, resulting in defects in autophagy (especially clearance of damaged mitochondria), lysosomal degradation, and endosomal trafficking (83,84,86,88,90). The disease mechanism for these *VCP* mutations is related to mitochondrial uncoupling and a decrease in cellular ATP followed by a failure to clear these damaged mitochondria (87,91,175,176). It is difficult to imagine a way in which our *cdc48* point mutations are having a similar effect in *S. pombe*, with the downstream result being a defect in SREBP activation at the Golgi.

As an alternative, our previous work showed that the Dsc E3 ligase enzymatic function is required for proper Golgi localization (73). One attractive hypothesis is that both Dsc E3 ligase function and Cdc48 activity are required for the same process, which permits traffic of the Dsc E3 ligase to the Golgi. Perhaps there is a protein in the ER that binds the Dsc E3 ligase and represses traffic to the Golgi, possibly by inhibiting packaging into COPII vesicles. To appropriately traffic to the Golgi, the Dsc E3 ligase may need to ubiquitylate the repressor, and then Cdc48 would extract it from the complex and/or membrane for degradation by the proteasome. This function would be consistent with Cdc48's activity as a separase, and is indeed analogous to its role in ERAD. This would provide a quality control mechanism to ensure that the Dsc E3 ligase is functional before being shipped to its final destination. Consistent with this hypothesis, the Sre1 precursor is not degraded in the *cdc48* mutants after Brefeldin A treatment, suggesting that the Dsc E3 ligase is unable to ubiquitylate Sre1 (**Fig. *A.3A***). To determine the identity of the repressor, I performed an overexpression screen, reasoning that overexpression of a repressor of Dsc E3 ligase transport would result in a failure to cleave Sre1 (**Fig. *A.4-A.6***). That screen failed to identify the repressor, but it may be that the removal of the repressor by the Dsc E3 ligase under normal conditions is too rapid for overexpression of the repressor to inhibit Sre1 cleavage. Future work may instead try to identify proteins bound to the Dsc E3 ligase under transport-inhibited conditions, such as in the *cdc48* mutants.

Beyond a role during Dsc E3 ligase Golgi localization, it is still relatively unclear what role Cdc48 is playing when bound to Rbd2. I hypothesize that Cdc48 could impact three steps of

substrate cleavage by Rbd2: (1) substrate identification/binding including substrate positioning, (2) enzymatic catalysis, and/or (3) substrate extraction after cleavage. Because Rbd2 functions after the Dsc E3 ligase in the SREBP cleavage activation pathway, it is difficult to dissect the impact of our *cdc48* point mutants on Cdc48 function at Rbd2. However, it is possible that these point mutants are also having an impact on cleavage by Rbd2, and that the effects we observe on SREBP cleavage are additive of both of these roles for Cdc48. In lieu of being able to study the effects of the *cdc48* point mutants on Rbd2, a previous report utilized mutation of the Cdc48 binding domain (SHP) on Rbd2 (71). That study concluded that Cdc48 functions as a substrate adaptor for Rbd2, bringing the SREBP and Rbd2 together in the Golgi membrane for cleavage. This hypothesis was based on the observation that overexpression of Rbd2 lacking the SHP domain, which cannot bind Cdc48, was able to rescue the SREBP cleavage defect of an *rbd2Δ* strain, indicating that Cdc48 binding to Rbd2 is not strictly required for cleavage (71). Additionally, no membrane-bound cleavage intermediate was observed in the absence of Cdc48 binding, as might be expected from a defect in substrate extraction. The literature suggests that rhomboid proteases have relatively little substrate affinity, and that substrate interaction is rate-limiting to cleavage (177). Therefore, an adaptor that increases interaction between Rbd2 and the SREBP would be very beneficial to the rate of SREBP activation, especially given that SREBPs are degraded by the proteasome when not cleaved by Rbd2, possibly in a time-dependent manner (71). Additionally, a recent report indicated that the length of the ubiquitin chain determines the ability of Cdc48 to unfold the client protein, with short chains showing interaction with Cdc48 but not induction of ATPase activity (81). Therefore it is possible that a short ubiquitin chain on the SREBP would allow recognition by Cdc48 without unfolding.

In counterpoint, while Cdc48 binding to Rbd2 can be readily observed in the cell, Cdc48 interaction with the SREBP substrate has not been shown (71). This may be due to the rapid processing and release of the SREBP under normal conditions, but it could also indicate that the Cdc48-Rbd2 interaction is more stable than the Cdc48-SREBP interaction, calling into question

its ability to bring substrates to Rbd2. Further, while the conclusion that Cdc48 acts as a substrate adaptor for Rbd2 is consistent with the expected mechanism for a rhomboid protease, it is not consistent with the Cdc48 literature. In fact, to my knowledge, such a role would be completely unprecedented in any species. Instead, Cdc48 has been very well described to perform the mechanical function of pulling and separating ubiquitylated substrates from protein complexes or membranes. This canonical function could be used to reorient the SREBP transmembrane domain for access by Rbd2, for example, if it was poorly positioned in the Golgi membrane. This role would still occur prior to Rbd2 cleavage, but would be more consistent with known activities of Cdc48.

Alternatively, a requirement for Cdc48 during extraction of the cleaved SREBP substrate from the Golgi membrane after cleavage (Step 3) would be completely consistent with the literature. Indeed, such a mechanism was demonstrated in mammals for substrate extraction after cleavage by the rhomboid protease RHBDL4 during ERAD (76). Consistently, Rbd2 is predicted to cleave the SREBP in the second transmembrane segment or luminal loop, leaving the N-terminus attached to the Golgi via the first transmembrane domain (71). A second Golgi protease could release the final transcription factor, but so far none has been identified. Instead, Cdc48 bound to Rbd2 could extract this intermediate from both the membrane and the complex with Rbd2, making it available to cytoplasmic proteases for further processing. If substrate extraction is the main role for Cdc48 at Rbd2, mutation of the SHP domain would be expected to produce SREBP cleavage intermediates trapped in the Golgi membrane. However, if extraction of the substrate by Cdc48 is required to release Rbd2 for subsequent rounds of catalytic activity, then the unextracted substrate could quickly clog and inhibit the available Rbd2, resulting in a cleavage block and accumulation of only a very small amount of cleavage intermediate that may not be visible by western blot. This would be improved by overexpression of the SHP mutant Rbd2, as was observed. Future work differentiating these potential roles for Cdc48 at Rbd2 would be aided by identification of cofactors involved in this process, and genetic bypass of the role for

Cdc48 at the Dsc E3 ligase (through identification of the repressor) so that the impact of the *cdc48* point mutants at this step can be evaluated.

5.3 What regulates other oxygen-responsive genes?

Only 38% of *S. pombe* anaerobically upregulated genes are transcriptional targets of either Mga2 or Sre1 (**Fig. *3.3B***). Thus, additional transcriptional regulators of low oxygen-responsive pathways remain to be discovered in both this and other fungal species (54). Carbohydrate catabolism and aerobic respiration are two conserved regulated pathways **(Fig. *1.1*)**. Enriched GO terms upregulated by low oxygen include carbohydrate metabolic process (GO:0005975), glucose catabolic process (GO:0006007), acetyl-CoA biosynthetic process from acetate (GO:0019427), and generation of precursor metabolites and energy (GO:0006091). In contrast, GO terms downregulated by low oxygen include aerobic respiration (GO:0009060) and respiratory electron transport chain (GO:0022904). Each molecule of glucose consumed via aerobic respiration requires six molecules of oxygen for full ATP output, whereas glucose metabolism via ethanol fermentation requires no oxygen (178). Therefore under low oxygen conditions, glycolysis is upregulated while aerobic respiration is downregulated. This serves to efficiently produce ATP and acetyl-CoA for lipid biosynthesis.

Regulation of carbohydrate synthesis in response to low oxygen has been relatively poorly studied in any fungal species. *S. cerevisiae* exhibit a unique reliance on fermentation even in the presence of oxygen due to a strong glucose-repression circuit, a phenomenon known as the Crabtree effect (179,180). Therefore *S. cerevisiae* have little regulation of carbohydrate metabolism in response to oxygen and only upregulate carbohydrate metabolic process (GO:0005975), instead showing regulation of carbohydrate metabolism almost entirely by carbon source (55,181). In contrast, carbohydrate metabolism in other fungi is more clearly regulated by oxygen. In *C. albicans*, the soluble bHLH transcription factor Tye7 and the soluble Gal4 transcription factor upregulate glycolytic gene expression in fermentative conditions as well as in

response to low oxygen (182). Interestingly, Tye7 is an Sre1N homolog (127). When *tye7* was deleted, *C. albicans* accumulated trehalose and glycogen under normoxic conditions, suggesting that *tye7* is required for directing the cells towards glycolysis and away from storage lipids (182). The homologs of *tye7* and *gal4* in *S. cerevisiae* also regulate glycolysis, although not in response to oxygen (183). In *C. parapsilosis*, glycolytic genes are induced by Upc2 in response to low oxygen, although to a lesser extent than ergosterol synthesis genes (57).

The transcriptional regulator of carbohydrate metabolism in *S. pombe* is unknown. This thesis work reports the full results of the first screen of the *S. pombe* non-essential haploid deletion collection version 1.0 for gene deletions sensitive to low oxygen (68,70). We expected that deletion of a transcription factor required for low oxygen adaptation would be sensitive to low oxygen and $CoCl_2$. However, *mga2* was the only transcription factor that satisfied these characteristics (**Supplementary Table 3.1**). It is possible that lipid homeostasis is more sensitive to low oxygen than other pathways. However, it is also the case that this deletion collection does not contain deletions of all non-essential genes, not to mention essential genes. Screening conditions may also have resulted in missed hits. Ryuko *et al.* previously performed a screen of the 3,004 *S. pombe* deletion collection version 2.0 strains for growth on 3.5 mM $CoCl_2$ (184). We used 1.6 mM $CoCl_2$ in our screen. They found 54 gene deletions sensitive to $CoCl_2$ and 56 gene deletions resistant to $CoCl_2$. Of the 67 deletions that we found sensitive to $CoCl_2$, only 11 were also identified by Ryuko *et al.* as sensitive to $CoCl_2$ (**Supplementary Table 3.3**). The small overlap between these studies may be due to the different concentrations of $CoCl_2$ used, leading to selection for different responses to the chemical. We chose a concentration sufficient to inhibit growth of *sre1*Δ cells in order to mimic hypoxia. By screening under two conditions (low oxygen and $CoCl_2$), we focused our search to those genes most likely to be involved in low oxygen response. Additionally, another group recently screened the 669 strains of deletion collection version 2.0 that are not present in deletion collection version 1.0 (screened in this study) for growth on both $CoCl_2$ and under low oxygen. They identified 33 genes required for growth under

low-oxygen and/or $CoCl_2$ conditions, although they only reported the identity of one, the rhomboid protease *rbd2* (138). A directed evaluation of transcription factor deletions or knock down in fission yeast may yet identify additional factors required for low oxygen adaptation that were missed in our screen.

Despite not identifying any additional transcription factor candidates, this deletion collection screen identified 105 gene deletions that resulted in sensitivity to low oxygen and/or the low oxygen mimetic $CoCl_2$, with 27 deletions resulting in sensitivity to both (68,70). Interestingly, we identified 19 genes that are required for adaptation to low oxygen stress but are not deficient in Sre1N accumulation (**Table 3.2**). These genes may represent other pathways required to adapt to oxygen stress. These genes include multiple players of three separate pathways (**Supplementary Tables 3.2-3.3**).

The first highly represented pathway sensitive to low oxygen and $CoCl_2$ is transport between the endosome and the Golgi or the vacuole (*ryh1, sec28, vsp8, vps17, vps24, vps26, vps29, vps32, vps35, vps36*). This transport could be required to maintain V-type H+ ATPase at the vacuole. It has been shown in budding yeast that in the absence of V-ATPase function, the cytosol acidifies (185). Normally, the plasma membrane proton pump Pma1 would compensate by hydrolyzing ATP and pumping out protons (186). However under low oxygen, reduced oxidative respiration may decrease cellular ATP (187), creating conditions that require full V-ATPase activity to maintain cytosolic pH.

The second pathway sensitive to both low oxygen and $CoCl_2$ is Mediator (*med20*, *nut2*). Highly conserved from yeast to humans, the Mediator complex, composed of 13 subunits in fission yeast, is required for regulated expression of most RNA polymerase II-dependent genes (188,189). A potential role of Mediator in regulating low oxygen adaptation in fission yeast is consistent with data in humans and *C. elegans* showing that Mediator is required for SREBP transcriptional activation of target genes, as well as lipid homeostasis and fatty acid desaturation

(190). Because mediator is required at a post-cleavage step in the SREBP pathway, the effects of these mutants may not be apparent in a cleavage assay.

A third pathway sensitive to only low oxygen in our screen is miRNA biogenesis (*arb1, arb2, dcr1*). Interestingly, a number of recent papers have suggested that chronic hypoxia induces downregulation of miRNA biogenesis in order to maintain HIFα induction in vascular endothelial and cancer cell lines (191-193). This adaptation is correlated with tumor progression and poor prognosis (192,193). However, other recent work has identified the micro-RNA miR-210 as a "master" hypoxia-regulated miRNA, exhibiting upregulation by HIF-1α under conditions of hypoxia (194-196). miR-210 promotes cell-cycle progression and evasion of apoptosis while compromising mitochondrial integrity and DNA repair in numerous cancer cell lines (196). Additional work is required to fully understand the complex interplay between miRNA biogenesis and hypoxia adaptation in human cells, as well as in fission yeast, which lack a HIF homolog.

In addition to *mga2*, this screen identified three genes that were required for Sre1N accumulation but were not rescued by exogenous Sre1N (**Fig. *3.1C***). Cpp1 is a subunit of protein farnesyltransferase required for farnesylation of small GTPases such as Ras and Rheb. *cpp1Δ* exhibits severe normoxia growth defects and temperature sensitivity as well as morphological defects, indicating a role for farnesylation in a number of processes, one of which may be Sre1 activation (197). Trx2 is a mitochondrial oxidoreductase that helps to maintain the mitochondrial redox state, especially in the absence of glutathione (198,199). Ppr6 is a mitochondrial membrane protein that regulates the mRNA stability of the mitochondrial ATP synthase subunit *atp9*. In the absence of *ppr6*, *atp9* mRNA is reduced and cells become sensitive to galactose and antimycin, indicating defects in aerobic respiration (200). Taken together, these data suggest a role for mitochondrial function in regulating Sre1 activation and cellular adaptation to low oxygen and $CoCl_2$, consistent with the microarray results.

5.4 Are these pathways conserved in other fungal species?

We believe the requirement for metabolic changes during successful adaptation to low oxygen is an exploitable "Achilles heel" of pathogenic fungal infection and a potential source of new antifungal targets. The success of azole drugs, which target ergosterol biosynthesis, supports this hypothesis. However, azoles only target a single enzyme of the ergosterol biosynthesis pathway, and there is nothing unique about sterol biosynthesis that makes it a preferred drug target over other metabolic pathways. Therefore, we consider ergosterol biosynthesis, fatty acid biosynthesis, and carbohydrate metabolism to be attractive open fields for targeted drug development. Conservation of the regulation of lipid homeostasis in response to low oxygen by Sre1 and Mga2 in other fungal species would indicate potential for targeting these pathways with antifungal drugs. Indeed over 20 fungal species, including human and plant pathogens, have predicted Sre1 homologs (**Table 1.1**), suggesting that this pathway may be a common mechanism for sterol regulation in response to oxygen. In the human pathogen *Aspergillus fumigatus*, the Sre1 homolog SrbA is activated by the Dsc E3 ligase homologs DscA-D and the Rbd2 homolog RbdB. This pathway is required for hypoxia adaptation and virulence in Invasive Pulmonary Aspergillosis mouse models (125,126,201). Interestingly there is no *scp1* homolog in *A. fumigatus* (202). Therefore it is unknown how SrbA cleavage is regulated by oxygen. Similarly in *Histoplasma capsulatum*, the *sre1* homolog *srb1* regulates ergosterol biosynthesis in response to low oxygen and is required for virulence in intranasal mouse infectivity studies (128). An *sre1* homolog called *srbA* was also recently identified in *Paracoccidioides* species, and *rbd2* is conserved in *Neurospora crassa* (201,203). No role for homologs of other pathway components has yet been examined in these species. Thus, the role of Sre1 homologs in the oxygen response and sterol regulation is conserved in other *Ascomycota* fungal species and is crucial for virulence in several pathogens.

Interestingly, *Cryptococcus* fungal species also have predicted *sre1* homologs, but the mechanism of activation is distinct from that described in *S. pombe*. In *Cryptococcus neoformans*,

the Sre1 low oxygen response is required for virulence in mouse models of meningoencephalitis (204). However, *C. neoformans* Sre1 is activated by a mammalian Site-2 protease homolog, Stp1, instead of the Dsc E3 ligase and rhomboid protease required in *S. pombe* (205). Site-2 protease homologs are predicted in at least seven *Basidiomycota* (including *Cryptococcus*) and *Zygomycota* fungal species. Interestingly, no *Basidiomycetes* have *rbd2* or *dsc4* homologs (**Table 1.1**). Therefore *C. neoformans* appears to have retained the Site-2 protease cleavage mechanism that was present in the common ancestor of fungi and humans (for an excellent review on the evolution of hypoxic gene regulation see (202)).

In contrast, during the evolution of *Saccharomycotina* fungi, including *Saccharomyces cerevisiae* and *Candida* spp., SREBP homologs (like *hms1* and *cph2*) lost the C-terminal DUF2014 domain and with it their role as regulators of sterol biosynthesis (59). This domain is required for Sre1 binding to Scp1; therefore it is likely that *cph2* proteins cannot sense and respond to sterol levels (206). Instead, *cph2* transcription factors regulate hyphal growth (207). Regulating sterol biosynthesis in their place is *upc2* (also called *mox4*), a GAL4-type zinc finger transcription factor. The last species that contains full-length orthologs of both *sre1* and *upc2* transcription factors is *Yarrowia lipolytica*, where Upc2 plays the predominant role in low oxygen sterol regulation, while Sre1 primarily regulates filamentation (59). Upc2 was initially characterized in *S. cerevisiae*, where it upregulates transcription of genes required for ergosterol biosynthesis in response to low sterols and low oxygen in a semi-redundant fashion with the homologous transcription factor Ecm22 (208-210). Like Sre1, Upc2 binds SRE elements in its own promoter, creating positive feedback within the system (210). Further studies in *Candida albicans, Candida glabrata, Candida parapsilosis*, and *Candida tropicalis* showed that Upc2 regulates ergosterol biosynthesis and sterol uptake (211-215). Recent structural and biophysical studies showed that Upc2 has a C-terminal ligand-binding domain that binds ergosterol *in vivo* (216). Additionally, Upc2, Ecm22, and *C. albicans* Upc2 form ligand-independent homodimers through interactions of the ligand binding domains (216).

Data on the cellular localization and activation mechanism of *S. cerevisiae* Upc2 and Ecm22 are conflicting. Prediction programs such as Phobius, TMHMM, and TMPred predict between 0-4 transmembrane domains with a single transmembrane domain near the C-terminus scoring the highest confidence. A C-terminally GFP-tagged Upc2 had ER or Golgi localization under normal conditions, and became more cytoplasmic and perinuclear upon inhibition of ergosterol biosynthesis (217). This result was replicated by indirect immunofluorescence using C-terminally FLAG-tagged Upc2. The authors proposed an SREBP-like activation mechanism for Upc2, where membrane-tethering through the transmembrane domain(s) inactivates Upc2 until low ergosterol conditions allow for membrane release (217).

In contrast, a recent report showed that N-terminally GFP-tagged Upc2, designed to avoid adverse interactions between GFP and the C-terminal ligand binding and activation domains, exhibited cytosolic localization in ergosterol-replete conditions and nuclear localization in ergosterol-depleted conditions (216). This nuclear localization is consistent with the role of Upc2 as a transcription factor. Importantly, Upc2 has an intrinsic nuclear localization sequence, and deletion of the ligand-binding domain caused constitutive nuclear localization, suggesting that ergosterol binding excludes Upc2 from the nucleus (216). However, it is important to note that the ligand-binding domain encompasses the strongest predicted transmembrane domain, and the effects of its deletion on potential membrane binding were not examined. These authors concluded that Upc2 is normally cytoplasmic, and that it senses ergosterol by extracting sterol from the plasma membrane based on the ability of Upc2 to extract ergosterol from liposomes *in vitro* (216). It is unclear what the dynamic range of ergosterol sensing would be for such a mechanism. Future studies will be needed to determine whether Upc2 is membrane-bound or cytosolic and to provide a clearer mechanism for ergosterol sensing in this system.

In addition to activation of ergosterol synthesis by Upc2, *S. cerevisiae* evolved a repressive system to turn off hypoxic-responsive genes under aerobic conditions. This system relies on two soluble transcriptional repressors, Mot3 and Rox1, a C2H2 zinc finger transcription

factor and an HMG-box Sox family transcription factor, respectively (218-222). Mot3 and Rox1 are in turn repressed by the soluble Hap1 GAL4-like zinc-finger transcription factor in a heme-dependent manner (223-225). Under normoxic conditions, Hap1 binds heme causing it to stop repressing Mot3 and Rox1, which go on to repress expression of low oxygen-responsive genes (225). Under low oxygen conditions, when heme is not synthesized, Hap1 repression of Mot3 and Rox1 allows expression of low oxygen-responsive genes. Mot3 and Rox1 work together with Upc2 to regulate ergosterol synthesis, but they also regulate the DAN/TIR group of hypoxic responsive genes involved in remodeling the cell wall in response to low oxygen (210,225). Interestingly, Rox1 is also thought to repress expression of the Δ9 fatty acid desaturase *OLE1* (226). Conservation of the Mot3-Rox1 regulation of ergosterol in response to oxygen has not been shown in other organisms, and Sre1 and Upc2 are thought to be the primary regulators of the sterol low oxygen response in fungi.

Interestingly, *S. cerevisiae* does have homologs to *S. pombe ofd1* and *nro1* called *TPA1* and *ETT1*, respectively. Deletion of either protein caused increased stop-codon read-through, suggesting that *TPA1* and *ETT1* act in the same direction, rather than *ETT1* inhibiting *TPA1* (227,228). More recent studies suggested that the effect on read-through is context dependent, with read-through in the absence of *TPA1* increasing in some cases and decreasing in others (94). These effects of Tpa1 on translational fidelity stem from Tpa1's role in the dihydroxylation of ribosomal protein Rps23 (94). Strikingly, a recent study found that Tpa1 is also involved in DNA damage repair, and deletion of *TPA1* resulted in sensitivity to alkylating agents that appears to be distinct from any role in stop-codon read through (229). Additional work is needed to understand how Tpa1 functions in genome maintenance and whether Tpa1 plays a role in the *S. cerevisiae* low oxygen response.

While Mga2 homologs in *S. cerevisiae* are well-established regulators of fatty acid desaturation and the fatty acid transcriptional response to low oxygen, conservation in other fungi has been less studied. One important consideration is that most fungi express multiple oxygen-

dependent fatty acid desaturases, Δ9, Δ12, and Δ15, and each desaturase may be regulated by a different transcription factor (230). Nevertheless, *mga2* has apparent homologs in at least 35 fungal species, including the fungal pathogens *A. fumigatus, A. flavus, H. capsulatum, C. neoformans, C. gattii, C. albicans,* and *C. glabrata.* These homologs are characterized by an IPT immunoglobulin-like DNA binding domain, an Ankyrin repeat, and a transmembrane domain near the C-terminus (231,232) (**Table 1.1**). Work in *Kluyveromyces lactis* showed that Mga2 regulates squalene epoxidase, fatty acid synthase, and alcohol acetyltransferase in response to low oxygen (233). Deletion of *MGA2* resulted in increased oleate, decreased polyunsaturated fatty acids, and decreased membrane fluidity (233). In *C. albicans*, *SPT23* (an *MGA2* homolog) is required for *OLE1* expression, and knock down of SPT23 results in cell inviability and a reduction in unsaturated fatty acids (234). However, another group analyzed the *C. albicans* transcriptional response to hypoxia and found that the soluble bHLH transcription factor *EFG1*, which regulates glycolysis, oxidative metabolism, and filamentous growth under normoxia, is required for the upregulation of fatty acid biosynthesis genes including *OLE1* under low oxygen (235). Further, they observed decreases in polyunsaturated fatty acids in the absence of *EFG1* under low oxygen conditions (235). It is not known whether *SPT23* and *EFG1* regulate fatty acid biosynthesis separately or in concert in *C. albicans*, but numerous studies of *EFG1* homologs in other fungi have not yet identified a role in regulation of fatty acid biosynthesis under low oxygen conditions. Clearly the *MGA2* family of transcription factors is conserved in a number of fungal species, but like for SREBPs, additional mechanisms for regulating fatty acid desaturation, GPL, and TAG biosynthesis may have evolved over time. Future studies will characterize *mga2* homologs in these organisms to determine if they also regulate pathways required for low oxygen adaptation and fungal virulence.

The coordination of these two oxygen responsive pathways in fission yeast may also be conserved in the over 20 fungal species that have predicted Sre1 and Mga2 homologs (**Table 1.1**). But whether and how the carbohydrate response is coordinated with lipid homeostasis in fission

yeast is yet to be determined. Other models of coordination exist in the literature. One alternative method to coordinate these disparate pathways is through a shared master transcription factor or transcription factor cascade. In *C. parapsilosis*, sterol and carbohydrate biosynthesis are both regulated by Upc2 (57). In *K. lactis*, low oxygen induction of *MGA2* is dependent on the plasma membrane glucose sensor Rag4, previously shown to inhibit the GAL4-like zinc-finger transcriptional repressor Rgt1 (233,236). This suggests that the *K. lactis* low oxygen lipid response is dependent on glucose availability. In *S. cerevisiae*, sphingolipid biosynthesis is dependent on sterols, although the mechanism of this coordination is not known (237).

Conservation of these low oxygen-responsive pathways and their coordination in other fungal species is important if these discoveries are to translate to antifungal drug development. Available research supports the relevance of these pathways to fungal pathogenesis. Sites of fungal infection are hypoxic and fungal pathogens require SREBP to adapt to these conditions and remain virulent, demonstrating conservation of this low oxygen-responsive pathway across yeast species (238). Consequently, the SREBP pathway is an important antifungal drug target (205,238-240). Indeed in *A. fumigatus*, *srbA*, the Dsc E3 ligase, and the rhomboid protease are required for azole drug resistance (125,201). Importantly, inhibition of the Sre1 pathway in *C. neoformans* not only reduced azole drug tolerance, but also converted azole drugs from fungistatic to fungicidal agents (204,205). This suggests synergy may exist between future inhibitors of the Sre1 activation pathway and current azole drugs. In contrast, in *S. cerevisiae, C. albicans, C. glabrata, C. parapsilosis*, and *C. tropicalis*, where there are no SREBP homologs, *UPC2* is required for azole resistance, suggesting that regardless of the transcription factor employed, transcriptional regulation of ergosterol biosynthesis affects the efficacy of azole drugs (211-216).

Finally, the Mga2 pathway represents a new avenue for antifungal drug discovery. Although no currently available antifungal drugs target the fatty acid biosynthesis pathway headed by Mga2, the antifungal cerulenin is used in biochemical studies to block fatty acid

synthase activity and has low (ug/mL) minimal inhibitory concentrations in a number of pathogenic fungal species (241). Therefore, there is potential for success in future development of antifungal drugs targeting this pathway. Additionally, unlike the SREBP transcription factors, Mga2 has no apparent homologs in humans, limiting the potential toxic effects of drugs targeting this pathway. Given the reported coordination between the fatty acid and sterol biosynthesis pathways, targeting of fatty acid biosynthesis may hit both of these important adaptations with a single drug. These data suggest that mechanisms of low oxygen adaptation are a largely untapped source for advances in treatment of pathogenic fungal infection.

5.5 Final thoughts

Recent years have yielded great advances in our understanding of the transcriptional regulation of the low oxygen response, resulting in the identification of many conserved pathways. However, in order to develop antifungal therapies that target low oxygen adaptation, additional work is needed to understand the mechanisms of these pathways. The identification of over a dozen regulators of low oxygen lipid homeostasis holds promise for targeted drug development (**Table 1.1**). But understanding how each of these proteins regulates the low oxygen response, as well as whether they play additional off-pathway roles in the cell, will be important for predicting drug outcomes. In addition to lipid homeostasis, changes in carbohydrate metabolism and aerobic respiration are important low oxygen responses, but the transcriptional regulators of this response are largely unidentified. *S. pombe* and *S. cerevisiae*, as well as the highly-annotated pathogens *A. fumigatus* and *C. albicans*, will prove valuable models for identification and dissection of these transcriptional pathways.

Experiments in pathogenic fungi highlight the importance of these metabolic pathways in low oxygen adaptation and virulence. However, many questions still remain about the pathogenic low oxygen response in the host. In addition to changes in oxygen availability, the host environment is distinct in other ways, including pH, carbon dioxide, and nutrient levels. It is

unknown how the pathogenic low oxygen response is coordinated with responses to these other factors. A broader view of the pathogen host response could be achieved through the combination of CRISPR/Cas9 gene deletion and pooled screening methods, in order to identify genes required for host adaptation directly in the animal (242-245). This analysis will be important to focus on the most important pathways for further research.

Finally, in the development of drugs targeting these pathways, a few important considerations need to be addressed. Can the promising results gained with deletion of transcription factors be recapitulated with chemical inhibition of these transcriptional pathways? Particularly, what is the time scale in which chemical inhibition of transcription leads to a block in pathogen growth, and how does this compare with the time scale of disease? There is a fundamental difference between pathogens that cannot initiate an infection due to chronic absence of a gene and those infections that are successfully treated by acute chemical inhibition of that gene product. If inhibition at the level of transcription takes too long to result in effective changes in lipid homeostasis, the host may succumb to the infection before the pathogen succumbs to the therapy. In this case, targeting enzymes in these metabolic pathways rather than transcription factors may be the most effective route. Additionally, does coordination of oxygen-responsive transcriptional pathways lend itself to development of drugs with pleiotropic effects? And what synergies exist between new targets and existing antifungal therapies? Multidrug combinations have the greatest promise for fungicidal effects and slowing of the development of antifungal resistance. Therefore, it will be important to test a variety of drug combinations and consider pathway coordination for greatest treatment success.

With growing concern about the threat of pathogenic fungi and the rise of antifungal resistance, the next decade is likely to produce answers to many of these questions as we see a renewed focus on both pathogenic and non-pathogenic fungal research.

Chapter A

Appendix

A.1 Summary

My thesis work answered many fundamental questions regarding how fission yeast regulate lipid homeostasis in response to oxygen, but a number of holes are yet to be filled, especially regarding the role of Cdc48 during SREBP cleavage. This section reports a few preliminary results that alone are largely inconclusive, but support the previous results or indicate an answer to these remaining questions. Future work and repetition is needed to evaluate the significance and meaning of these results.

A.2 Results

sum3 does not have a large effect on Sre1 cleavage – The RNA helicase *sum3* was identified as required for Sre1 activity by whole genome sequencing of two linked MMS mutagenesis strains (**Fig. *2.1***). To test whether a failure to produce Sre1N caused the observed growth rescue on 5-FOA, we expressed *sre1N* from a plasmid and assayed growth on $CoCl_2$. We observed rescue of growth for the control *sre1Δ* strain, but no rescue of growth for the *sum3-1* strain (**Fig. *A.1A***). To directly assess Sre1N production in the *sum3-1* mutant, we assayed Sre1 cleavage by western blot. We cultured wild-type, *sre1Δ,* and *sum3-1* mutant cells for 4 h plus or minus oxygen. We then probed whole cell lysates with anti-Sre1N, which detects both the full-length ER-membrane bound precursor form (P) as well as the cleaved N-terminal transcription factor form (N). Wild-type cells accumulated Sre1N after 4 hours of growth under low oxygen (**Fig. *A.1B***, lanes 1-2). The *sum3-1* mutant strain showed a partial Sre1N accumulation defect (**Fig. *A.1B***, lanes 10-11). Together, these data suggest that *sum3-1* does not play a large role in Sre1 activation, and is likely affecting more general rates of translation during the stress response to 5-FOA.

ubx3 required for efficient Sre1 activation – The p47 homolog *ubx3* was identified in the Cdc48 binding protein mass spectrometry analysis (**Fig. *2.4***). To test whether it is required for low oxygen adaptation, we assayed growth of the deletion on $CoCl_2$ with *sre1N* or empty vector

expressed on a plasmid. Growth of the deletion was partially defective on $CoCl_2$, and that defect was rescued with *sre1N* expression (**Fig. *A.2A***). To determine the effects of *ubx3* deletion on Sre1 cleavage, we assayed Sre1N accumulation by western blot. We cultured wild-type, *ubx3Δ,* and *sre1Δ* cells in anoxic conditions for 0 or 4 hours. *ubx3Δ* cells displayed a partial Sre1 cleavage defect under low oxygen conditions (**Fig. *A.2B***) indicating that *ubx3* is required for efficient Sre1 activation. To determine whether that role for *ubx3* is during Dsc E3 ligase transport to the Golgi, we examined Dsc1 glycosylation in the *ubx3Δ* cells. In the absence of *ubx3*, the glycosylation pattern looked similar to wild-type, with accumulation of primarily the mature glycosylated form indicating arrival of Dsc1 in the Golgi (**Fig. *A.2C,*** lanes 1-2). This is in contrast to *cdc48-8* and *dsc2Δ*, which accumulated the intermediate, ER localized Dsc1 (**Fig. *A.2C***, lanes 3-4). Therefore, we conclude that *ubx3* may have a role in Sre1 activation but it is not during Dsc E3 ligase Golgi localization.

Instead, *ubx3* could be required during the interaction between Cdc48 and Rbd2 (71). To determine whether Ubx3 physically associates with Cdc48 when bound to Rbd2, we performed an *in vitro* pull-down experiment from *ufd1-13xmyc* and *ubx3-13xmyc* lysates using GST-tagged Dsc5 UBX domain, GST-tagged Rbd2 SHP domain, or GST alone. As previously shown, Ufd1-13xMyc was pulled down by GST-UBX but not GST-SHP (**Fig. *A.2D***, lanes 11 vs 13). In contrast, Ubx3-13xMyc was not pulled down by either domain, suggesting that Ubx3 does not interact with Cdc48 at Dsc5 or Rbd2 (**Fig. *A.2D***, lanes 12 and 14). However, direct immunoprecipitation of Cdc48 in the *ubx3-13xmyc* and *ufd1-13xmyc* cells also pulled down very little Ubx3-13xMyc relative to the amount of Ufd1-13xMyc (**Fig. *A.2E,*** lanes 5 vs 6). Further, the reciprocal immunoprecipitation against Myc showed the opposite result, with much more Cdc48 pulled down from the *ubx3-13xmyc* cells relative to the *ufd1-13xmyc* cells (**Fig. *A.2F,*** lanes 8 vs 9). This is despite the fact that both showed similar input levels and both were similarly enriched in the Cdc48 mass spectrometry results (**Table 2.1**). It is possible that the polyclonal Cdc48 antibody interferes with the interaction between Cdc48 and its cofactors. It may be that the GST-

tagged Cdc48 binding domains also interfere with this interaction, leaving open the possibility that Ubx3 interacts with Cdc48 while at Rbd2.

What is Cdc48 doing at the Dsc E3 ligase? – Our published data indicate that Cdc48-Ufd1 is required for Dsc E3 ligase Golgi localization, but it is unclear what specifically it is doing there. To determine why the Dsc E3 ligase is mislocalized in the *cdc48* mutants, we assayed Dsc E3 ligase complex function using a Brefeldin A (BFA) assay. BFA blocks transport from the ER to the Golgi, thereby merging the ER and Golgi compartments since Golgi proteins recycle to the ER (68). We previously showed that incubation of fission yeast with BFA results in degradation of the Sre1 precursor in a Dsc E3 ligase-dependent manner (68). Therefore, this assay reports on the function of the Dsc E3 ligase in mutant strains. After 2 h incubation with BFA, *WT* cells showed degradation of Sre1-P as expected (**Fig. *A.3A***, lane 2). In contrast, in *dsc2Δ* cells, Sre1-P was stabilized after 2 h incubation with BFA, confirming that the Dsc E3 ligase is required for the degradation observed in *WT* cells (**Fig. *A.3A***, lane 12). In all the *cdc48* mutants tested, Sre1-P was also stabilized after 2 h incubation with BFA (**Fig. *A.3A***, lanes 3-10). This suggests that *cdc48* is required, not just for Dsc E3 ligase localization, but for Dsc E3 ligase-dependent degradation of SREBP, and that without this Cdc48 activity the E3 ligase fails to traffic to the Golgi and cleave SREBPs. However, because *cdc48* is required for a number of cellular degradative processes, a caveat of this experiment is that *cdc48* may be required for the degradation of the Sre1-P subsequent to its ubiquitylation, rather than ubiquitylation by the Dsc E3 ligase, resulting in stabilizing of the Sre1-P. However, in that case we might expect accumulation of a higher molecular weight ubiquitylated Sre1-P band in the 2 h lanes when *cdc48* is mutated, which is not observed upon three repeated experiments.

In addition to the role for Cdc48 at the Dsc E3 ligase, it is also unclear what effect the *cdc48* and *ufd1* mutants are having on the Cdc48-Ufd1 complex. To assay the effect of these mutants on Cdc48-Ufd1 complex formation, we performed immunoprecipitations of either Ufd1-13xMyc (anti-Myc) in the *cdc48* mutant backgrounds, or Cdc48 in the *ufd1* mutant backgrounds.

Interestingly, Ufd1-13xMyc binding to Cdc48 was weakest in the wild-type strains and stronger in the mutant strains (**Fig. *A3.B***, lanes 8,11 vs 9,10,12-14). The reciprocal experiment analyzing *ufd1* mutants was less easy to interpret, because expression level of Ufd1-13xMyc was variable (**Fig. *A3.C***). A strengthened interaction between Cdc48 and its cofactor resulting in a phenotypic defect has precedent in the literature, and may indicate a reduced rate of ATP hydrolysis (81,246).

Overexpression screen for genes repressing Sre1 activity – Based on the role for Cdc48-Ufd1 during Dsc E3 ligase Golgi localization, we hypothesized that there may be a protein that represses Dsc E3 ligase export from the ER unless ubiquitylated by Dsc1 and extracted by Cdc48-Ufd1 (see **Chapter 5.2**). To identify such a repressor, we reasoned that overexpression of that protein may inhibit Sre1 cleavage. Therefore we generated a reporter strain in which Sre1 binding sites were in the promoter of the *ura4* gene, so that when Sre1 is functional, orotidine 5'-phosphate decarboxylase (Ura4) is produced (69). We deleted the Sre1 inhibitor *ofd1* in this strain so that basal Sre1 activity would be increased and to avoid isolating regulators of the Ofd1-Nro1 interaction (95). When this reporter strain was plated on 5-fluoroorotic acid (5-FOA), it was converted to the toxic 5-fluorouracil by Ura4 and killed the cells. We transformed this reporter strain with an *S. pombe* cDNA library, and reasoned that any gene whose overexpression blocked Sre1 cleavage would rescue growth on 5-FOA.

This experiment screened 6.1×10^5 transformants and isolated 183 colonies that were resistant to 5-FOA, encompassing 86 genes (**Supplementary Table A.1**). As expected based on the screen design, *ofd1* was the most common gene, isolated 22 times. To approximate the likelihood that a gene was a false positive, we compared the cellular RNA abundance of that gene (247) to the number of times it was isolated from the screen. Therefore, *ofd1* had a ratio of 0.23, whereas a highly abundant gene that was isolated only once could have a ratio of 160 or more. All plasmids with ratios less than 3 were retransformed into the selection strain and retested for rescue of growth on 5-FOA. 26/30 of those were reconfirmed to rescue growth (**Supplementary Table A.2**).

To determine the effects of overexpressing these genes on Sre1 cleavage, we assayed Sre1N accumulation by western blot. We cultured wild-type and cells overexpressing the indicated gene in EMM-L overnight, then transferred to YES rich medium and cultured in normoxic or anoxic conditions for 4 hours and assayed Sre1N accumulation by western blot (**Fig. *A.4***). Of the genes tested, *dsc5, SPBC1E8.02* (E8.02)*, sre1-C* (C-terminus truncation), *ofd1, SPAC24B11.05* (11.05), *ppk1,* and *erg27* overexpression showed Sre1 cleavage defects (**Fig. *A.4***). Repeated transformation of the *SPBC1E8.02* plasmid did not recapitulate the Sre1 cleavage result (data not shown). To determine whether any of these genes affected Dsc E3 ligase localization, we examined Dsc1 glycosylation in the transformed cells. No gene expression blocked Dsc1 glycosylation as compared with *dsc2Δ*, although *dsc5* appeared to have an effect on Dsc1 expression (**Fig. *A.5***). Therefore, we conclude that none of these genes is affecting Sre1 activity by inhibiting Dsc E3 ligase transport.

Despite not identifying a repressor of Dsc E3 ligase transport, a few interesting preliminary conclusions can be made from this screen. *SPAC24B11.05* is expected to cause increased resistance to 5-FOA, outside of its effects on the Sre1 pathway (248). However, it also appeared to result in loss of the Sre1 precursor, therefore it may be playing a role in transcription (**Fig. *A.4***). First, *dap1* (cytochrome p450 regulator) and *erg27* (3-keto sterol reductase) promote sterol biosynthesis, while *sur2* (sphingosine hydroxylase) promotes sphingolipid biosynthesis. When we evaluated Sre1 cleavage over a low oxygen time course of 2 h in these overexpression strains, we observed a delay in Sre1 cleavage induction rather than a complete block (**Fig. *A.6A-B***). This may indicate that when these genes are overexpressed, basal sterol levels in the ER increase resulting in a delay in Sre1 activation by low oxygen.

Second, we observed a defect in Sre1 cleavage when *dsc5* was overexpressed, despite the fact that deletion of *dsc5* also blocked Sre1 cleavage (69). When we evaluated expression of Dsc complex members in this overexpression strain, we observed decreased Dsc1, Dsc3, and Dsc4 levels (**Fig. *A.6C***). Previous work in the lab had noted that when *dsc2* was deleted, Dsc4

expression was also reduced (172). That work also found that in addition to the 5-member Dsc E3 ligase complex, Dsc2 and Dsc5 can form an independent subcomplex in wild-type cells, the function of which is unknown (172). Considering that data, it is possible that overexpression of Dsc5 sequesters some Dsc2 away from the Dsc E3 ligase complex, resulting in reduced Dsc4 stability and blocking Sre1 cleavage. Whether we can see that change in complex formation by immunoprecipitation and why it would result in such a strong block in cleavage is yet to be determined.

Finally, this screen identified 16 cDNAs expressing Sre1 that blocked Sre1 cleavage (**Supplementary Table A.1**). This is counterintuitive, but closer inspection revealed that all of these lacked the N-terminus of the gene (11 different start sites), and the majority of these did not contain the full bHLH transcription factor domain, indicating that they would not produce a functional Sre1N transcription factor (**Fig. *A.6D***). Therefore, this result suggests that overexpression of the Sre1 C-terminus inhibits Sre1 cleavage. As the C-terminus is the domain that binds Scp1, it may be that overexpressing the C-terminus sequesters Scp1 away from full length Sre1, blocking it from trafficking to the Golgi for cleavage.

A.3 Experimental procedures

Whole genome sequencing – Strains PEY1516, ESY58-25, ESY58-329 were grown to a cell density of 1×10^8 cells/ml in 10 ml and resuspended in 1 ml sterile water. To collect genomic DNA, samples were divided into 2, cells were pelleted the resuspended in 500 µl Buffer A [2% Triton X-100, 1% SDS, 100 mM NaCl, 10 mM Tris-HCl pH 8.0, 1 mM EDTA pH 8.0], 500 µl phenol:chloroform:isoamylalcohol (25:24:1), and 200 µl glass beads. Tubes were vortexed for 3 min at 4°C then centrifuged 10 min, 14,000 rpm, at 4°C. Aqueous layer was removed to a new tube and 1 ml 100% EtOH was added. Samples were incubated at -20°C for 15 min then centrifuged 10 min, 14,000 rpm, at 4°C to pellet DNA. Pellet was resuspended in 200 µl Tris-HCl/EDTA + 50 µg/ml RNase and incubated at room temperature for 30 min. DNA was

precipitated with 20 µl 3M NaOAc and 1 ml 100% EtOH by incubation at -20°C for 15 min. Samples were centrifuged 15 min, 14,000 rpm, at 4°C to pellet DNA, supernatant was aspirated and pellets were rinsed with 250 µl ice-cold 70% EtOH. Pellets were dried by aspirating and resuspended in 20 µl Tris-HCl/EDTA.

All DNA quantification for library preparation was performed using Quant-iT Pico Green dsDNA assay [Thermo Fisher] for improved accuracy over Nanodrop. Samples were diluted with elution buffer [10 mM Tris-Cl, pH 8.5, Qiagen] to a DNA concentration of 0.1-10 µg/µl. Genomic DNA was sheared 5 min per sample to ~200 bp on a Covaris E220 [Covaris Inc.]. Libraries were prepared with NEBNext DNA Library Prep Master Mix Set [Illumina, NEB #E6040S] using multiplex oligos following manufacturer's instructions. 6 cycles of PCR were used during enrichment of adaptor ligated DNA. 7.5 ng/µl library in 5 µl was assayed using a Qubit Fluorometric Quantitation [Thermo Fisher] and a Bioanalyzer DNA High-Sensitivity Chip [Agilent] for determination of library quantity, quality, and size distribution. Samples were diluted to 2 nM and analyzed in a single lane on an Illumina HiSeq 2000 by the Genomic Research Core Facility. Sequences were aligned using ClustalW and SNP analysis was performed against the reference genome (972h-). I then compared the ESY58 SNPs with those present in PEY1516. Accounting for mutational hotspots and assuming the mutation should be in the coding region to have an effect, *sum3* was the top hit.

Overexpression screen – Strain REBY206 (*ura4-D18::4xSRE Ura4::KanR, his3-D1::4xSRE lacZ::KanR, ofd1Δ::KanR*) was generated as described previously using four tandem copies of the Tf2–1 sterol-regulatory element to drive *ura4*$^{+}$ and *lacZ*$^{+}$ reporter gene activation (92). The strain included deletion of the Sre1 inhibitor *ofd1* to increase the amount of Sre1 activity under normoxic, uninduced conditions. REBY206 cells were grown to a cell density of 1 × 10^{7} cells/ml in 10 ml then washed 4x with 1 ml ice-cold 1.2M sorbitol. Cells were resuspended in 1.2M sorbitol at a density of 2 × 10^{6} cells/ml and 1 µg SPLE-1 library or pLEV3 vector was

added. The SPLE-1 cDNA library was a kind gift from C. Hoffman (Boston College University) and contains 6×10^5 clones promoted by *adh*, 67% of which carry inserts of 1 kb or more (249). Cell suspension was transferred to an electroporation cuvette and cells were transformed by electroporation at 2.25 kV, 200 Ω, 25 μF. 1% of cell suspension was plated on EMM-Leu [2% (w/v) agar, 20 g/L glucose, 225 mg/L each of adenine and histidine, 50.25 mg/L uracil] for determination of transformation efficiency. The remainder was plated on EMM-Leu, incubated at 30°C for 48 h, then replica plated to EMM-Leu+5-FOA [2% (w/v) agar, 20 g/L glucose, 225 mg/L each of adenine and histidine, 50.25 mg/L uracil, 0.1% (w/v) 5-FOA]. Plates were wrapped in foil and incubated at 30°C for 7 days. Colonies were picked and restreaked onto EMM-Leu+5-FOA twice. Surviving colonies were patched onto EMM-Leu+5-FOA. This process was repeated 12 times at a transformation efficiency of 2-8 $\times 10^4$ for a total of 6.1×10^5 colonies examined, or about 1x coverage of the library. Rescue plasmids were isolated by collecting total DNA from strains of interest then directly transforming electrocompetent *E. coli* and plating on selective plates before isolating plasmids by miniprep. Plasmids were sequenced using a primer in the backbone for insert identification. Plasmids were retransformed into REBY206 for confirmation of result and downstream analysis.

Immunoprecipitation - Exponentially growing cells (5 x 10^8) were resuspended in 200 μl NP-40 lysis buffer [50 mM HEPES pH 7.4, 100 mM NaCl, 1.5 mM MgCl2, 1% NP-40 (v/v), 2x PI, 2x Complete EDTA-free PI]. Cells were lysed by bead beating for 10 min at 4°C, then beads were washed with 800 μl NP-40 lysis buffer to collect all lysate. Lysate was incubated with rotation for 40 min at 4°C then centrifuged for 5 min at 500 x g to clear intact cells and nuclei. 3 mg of supernatant protein was incubated with 4 μg relevant antiserum for 15 min then incubated with 80 μl protein A or G magnetic beads (NEB) for 2 h at 4°C. Beads were washed 3x with NP-40 lysis buffer, and the bound fraction was eluted into SDS lysis buffer + 1x PI and 1x loading dye at 95°C for 5 min.

A.4 Figures

FIGURE A.1 ***sum3*** **does not have a large effect on Sre1 cleavage.** *A,* wild-type or the indicated mutant strains carrying empty vector or a plasmid expressing *sre1N* were grown on YES+$CoCl_2$ or selection medium + 5-FOA plates. *B,* western blots imaged by film probed with anti-Sre1 IgG of lysates from wild-type cells or the indicated mutant strains grown for 4 h in the presence or absence of oxygen. P and N denote precursor and cleaved N-terminal transcription factor forms, respectively.

FIGURE A.2 ***ubx3*** **required for efficient Sre1 activation.** *A,* wild-type or the indicated deletion strains carrying empty vector or a plasmid expressing *sre1N* were grown on YES or YES+$CoCl_2$ plates. *B,* western blots imaged by film probed with anti-Sre1 IgG of lysates from wild-type cells or the indicated mutant strains grown for 0 or 4 h in the absence of oxygen. P and N denote precursor and cleaved N-terminal transcription factor forms, respectively. *C,* western blot imaged by film probed with polyclonal anti-Dsc1 IgG of NP-40-solubilized membrane protein from *WT, ubx3Δ*, *cdc48-8,* or *dsc2Δ* cells grown in the presence of oxygen. M and I indicate mature and intermediate glycosylated forms, respectively. *D,* recombinant GST-HA-V5 control (GST), GST-Dsc5 UBX ($Dsc5_{323–425}$, UBX), and GST-Rbd2 C-terminus ($Rbd2_{200–251}$, SHP) were bound to GST magnetic beads and incubated with *S. pombe* cytosol from *ufd1-13xmyc* or *ubx3-13xmyc* cells. Input, unbound, and 10-fold enriched bound fractions were probed with monoclonal anti-Myc IgG, polyclonal anti-Cdc48 IgG, and monoclonal anti-GST IgG. *E-F, WT, ufd1-13xmyc,* or *ubx3-13xmyc* cells were grown in the presence of oxygen, and Cdc48 (*E*) or Myc (*F*) was immunoprecipitated from NP-40-solubilized cell lysate. Input, unbound, and 10-fold enriched bound fractions were analyzed by western blot and imaged by Li-Cor using polyclonal anti-Cdc48 IgG and polyclonal anti-Myc IgG.

FIGURE A.3 **What is Cdc48 doing at the Dsc E3 ligase?** *A, w*estern blot imaged by Li-Cor probed with polyclonal anti-Sre1 IgG and monoclonal anti-actin (for loading) of lysates from *WT, cdc48* mutant, or *dsc2Δ* cells treated with Brefeldin A (100 µg/mL, BFA) or EtOH vehicle for 2 h in the presence of oxygen. *B-C, cdc48^{m} ufd1-13xmyc (B),* or *ufd1^{m}-13xmyc (C)* cells were grown in the presence of oxygen, and Myc (*B*) or Cdc48 *(C)* was immunoprecipitated from NP-40-solubilized cell lysate. Input, unbound, and 10-fold enriched bound fractions were analyzed by western blot and imaged by Li-Cor using polyclonal anti-Cdc48 IgG and polyclonal anti-Myc IgG.

FIGURE A.4 **Overexpression screen for genes repressing Sre1 activity – Sre1 cleavage effects.** western blots imaged by Li-Cor probed with anti-Sre1 IgG of lysates from REBY206 cells transformed with the indicated overexpression plasmids and grown for 4 h in YES in the presence or absence of oxygen. P and N denote precursor and cleaved N-terminal transcription factor forms, respectively.

FIGURE A.5 **Overexpression screen for genes repressing Sre1 activity – Dsc1 glycosylation effects.** western blots imaged by Li-Cor probed with polyclonal anti-Dsc1 IgG of NP-40-solubilized membrane protein from REBY206 cells transformed with the indicated overexpression plasmids and grown in the presence of oxygen. M and I indicate mature and intermediate glycosylated forms, respectively.

FIGURE A.6 **Overexpression screen for genes repressing Sre1 activity – preliminary conclusions.** *A-B,* western blots imaged by Li-Cor probed with anti-Sre1 IgG of lysates from *sre1Δ* cells or REBY206 cells transformed with the indicated overexpression plasmids and grown for 0-2 h in YES in the absence of oxygen. P and N denote precursor and cleaved N-terminal transcription factor forms, respectively. *C,* western blots imaged by Li-Cor probed with the

indicated IgG of lysates from REBY206 cells transformed with vector or *dsc5* overexpression plasmid. *D,* alignment against the Sre1 coding sequence (blue) of *sre1* inserts isolated during the overexpression screen. Unfilled portion indicates non-homologous (vector) sequence, red indicates aligned sequence, arrow indicates direction of sequencing.

Figure A.1

A Cobalt Chloride Growth Assay

Strain	*WT*		*sre1*Δ		*sum3-1*	
Sre1N	+	-	+	-	+	-
+$CoCl_2$						

5-FOA Growth Assay

Strain	*WT*	*sre1*Δ	*scp1*Δ	*sum3-1*

B Western Blot

Strain	*WT*			*sre1*Δ			*sre1*Δ			*sum3-1*	
O_2 (4h)	+	-		+	-		+	-		+	-
Lane	1	2	3	4	5	6	7	8	9	10	11

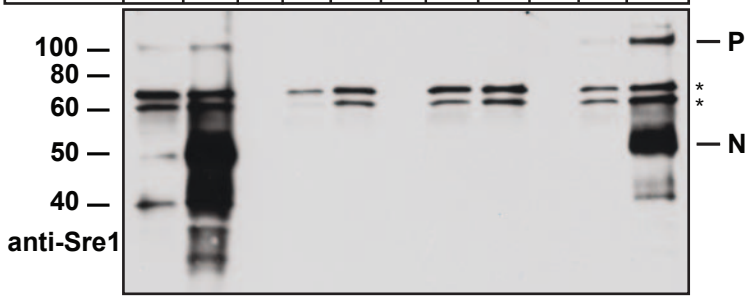

Figure A.2

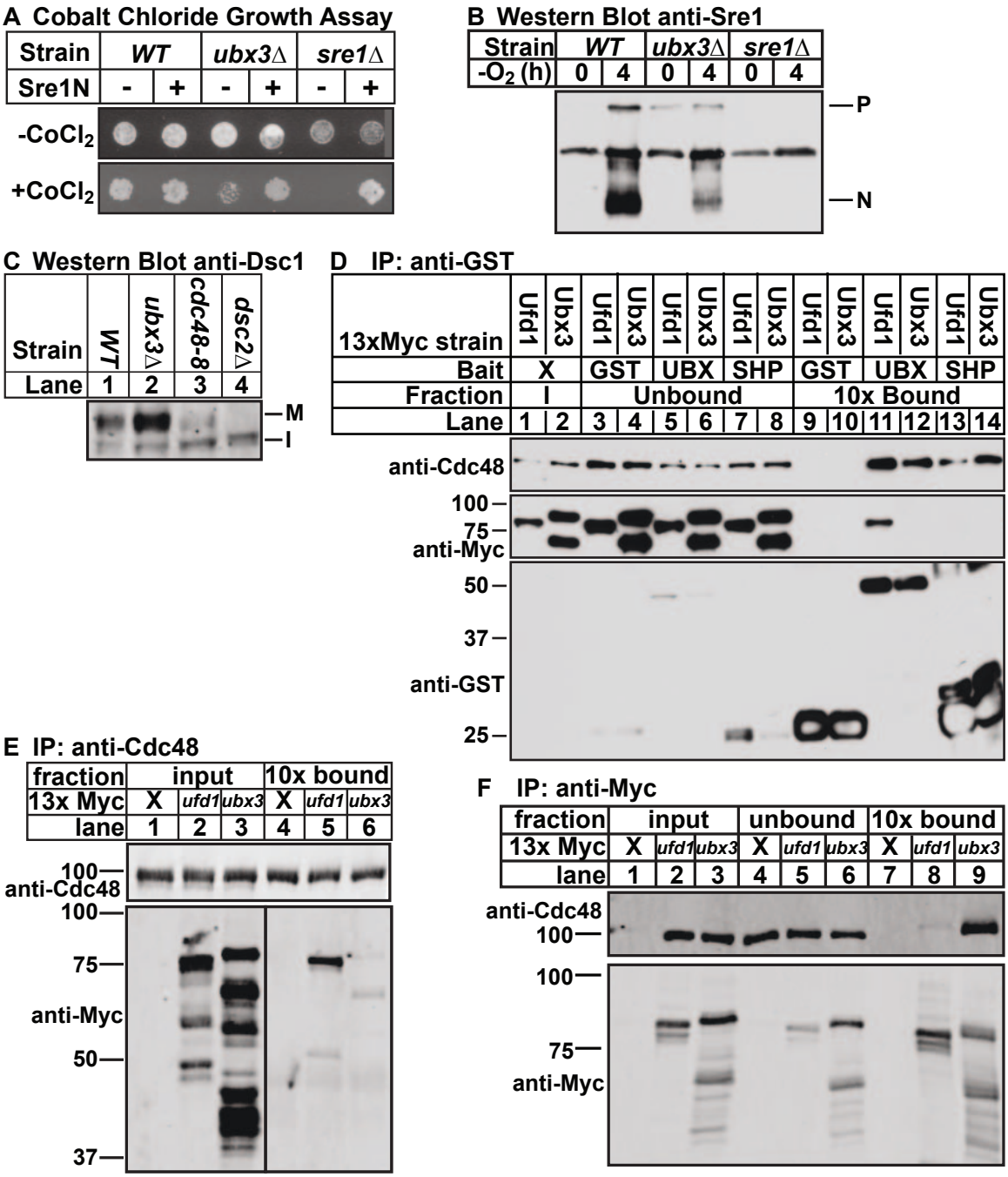
A Cobalt Chloride Growth Assay
Strain
WT
ubx3Δ
sre1Δ
Sre1N
-
+
-CoCl2
+CoCl2
B Western Blot anti-Sre1
Strain
WT
ubx3Δ
sre1Δ
-O2 (h)
0
4
P
N
C Western Blot anti-Dsc1
Strain
WT
ubx3Δ
cdc48-8
dsc2Δ
Lane
1
2
3
4
M
I
D IP: anti-GST
13xMyc strain
Ufd1
Ubx3
Bait
X
GST
UBX
SHP
Fraction
I
Unbound
10x Bound
Lane
anti-Cdc48
100
75
anti-Myc
50
37
anti-GST
25
E IP: anti-Cdc48
fraction
input
10x bound
13x Myc
X
ufd1
ubx3
lane
anti-Cdc48
anti-Myc
F IP: anti-Myc
fraction
input
unbound
10x bound

Figure A.3

A Western Blot

Strain	*WT*		*48-5*		*48-8*		*48-9*		*48-10*		*dsc2Δ*	
BFA (h)	0	2	0	2	0	2	0	2	0	2	0	2
Lane	1	2	3	4	5	6	7	8	9	10	11	12

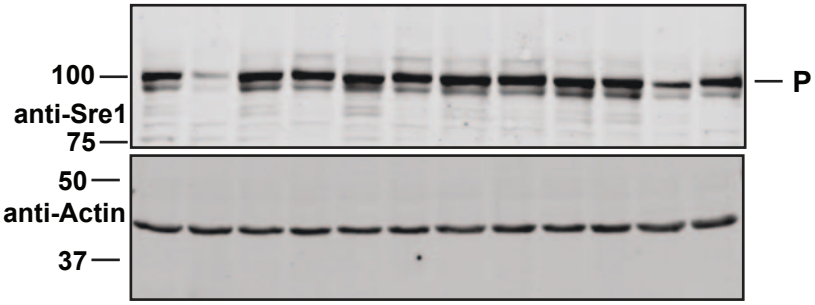

B IP: anti-Myc (Ufd1-13xMyc)

Fraction	Input							10x Bound						
Strain	*WT*	*48-5*	*48-6*	*48-7*	*48-8*	*48-9*	*48-10*	*WT*	*48-5*	*48-6*	*48-7*	*48-8*	*48-9*	*48-10*
Lane	1	2	3	4	5	6	7	8	9	10	11	12	13	14

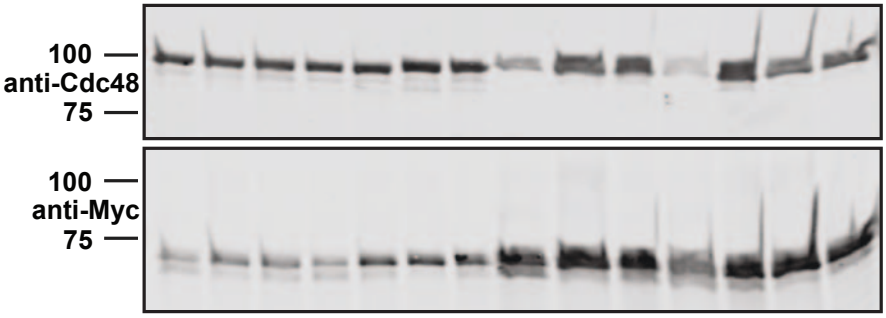

C IP: anti-Cdc48

Fraction	Input				Unbound				10x Bound			
Strain	*WT*	*1-5*	*1-7*	*1-8*	*WT*	*1-5*	*1-7*	*1-8*	*WT*	*1-5*	*1-7*	*1-8*
Lane	1	2	3	4	5	6	7	8	9	10	11	12

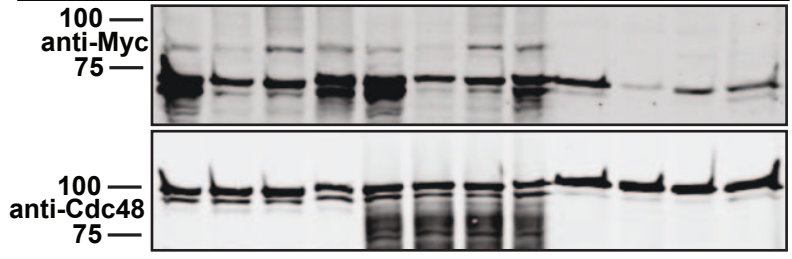

Figure A.4

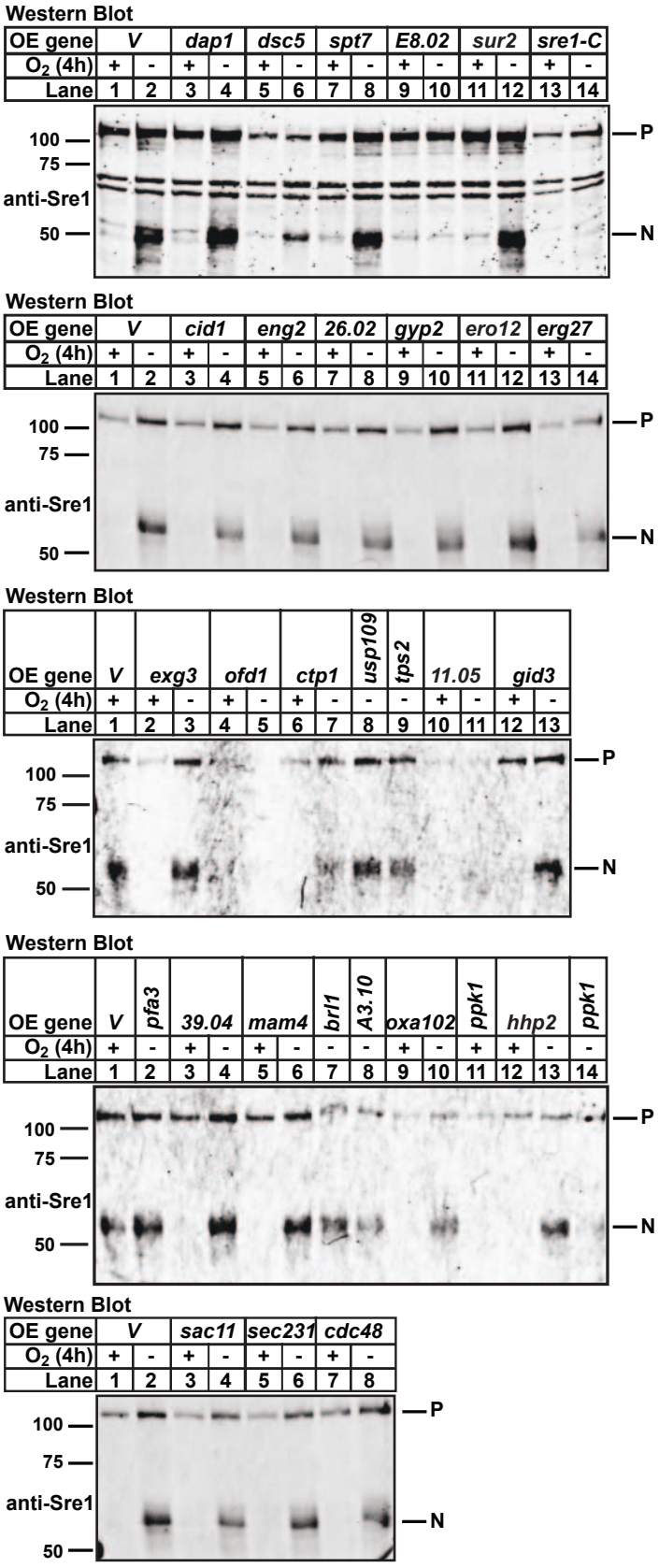
Western Blot
OE gene V dap1 dsc5 spt7 E8.02 sur2 sre1-C
O2 (4h) + - + - + - + - + - + - + -
Lane 1 2 3 4 5 6 7 8 9 10 11 12 13 14
100
75
anti-Sre1
50
P
N
Western Blot
OE gene V cid1 eng2 26.02 gyp2 ero12 erg27
O2 (4h) + - + - + - + - + - + - + -
Lane 1 2 3 4 5 6 7 8 9 10 11 12 13 14
100
75
anti-Sre1
50
P
N
Western Blot
OE gene V exg3 ofd1 ctp1 usp109 tps2 11.05 gid3
O2 (4h) + + - + - + - - - + - + -
Lane 1 2 3 4 5 6 7 8 9 10 11 12 13
100
75
anti-Sre1
50
P
N
Western Blot
OE gene V pfa3 39.04 mam4 brl1 A3.10 oxa102 ppk1 hhp2 ppk1
O2 (4h) + - + - + - - - + - + + - -
Lane 1 2 3 4 5 6 7 8 9 10 11 12 13 14
100
75
anti-Sre1
50
P
N
Western Blot
OE gene V sac11 sec231 cdc48
O2 (4h) + - + - + - + -
Lane 1 2 3 4 5 6 7 8
100
75
anti-Sre1
50
P
N

Figure A.5

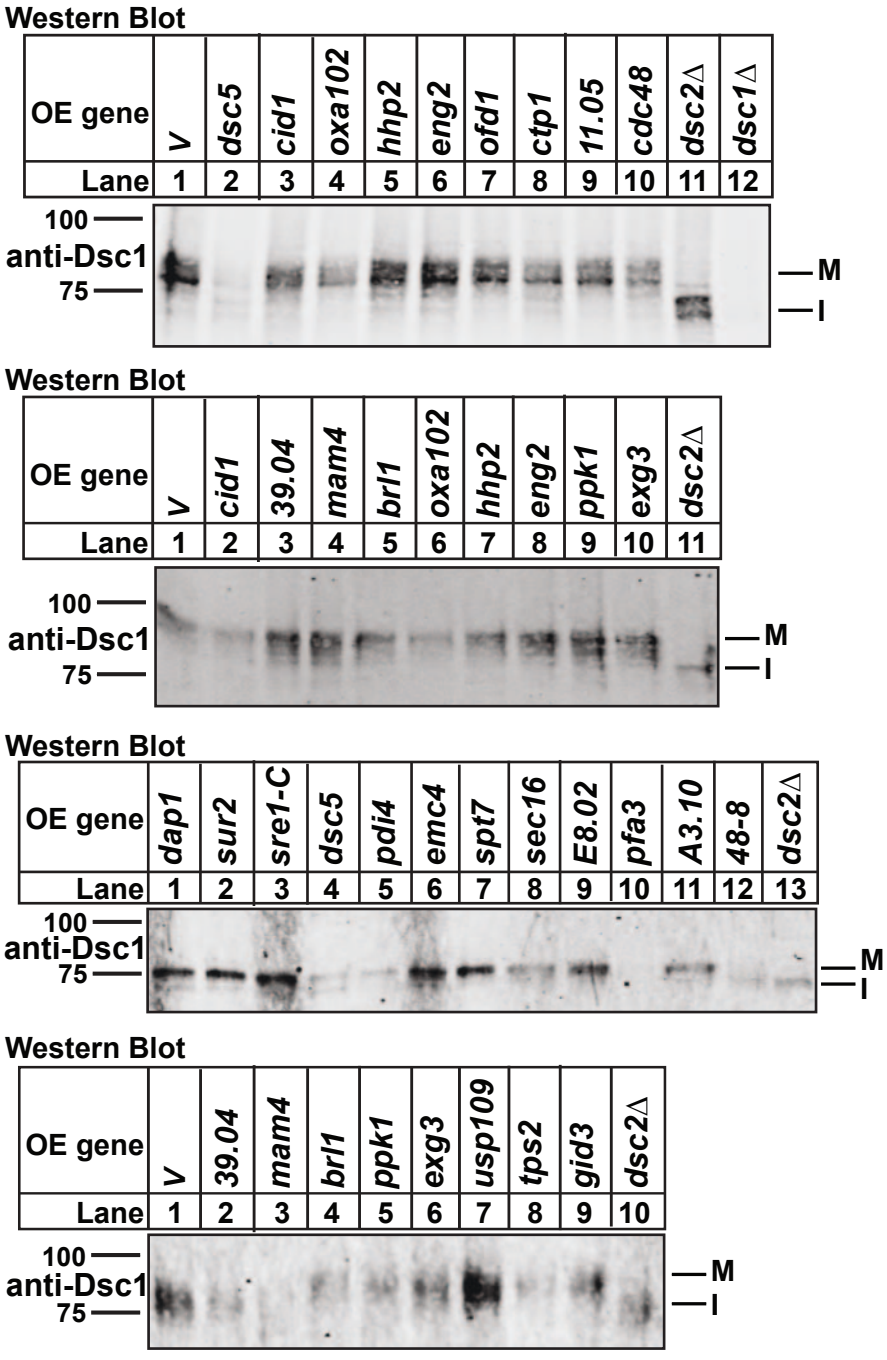
Western Blot
OE gene
V
dsc5
cid1
oxa102
hhp2
eng2
ofd1
ctp1
11.05
cdc48
dsc2Δ
dsc1Δ
Lane
1 2 3 4 5 6 7 8 9 10 11 12
100
anti-Dsc1
75
M
I
Western Blot
OE gene
V
cid1
39.04
mam4
brl1
oxa102
hhp2
eng2
ppk1
exg3
dsc2Δ
Lane
1 2 3 4 5 6 7 8 9 10 11
100
anti-Dsc1
75
M
I
Western Blot
OE gene
dap1
sur2
sre1-C
dsc5
pdi4
emc4
spt7
sec16
E8.02
pfa3
A3.10
48-8
dsc2Δ
Lane
1 2 3 4 5 6 7 8 9 10 11 12 13
100
anti-Dsc1
75
M
I
Western Blot
OE gene
V
39.04
mam4
brl1
ppk1
exg3
usp109
tps2
gid3
dsc2Δ
Lane
1 2 3 4 5 6 7 8 9 10
100
anti-Dsc1
75
M
I

Figure A.6

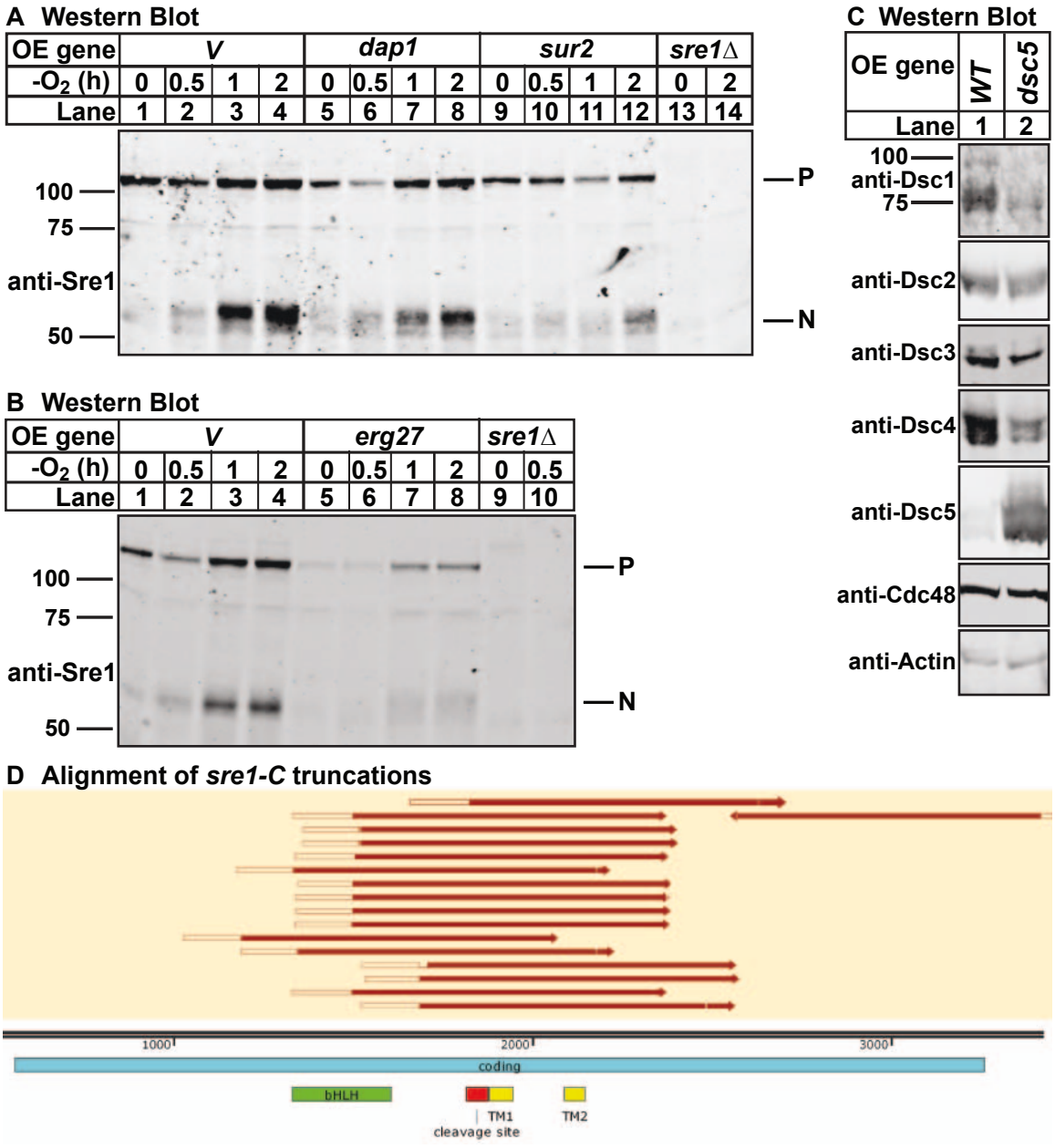
A Western Blot
OE gene | V | dap1 | sur2 | sre1Δ
-O2 (h) | 0 0.5 1 2 | 0 0.5 1 2 | 0 0.5 1 2 | 0 2
Lane | 1 2 3 4 | 5 6 7 8 | 9 10 11 12 | 13 14
100
75
anti-Sre1
50
P
N
B Western Blot
OE gene | V | erg27 | sre1Δ
-O2 (h) | 0 0.5 1 2 | 0 0.5 1 2 | 0 0.5
Lane | 1 2 3 4 | 5 6 7 8 | 9 10
100
75
anti-Sre1
50
P
N
C Western Blot
OE gene | WT | dsc5
Lane | 1 | 2
100
anti-Dsc1
75
anti-Dsc2
anti-Dsc3
anti-Dsc4
anti-Dsc5
anti-Cdc48
anti-Actin
D Alignment of sre1-C truncations
1000
2000
3000
coding
bHLH
TM1
cleavage site
TM2

References

1. Grahl, N., Shepardson, K. M., Chung, D., and Cramer, R. A. (2012) Hypoxia and fungal pathogenesis: to air or not to air? *Eukaryot Cell* **11**, 560-570
2. Hughes, I. A., Davies, J. D., Bunch, T. I., Pasterski, V., Mastroyannopoulou, K., and MacDougall, J. (2012) Androgen insensitivity syndrome. *Lancet* **380**, 1419-1428
3. Kurtoglu, S., and Hatipoglu, N. (2016) Growth hormone insensitivity: diagnostic and therapeutic approaches. *Journal of endocrinological investigation* **39**, 19-28
4. Semple, R. K., Savage, D. B., Cochran, E. K., Gorden, P., and O'Rahilly, S. (2011) Genetic syndromes of severe insulin resistance. *Endocrine reviews* **32**, 498-514
5. Toka, H. R., and Pollak, M. R. (2014) The role of the calcium-sensing receptor in disorders of abnormal calcium handling and cardiovascular disease. *Current opinion in nephrology and hypertension* **23**, 494-501
6. Semenza, G. L. (2014) Oxygen sensing, hypoxia-inducible factors, and disease pathophysiology. *Annu Rev Pathol* **9**, 47-71
7. Soyal, S. M., Nofziger, C., Dossena, S., Paulmichl, M., and Patsch, W. (2015) Targeting SREBPs for treatment of the metabolic syndrome. *Trends in pharmacological sciences* **36**, 406-416
8. Moon, Y. A., Liang, G., Xie, X., Frank-Kamenetsky, M., Fitzgerald, K., Koteliansky, V., Brown, M. S., Goldstein, J. L., and Horton, J. D. (2012) The Scap/SREBP pathway is essential for developing diabetic fatty liver and carbohydrate-induced hypertriglyceridemia in animals. *Cell Metab* **15**, 240-246
9. Leoni, V., and Caccia, C. (2015) The impairment of cholesterol metabolism in Huntington disease. *Biochim Biophys Acta* **1851**, 1095-1105
10. Baenke, F., Peck, B., Miess, H., and Schulze, A. (2013) Hooked on fat: the role of lipid synthesis in cancer metabolism and tumour development. *Disease models & mechanisms* **6**, 1353-1363
11. Dowhan, W. (1997) Molecular basis for membrane phospholipid diversity: why are there so many lipids? *Annu Rev Biochem* **66**, 199-232
12. van Meer, G., Voelker, D. R., and Feigenson, G. W. (2008) Membrane lipids: where they are and how they behave. *Nat Rev Mol Cell Biol* **9**, 112-124
13. McMahon, H. T., and Boucrot, E. (2015) Membrane curvature at a glance. *J Cell Sci* **128**, 1065-1070
14. Chang, W. C., Song, H., Liu, H. W., and Liu, P. (2013) Current development in isoprenoid precursor biosynthesis and regulation. *Current opinion in chemical biology* **17**, 571-579
15. Robinson, J. A. (1991) Polyketide synthase complexes: their structure and function in antibiotic biosynthesis. *Philosophical transactions of the Royal Society of London. Series B, Biological sciences* **332**, 107-114
16. Bohdanowicz, M., and Grinstein, S. (2013) Role of phospholipids in endocytosis, phagocytosis, and macropinocytosis. *Physiological reviews* **93**, 69-106
17. Martin, C. E., Oh, C. S., and Jiang, Y. (2007) Regulation of long chain unsaturated fatty acid synthesis in yeast. *Biochim Biophys Acta* **1771**, 271-285
18. Hajra, A. K. (1995) Glycerolipid biosynthesis in peroxisomes (microbodies). *Progress in lipid research* **34**, 343-364
19. Chang, T. Y., Li, B. L., Chang, C. C., and Urano, Y. (2009) Acyl-coenzyme A:cholesterol acyltransferases. *American journal of physiology. Endocrinology and metabolism* **297**, E1-9
20. Dickson, R. C. (2008) Thematic review series: sphingolipids. New insights into sphingolipid metabolism and function in budding yeast. *J Lipid Res* **49**, 909-921

21. Houten, S. M., and Wanders, R. J. (2010) A general introduction to the biochemistry of mitochondrial fatty acid beta-oxidation. *Journal of inherited metabolic disease* **33**, 469-477
22. Settembre, C., and Ballabio, A. (2014) Lysosome: regulator of lipid degradation pathways. *Trends Cell Biol* **24**, 743-750
23. Bjorkhem, I. (2002) Do oxysterols control cholesterol homeostasis? *J.Clin.Invest* **110**, 725-730
24. Horton, J. D., Goldstein, J. L., and Brown, M. S. (2002) SREBPs: transcriptional mediators of lipid homeostasis. *Cold Spring Harb.Symp.Quant.Biol.* **67**, 491-498
25. Nohturfft, A., DeBose-Boyd, R. A., Scheek, S., Goldstein, J. L., and Brown, M. S. (1999) Sterols regulate cycling of SREBP cleavage-activating protein (SCAP) between endoplasmic reticulum and Golgi. *Proceedings of the National Academy of Sciences of the United States of America* **96**, 11235-11240
26. Sakai, J., Rawson, R. B., Espenshade, P. J., Cheng, D., Seegmiller, A. C., Goldstein, J. L., and Brown, M. S. (1998) Molecular identification of the sterol-regulated luminal protease that cleaves SREBPs and controls lipid composition of animal cells. *Mol.Cell* **2**, 505-514
27. Shao, W., and Espenshade, P. J. (2014) Sterol regulatory element-binding protein (SREBP) cleavage regulates Golgi-to-endoplasmic reticulum recycling of SREBP cleavage-activating protein (SCAP). *J Biol Chem* **289**, 7547-7557
28. Eberle, D., Hegarty, B., Bossard, P., Ferre, P., and Foufelle, F. (2004) SREBP transcription factors: master regulators of lipid homeostasis. *Biochimie* **86**, 839-848
29. Kaelin, W. G., Jr., and Ratcliffe, P. J. (2008) Oxygen sensing by metazoans: the central role of the HIF hydroxylase pathway. *Mol Cell* **30**, 393-402
30. Lando, D., Peet, D. J., Gorman, J. J., Whelan, D. A., Whitelaw, M. L., and Bruick, R. K. (2002) FIH-1 is an asparaginyl hydroxylase enzyme that regulates the transcriptional activity of hypoxia-inducible factor. *Genes Dev.* **16**, 1466-1471
31. Koivunen, P., Hirsila, M., Gunzler, V., Kivirikko, K. I., and Myllyharju, J. (2004) Catalytic properties of the asparaginyl hydroxylase (FIH) in the oxygen sensing pathway are distinct from those of its prolyl 4-hydroxylases. *J Biol Chem* **279**, 9899-9904
32. Rankin, E. B., Rha, J., Selak, M. A., Unger, T. L., Keith, B., Liu, Q., and Haase, V. H. (2009) Hypoxia-inducible factor 2 regulates hepatic lipid metabolism. *Mol Cell Biol* **29**, 4527-4538
33. Bensaad, K., Favaro, E., Lewis, C. A., Peck, B., Lord, S., Collins, J. M., Pinnick, K. E., Wigfield, S., Buffa, F. M., Li, J. L., Zhang, Q., Wakelam, M. J., Karpe, F., Schulze, A., and Harris, A. L. (2014) Fatty acid uptake and lipid storage induced by HIF-1alpha contribute to cell growth and survival after hypoxia-reoxygenation. *Cell reports* **9**, 349-365
34. Trust, T. F. I. (2011, updated 2016) How common are fungal diseases? in *Fungal Research Trust 20th Anniversary meeting*, London
35. Richardson, M., and Lass-Florl, C. (2008) Changing epidemiology of systemic fungal infections. *Clinical microbiology and infection : the official publication of the European Society of Clinical Microbiology and Infectious Diseases* **14 Suppl 4**, 5-24
36. Rammaert, B., Lanternier, F., Zahar, J. R., Dannaoui, E., Bougnoux, M. E., Lecuit, M., and Lortholary, O. (2012) Healthcare-associated mucormycosis. *Clinical infectious diseases : an official publication of the Infectious Diseases Society of America* **54 Suppl 1**, S44-54
37. Roden, M. M., Zaoutis, T. E., Buchanan, W. L., Knudsen, T. A., Sarkisova, T. A., Schaufele, R. L., Sein, M., Sein, T., Chiou, C. C., Chu, J. H., Kontoyiannis, D. P., and Walsh, T. J. (2005) Epidemiology and outcome of zygomycosis: a review of 929 reported

cases. *Clinical infectious diseases : an official publication of the Infectious Diseases Society of America* **41**, 634-653
38. Malcolm, T. R., and Chin-Hong, P. V. (2013) Endemic mycoses in immunocompromised hosts. *Current infectious disease reports* **15**, 536-543
39. Suleyman, G., and Alangaden, G. J. (2016) Nosocomial Fungal Infections: Epidemiology, Infection Control, and Prevention. *Infectious disease clinics of North America* **30**, 1023-1052
40. Oren, I., and Paul, M. (2014) Up to date epidemiology, diagnosis and management of invasive fungal infections. *Clinical microbiology and infection : the official publication of the European Society of Clinical Microbiology and Infectious Diseases* **20 Suppl 6**, 1-4
41. Greenberg, R. N., Scott, L. J., Vaughn, H. H., and Ribes, J. A. (2004) Zygomycosis (mucormycosis): emerging clinical importance and new treatments. *Current opinion in infectious diseases* **17**, 517-525
42. Prasad, R., Shah, A. H., and Rawal, M. K. (2016) Antifungals: Mechanism of Action and Drug Resistance. *Advances in experimental medicine and biology* **892**, 327-349
43. Sheehan, D. J., Hitchcock, C. A., and Sibley, C. M. (1999) Current and emerging azole antifungal agents. *Clinical Microbiology Reviews* **12**, 40-79
44. Denning, D. W. (2003) Echinocandin antifungal drugs. *Lancet* **362**, 1142-1151
45. Wiederhold, N. P., and Patterson, T. F. (2015) What's new in antifungals: an update on the in-vitro activity and in-vivo efficacy of new and investigational antifungal agents. *Current opinion in infectious diseases* **28**, 539-545
46. Lockhart, S. R., Iqbal, N., Cleveland, A. A., Farley, M. M., Harrison, L. H., Bolden, C. B., Baughman, W., Stein, B., Hollick, R., Park, B. J., and Chiller, T. (2012) Species identification and antifungal susceptibility testing of Candida bloodstream isolates from population-based surveillance studies in two U.S. cities from 2008 to 2011. *Journal of clinical microbiology* **50**, 3435-3442
47. Alexander, B. D., Johnson, M. D., Pfeiffer, C. D., Jimenez-Ortigosa, C., Catania, J., Booker, R., Castanheira, M., Messer, S. A., Perlin, D. S., and Pfaller, M. A. (2013) Increasing echinocandin resistance in Candida glabrata: clinical failure correlates with presence of FKS mutations and elevated minimum inhibitory concentrations. *Clinical infectious diseases : an official publication of the Infectious Diseases Society of America* **56**, 1724-1732
48. Vallabhaneni, S., Cleveland, A. A., Farley, M. M., Harrison, L. H., Schaffner, W., Beldavs, Z. G., Derado, G., Pham, C. D., Lockhart, S. R., and Smith, R. M. (2015) Epidemiology and Risk Factors for Echinocandin Nonsusceptible Candida glabrata Bloodstream Infections: Data From a Large Multisite Population-Based Candidemia Surveillance Program, 2008-2014. *Open forum infectious diseases* **2**, ofv163
49. CDC. Candida Auris Alert.
50. Hull, C. M., Purdy, N. J., and Moody, S. C. (2014) Mitigation of human-pathogenic fungi that exhibit resistance to medical agents: can clinical antifungal stewardship help? *Future microbiology* **9**, 307-325
51. Grahl, N., and Cramer, R. A., Jr. (2010) Regulation of hypoxia adaptation: an overlooked virulence attribute of pathogenic fungi? *Med Mycol* **48**, 1-15
52. Blackwell, M. (2011) The fungi: 1, 2, 3 ... 5.1 million species? *American journal of botany* **98**, 426-438
53. Brahimi-Horn, M. C., and Pouyssegur, J. (2007) Oxygen, a source of life and stress. *FEBS Lett* **581**, 3582-3591
54. Todd, B. L., Stewart, E. V., Burg, J. S., Hughes, A. L., and Espenshade, P. J. (2006) Sterol regulatory element binding protein is a principal regulator of anaerobic gene expression in fission yeast. *Mol.Cell Biol.* **26**, 2817-2831

55. Protchenko, O., Shakoury-Elizeh, M., Keane, P., Storey, J., Androphy, R., and Philpott, C. C. (2008) Role of PUG1 in inducible porphyrin and heme transport in Saccharomyces cerevisiae. *Eukaryot Cell* **7**, 859-871
56. Synnott, J. M., Guida, A., Mulhern-Haughey, S., Higgins, D. G., and Butler, G. (2010) Regulation of the hypoxic response in Candida albicans. *Eukaryot Cell* **9**, 1734-1746
57. Guida, A., Lindstadt, C., Maguire, S. L., Ding, C., Higgins, D. G., Corton, N. J., Berriman, M., and Butler, G. (2011) Using RNA-seq to determine the transcriptional landscape and the hypoxic response of the pathogenic yeast Candida parapsilosis. *BMC Genomics* **12**, 628
58. Masuo, S., Terabayashi, Y., Shimizu, M., Fujii, T., Kitazume, T., and Takaya, N. (2010) Global gene expression analysis of Aspergillus nidulans reveals metabolic shift and transcription suppression under hypoxia. *Molecular genetics and genomics : MGG* **284**, 415-424
59. Maguire, S. L., Wang, C., Holland, L. M., Brunel, F., Neuveglise, C., Nicaud, J. M., Zavrel, M., White, T. C., Wolfe, K. H., and Butler, G. (2014) Zinc finger transcription factors displaced SREBP proteins as the major Sterol regulators during Saccharomycotina evolution. *PLoS Genet* **10**, e1004076
60. Barker, B. M., Kroll, K., Vodisch, M., Mazurie, A., Kniemeyer, O., and Cramer, R. A. (2012) Transcriptomic and proteomic analyses of the Aspergillus fumigatus hypoxia response using an oxygen-controlled fermenter. *BMC Genomics* **13**, 62
61. Summons, R. E., Bradley, A. S., Jahnke, L. L., and Waldbauer, J. R. (2006) Steroids, triterpenoids and molecular oxygen. *Philosophical transactions of the Royal Society of London. Series B, Biological sciences* **361**, 951-968
62. Hughes, A. L., Todd, B. L., and Espenshade, P. J. (2005) SREBP pathway responds to sterols and functions as an oxygen sensor in fission yeast. *Cell* **120**, 831-842
63. Burg, J. S., Powell, D. W., Chai, R., Hughes, A. L., Link, A. J., and Espenshade, P. J. (2008) Insig regulates HMG-CoA reductase by controlling enzyme phosphorylation in fission yeast. *Cell Metab* **8**, 522-531
64. Hughes, B. T., Nwosu, C. C., and Espenshade, P. J. (2009) Degradation of SREBP precursor requires the ERAD components UBC7 and HRD1 in fission yeast. *J.Biol.Chem.* **284** 20512-20521
65. Porter, J. R., Burg, J. S., Espenshade, P. J., and Iglesias, P. A. (2010) Ergosterol regulates sterol regulatory element binding protein (SREBP) cleavage in fission yeast. *J Biol Chem* **285**, 41051-41061
66. Cheung, R., and Espenshade, P. J. (2013) Structural requirements for sterol regulatory element-binding protein (SREBP) cleavage in fission yeast. *J Biol Chem* **288**, 20351-20360
67. Kwon, E. J., Laderoute, A., Chatfield-Reed, K., Vachon, L., Karagiannis, J., and Chua, G. (2012) Deciphering the transcriptional-regulatory network of flocculation in Schizosaccharomyces pombe. *PLoS Genet* **8**, e1003104
68. Stewart, E. V., Nwosu, C. C., Tong, Z., Roguev, A., Cummins, T. D., Kim, D. U., Hayles, J., Park, H. O., Hoe, K. L., Powell, D. W., Krogan, N. J., and Espenshade, P. J. (2011) Yeast SREBP cleavage activation requires the Golgi Dsc E3 ligase complex. *Mol Cell* **42**, 160-171
69. Stewart, E. V., Lloyd, S. J., Burg, J. S., Nwosu, C. C., Lintner, R. E., Daza, R., Russ, C., Ponchner, K., Nusbaum, C., and Espenshade, P. J. (2012) Yeast sterol regulatory element-binding protein (SREBP) cleavage requires Cdc48 and Dsc5, a ubiquitin regulatory X domain-containing subunit of the Golgi Dsc E3 ligase. *J Biol Chem* **287**, 672-681

70. Burr, R., Stewart, E. V., Shao, W., Zhao, S., Hannibal-Bach, H. K., Ejsing, C. S., and Espenshade, P. J. (2016) Mga2 Transcription Factor Regulates an Oxygen-responsive Lipid Homeostasis Pathway in Fission Yeast. *J Biol Chem* **291**, 12171-12183
71. Hwang, J., Ribbens, D., Raychaudhuri, S., Cairns, L., Gu, H., Frost, A., Urban, S., and Espenshade, P. J. (2016) A Golgi rhomboid protease Rbd2 recruits Cdc48 to cleave yeast SREBP. *EMBO J* **35**, 2332-2349
72. Li, M., Koshi, T., and Emr, S. D. (2015) Membrane-anchored ubiquitin ligase complex is required for the turnover of lysosomal membrane proteins. *J Cell Biol* **211**, 639-652
73. Raychaudhuri, S., and Espenshade, P. J. (2015) Endoplasmic Reticulum Exit of Golgi-resident Defective for SREBP Cleavage (Dsc) E3 Ligase Complex Requires Its Activity. *J Biol Chem* **290**, 14430-14440
74. Dobzinski, N., Chuartzman, S. G., Kama, R., Schuldiner, M., and Gerst, J. E. (2015) Starvation-Dependent Regulation of Golgi Quality Control Links the TOR Signaling and Vacuolar Protein Sorting Pathways. *Cell reports* **12**, 1876-1886
75. Bat-Ochir, C., Kwak, J. Y., Koh, S. K., Jeon, M. H., Chung, D., Lee, Y. W., and Chae, S. K. (2016) The signal peptide peptidase SppA is involved in sterol regulatory element-binding protein cleavage and hypoxia adaptation in Aspergillus nidulans. *Mol Microbiol* **100**, 635-655
76. Fleig, L., Bergbold, N., Sahasrabudhe, P., Geiger, B., Kaltak, L., and Lemberg, M. K. (2012) Ubiquitin-dependent intramembrane rhomboid protease promotes ERAD of membrane proteins. *Mol Cell* **47**, 558-569
77. Yeung, H. O., Kloppsteck, P., Niwa, H., Isaacson, R. L., Matthews, S., Zhang, X., and Freemont, P. S. (2008) Insights into adaptor binding to the AAA protein p97. *Biochem Soc Trans* **36**, 62-67
78. Meyer, H., Bug, M., and Bremer, S. (2012) Emerging functions of the VCP/p97 AAA-ATPase in the ubiquitin system. *Nat Cell Biol* **14**, 117-123
79. Verma, R., Oania, R. S., Kolawa, N. J., and Deshaies, R. J. (2013) Cdc48/p97 promotes degradation of aberrant nascent polypeptides bound to the ribosome. *eLife* **2**, e00308
80. Nishikori, S., Esaki, M., Yamanaka, K., Sugimoto, S., and Ogura, T. (2011) Positive cooperativity of the p97 AAA ATPase is critical for essential functions. *J Biol Chem* **286**, 15815-15820
81. Bodnar, N. O., and Rapoport, T. A. (2017) Molecular Mechanism of Substrate Processing by the Cdc48 ATPase Complex. *Cell* **169**, 722-735 e729
82. Zhang, X., Gui, L., Zhang, X., Bulfer, S. L., Sanghez, V., Wong, D. E., Lee, Y., Lehmann, L., Lee, J. S., Shih, P. Y., Lin, H. J., Iacovino, M., Weihl, C. C., Arkin, M. R., Wang, Y., and Chou, T. F. (2015) Altered cofactor regulation with disease-associated p97/VCP mutations. *Proc Natl Acad Sci U S A* **112**, E1705-1714
83. Buchberger, A. (2010) Control of ubiquitin conjugation by cdc48 and its cofactors. *Sub-cellular biochemistry* **54**, 17-30
84. Schuetz, A. K., and Kay, L. E. (2016) A Dynamic molecular basis for malfunction in disease mutants of p97/VCP. *eLife* **5**
85. Erzurumlu, Y., Kose, F. A., Gozen, O., Gozuacik, D., Toth, E. A., and Ballar, P. (2013) A unique IBMPFD-related P97/VCP mutation with differential binding pattern and subcellular localization. *Int J Biochem Cell Biol* **45**, 773-782
86. Watts, G. D., Wymer, J., Kovach, M. J., Mehta, S. G., Mumm, S., Darvish, D., Pestronk, A., Whyte, M. P., and Kimonis, V. E. (2004) Inclusion body myopathy associated with Paget disease of bone and frontotemporal dementia is caused by mutant valosin-containing protein. *Nat Genet* **36**, 377-381
87. Kimura, Y., Fukushi, J., Hori, S., Matsuda, N., Okatsu, K., Kakiyama, Y., Kawawaki, J., Kakizuka, A., and Tanaka, K. (2013) Different dynamic movements of wild-type and

pathogenic VCPs and their cofactors to damaged mitochondria in a Parkin-mediated mitochondrial quality control system. *Genes Cells* **18**, 1131-1143

88. Johnson, J. O., Mandrioli, J., Benatar, M., Abramzon, Y., Van Deerlin, V. M., Trojanowski, J. Q., Gibbs, J. R., Brunetti, M., Gronka, S., Wuu, J., Ding, J., McCluskey, L., Martinez-Lage, M., Falcone, D., Hernandez, D. G., Arepalli, S., Chong, S., Schymick, J. C., Rothstein, J., Landi, F., Wang, Y. D., Calvo, A., Mora, G., Sabatelli, M., Monsurro, M. R., Battistini, S., Salvi, F., Spataro, R., Sola, P., Borghero, G., Consortium, I., Galassi, G., Scholz, S. W., Taylor, J. P., Restagno, G., Chio, A., and Traynor, B. J. (2010) Exome sequencing reveals VCP mutations as a cause of familial ALS. *Neuron* **68**, 857-864
89. Ju, J. S., Fuentealba, R. A., Miller, S. E., Jackson, E., Piwnica-Worms, D., Baloh, R. H., and Weihl, C. C. (2009) Valosin-containing protein (VCP) is required for autophagy and is disrupted in VCP disease. *J Cell Biol* **187**, 875-888
90. Niwa, H., Ewens, C. A., Tsang, C., Yeung, H. O., Zhang, X., and Freemont, P. S. (2012) The role of the N-domain in the ATPase activity of the mammalian AAA ATPase p97/VCP. *J Biol Chem* **287**, 8561-8570
91. Kim, N. C., Tresse, E., Kolaitis, R. M., Molliex, A., Thomas, R. E., Alami, N. H., Wang, B., Joshi, A., Smith, R. B., Ritson, G. P., Winborn, B. J., Moore, J., Lee, J. Y., Yao, T. P., Pallanck, L., Kundu, M., and Taylor, J. P. (2013) VCP is essential for mitochondrial quality control by PINK1/Parkin and this function is impaired by VCP mutations. *Neuron* **78**, 65-80
92. Hughes, B. T., and Espenshade, P. J. (2008) Oxygen-regulated degradation of fission yeast SREBP by Ofd1, a prolyl hydroxylase family member. *EMBO J.* **27**, 1491-1501
93. Yeh, T. L., Lee, C. Y., Amzel, L. M., Espenshade, P. J., and Bianchet, M. A. (2011) The hypoxic regulator of sterol synthesis nro1 is a nuclear import adaptor. *Structure* **19**, 503-514
94. Loenarz, C., Sekirnik, R., Thalhammer, A., Ge, W., Spivakovsky, E., Mackeen, M. M., McDonough, M. A., Cockman, M. E., Kessler, B. M., Ratcliffe, P. J., Wolf, A., and Schofield, C. J. (2014) Hydroxylation of the eukaryotic ribosomal decoding center affects translational accuracy. *Proc Natl Acad Sci U S A* **111**, 4019-4024
95. Lee, C. Y. S., Yeh, T. L., Hughes, B. T., and Espenshade, P. J. (2011) Regulation of the Sre1 hypoxic transcription factor by oxygen-dependent control of DNA binding. *Molecular Cell* **44**, 225-234
96. Porter, J. R., Lee, C. Y., Espenshade, P. J., and Iglesias, P. A. (2012) Regulation of SREBP during hypoxia requires Ofd1-mediated control of both DNA binding and degradation. *Mol Biol Cell* **23**, 3764-3774
97. Lee, C. Y., Stewart, E. V., Hughes, B. T., and Espenshade, P. J. (2009) Oxygen-dependent binding of Nro1 to the prolyl hydroxylase Ofd1 regulates SREBP degradation in yeast. *EMBO J.* **28**, 135-143
98. Singleton, R. S., Liu-Yi, P., Formenti, F., Ge, W., Sekirnik, R., Fischer, R., Adam, J., Pollard, P. J., Wolf, A., Thalhammer, A., Loenarz, C., Flashman, E., Yamamoto, A., Coleman, M. L., Kessler, B. M., Wappner, P., Schofield, C. J., Ratcliffe, P. J., and Cockman, M. E. (2014) OGFOD1 catalyzes prolyl hydroxylation of RPS23 and is involved in translation control and stress granule formation. *Proc Natl Acad Sci U S A* **111**, 4031-4036
99. Nakamura, M. T., and Nara, T. Y. (2004) Structure, function, and dietary regulation of delta6, delta5, and delta9 desaturases. *Annual review of nutrition* **24**, 345-376
100. Kwast, K. E., Burke, P. V., and Poyton, R. O. (1998) Oxygen sensing and the transcriptional regulation of oxygen-responsive genes in yeast. *J.Exp.Biol.* **201**, 1177-1195

101. Jiang, Y., Vasconcelles, M. J., Wretzel, S., Light, A., Martin, C. E., and Goldberg, M. A. (2001) MGA2 is involved in the low-oxygen response element-dependent hypoxic induction of genes in Saccharomyces cerevisiae. *Mol Cell Biol* **21**, 6161-6169
102. Kaliszewski, P., Szkopinska, A., Ferreira, T., Swiezewska, E., Berges, T., and Zoladek, T. (2008) Rsp5p ubiquitin ligase and the transcriptional activators Spt23p and Mga2p are involved in co-regulation of biosynthesis of end products of the mevalonate pathway and triacylglycerol in yeast Saccharomyces cerevisiae. *Biochim Biophys Acta* **1781**, 627-634
103. Zhang, S., Skalsky, Y., and Garfinkel, D. J. (1999) MGA2 or SPT23 is required for transcription of the delta9 fatty acid desaturase gene, OLE1, and nuclear membrane integrity in Saccharomyces cerevisiae. *Genetics* **151**, 473-483
104. Burkett, T. J., and Garfinkel, D. J. (1994) Molecular characterization of the SPT23 gene: a dosage-dependent suppressor of Ty-induced promoter mutations from Saccharomyces cerevisiae. *Yeast* **10**, 81-92
105. Chellappa, R., Kandasamy, P., Oh, C. S., Jiang, Y., Vemula, M., and Martin, C. E. (2001) The membrane proteins, Spt23p and Mga2p, play distinct roles in the activation of Saccharomyces cerevisiae OLE1 gene expression. Fatty acid-mediated regulation of Mga2p activity is independent of its proteolytic processing into a soluble transcription activator. *J Biol Chem* **276**, 43548-43556
106. Kandasamy, P., Vemula, M., Oh, C. S., Chellappa, R., and Martin, C. E. (2004) Regulation of unsaturated fatty acid biosynthesis in Saccharomyces: the endoplasmic reticulum membrane protein, Mga2p, a transcription activator of the OLE1 gene, regulates the stability of the OLE1 mRNA through exosome-mediated mechanisms. *J Biol Chem* **279**, 36586-36592
107. Nakagawa, Y., Sakumoto, N., Kaneko, Y., and Harashima, S. (2002) Mga2p is a putative sensor for low temperature and oxygen to induce OLE1 transcription in Saccharomyces cerevisiae. *Biochem Biophys Res Commun* **291**, 707-713
108. Hoppe, T., Matuschewski, K., Rape, M., Schlenker, S., Ulrich, H. D., and Jentsch, S. (2000) Activation of a membrane-bound transcription factor by regulated ubiquitin/proteasome-dependent processing. *Cell* **102**, 577-586
109. Rape, M., Hoppe, T., Gorr, I., Kalocay, M., Richly, H., and Jentsch, S. (2001) Mobilization of processed, membrane-tethered SPT23 transcription factor by CDC48(UFD1/NPL4), a ubiquitin-selective chaperone. *Cell* **107**, 667-677
110. Covino, R., Ballweg, S., Stordeur, C., Michaelis, J. B., Puth, K., Wernig, F., Bahrami, A., Ernst, A. M., Hummer, G., and Ernst, R. (2016) A Eukaryotic Sensor for Membrane Lipid Saturation. *Mol Cell* **63**, 49-59
111. Priebe, S., Kreisel, C., Horn, F., Guthke, R., and Linde, J. (2015) FungiFun2: a comprehensive online resource for systematic analysis of gene lists from fungal species. *Bioinformatics* **31**, 445-446
112. Supek, F., Bosnjak, M., Skunca, N., and Smuc, T. (2011) REVIGO summarizes and visualizes long lists of gene ontology terms. *PloS one* **6**, e21800
113. Thompson, A., Schafer, J., Kuhn, K., Kienle, S., Schwarz, J., Schmidt, G., Neumann, T., Johnstone, R., Mohammed, A. K., and Hamon, C. (2003) Tandem mass tags: a novel quantification strategy for comparative analysis of complex protein mixtures by MS/MS. *Anal Chem* **75**, 1895-1904
114. Kim, D. U., Hayles, J., Kim, D., Wood, V., Park, H. O., Won, M., Yoo, H. S., Duhig, T., Nam, M., Palmer, G., Han, S., Jeffery, L., Baek, S. T., Lee, H., Shim, Y. S., Lee, M., Kim, L., Heo, K. S., Noh, E. J., Lee, A. R., Jang, Y. J., Chung, K. S., Choi, S. J., Park, J. Y., Park, Y., Kim, H. M., Park, S. K., Park, H. J., Kang, E. J., Kim, H. B., Kang, H. S., Park, H. M., Kim, K., Song, K., Song, K. B., Nurse, P., and Hoe, K. L. (2010) Analysis of a genome-wide set of gene deletions in the fission yeast Schizosaccharomyces pombe. *Nat Biotechnol* **28**, 617-623

115. Nie, M., Aslanian, A., Prudden, J., Heideker, J., Vashisht, A. A., Wohlschlegel, J. A., Yates, J. R., 3rd, and Boddy, M. N. (2012) Dual recruitment of Cdc48 (p97)-Ufd1-Npl4 ubiquitin-selective segregase by small ubiquitin-like modifier protein (SUMO) and ubiquitin in SUMO-targeted ubiquitin ligase-mediated genome stability functions. *J Biol Chem* **287**, 29610-29619
116. Meyer, H. H., Shorter, J. G., Seemann, J., Pappin, D., and Warren, G. (2000) A complex of mammalian ufd1 and npl4 links the AAA-ATPase, p97, to ubiquitin and nuclear transport pathways. *EMBO J* **19**, 2181-2192
117. Wolf, D. H., and Stolz, A. (2012) The Cdc48 machine in endoplasmic reticulum associated protein degradation. *Biochim Biophys Acta* **1823**, 117-124
118. Ye, Y., Meyer, H. H., and Rapoport, T. A. (2003) Function of the p97-Ufd1-Npl4 complex in retrotranslocation from the ER to the cytosol: dual recognition of nonubiquitinated polypeptide segments and polyubiquitin chains. *J Cell Biol* **162**, 71-84
119. Bruderer, R. M., Brasseur, C., and Meyer, H. H. (2004) The AAA ATPase p97/VCP interacts with its alternative co-factors, Ufd1-Npl4 and p47, through a common bipartite binding mechanism. *J Biol Chem* **279**, 49609-49616
120. Reggiori, F., and Pelham, H. R. (2002) A transmembrane ubiquitin ligase required to sort membrane proteins into multivesicular bodies. *Nat.Cell Biol.* **4**, 117-123
121. Alexandru, G., Graumann, J., Smith, G. T., Kolawa, N. J., Fang, R., and Deshaies, R. J. (2008) UBXD7 binds multiple ubiquitin ligases and implicates p97 in HIF1alpha turnover. *Cell* **134**, 804-816
122. Hartmann-Petersen, R., Wallace, M., Hofmann, K., Koch, G., Johnsen, A. H., Hendil, K. B., and Gordon, C. (2004) The Ubx2 and Ubx3 cofactors direct Cdc48 activity to proteolytic and nonproteolytic ubiquitin-dependent processes. *Curr Biol* **14**, 824-828
123. Forsburg, S. L. (1993) Comparison of Schizosaccharomyces pombe expression systems. *Nucleic Acids Res.* **21**, 2955-2956
124. Burr, R., Stewart, E. V., and Espenshade, P. J. (2017) Coordinate Regulation of Yeast Sterol Regulatory Element-binding Protein (SREBP) and Mga2 Transcription Factors. *J Biol Chem* **292**, 5311-5324
125. Willger, S. D., Cornish, E. J., Chung, D., Fleming, B. A., Lehmann, M. M., Puttikamonkul, S., and Cramer, R. A. (2012) Dsc orthologs are required for hypoxia adaptation, triazole drug responses, and fungal virulence in Aspergillus fumigatus. *Eukaryot Cell* **11**, 1557-1567
126. Willger, S. D., Puttikamonkul, S., Kim, K. H., Burritt, J. B., Grahl, N., Metzler, L. J., Barbuch, R., Bard, M., Lawrence, C. B., and Cramer, R. A., Jr. (2008) A sterol-regulatory element binding protein is required for cell polarity, hypoxia adaptation, azole drug resistance, and virulence in Aspergillus fumigatus *PLoS.Pathog.* **4**, e1000200
127. Lane, S., Di Lena, P., Tormanen, K., Baldi, P., and Liu, H. (2015) Function and Regulation of Cph2 in Candida albicans. *Eukaryot Cell* **14**, 1114-1126
128. DuBois, J. C., Pasula, R., Dade, J. E., and Smulian, A. G. (2016) Yeast Transcriptome and In Vivo Hypoxia Detection Reveals Histoplasma capsulatum Response to Low Oxygen Tension. *Med Mycol* **54**, 40-58
129. Kelley, R., and Ideker, T. (2009) Genome-wide fitness and expression profiling implicate Mga2 in adaptation to hydrogen peroxide. *PLoS Genet* **5**, e1000488
130. Ferreira, T., Regnacq, M., Alimardani, P., Moreau-Vauzelle, C., and Berges, T. (2004) Lipid dynamics in yeast under haem-induced unsaturated fatty acid and/or sterol depletion. *Biochem J* **378**, 899-908
131. Ejsing, C. S., Sampaio, J. L., Surendranath, V., Duchoslav, E., Ekroos, K., Klemm, R. W., Simons, K., and Shevchenko, A. (2009) Global analysis of the yeast lipidome by quantitative shotgun mass spectrometry. *Proc Natl Acad Sci U S A* **106**, 2136-2141

132. Bloomfield, D. K., and Bloch, K. (1960) The formation of delta 9-unsaturated fatty acids. *J Biol Chem* **235**, 337-345
133. Klein, H. P., Eaton, N. R., and Murphy, J. C. (1954) Net synthesis of sterols in resting cells of Saccharomyces cerevisiae. *Biochim Biophys Acta* **13**, 591
134. Jahnke, L., and Klein, H. P. (1983) Oxygen requirements for formation and activity of the squalene epoxidase in Saccharomyces cerevisiae. *J Bacteriol* **155**, 488-492
135. Holic, R., Yazawa, H., Kumagai, H., and Uemura, H. (2012) Engineered high content of ricinoleic acid in fission yeast Schizosaccharomyces pombe. *Applied microbiology and biotechnology* **95**, 179-187
136. Horton, J. D., Shah, N. A., Warrington, J. A., Anderson, N. N., Park, S. W., Brown, M. S., and Goldstein, J. L. (2003) Combined analysis of oligonucleotide microarray data from transgenic and knockout mice identifies direct SREBP target genes. *Proc.Natl.Acad.Sci.U.S.A* **100**, 12027-12032
137. Henry, S. A., Kohlwein, S. D., and Carman, G. M. (2012) Metabolism and regulation of glycerolipids in the yeast Saccharomyces cerevisiae. *Genetics* **190**, 317-349
138. Kim, J., Ha, H. J., Kim, S., Choi, A. R., Lee, S. J., Hoe, K. L., and Kim, D. U. (2015) Identification of Rbd2 as a candidate protease for sterol regulatory element binding protein (SREBP) cleavage in fission yeast. *Biochem Biophys Res Commun* **468**, 606-610
139. Radhakrishnan, A., Sun, L. P., Kwon, H. J., Brown, M. S., and Goldstein, J. L. (2004) Direct binding of cholesterol to the purified membrane region of SCAP: mechanism for a sterol-sensing domain. *Mol.Cell* **15**, 259-268
140. Hua, X. X., Nohturfft, A., Goldstein, J. L., and Brown, M. S. (1996) Sterol resistance in CHO cells traced to point mutation in SREBP cleavage-activating protein. *Cell* **87**, 415-426
141. Hannah, V. C., Ou, J. F., Luong, A., Goldstein, J. L., and Brown, M. S. (2001) Unsaturated fatty acids down-regulate SREBP isoforms 1a and 1c by two mechanisms in HEK-293 cells. *Journal of Biological Chemistry* **276**, 4365-4372
142. Prevorovsky, M., Oravcova, M., Tvaruzkova, J., Zach, R., Folk, P., Puta, F., and Bahler, J. (2015) Fission Yeast CSL Transcription Factors: Mapping Their Target Genes and Biological Roles. *PloS one* **10**, e0137820
143. Pancaldi, V., Sarac, O. S., Rallis, C., McLean, J. R., Prevorovsky, M., Gould, K., Beyer, A., and Bahler, J. (2012) Predicting the fission yeast protein interaction network. *G3* **2**, 453-467
144. Jarriault, S., Brou, C., Logeat, F., Schroeter, E. H., Kopan, R., and Israel, A. (1995) Signalling downstream of activated mammalian Notch. *Nature* **377**, 355-358
145. Beres, T. M., Masui, T., Swift, G. H., Shi, L., Henke, R. M., and MacDonald, R. J. (2006) PTF1 is an organ-specific and Notch-independent basic helix-loop-helix complex containing the mammalian Suppressor of Hairless (RBP-J) or its paralogue, RBP-L. *Mol Cell Biol* **26**, 117-130
146. Edgar, R., Domrachev, M., and Lash, A. E. (2002) Gene Expression Omnibus: NCBI gene expression and hybridization array data repository. *Nucleic Acids Res* **30**, 207-210
147. Husen, P., Tarasov, K., Katafiasz, M., Sokol, E., Vogt, J., Baumgart, J., Nitsch, R., Ekroos, K., and Ejsing, C. S. (2013) Analysis of lipid experiments (ALEX): a software framework for analysis of high-resolution shotgun lipidomics data. *PloS one* **8**, e79736
148. Casanovas, A., Sprenger, R. R., Tarasov, K., Ruckerbauer, D. E., Hannibal-Bach, H. K., Zanghellini, J., Jensen, O. N., and Ejsing, C. S. (2015) Quantitative analysis of proteome and lipidome dynamics reveals functional regulation of global lipid metabolism. *Chem Biol* **22**, 412-425
149. Brown, M. S., Faust, J. R., Goldstein, J. L., Kaneko, I., and Endo, A. (1978) Induction of 3-hydroxy-3-methylglutaryl coenzyme-A reductase-activity in human fibroblasts

incubated with compactin (Ml-236B), a competitive inhibitor of reductase. *Journal of Biological Chemistry* **253**, 1121-1128
150. Hughes, A. L., Stewart, E. V., and Espenshade, P. J. (2008) Identification of twenty-three mutations in fission yeast Scap that constitutively activate SREBP. *J.Lipid Res.* **49**, 2001-2012
151. Lande, M. B., Donovan, J. M., and Zeidel, M. L. (1995) The relationship between membrane fluidity and permeabilities to water, solutes, ammonia, and protons. *The Journal of general physiology* **106**, 67-84
152. Brenner, R. R. (1984) Effect of unsaturated acids on membrane structure and enzyme kinetics. *Progress in lipid research* **23**, 69-96
153. Los, D. A., and Murata, N. (2000) Regulation of enzymatic activity and gene expression by membrane fluidity. *Sci STKE* **2000**, pe1
154. Matynia, A., Salus, S. S., and Sazer, S. (2002) Three proteins required for early steps in the protein secretory pathway also affect nuclear envelope structure and cell cycle progression in fission yeast. *J.Cell Sci.* **115**, 421-431
155. Jiang, Y., Vasconcelles, M. J., Wretzel, S., Light, A., Gilooly, L., McDaid, K., Oh, C. S., Martin, C. E., and Goldberg, M. A. (2002) Mga2p processing by hypoxia and unsaturated fatty acids in Saccharomyces cerevisiae: impact on LORE-dependent gene expression. *Eukaryot Cell* **1**, 481-490
156. Matsuoka, K., Orci, L., Amherdt, M., Bednarek, S. Y., Hamamoto, S., Schekman, R., and Yeung, T. (1998) COPII-coated vesicle formation reconstituted with purified coat proteins and chemically defined liposomes. *Cell* **93**, 263-275
157. Shindiapina, P., and Barlowe, C. (2010) Requirements for transitional endoplasmic reticulum site structure and function in Saccharomyces cerevisiae. *Mol Biol Cell* **21**, 1530-1545
158. Magdeleine, M., Gautier, R., Gounon, P., Barelli, H., Vanni, S., and Antonny, B. (2016) A filter at the entrance of the Golgi that selects vesicles according to size and bulk lipid composition. *eLife* **5**
159. Miyazaki, M., Dobrzyn, A., Man, W. C., Chu, K., Sampath, H., Kim, H. J., and Ntambi, J. M. (2004) Stearoyl-CoA desaturase 1 gene expression is necessary for fructose-mediated induction of lipogenic gene expression by sterol regulatory element-binding protein-1c-dependent and -independent mechanisms. *J Biol Chem* **279**, 25164-25171
160. Horton, J. D. (2002) Sterol regulatory element-binding proteins: transcriptional activators of lipid synthesis. *Biochem Soc Trans* **30**, 1091-1095
161. Vallett, S. M., Sanchez, H. B., Rosenfeld, J. M., and Osborne, T. F. (1996) A direct role for sterol regulatory element binding protein in activation of 3-hydroxy-3-methylglutaryl coenzyme A reductase gene. *J Biol Chem* **271**, 12247-12253
162. Lopez, J. M., Bennett, M. K., Sanchez, H. B., Rosenfeld, J. M., and Osborne, T. F. (1996) Sterol regulation of acetyl coenzyme A carboxylase: a mechanism for coordinate control of cellular lipid. *Proc Natl Acad Sci U S A* **93**, 1049-1053
163. Magana, M. M., and Osborne, T. F. (1996) Two tandem binding sites for sterol regulatory element binding proteins are required for sterol regulation of fatty-acid synthase promoter. *J.Biol.Chem.* **271**, 32689-32694
164. Bennett, M. K., Lopez, J. M., Sanchez, H. B., and Osborne, T. F. (1995) Sterol regulation of fatty acid synthase promoter. Coordinate feedback regulation of two major lipid pathways. *J Biol Chem* **270**, 25578-25583
165. Worgall, T. S., Sturley, S. L., Seo, T., Osborne, T. F., and Deckelbaum, R. J. (1998) Polyunsaturated fatty acids decrease expression of promoters with sterol regulatory elements by decreasing levels of mature sterol regulatory element-binding protein. *J Biol Chem* **273**, 25537-25540

166. Lee, J. N., Zhang, X., Feramisco, J. D., Gong, Y., and Ye, J. (2008) Unsaturated fatty acids inhibit proteasomal degradation of Insig-1 at a postubiquitination step. *J Biol Chem* **283**, 33772-33783
167. Takeuchi, Y., Yahagi, N., Izumida, Y., Nishi, M., Kubota, M., Teraoka, Y., Yamamoto, T., Matsuzaka, T., Nakagawa, Y., Sekiya, M., Iizuka, Y., Ohashi, K., Osuga, J., Gotoda, T., Ishibashi, S., Itaka, K., Kataoka, K., Nagai, R., Yamada, N., Kadowaki, T., and Shimano, H. (2010) Polyunsaturated fatty acids selectively suppress sterol regulatory element-binding protein-1 through proteolytic processing and autoloop regulatory circuit. *J Biol Chem* **285**, 11681-11691
168. Thewke, D. P., Panini, S. R., and Sinensky, M. (1998) Oleate potentiates oxysterol inhibition of transcription from sterol regulatory element-1-regulated promoters and maturation of sterol regulatory element-binding proteins. *J Biol Chem* **273**, 21402-21407
169. Melser, S., Molino, D., Batailler, B., Peypelut, M., Laloi, M., Wattelet-Boyer, V., Bellec, Y., Faure, J. D., and Moreau, P. (2011) Links between lipid homeostasis, organelle morphodynamics and protein trafficking in eukaryotic and plant secretory pathways. *Plant cell reports* **30**, 177-193
170. Steck, T. L., and Lange, Y. (2010) Cell cholesterol homeostasis: mediation by active cholesterol. *Trends Cell Biol* **20**, 680-687
171. Moreno, S., Klar, A., and Nurse, P. (1991) Molecular genetic analysis of fission yeast Schizosaccharomyces pombe. *Methods Enzymol.* **194**, 795-823
172. Lloyd, S. J., Raychaudhuri, S., and Espenshade, P. J. (2013) Subunit architecture of the Golgi Dsc E3 ligase required for Sterol Regulatory Element-Binding Protein (SREBP) cleavage in fission yeast. *J Biol Chem* **288**, 21043-21054
173. Chou, T. F., Bulfer, S. L., Weihl, C. C., Li, K., Lis, L. G., Walters, M. A., Schoenen, F. J., Lin, H. J., Deshaies, R. J., and Arkin, M. R. (2014) Specific inhibition of p97/VCP ATPase and kinetic analysis demonstrate interaction between D1 and D2 ATPase domains. *J Mol Biol* **426**, 2886-2899
174. Marinova, I. N., Engelbrecht, J., Ewald, A., Langholm, L. L., Holmberg, C., Kragelund, B. B., Gordon, C., Nielsen, O., and Hartmann-Petersen, R. (2015) Single site suppressors of a fission yeast temperature-sensitive mutant in cdc48 identified by whole genome sequencing. *PloS one* **10**, e0117779
175. Nalbandian, A., Llewellyn, K. J., Kitazawa, M., Yin, H. Z., Badadani, M., Khanlou, N., Edwards, R., Nguyen, C., Mukherjee, J., Mozaffar, T., Watts, G., Weiss, J., and Kimonis, V. E. (2012) The homozygote VCP(R(1)(5)(5)H/R(1)(5)(5)H) mouse model exhibits accelerated human VCP-associated disease pathology. *PloS one* **7**, e46308
176. Bartolome, F., Wu, H. C., Burchell, V. S., Preza, E., Wray, S., Mahoney, C. J., Fox, N. C., Calvo, A., Canosa, A., Moglia, C., Mandrioli, J., Chio, A., Orrell, R. W., Houlden, H., Hardy, J., Abramov, A. Y., and Plun-Favreau, H. (2013) Pathogenic VCP mutations induce mitochondrial uncoupling and reduced ATP levels. *Neuron* **78**, 57-64
177. Dickey, S. W., Baker, R. P., Cho, S., and Urban, S. (2013) Proteolysis inside the membrane is a rate-governed reaction not driven by substrate affinity. *Cell* **155**, 1270-1281
178. Slater, E. C. (2003) Keilin, cytochrome, and the respiratory chain. *J Biol Chem* **278**, 16455-16461
179. Gancedo, J. M. (1998) Yeast carbon catabolite repression. *Microbiology and molecular biology reviews : MMBR* **62**, 334-361
180. Crabtree, H. G. (1928) The carbohydrate metabolism of certain pathological overgrowths. *Biochem J* **22**, 1289-1298
181. Lai, L. C., Kosorukoff, A. L., Burke, P. V., and Kwast, K. E. (2006) Metabolic-state-dependent remodeling of the transcriptome in response to anoxia and subsequent reoxygenation in Saccharomyces cerevisiae. *Eukaryot Cell* **5**, 1468-1489

182. Askew, C., Sellam, A., Epp, E., Hogues, H., Mullick, A., Nantel, A., and Whiteway, M. (2009) Transcriptional regulation of carbohydrate metabolism in the human pathogen Candida albicans. *PLoS Pathog* **5**, e1000612
183. Sato, T., Lopez, M. C., Sugioka, S., Jigamia, Y., Baker, H. V., and Uemura, H. (1999) The E-box DNA binding protein Sgc1p suppresses the gcr2 mutation, which is involved in transcriptional activation of glycolytic genes in Saccharomyces cerevisiae *Febs Letters* **463**, 307-311
184. Ryuko, S., Ma, Y., Ma, N., Sakaue, M., and Kuno, T. (2012) Genome-wide screen reveals novel mechanisms for regulating cobalt uptake and detoxification in fission yeast. *Molecular genetics and genomics : MGG* **287**, 651-662
185. Tarsio, M., Zheng, H., Smardon, A. M., Martinez-Munoz, G. A., and Kane, P. M. (2011) Consequences of loss of Vph1 protein-containing vacuolar ATPases (V-ATPases) for overall cellular pH homeostasis. *J Biol Chem* **286**, 28089-28096
186. Martinez-Munoz, G. A., and Kane, P. (2008) Vacuolar and plasma membrane proton pumps collaborate to achieve cytosolic pH homeostasis in yeast. *J Biol Chem* **283**, 20309-20319
187. Solaini, G., Baracca, A., Lenaz, G., and Sgarbi, G. (2010) Hypoxia and mitochondrial oxidative metabolism. *Biochim Biophys Acta* **1797**, 1171-1177
188. Spahr, H., Samuelsen, C. O., Baraznenok, V., Ernest, I., Huylebroeck, D., Remacle, J. E., Samuelsson, T., Kieselbach, T., Holmberg, S., and Gustafsson, C. M. (2001) Analysis of Schizosaccharomyces pombe mediator reveals a set of essential subunits conserved between yeast and metazoan cells. *Proc Natl Acad Sci U S A* **98**, 11985-11990
189. Conaway, R. C., and Conaway, J. W. (2011) Origins and activity of the Mediator complex. *Seminars in cell & developmental biology* **22**, 729-734
190. Yang, F., Vought, B. W., Satterlee, J. S., Walker, A. K., Jim Sun, Z. Y., Watts, J. L., DeBeaumont, R., Saito, R. M., Hyberts, S. G., Yang, S., Macol, C., Iyer, L., Tjian, R., van den Heuvel, S., Hart, A. C., Wagner, G., and Naar, A. M. (2006) An ARC/Mediator subunit required for SREBP control of cholesterol and lipid homeostasis. *Nature* **442**, 700-704
191. Ho, J. J., Metcalf, J. L., Yan, M. S., Turgeon, P. J., Wang, J. J., Chalsev, M., Petruzziello-Pellegrini, T. N., Tsui, A. K., He, J. Z., Dhamko, H., Man, H. S., Robb, G. B., Teh, B. T., Ohh, M., and Marsden, P. A. (2012) Functional importance of Dicer protein in the adaptive cellular response to hypoxia. *J Biol Chem* **287**, 29003-29020
192. van den, B. T., Koritzinsky, M., and Wouters, B. G. (2006) Translational control of gene expression during hypoxia. *Cancer Biol.Ther.* **5**, 749-755
193. Rupaimoole, R., Wu, S. Y., Pradeep, S., Ivan, C., Pecot, C. V., Gharpure, K. M., Nagaraja, A. S., Armaiz-Pena, G. N., McGuire, M., Zand, B., Dalton, H. J., Filant, J., Miller, J. B., Lu, C., Sadaoui, N. C., Mangala, L. S., Taylor, M., van den Beucken, T., Koch, E., Rodriguez-Aguayo, C., Huang, L., Bar-Eli, M., Wouters, B. G., Radovich, M., Ivan, M., Calin, G. A., Zhang, W., Lopez-Berestein, G., and Sood, A. K. (2014) Hypoxia-mediated downregulation of miRNA biogenesis promotes tumour progression. *Nature communications* **5**, 5202
194. Fasanaro, P., D'Alessandra, Y., Di Stefano, V., Melchionna, R., Romani, S., Pompilio, G., Capogrossi, M. C., and Martelli, F. (2008) MicroRNA-210 modulates endothelial cell response to hypoxia and inhibits the receptor tyrosine kinase ligand Ephrin-A3. *J Biol Chem* **283**, 15878-15883
195. Fasanaro, P., Greco, S., Lorenzi, M., Pescatori, M., Brioschi, M., Kulshreshtha, R., Banfi, C., Stubbs, A., Calin, G. A., Ivan, M., Capogrossi, M. C., and Martelli, F. (2009) An integrated approach for experimental target identification of hypoxia-induced miR-210. *J Biol Chem* **284**, 35134-35143

196. Dang, K., and Myers, K. A. (2015) The role of hypoxia-induced miR-210 in cancer progression. *International journal of molecular sciences* **16**, 6353-6372
197. Yang, W., Urano, J., and Tamanoi, F. (2000) Protein farnesylation is critical for maintaining normal cell morphology and canavanine resistance in Schizosaccharomyces pombe. *J Biol Chem* **275**, 429-438
198. Song, J. Y., Cha, J., Lee, J., and Roe, J. H. (2006) Glutathione reductase and a mitochondrial thioredoxin play overlapping roles in maintaining iron-sulfur enzymes in fission yeast. *Eukaryot Cell* **5**, 1857-1865
199. Song, J. Y., Kim, K. D., and Roe, J. H. (2008) Thiol-independent action of mitochondrial thioredoxin to support the urea cycle of arginine biosynthesis in Schizosaccharomyces pombe. *Eukaryot Cell* **7**, 2160-2167
200. Kuhl, I., Dujeancourt, L., Gaisne, M., Herbert, C. J., and Bonnefoy, N. (2011) A genome wide study in fission yeast reveals nine PPR proteins that regulate mitochondrial gene expression. *Nucleic Acids Res* **39**, 8029-8041
201. Dhingra, S., Kowlaski, C. H., Thammahong, A., Beattie, S. R., Bultman, K. M., and Cramer, R. A. (2016) RbdB, a Rhomboid Protease Critical for SREBP Activation and Virulence in Aspergillus fumigatus. *mSphere* **1**
202. Butler, G. (2013) Hypoxia and gene expression in eukaryotic microbes. *Annual review of microbiology* **67**, 291-312
203. Lima Pde, S., Chung, D., Bailao, A. M., Cramer, R. A., and Soares, C. M. (2015) Characterization of the Paracoccidioides Hypoxia Response Reveals New Insights into Pathogenesis Mechanisms of This Important Human Pathogenic Fungus. *PLoS neglected tropical diseases* **9**, e0004282
204. Chang, Y. C., Bien, C. M., Lee, H., Espenshade, P. J., and Kwon-Chung, K. J. (2007) Sre1p, a regulator of oxygen sensing and sterol homeostasis, is required for virulence in Cryptococcus neoformans *Mol.Microbiol.* **64**, 614-629
205. Bien, C. M., Chang, Y. C., Nes, W. D., Kwon-Chung, K. J., and Espenshade, P. J. (2009) Cryptococcus neoformans Site-2 protease is required for virulence and survival in the presence of azole drugs. *Molecular Microbiology* **74**, 672-690
206. Gong, X., Qian, H., Shao, W., Li, J., Wu, J., Liu, J. J., Li, W., Wang, H. W., Espenshade, P., and Yan, N. (2016) Complex structure of the fission yeast SREBP-SCAP binding domains reveals an oligomeric organization. *Cell Res* **26**, 1197-1211
207. Lane, S., Zhou, S., Pan, T., Dai, Q., and Liu, H. P. (2001) The basic helix-loop-helix transcription factor Cph2 regulates hyphal development in Candida albicans partly via Tec1. *Molecular and Cellular Biology* **21**, 6418-6428
208. Crowley, J. H., Leak, F. W., Jr., Shianna, K. V., Tove, S., and Parks, L. W. (1998) A mutation in a purported regulatory gene affects control of sterol uptake in Saccharomyces cerevisiae. *J Bacteriol* **180**, 4177-4183
209. Vik, A., and Rine, J. (2001) Upc2p and Ecm22p, dual regulators of sterol biosynthesis in Saccharomyces cerevisiae *Mol.Cell Biol.* **21**, 6395-6405
210. Abramova, N. E., Cohen, B. D., Sertil, O., Kapoor, R., Davies, K. J., and Lowry, C. V. (2001) Regulatory mechanisms controlling expression of the DAN/TIR mannoprotein genes during anaerobic remodeling of the cell wall in Saccharomyces cerevisiae. *Genetics* **157**, 1169-1177
211. Silver, P. M., Oliver, B. G., and White, T. C. (2004) Role of Candida albicans transcription factor Upc2p in drug resistance and sterol metabolism. *Eukaryot Cell* **3**, 1391-1397
212. MacPherson, S., Akache, B., Weber, S., De Deken, X., Raymond, M., and Turcotte, B. (2005) Candida albicans zinc cluster protein Upc2p confers resistance to antifungal drugs and is an activator of ergosterol biosynthetic genes. *Antimicrobial Agents and Chemotherapy* **49**, 1745-1752

213. Branco, J., Ola, M., Silva, R. M., Fonseca, E., Gomes, N. C., Martins-Cruz, C., Silva, A. P., Silva-Dias, A., Pina-Vaz, C., Erraught, C., Brennan, L., Rodrigues, A. G., Butler, G., and Miranda, I. M. (2017) Impact of ERG3 mutations and expression of ergosterol genes controlled by UPC2 and NDT80 in Candida parapsilosis azole resistance. *Clinical microbiology and infection : the official publication of the European Society of Clinical Microbiology and Infectious Diseases*
214. Jiang, C., Ni, Q., Dong, D., Zhang, L., Li, Z., Tian, Y., and Peng, Y. (2016) The Role of UPC2 Gene in Azole-Resistant Candida tropicalis. *Mycopathologia* **181**, 833-838
215. Nagi, M., Nakayama, H., Tanabe, K., Bard, M., Aoyama, T., Okano, M., Higashi, S., Ueno, K., Chibana, H., Niimi, M., Yamagoe, S., Umeyama, T., Kajiwara, S., Ohno, H., and Miyazaki, Y. (2011) Transcription factors CgUPC2A and CgUPC2B regulate ergosterol biosynthetic genes in Candida glabrata. *Genes Cells* **16**, 80-89
216. Yang, H., Tong, J., Lee, C. W., Ha, S., Eom, S. H., and Im, Y. J. (2015) Structural mechanism of ergosterol regulation by fungal sterol transcription factor Upc2. *Nature communications* **6**, 6129
217. Marie, C., Leyde, S., and White, T. C. (2008) Cytoplasmic localization of sterol transcription factors Upc2p and Ecm22p in S. cerevisiae. *Fungal genetics and biology : FG & B* **45**, 1430-1438
218. Lowry, C. V., and Zitomer, R. S. (1988) ROX1 encodes a heme-induced repression factor regulating ANB1 and CYC7 of Saccharomyces cerevisiae. *Mol Cell Biol* **8**, 4651-4658
219. Balasubramanian, B., Lowry, C. V., and Zitomer, R. S. (1993) The Rox1 repressor of the Saccharomyces cerevisiae hypoxic genes is a specific DNA-binding protein with a high-mobility-group motif. *Mol Cell Biol* **13**, 6071-6078
220. Grishin, A. V., Rothenberg, M., Downs, M. A., and Blumer, K. J. (1998) Mot3, a Zn finger transcription factor that modulates gene expression and attenuates mating pheromone signaling in Saccharomyces cerevisiae. *Genetics* **149**, 879-892
221. Madison, J. M., Dudley, A. M., and Winston, F. (1998) Identification and analysis of Mot3, a zinc finger protein that binds to the retrotransposon Ty long terminal repeat (delta) in Saccharomyces cerevisiae. *Mol Cell Biol* **18**, 1879-1890
222. Hongay, C., Jia, N., Bard, M., and Winston, F. (2002) Mot3 is a transcriptional repressor of ergosterol biosynthetic genes and is required for normal vacuolar function in Saccharomyces cerevisiae. *EMBO J* **21**, 4114-4124
223. Keng, T. (1992) HAP1 and ROX1 form a regulatory pathway in the repression of HEM13 transcription in Saccharomyces cerevisiae. *Mol Cell Biol* **12**, 2616-2623
224. Becerra, M., Lombardia-Ferreira, L. J., Hauser, N. C., Hoheisel, J. D., Tizon, B., and Cerdan, M. E. (2002) The yeast transcriptome in aerobic and hypoxic conditions: effects of hap1, rox1, rox3 and srb10 deletions. *Mol.Microbiol.* **43**, 545-555
225. Sertil, O., Kapoor, R., Cohen, B. D., Abramova, N., and Lowry, C. V. (2003) Synergistic repression of anaerobic genes by Mot3 and Rox1 in Saccharomyces cerevisiae. *Nucleic Acids Res* **31**, 5831-5837
226. Zitomer, R. S., and Lowry, C. V. (1992) Regulation of gene expression by oxygen in Saccharomyces cerevisiae. *Microbiological reviews* **56**, 1-11
227. Keeling, K. M., Salas-Marco, J., Osherovich, L. Z., and Bedwell, D. M. (2006) Tpa1p is part of an mRNP complex that influences translation termination, mRNA deadenylation, and mRNA turnover in Saccharomyces cerevisiae *Mol.Cell Biol.* **26**, 5237-5248
228. Henri, J., Rispal, D., Bayart, E., van Tilbeurgh, H., Seraphin, B., and Graille, M. (2010) Structural and functional insights into Saccharomyces cerevisiae Tpa1, a putative prolylhydroxylase influencing translation termination and transcription. *J Biol Chem* **285**, 30767-30778

229. Shivange, G., Kodipelli, N., Monisha, M., and Anindya, R. (2014) A role for Saccharomyces cerevisiae Tpa1 protein in direct alkylation repair. *J Biol Chem* **289**, 35939-35952
230. Tocher, D. R., Leaver, M. J., and Hodgson, P. A. (1998) Recent advances in the biochemistry and molecular biology of fatty acyl desaturases. *Progress in lipid research* **37**, 73-117
231. Bork, P. (1993) Hundreds of ankyrin-like repeats in functionally diverse proteins: mobile modules that cross phyla horizontally? *Proteins* **17**, 363-374
232. Bork, P., Doerks, T., Springer, T. A., and Snel, B. (1999) Domains in plexins: links to integrins and transcription factors. *Trends Biochem Sci* **24**, 261-263
233. Micolonghi, C., Ottaviano, D., Di Silvio, E., Damato, G., Heipieper, H. J., and Bianchi, M. M. (2012) A dual signalling pathway for the hypoxic expression of lipid genes, dependent on the glucose sensor Rag4, is revealed by the analysis of the KlMGA2 gene in Kluyveromyces lactis. *Microbiology* **158**, 1734-1744
234. Oh, C. S., and Martin, C. E. (2006) Candida albicans Spt23p controls the expression of the Ole1p Delta9 fatty acid desaturase and regulates unsaturated fatty acid biosynthesis. *J Biol Chem* **281**, 7030-7039
235. Setiadi, E. R., Doedt, T., Cottier, F., Noffz, C., and Ernst, J. F. (2006) Transcriptional response Candida albicans to hypoxia: Linkage of oxygen sensing and Efg1p-regulatory networks. *Journal of Molecular Biology* **361**, 399-411
236. Rolland, S., Hnatova, M., Lemaire, M., Leal-Sanchez, J., and Wesolowski-Louvel, M. (2006) Connection between the Rag4 glucose sensor and the KlRgt1 repressor in Kluyveromyces lactis. *Genetics* **174**, 617-626
237. Swain, E., Baudry, K., Stukey, J., McDonough, V., Germann, M., and Nickels, J. T., Jr. (2002) Sterol-dependent regulation of sphingolipid metabolism in Saccharomyces cerevisiae. *J Biol Chem* **277**, 26177-26184
238. Bien, C. M., and Espenshade, P. J. (2010) Sterol regulatory element binding proteins in fungi: hypoxic transcription factors linked to pathogenesis. *Eukaryot Cell* **9**, 352-359
239. Lee, H., Bien, C. M., Hughes, A. L., Espenshade, P. J., Kwon-Chung, K. J., and Chang, Y. C. (2007) Cobalt chloride, a hypoxia-mimicking agent, targets sterol synthesis in the pathogenic fungus Cryptococcus neoformans *Mol.Microbiol.* **65**, 1018-1033
240. Blatzer, M., Barker, B. M., Willger, S. D., Beckmann, N., Blosser, S. J., Cornish, E. J., Mazurie, A., Grahl, N., Haas, H., and Cramer, R. A. (2011) SREBP coordinates iron and ergosterol homeostasis to mediate triazole drug and hypoxia responses in the human fungal pathogen Aspergillus fumigatus. *PLoS Genet* **7**, e1002374
241. Omura, S. (1976) The antibiotic cerulenin, a novel tool for biochemistry as an inhibitor of fatty acid synthesis. *Bacteriological reviews* **40**, 681-697
242. Liu, O. W., Chun, C. D., Chow, E. D., Chen, C., Madhani, H. D., and Noble, S. M. (2008) Systematic genetic analysis of virulence in the human fungal pathogen Cryptococcus neoformans. *Cell* **135**, 174-188
243. Noble, S. M., French, S., Kohn, L. A., Chen, V., and Johnson, A. D. (2010) Systematic screens of a Candida albicans homozygous deletion library decouple morphogenetic switching and pathogenicity. *Nat Genet* **42**, 590-598
244. Brunke, S., Quintin, J., Kasper, L., Jacobsen, I. D., Richter, M. E., Hiller, E., Schwarzmuller, T., d'Enfert, C., Kuchler, K., Rupp, S., Hube, B., and Ferrandon, D. (2015) Of mice, flies--and men? Comparing fungal infection models for large-scale screening efforts. *Disease models & mechanisms* **8**, 473-486
245. Krappmann, S. (2017) CRISPR-Cas9, the new kid on the block of fungal molecular biology. *Med Mycol* **55**, 16-23
246. Fernandez-Saiz, V., and Buchberger, A. (2010) Imbalances in p97 co-factor interactions in human proteinopathy. *EMBO reports* **11**, 479-485

247. Marguerat, S., Schmidt, A., Codlin, S., Chen, W., Aebersold, R., and Bahler, J. (2012) Quantitative analysis of fission yeast transcriptomes and proteomes in proliferating and quiescent cells. *Cell* **151**, 671-683
248. Shimoaraiso, M., Nakanishi, T., Kubo, T., and Natori, S. (2000) Transcription elongation factor S-II confers yeast resistance to 6-azauracil by enhancing expression of the SSM1 gene. *J Biol Chem* **275**, 29623-29627
249. Janoo, R. T., Neely, L. A., Braun, B. R., Whitehall, S. K., and Hoffman, C. S. (2001) Transcriptional regulators of the Schizosaccharomyces pombe fbp1 gene include two redundant Tup1p-like corepressors and the CCAAT binding factor activation complex. *Genetics* **157**, 1205-1215

Curriculum Vitae

Risa Burr

The Johns Hopkins University School of Medicine
rburr4@jhmi.edu
781-264-7835
August, 2017

Educational History

Ph.D., Biochemistry, Cellular, and Molecular Biology, Johns Hopkins University School of Medicine, Baltimore, MD, 2011-2017
Advisor: Dr. Peter Espenshade

B.S., Biochemistry and Molecular Biology, Brown University, Providence, RI, 2007-2011
Advisor: Dr. Alexander Brodsky

Professional Experience

2016	**Managing Science in Biotech Industry Course,** ASCB-KGI
2012	**Research Rotation,** JHU-SOM, Lab of Dr. Rachel Green
2011	**Research Rotation,** JHU-SOM, Lab of Dr. Denise Montell
2009	**Intern,** Oncology Drug Development, AstraZeneca Pharmaceuticals
2008	**Intern,** FAS Center for Systems Biology, Harvard University

Honors and Awards

2012	Travel Award to Genetics Society of America Conference from JHU-SOM
2011	Sigma Xi, Brown University chapter
2011	Graduated with Honors, Brown University
2010	Undergraduate Teaching and Research Grant, Brown University

Publications

1. **Burr R,** Ribbens DJ, Raychaudhuri S, Stewart EV, Ho J, and Espenshade PJ. (Submitted) Dsc E3 ligase Golgi localization requires the ATPase Cdc48 and cofactor Ufd1 for Sterol Regulatory Element-binding Protein activation in fission yeast.
2. **Burr R** and Espenshade PJ. (Submitted) Oxygen-responsive transcriptional regulation of lipid homeostasis in fungi: Implications for anti-fungal drug development. *Semin. Cell Dev. Biol.*

3. **Burr R,** Stewart EV, and Espenshade PJ. (2017) Coordinate Regulation of Yeast Sterol Regulatory Element-binding Protein (SREBP) and Mga2 Transcription Factors. *JBC* 292(13): 5311-5324.
4. **Burr R**, Stewart EV, Shao W, Zhao S, Hannibal-Bach HK, Ejsing CS, and Espenshade PJ. (2016) Mga2 transcription factor regulates an oxygen-responsive lipid homeostasis pathway in fission yeast. *JBC* 291(23): 12171–83.
5. Miller DH, Fischer AK, Chu KF, **Burr R**, Hillenmeyer S, Brard L, and Brodsky AS. (2011) T090137 inhibits cisplatin induced apoptosis in ovarian cancer cells. *Int. Jour. of Gyn. Cancer* 21: 1350–56.

Posters

The Ubiquitin Family Meeting, CSHL, 2015
Cdc48 Complexes Required for Multiple Steps of SREBP Cleavage in S. pombe

Lipid Research Conference, ASCB, 2014
SREBP activation in S. pombe requires unsaturated fatty acid maintenance by the transcriptional activator mga2

Yeast Molecular Biology and Genetics Meeting, GSA, 2012
Regulation of the Hypoxic Response in Schizosaccharomyces pombe

Service and Leadership

2015-2016 **Vice-President Finance of Graduate Student Association,** JHU-SOM
2013-2015 **Graduate Student Representative to Committee on Masters and PhD Programs,** JHU-SOM
2013-2015 **Student Representative to BCMB Policy Committee,** JHU-SOM

Citizenship

Born Buffalo, NY - 1989